University College London

An Investigation into the Effects of Variable Valve Actuation on Combustion and Emissions in an SI Engine

Ph.D. Thesis

Ahmar Ghauri

August 1999

This thesis is submitted in partial fulfilment of the requirements for the degree of Doctor of Philosophy

Abstract

The work reported in this thesis was conducted to study the effects of variable valve actuation on combustion, emissions, and fuel economy in a modern design of 4-valve per cylinder SI engine. The use of statistically-based procedures for the design of experiments allowed a limited number of tests to be used to explore a wide region of each of the experimental variables.

A series of steady-flow tests was conducted to assess the effects of valve lift on flow past the valves and the nature of any in-cylinder motion generated. Results from the former were incorporated into a filling and emptying model that allowed levels of trapped residuals and pumping work to be estimated for different valve strategies. The in-cylinder motion tests explored asymmetric valve lifts, that is to say where the two valves were opened by a different amount. These results allowed a pair of response surfaces to be established to model the intensity of both axial and barrel swirl within the cylinder over the range of valve lifts.

Engine tests were conducted in two parts. The first explored the effects of changes in exhaust event phasing, intake event phasing, intake event duration, and peak intake valve lift. The design of the experiment allowed linear, quadratic, and interactions between the variables to be modelled using regression analysis. Statistical analysis allowed the most influential factors (both main effects and interactions) to be identified. Contour plots of the modelled response were used to draw conclusions about the nature of the response surface and to isolate the effects of valve opening and closure angles as well as overlap. The results were correlated with those from the steady-flow tests and from the computer model.

The strategy for the second phase of tests was chosen after considering the previous results. The steady-flow tests indicated that there was considerable potential for enhancing in-cylinder motion by adopting a valve deactivation strategy and combining it with a low lift of the active intake valve. The second phase investigated the use of such a technique in conjunction with large overlaps over a range of duration of the intake valve event.

The results from both phases of engine tests indicated possible strategies to reduce emissions from future engines.

To my mother

Acknowledgements

Many individuals and organisations have assisted me in various ways throughout the course of my studies. I am especially indebted to my supervisor Chris Nightingale, this thesis would not have been possible without his continuous support and encouragement, and I will always be grateful for his patience, guidance and understanding.

My wife, Shazia who has supported me throughout this project which took many hours away from her. For her consideration and sacrifice, I will always be grateful.

I would also like to thank those at Jaguar Cars involved in the project. In particular, Steve Richardson, Martin Joyce, Xiang Dong Chen, Gordon Leeming, and Chris Atkinson, who provided invaluable support and assistance.

The IC engine research group members at UCL provided a stimulating and enjoyable environment within which to work, and the technical and support staff ensured things ran smoothly throughout my time at UCL.

Gregg Allin of Signal Instruments loaned exhaust gas analysis equipment during the initial phase of testing.

All the test fuel was kindly supplied by Paul Bennett from BP who was able to arrange and advise on supplies at short notice.

The earlier work of Dr Justin Seabrook during his time at UCL led to the development of some of the programs used for the analysis of the engine results and this is duly acknowledged.

The research work was supported by the Engineering and Physical Sciences Research Council through a CASE award, with further support from Jaguar Cars, and this is most gratefully acknowledged.

Finally, I would like to express my gratitude towards all my friends and family who have 'been there' in times of need.

Table of Contents

List of Figures

Chapter 1

Chapter 2

Chapter 3

Chapter 4

Chapter 5

Chapter 6

Chapter 7

List of Tables

Nomenclature

AAA	air-assisted atomiser
aBDC	after bottom dead centre
AFR	air-fuel ratio
aTDC	after top dead centre
AVT	Active valve train
bBDC	before bottom dead centre
BDC	bottom dead centre
BMEP	brake mean effective pressure
BSCO	brake specific carbon monoxide
BSFC	brake specific fuel consumption
bTDC	before top dead centre
ca	crank angle
CCRD	central composite rotatable design
CLA	chemi-luminescence analyser
CO	carbon monoxide
CO_2	carbon dioxide
DI	direct injection
DVM	digital volt meter
ECU	engine control unit
EGR	exhaust gas re-circulation
EIVC	early intake valve closure
EMS	engine management system
EVC	exhaust valve closure
EVO	exhaust valve opening
EVT	exhaust valve timing
FID	flame ionisation detector
FTP	federal test procedure
GFEE	general flow energy equation
HC	unburned hydrocarbon
HEGO	heated exhaust gas oxygen (sensor)
IC	internal combustion
IMEP	indicated mean effective pressure
IVC	inlet valve closure
IVO	inlet valve opening
IVT	inlet valve timing
LDV	laser doppler velocimetry
LIVC	late inlet valve closure

MBT	maximum brake torque
MFB	mass fraction burned
MOP	maximum opening point
MY	model year
NDIR	non-dispersive infra-red
NMHC	non-methane hydrocarbons
NMOG	non-methane organic gases
NO	nitric oxide
NO_2	nitrogen dioxide
NO_x	oxides of nitrogen
OOP	object oriented programming
PMEP	pumping mean effective pressure
RGF	residual gas fraction
Smd	Sauter mean diameter
SI	spark ignition
TDC	top dead centre
VIS	variable intake system
VOC	volatile organic compounds
VVA	variable valve actuation
VVT	variable valve timing
WOT	wide open throttle
ZEV	zero emission vehicle

Chapter 1

COMBUSTION AND EMISSIONS IN AN SI ENGINE

A Literature Survey

1. Combustion and Emissions in an SI Engine

1.1. Introduction

Increasingly stringent legislation to limit emissions from Internal Combustion (IC) engines presents a considerable challenge to the engineer. Novel solutions are being sought to overcome some of the compromises inherent in designs of the past while research continues into gaining a more fundamental understanding of the mechanisms at work during the combustion gas exchange processes. The demand for improvements in performance continues unabated while emissions targets become more difficult to achieve. The wide use of the Spark Ignition (SI) engine as the principal prime mover means that great improvements are necessary if further damage to the environment is to be minimised.

The aim of this chapter is to give a brief review of the IC engine before moving on to look at future strategies which may be adopted to meet the performance demands of the consumer as well as the legislative requirements of the future.

1.2. The 4-stroke IC engine

1.2.1. Thermodynamic analysis applied to 4-stroke IC engines

In order to understand the limitations of real engines, it is necessary to identify the factors that significantly affect their performance. The most fundamental of these can be assessed to some extent by use of thermodynamic models, the simplest of which are based on the pressure-volume characteristics of the cylinder contents. Much of the following analysis can be found in standard texts on internal combustion engines [Heywood (1988), Stone (1992)]. Figure 1.1 shows a pressure-volume diagram taken from an actual SI engine under part throttle conditions.

This processes within a real engine can be modelled either by the constant volume thermodynamic cycle (often referred to as the Otto cycle) or a mechanical cycle [Heywood (1988)] based on the same principle. Representations of these are shown in Figure 1.2.

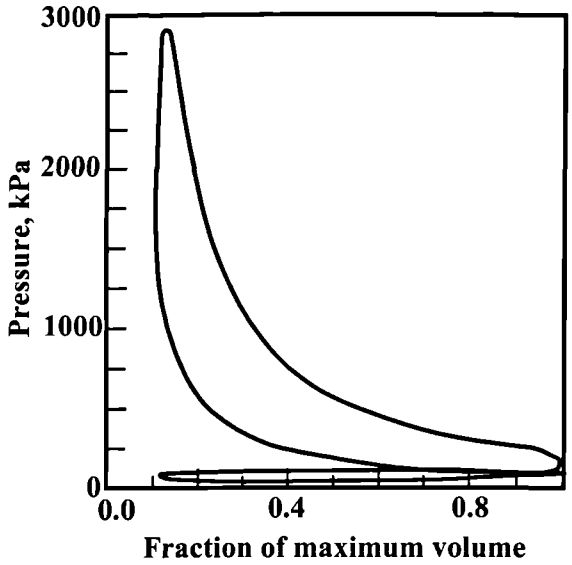

Figure 1.1
Pressure-volume diagram for a 4-stroke SI engine under part throttle conditions [Heywood (1988)]

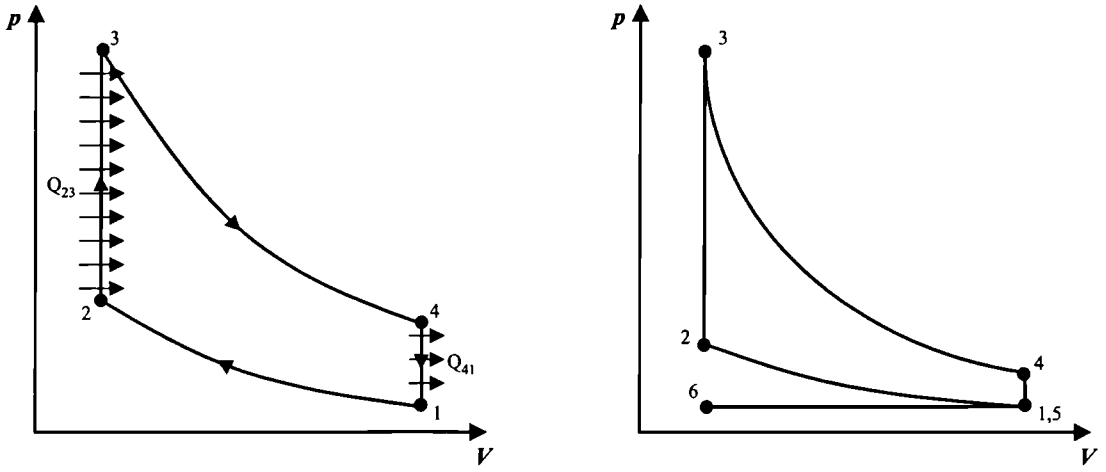

Figure 1.2
Pressure-volume diagrams for constant volume cycles (a) thermodynamic cycle and (b) mechanical cycle (adapted from Stone (1992))

The fundamental difference between these two approaches is that the cycle of Figure 1.2(a) represents a system in which the working fluid passes through a cycle with the only interactions being transfers of heat and work at the appropriate points. The cycle of Figure 1.2(b) refers to a mechanical cycle, additionally allowing mass transfer of the working fluid to take place. It also caters for internal combustion rather than simple heat transfer. The term constant volume in these two models refers to the fact that heat transfer or combustion takes place at a constant volume. The processes shown in Figure 1.2 can be summarised as follows:

- 1 - 2 Adiabatic and reversible (hence isentropic) compression.
- 2 - 3 Heat transfer (addition) to the system or internal combustion; both at constant volume.
- 3 - 4 Adiabatic and reversible (isentropic) expansion.
- 4 - 1 For the thermodynamic cycle, heat rejection at constant volume.
- 4 - 5 For the mechanical cycle, exhausting of gas from the cylinder.
- 5 - 6 For the mechanical cycle, induction of fresh charge into the cylinder.

Since the mechanical cycle more closely resembles the actual processes within an engine, it will be used from here on. Whichever model is used, each should give identical results for the key parameters to be discussed in the following.

The fuel conversion efficiency can be written in terms of the work produced (W), the mass of fuel m_f, and the lower calorific value of the fuel Q_{LCV}:

$$\eta_{f,i} = \frac{W}{m_f Q_{LCV}} \tag{1.1}$$

Assuming the working fluid to be ideal with constant specific heats (c_p and c_v), equation (1.1) reduces to:

$$\eta_{f,i} = 1 - \frac{1}{r_c^{\gamma-1}} \tag{1.2}$$

Where r_c is the volumetric compression ratio of the engine and γ is the ratio of the principal specific heats.

Equation (1.2) shows that for constant volume combustion, efficiency is a function of compression ratio only. However, the ideal of constant volume combustion cannot be realised due to the finite time taken for combustion and the rapid motion of the piston. A possible variation arises if the combustion process is contrived to occur at constant pressure. In this case combustion takes place over a finite time period and another simple model may be used to describe the cycle. Figure 1.3 shows the pressure-volume diagram for such a cycle. Using a similar method of analysis, it can be shown that the cycle efficiency will be given by:

$$\eta_{f,i} = 1 - \frac{1}{r_c^{\gamma-1}}\left[\frac{\alpha^{\gamma} - 1}{\gamma(\alpha - 1)}\right] \tag{1.3}$$

Where:

$$\alpha = \frac{V_3}{V_2} \tag{1.4}$$

Equation (1.3) is similar to (1.2) apart from the term in square brackets, which is always greater than unity. Consequently, the efficiency for a constant pressure cycle is always less than that of the Otto cycle. Comparison of Equation (1.2) to (1.3) demonstrates that the combustion process should occur over the shortest period possible in order to obtain high efficiency.

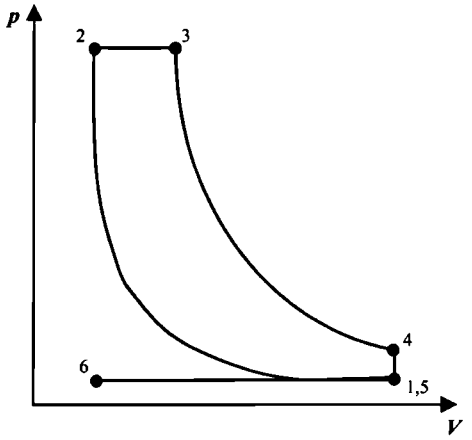

Figure 1.3
Pressure-volume diagram for constant pressure combustion cycle (adapted from Stone (1992))

1.2.2. Combustion in a 4-stroke SI engine

Combustion is initiated by a spark produced between a set of electrodes as the piston approaches Top Dead Centre (TDC). The spark provides the necessary activation energy for the combustion reactions to begin. Combustion starts in the gap between the electrodes as a spherical nucleus of flame, often referred to as a 'flame kernel', which grows as the flame front propagates through the combustion chamber. The flame is extinguished upon arrival at the chamber walls, at which point approximately 90% of the cylinder contents have been burned [Heywood (1988)]. Further oxidation reactions continue on a smaller scale in the post-flame gases.

The most important factor in combustion is the overall time taken for the combustion process to occur. Assuming laminar flame propagation, the time taken to complete combustion would be an order of magnitude greater than that available in a typical IC engine. Thus methods which improve flame propagation rates must be utilised. The primary method of reducing the time for combustion is by effective use of turbulence within the cylinder. Turbulence enhances combustion by 'wrinkling' the flame front, increasing the surface area of the flame to bring a greater quantity of fresh charge into the reaction zone [Stone (1992)]. Figure 1.4 shows the development of the flame.

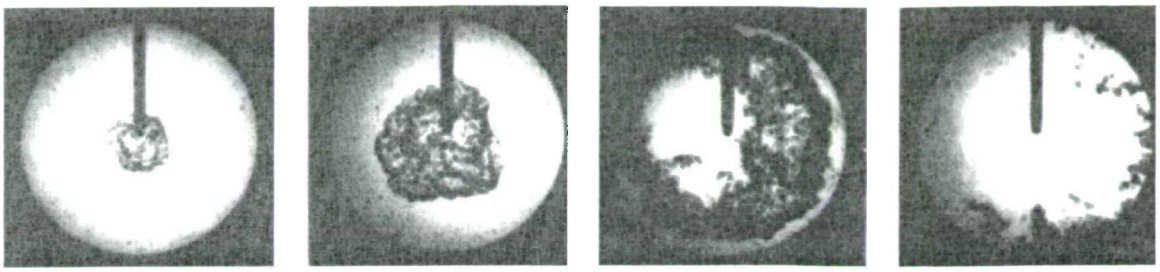

Figure 1.4
Development of the combustion process [Heywood (1988)]

Turbulence can be arranged to occur in a systematic way by controlling the bulk flow into the cylinder through the intake system. Intake generated in-cylinder motion is fundamental to achieving combustion improvements [de Boer *et al.* (1990)]. Figure 1.5 shows the two main types of controlled air motion regimes that can be arranged to occur.

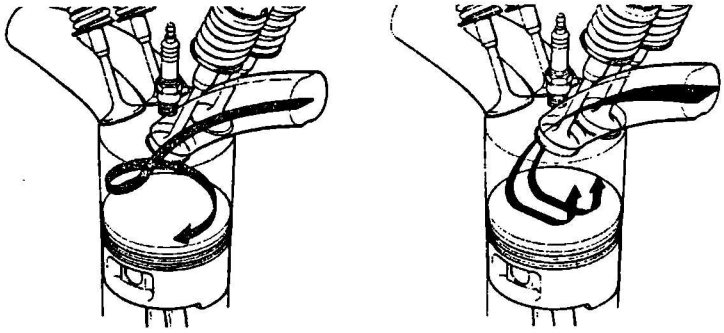

(a) Axial Swirl

(b) Barrel Swirl
(tumble)

Figure 1.5
In-cylinder air motion regimes. (a) Axial swirl and (b) barrel swirl (adapted from Wilson *et al.* (1993))

In-cylinder charge motion and turbulence are mainly determined by the intake flow characteristics during the induction stroke [Endres *et al.* (1992)]. The two motions tend to affect combustion to differing extents due to the behaviour of the flow as the piston approaches TDC. In the case of axial swirl, the rising piston does not completely destroy the gas motion. In fact the motion may be enhanced by use of certain types of combustion chambers (pent-roof for example) which induce an inward radially directed displacement (often referred to as squish). The fact that the rotating charge is forced towards its axis causes its angular velocity to increase. In general, swirl is not destroyed when combustion begins and may even persist well into the expansion stroke. Tumble differs fundamentally in that the motion suddenly degenerates into 'micro-turbulence' as the piston approaches TDC. This collapse of bulk flow is primarily due to the shape of the combustion chamber. The importance of this feature is that it ensures there is less chance of the flame kernel being swept away from its initial location. Instead the smaller

scale of turbulence is more effective in wrinkling the flame front. Another feature of tumble is that it is inherent to designs featuring two or more intake valves per cylinder. However, the required degree of in-cylinder motion can only be achieved by careful optimisation of the intake system, with the main aim being to keep the flow velocities high. Such an approach can be detrimental to high-speed performance so inevitably a compromise is required.

Numerous experimental studies correlating in-cylinder motion and its effects on combustion have been carried out (for example Endres et al. (1992), de Boer *et al.* (1990), Kyriakides and Glover (1989)). In general it has been found that tumble is preferable to swirl in reducing both the delay and overall duration of combustion provided that the initial flow velocities are high enough to ensure a strong tumbling motion. This requirement can be a problem at lower speeds for engines optimised for Wide Open Throttle (WOT) performance. In their study, Kyriakides and Glover (1989) found that tumble was more useful in that not only did it degenerate into 'micro-turbulence', but also it did so at approximately 40° bTDC (see Figure 1.6) making it particularly useful in promoting flame development during the initial phase of combustion.

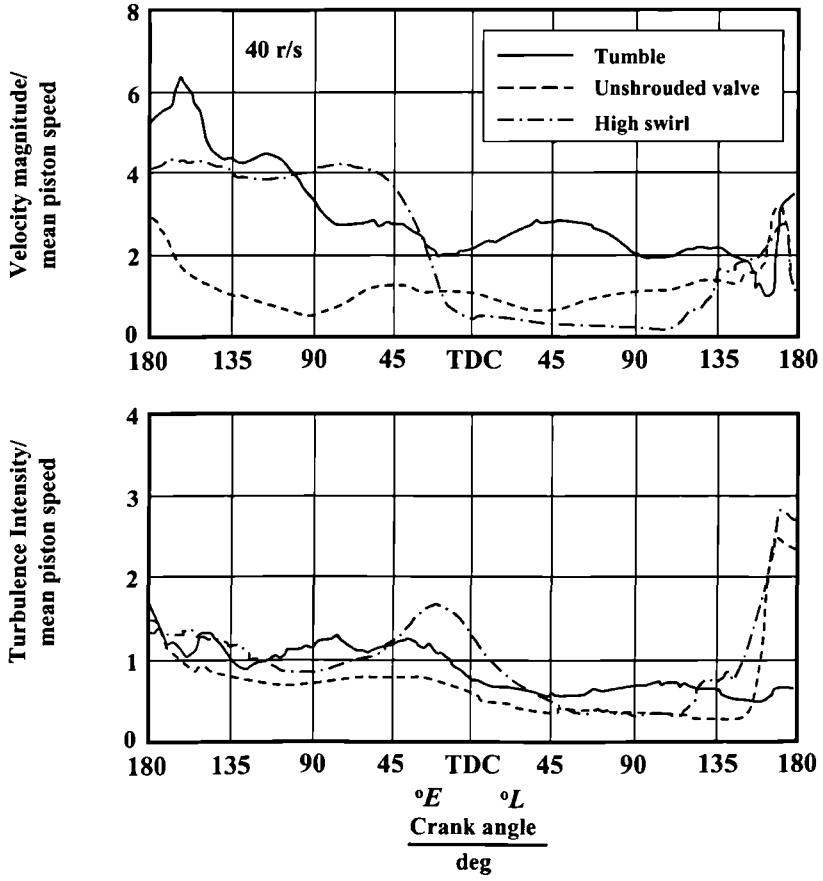

Figure 1.6
Variation of turbulence intensity with crank angle for different in-cylinder flow regimes [Kyriakides and Glover (1989)]

The burn rate, although primarily influenced by turbulence within the combustion chamber, is also dependent on a number of secondary factors. One of these is the reduction under lean mixture operation. Using a weaker mixture can give rise to a number of attendant benefits. In particular, it is widely recognised that lean combustion is the most promising method of improving fuel economy [Inoue *et al.* (1993)]. Turbulence in this case becomes even more of a necessity, due to the lower flame velocities in lean mixtures. Figure 1.7 shows the effect of fuel/air equivalence ratio on the laminar burning velocity, clearly indicating that the peak occurs for slightly rich mixtures. Lean operation also requires improved mixture preparation if misfire is to be avoided.

An extension of lean burn operation is the concept of stoichiometric combustion with high levels of Residual Gas Fraction (RGF). In particular Exhaust Gas Re-circulation (EGR) allows dramatic reductions in NOx emissions coupled with improvements in fuel economy. Mixture dilution with exhaust gas tends to slow combustion to a greater degree than use of air as the diluent. The subjects of lean burn and EGR will be dealt with in greater detail later.

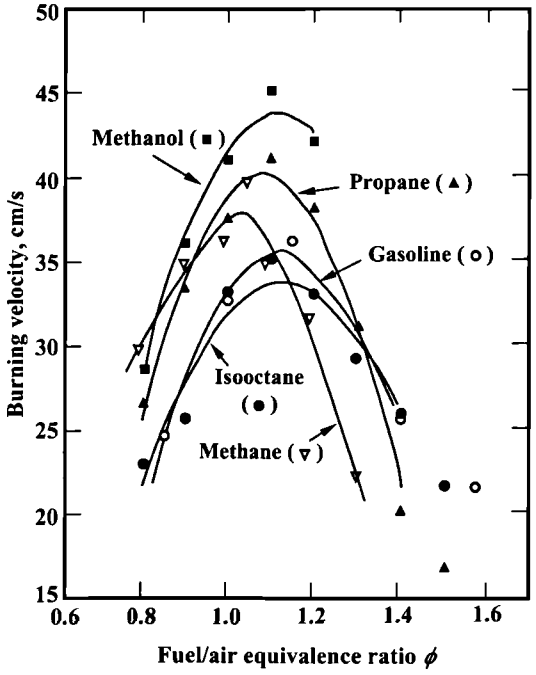

Figure 1.7
Laminar burning velocity for several fuels as a function of equivalence ratio [Heywood (1988)]

1.2.3. Port and combustion chamber design

The intensity and structure of the charge motion within the cylinder is predominantly a function of the intake port geometry. An optimally designed port will allow a high degree of turbulence to be generated at little expense to the volumetric efficiency (η_v) of the engine. The design of the

ports depends on the type of in-cylinder flow motion that is required. Those promoting axial swirl are prevalent in designs with 2-valves per cylinder, while tumble inducing ones are preferred in 4-valve engines.

Axial swirl can be induced by arranging the flow to enter the cylinder tangentially. In order to maximise the level of swirl, a helical inlet port is often used. Although this helps in promoting swirl, care is needed in order to avoid too great a reduction in volumetric efficiency as this would lead to a corresponding reduction in maximum power output [Stone (1992)].

Tumble is inherent in engines with four or more valves per cylinder. Such designs also exhibit a higher volumetric efficiency because of the larger flow area available. The inlet tracts are usually designed to be almost horizontal and converging slightly [Stone *et al.* (1993)]. The flow thus tends to be biased towards the top of the valve and enters the pent-roof combustion chambers heading towards the exhaust valves. Figure 1.8 shows the main parameters affecting the tumble generating capabilities of such induction systems. Inlet ports of multi-valve engines designed for tumble can also be used to provide swirl by restricting flow to all but one of the valves per cylinder (Figure 1.9). Such deactivation can be achieved either by preventing one valve from opening or by use of a throttle located in the inlet port to be disabled. Under such conditions, the flow enters the cylinder tangentially through the single open valve, hence producing axial swirl.

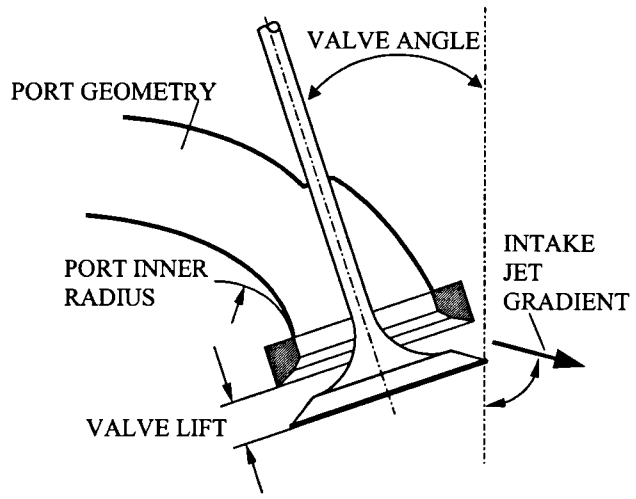

Figure 1.8
Parameters influencing the tumble generation of induction systems (adapted from Endres *et al.* (1992))

An example of deactivation through restriction of valve lift is described by Horie *et al.* (1992). In the Honda VTEC-E mechanism that they describe, the deactivated valve is opened slightly to avoid fuel collecting in the port. Swirl ratios of up to 2.8 have been quoted using this technique although their definition for the swirl ratio is not given.

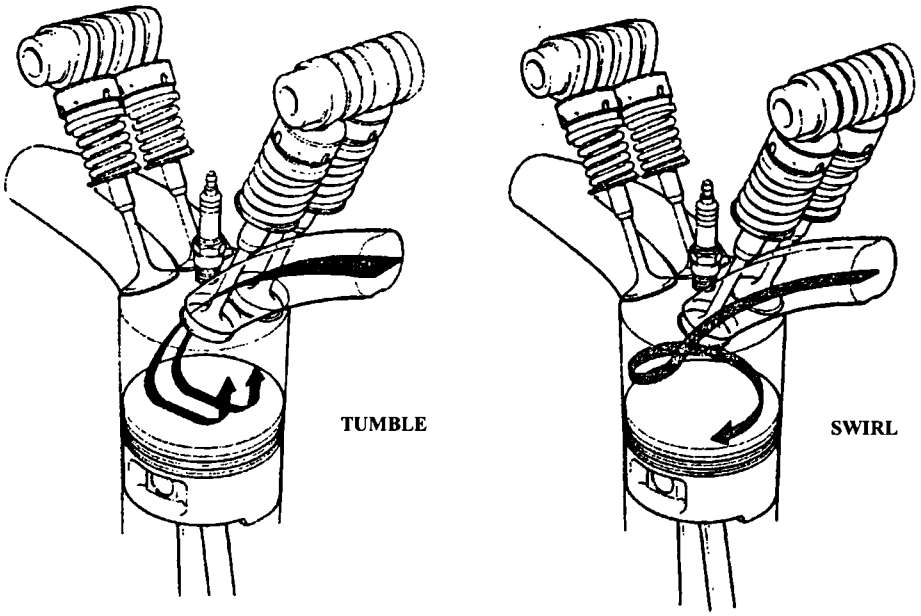

Figure 1.9
Use of valve deactivation to induce axial swirl in 4-valve engines
[Wilson *et al.* (1993)]

The advantage of port deactivation is that it can be used at low speeds when flow velocities under normal operation would be too low to induce any degree of in-cylinder tumble. The advantages of high volumetric efficiency are not compromised at higher loads since the deactivated port or valve can then be brought into operation. An extension of this technique is to retain one normal port (which can be deactivated) and to use a helical one for the primary port to further enhance the swirl inducing capabilities at low speed. There is, however, a slight penalty in volumetric efficiency at high speed.

The combustion chamber design plays a crucial role in utilising the in-cylinder motion to enhance the combustion process, particularly in four-valve engines. The ordered motion created during the induction stroke is broken down to form a region of highly turbulent eddies. In general, the selection of a combustion chamber is based on the optimisation of a number of criteria. Heywood (1988) suggests that these may include:

- a fast combustion process with low cycle-to-cycle variability over the full engine operating range
- a high volumetric efficiency at WOT
- minimum heat loss to combustion chamber walls
- a low fuel octane requirement

The fast burn capability can only be achieved by effective use of in-cylinder motion, thus it is preferable to have a system which, for example, promotes tumble. A consequence of fast burn is the reduction in cyclic variability and the ability to run under leaner conditions without loss of combustion quality. The location of the spark plug relative to the cylinder walls can also help in improving combustion speed. A number of approaches have been employed, including the use of more than one plug. However, it seems that the simplest practical solution is the use of a centrally-located plug as this limits the overall distance that the flame must travel in any direction.

A high volumetric efficiency implies the use of a multi-valve cylinder head that presents less of a restriction to the incoming charge. Using multi-valve heads constrains the shape that the combustion chamber can take since the valves should be able to open sufficiently without striking either one another or the piston.

The heat loss through the combustion chamber walls is a function of the surface area to volume ratio. A large surface area will have a greater potential for heat loss. Highly turbulent flows such as those generated by tumble ports will inevitably result in greater heat transfer. Heat transfer will additionally depend on the gas and wall temperatures.

The octane requirement of any chamber design is dictated by the onset of knock, which itself is one of the most difficult factors to judge quantitatively. The onset of knock limits the maximum compression ratio that can be used, consequently placing a direct limit on engine efficiency. The knock performance of any chamber design is influenced by, amongst other things, the temperatures of the exhaust valves and the end gas. Hot exhaust valves make a chamber more prone to knock. The exhaust valves will almost inevitably be the hottest regions of the combustion chamber, so it is preferable to ensure that the charge in the vicinity of the exhaust valves is burnt as early as possible. Placing the spark plug close to the exhaust valves will aid in achieving the shorter flame distances required.

A design of particular interest is the pent-roof combustion chamber as this is typical of modern 4-valve engines (Figure 1.10). Such a chamber satisfies a number of the criteria discussed above. In particular the pent-roof chamber offers a compact design with good surface area to volume ratio, a centrally-located spark plug which limits maximum flame travel distances as well as being close to the exhaust valves, and a shape which promotes tumble and then helps in its degeneration into micro-turbulence. In addition the exhaust valves are cooled by the incoming flow of gas during the induction stroke. These benefits allow pent-roof chambers to operate at higher compression ratios than most alternative designs.

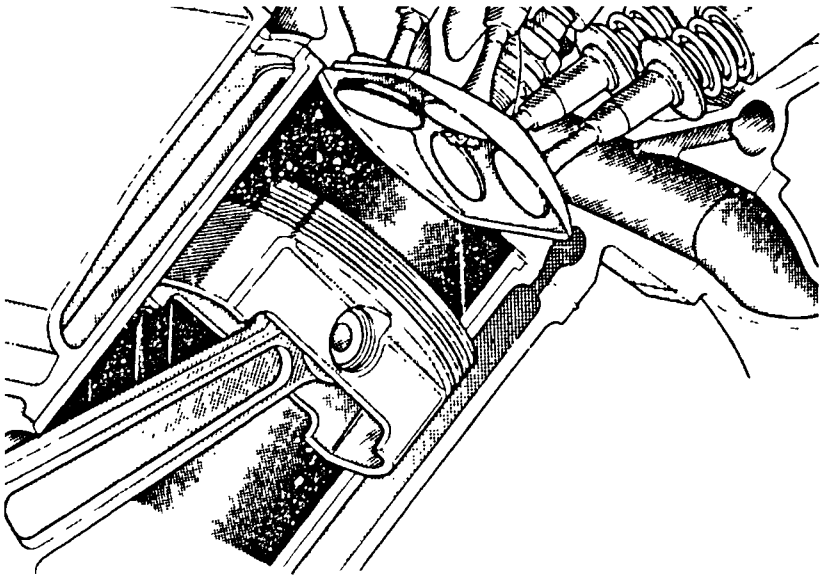

Figure 1.10
4-valve pent-roof combustion chamber (adapted from Titolo (1991))

1.2.4. Mixture preparation

Spark ignition engines use a mixture of hydrocarbon-based fuel and the oxygen from air for combustion. The process by which this is achieved is known as mixture preparation. The fuel must first be added in the correct proportion to the air entering the engine, and then be fully vaporised as it is incapable of burning in its liquid state.

Port fuel injection

Fuel is normally added by an injector located in the port (Carburettors and single-point injection may also used, but they are not discussed here). The injectors are fed by a pressurised supply of fuel, which is regulated by a pressure relief valve. The injector itself is a solenoid-controlled valve that allows accurate metering of the fuel being supplied to the engine. The fuel exits the injector as a spray consisting of relatively large droplets, typically for a pintle-type injector of the order of 100 μm Sauter Mean Diameter (Smd). The process of atomisation produces a very high surface to mass ratio in the liquid phase, thereby promoting rapid evaporation [Saikalis *et al.* (1993)]. The aim of the injector is to produce a fine spray with small droplets that will evaporate quickly to produce a homogenous mixture. Small drops are carried with the airflow while larger droplets are not influenced by the airflow to such a degree and are normally found to impinge on the port surfaces where they form a film. Nogi *et al.* (1988) demonstrated that, with an airflow velocity of 10 m/s, droplets of less than 30 μm in diameter were able to follow the airflow around an inlet valve. Those above 50 μm in diameter had sufficient momentum so as to cause them to impact on surfaces in the area. This mechanism is referred to as 'wall wetting' and is one

of the three ways in which fuel enters the cylinder, the other two being small droplets carried by the flow and fuel which has already been vaporised. The quantity of fuel left as a liquid, both on the walls and as droplets, can have a bearing on emissions of unburned hydrocarbons. This is because some of the fuel entering the cylinder may still be in its liquid state at the end of combustion and thus unable to burn. Figure 1.11 summarises the pathways by which fuel enters the engine.

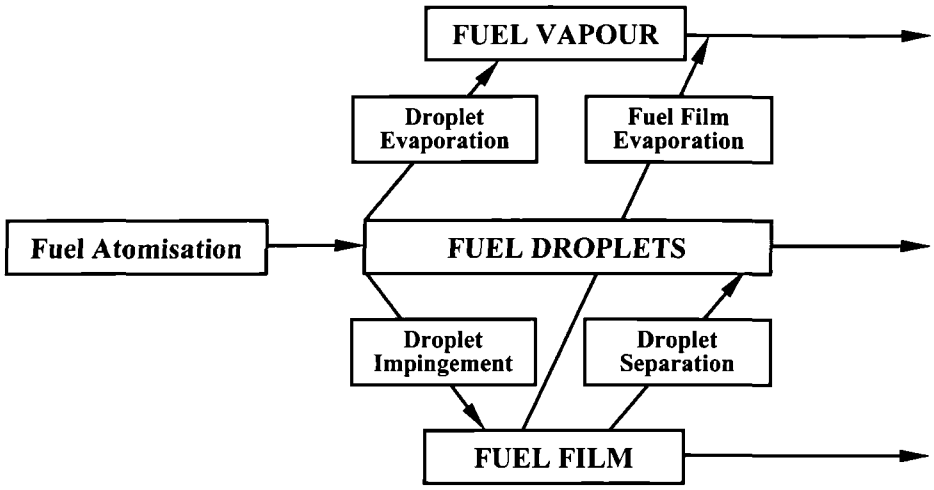

Figure 1.11
Possible pathways for fuel entering the cylinder
(adapted form Rokita *et al.* (1993))

Port fuel injection systems pose a number of problems. First, locating the injector close to the valve means that there is very little time available for the fuel to evaporate. For this reason, most systems adopt a strategy of targeting the fuel spray onto the back of the inlet valve when it is closed. The combination of increased residence time in the port, and the heat transfer from the valve greatly facilitates evaporation. The reverse is true during cold-starts and warm-up since fuel simply collects on the valve forming a puddle and enters as a liquid when the valve opens. The second problem is that accurate targeting of the fuel spray is required in order to avoid excessive wall wetting. This is particularly so in 4-valve engines, which suffer extensive wetting on the partition between the ports. Excessive wall wetting causes a deterioration in transient performance as fuel injected in one cycle may enter the cylinder in subsequent ones. Thus the injection system has to meet the following two requirements [Harada (1992)]:

- Fuel atomisation, to ensure a homogeneous fuel/air mixture.
- Optimisation of spray direction to minimise wall wetting.

Mixture preparation requirements are different for cold-start and warm-up than for normal, fully warm operation. They are most arduous during the cold-start and warm-up period because there

is very little heat transfer to the fuel from the cold surfaces in the port. As a consequence a greater amount of fuel is required to ensure a sufficient quantity has vaporised for combustion. The amount of enrichment can be reduced if the fuel droplets in the spray are smaller or if the fuel is vaporised by some other means. A number of methods have been proposed to help achieve such mixture preparation. These include use of Air Assisted Atomisers (AAAs), ultrasonic atomisers and electrostatic atomisers [Fry (1994)]. The AAA seems to be a particularly simple and promising method of giving the required droplet sizes. Figure 1.12 shows schematic representations of AAAs developed by three manufacturers.

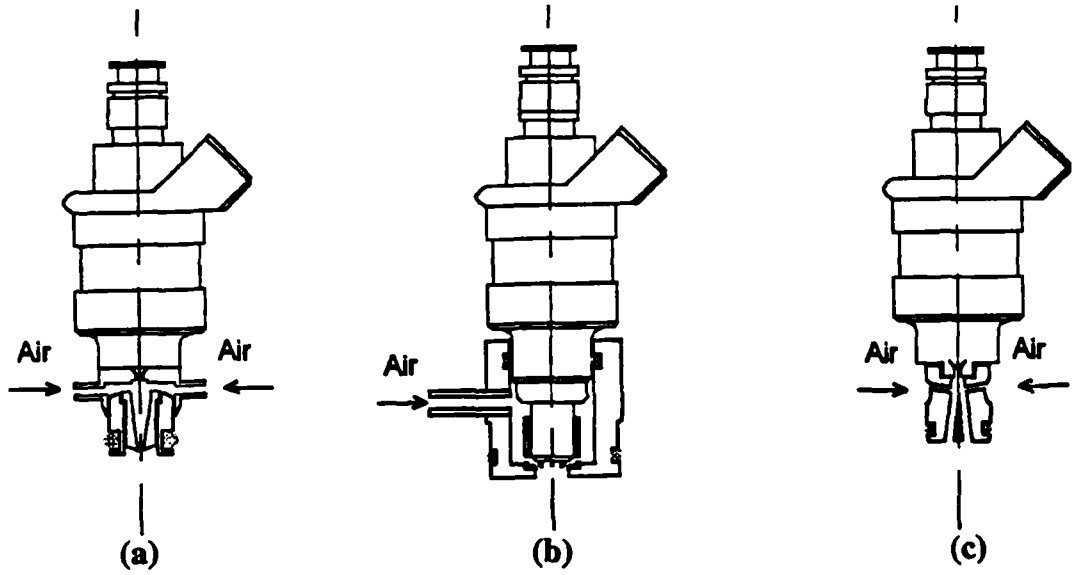

Figure 1.12
Schematics of air assisted atomisers by (a) Lucas, (b) Nippondenso and (c) Toyota (taken from Fry (1994), originally from Lucas, Nippondenso and Harada (1992) respectively)

These AAAs are based on the standard pintle injector with the nozzle modified so that pressurised air is mixed with the fuel. The high shear forces generated between the fuel and air cause the spray to be broken down into smaller droplets. The air can be added either before the metering orifice (as in the Lucas and Toyota designs), or afterwards as in the Nippondenso design. Although a separate pressurised air supply can be used, it is normally more convenient to use atmospheric air which can be arranged to bypass the throttle. The disadvantage of the latter is that the amount of air assistance diminishes with rising manifold pressure. In their study, Rokita *et al.* (1993) studied the effect of air assistance pressure on droplet size (Figure 1.13) using an AAA similar in principle to the Nippondenso device. They concluded "even a small air assistance pressure is very helpful".

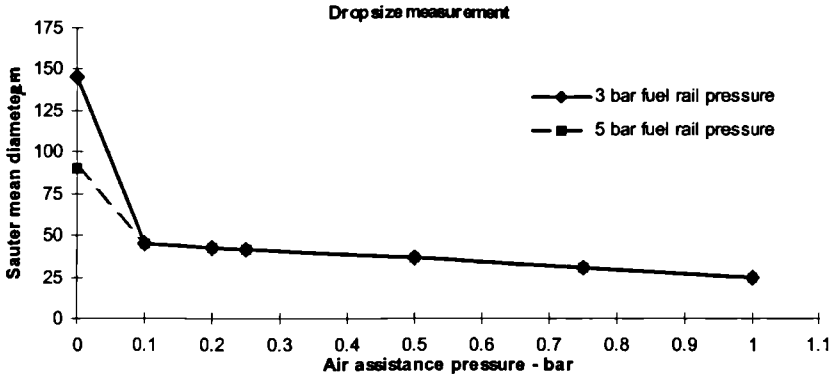

Figure 1.13
Influence of air assistance pressure on droplet size
(adapted from Rokita *et al.* (1993))

Effects of in-port conditions on mixture preparation

The conditions within the port have a profound effect on the mixture preparation process. These conditions are not only dependent on the thermal environment in the port, but are also varying continually with crank angle and with engine speed. This is because the induction process is unsteady in nature.

The induction process can be broken down into a number of discrete steps. In the case of closed valve injection, fuel would have already been injected by the time the inlet valve opens. Under part load conditions, the combination of low manifold pressure and a lack of gas dynamic effects mean that there will be a backflow of hot exhaust gases from the cylinder into the port. Once the pressures in the port and cylinder have equalised, the flow reverts to the forward direction, allowing fresh charge to enter the cylinder. Under part-throttle conditions, there will be another reverse flow period towards the end of the induction phase as the inlet valve normally closes after BDC. Shin *et al.* (1995) carried out tests on a single cylinder engine using a Volvo 4-valve cylinder head with pent-roof combustion chamber. The tests were carried out under simulated warm-up conditions by maintaining the coolant temperature at 25 °C. The investigation confirmed the presence of the above affects, and the authors were able to put forward some suggestions as to the impact each had on the mixture preparation process. The initial backflow not only helped in changing the thermal environment of the intake port, but also 'strip-atomised' the liquid fuel film in the vicinity of the inlet valve. The resulting droplets were transported up the intake port, thus facilitating evaporation by distributing fuel over a larger area. The transportation of liquid fuel into the cylinder was found to be mainly due to wall films on the port surfaces and the valves. The liquid was again strip-atomised as it entered the cylinder. The investigation also showed that some of the fuel injected in one cycle may be left in the port to be

inducted in subsequent ones [Shin *et al.* (1995)]. Although these effects were observed with a low coolant temperature, it is reasonable to assume that they may still be present, albeit to a lesser extent, under normal running conditions.

Mixture preparation within the cylinder

In-cylinder motion and heat transfer play the final part in the mixture preparation process. The charge motion allows further mixing of the fuel and air, whilst heat transfer from the surrounding surfaces helps in vaporising the droplets present. In practice much of the fuel entering may impact on cylinder surfaces, making this effect more significant than in-cylinder motion.

1.2.5. Emissions, mechanisms for their formation and legislation for their control

The four main pollutants emitted from the exhaust of a 4-stroke internal combustion engine are:

- carbon dioxide (CO_2)
- carbon monoxide (CO)
- unburned hydrocarbons (HC)
- oxides of nitrogen (NOx).

Carbon Dioxide

CO_2 can only be reduced by improvements in the Brake Specific Fuel Consumption (BSFC) of the engine. The other three are to some extent controllable by careful design of the engine and after-treatment of the exhaust gases. Although CO_2 is not toxic, and is not currently legislated against, it is a greenhouse gas, which makes it likely that it will fall within the remit of future legislation.

Carbon Monoxide

The presence of carbon monoxide is normally due to incomplete combustion. This is particularly so under rich conditions when there is insufficient oxygen to completely oxidise the fuel. However, even with lean mixtures, CO cannot completely be removed due to dissociation of the chemical species at the high temperatures within the chamber. During the expansion stroke, the fall in cylinder temperature effectively 'freezes' the reverse dissociation reactions thus preventing the oxidation of CO to CO_2. Carbon monoxide levels are also dependent on the degree of air/fuel homogeneity. Inconsistent mixing of air and fuel may lead to local regions containing a rich mixture causing incomplete combustion. Effective use of in-cylinder motion should help to reduce this effect.

Unburned Hydrocarbons

Hydrocarbons are one of the two main pollutants (together with oxides of nitrogen), emitted from engine exhausts and extensive work has been carried out to investigate the mechanisms that may account for their presence. They are found in the exhaust of SI engines due to a portion of the inducted fuel escaping combustion and exiting the cylinder partially or completely unoxidised [Thompson and Wallace (1994)]. A number of ideas have been put forward to explain this, in particular, it seems likely that there is more than one mechanism at work. The generally accepted explanation is that part of the fuel becomes trapped in such a way that the flame cannot reach it. Regions not reached by the flame are called 'crevices' and include such areas as the piston ring pack, the head gasket, spark plug thread and valve seats. In addition absorption and subsequent desorption may occur from the oil film on the cylinder wall and any deposits which may have accumulated in the combustion chamber. Min *et al.* (1994), have identified six mechanisms and pathways for unburned hydrocarbons in the exhaust:

- combustion chamber crevices
- absorption and desorption of fuel in oil layers
- absorption and desorption of fuel in deposits
- flame quenching at the wall and in the bulk of the contents
- presence of liquid fuel in the chamber
- exhaust valve leakage.

A number of studies (Wentworth (1968), Namazian and Heywood (1982), Boam *et al.* (1992), Min *et al.* (1994) and Thompson and Wallace (1994)) have identified crevices as the largest single factor affecting hydrocarbon levels. The consensus seems to be that the crevice formed by the piston top ring land in particular, and that between the top and second ring, are the most significant contributors. Wentworth (1968) reported a decrease in hydrocarbon emission of up to 74% when the top land was virtually eliminated.

During compression, unburned mixture is forced into the crevices where, because of the adverse surface to volume ratio, it cools down quickly to near-wall temperature. This process continues well into combustion as the cylinder pressure continues to rise, until the flame front arrives, at which point one of a number of things can occur. The flame can either enter to partially or completely oxidise the fuel, or it can be extinguished at the entrance or part-way inside. As the pressure falls, the crevice gas then joins the bulk gases in the cylinder, thus allowing a substantial amount to escape unoxidised. The mechanism for the transportation into the bulk gases is shown schematically in Figure 1.14.

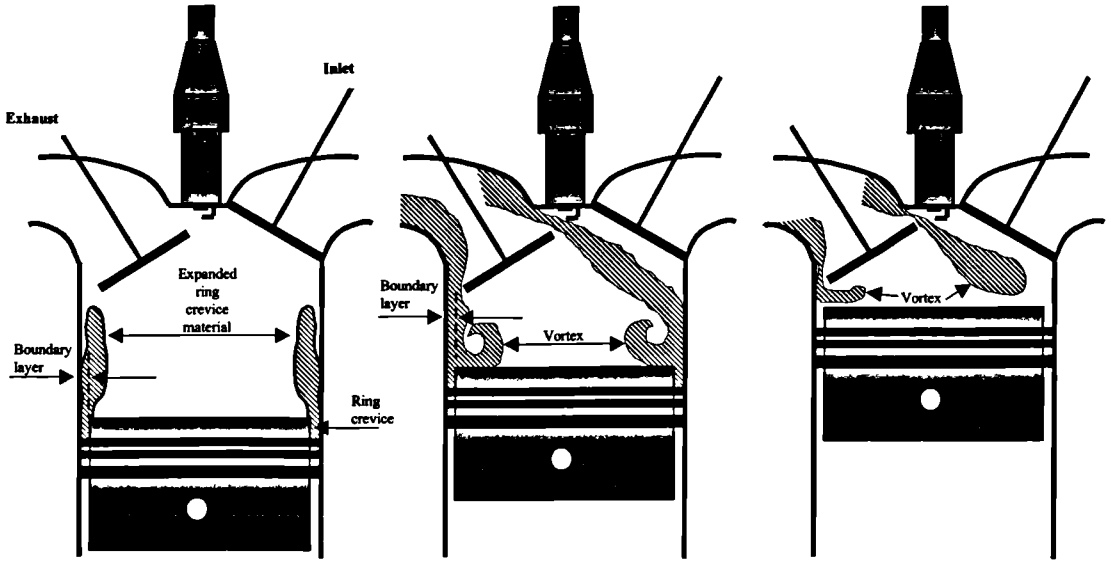

Figure 1.14
Schematic of transport mechanisms for unburned hydrocarbons out of the cylinder (adapted from Heywood (1988))

As the pressure falls during expansion, the crevice gas begins to expand with most of it being laid along the cylinder walls. A second flow, observed by Namazian and Heywood (1982), enters the cylinder as a turbulent jet. This is thought to be the gas contained between the top and second ring issuing through the top ring gap. Depending on in-cylinder conditions, part of this gas rich in hydrocarbons will become entrained in the bulk gas and be partially oxidised. The remainder of the gases laid along the wall, including any which have been desorbed from the oil film, are scrolled off as the piston rises during the exhaust stroke. Again some of this may be oxidised, but a large portion will leave unaffected.

Oxides of nitrogen

Oxides of nitrogen (NOx) are formed during combustion by the oxidation of nitrogen under the high temperature conditions in the cylinder. The major component is nitric oxide (NO) although there are much smaller amounts of nitrogen dioxide (NO_2).

According to Heywood (1988), NO forms in both the flame front and the post flame gases. However, as the flame front is extremely thin, residence time is extremely short, so it can be assumed that NO is formed behind the flame front. The rate of formation of NO increases exponentially with temperature (Figure 1.15). In particular the gases from the early stages of combustion, close to the spark plug, will continue to rise in temperature as the pressure rises. This early burning region therefore contributes significantly to NO production.

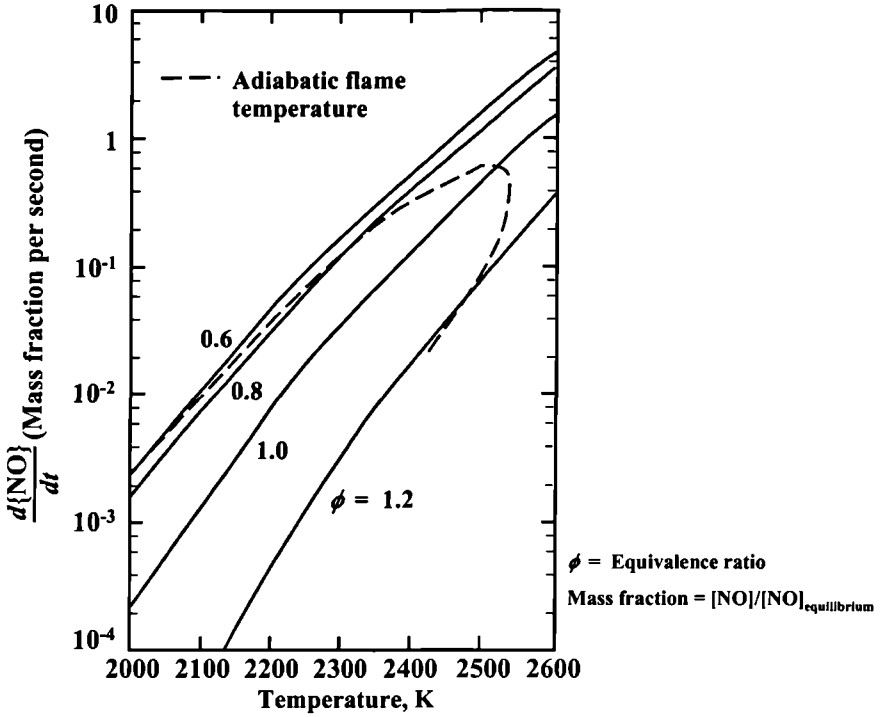

Figure 1.15
Variation in NO formation rate with temperature [Heywood (1988)]

The rate constants for the reverse reactions are lower than those for the forward ones. As the temperature falls, there is a higher quantity of NO than would be predicted under equilibrium conditions. The mechanisms for CO, hydrocarbons and NOx emissions are summarised in Figure 1.16.

Methods of Controlling Emissions

There are basically two strategies for controlling tailpipe emissions, namely strategies that limit their production by control of in-cylinder conditions and, secondly, after-treatment of the exhaust gases. These will be dealt with separately.

As mentioned earlier, CO production within the cylinder is effectively a function of air/fuel ratio. Thus, it is important to achieve an accurate control of the fuel-air mixture, which in turn requires an engine management system incorporating fuel injection to provide the necessary degree of control. Hydrocarbons, on the other hand, can be reduced by employing a number of techniques. Firstly it is important to minimise the major sources of HC emissions, i.e. the crevices. This can be achieved by using pistons with a very small top land, although this would always be limited by mechanical and thermal considerations. Use of lubricants which absorb less fuel is another obvious factor as well as improved methods of mixture preparation particularly during cold starts and warm-up. Another method is to promote the post-combustion oxidation reactions which take

place during the expansion stroke. These help oxidise part of the unburned hydrocarbons before they leave the cylinder. The primary factor affecting the extent of these reactions is the temperature of the cylinder contents during this period. Higher temperatures promote continued oxidation of the fuel. This can be achieved by delaying combustion slightly, for example by retarding the ignition timing.

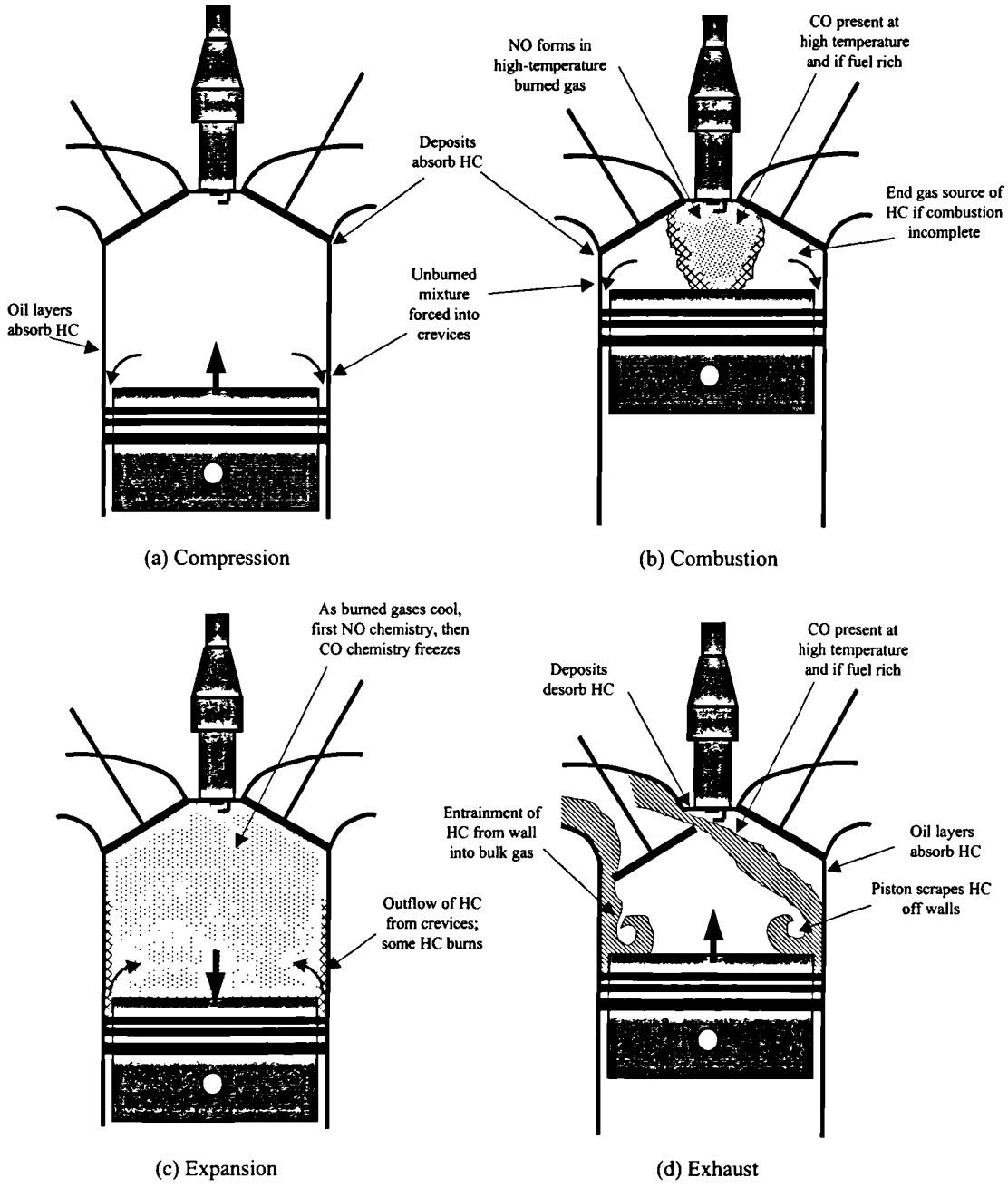

Figure 1.16
Summary of HC, CO, and NO pollutant formation mechanisms in an SI engine (adapted from Heywood (1988))

Since NOx formation is an exponential function of temperature, the obvious method of inhibiting its production is to reduce the peak temperatures during combustion. This can be accomplished

by adding a secondary gas to dilute the mixture. The gas acts as a heat sink serving to limit peak temperatures during combustion. It must be borne in mind that the Residual Gas Fraction (RGF) in the cylinder will also contribute to this effect. The diluting gas can either be air or re-circulated exhaust gas added just downstream of the throttle. EGR is used commonly as it can be used in conjunction with a three-way catalytic converter. The term external EGR can be applied to such a scheme since the exhaust gas is taken from the exhaust port and added to the intake port. Internal EGR, on the other hand, refers to a system designed to retain a controlled amount of the RGF inside the cylinder. The amount of EGR that a particular engine can tolerate is dependent on the combustion chamber type. Fast burn combustion chambers can tolerate a higher degree of EGR as they are less susceptible to cyclic variation under such conditions. In addition to reduced NOx emissions, EGR offers improvements in efficiency through a number of means. Heywood [1988] cites these as being, the reduction in pumping losses due to higher manifold pressures, less heat transfer to the walls due to the lower combustion temperatures, and a reduction in dissociation reactions in the high temperature gases which allows more of the fuel's energy to be released near to TDC.

After-treatment of exhaust gases (three-way catalyst)

After-treatment of the exhaust gases is the most important method currently available for achieving reductions in tail-pipe emissions. Treatment of the exhaust gases occurs in a catalytic converter, which oxidises CO and HC while simultaneously reducing NOx. Figure 1.17 shows the effect of air/fuel ratio on the conversion efficiency for each of the reactions.

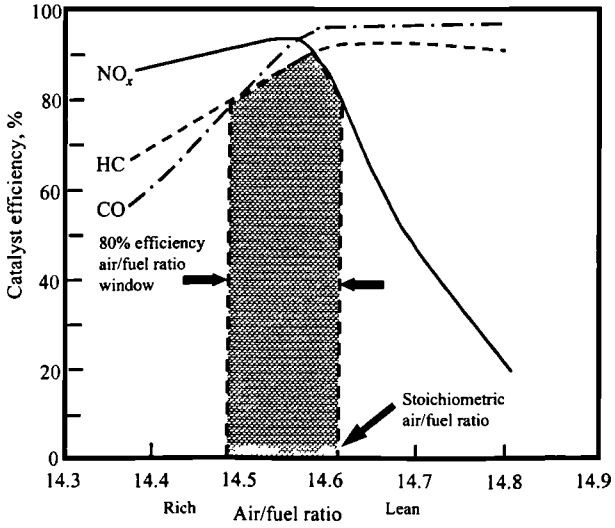

Figure 1.17
Variation in catalytic conversion efficiency with air/fuel ratio for a three-way catalyst [Heywood (1988)]

In order to achieve the degree of control necessary, engines equipped with such devices are normally operated under closed loop control. The oxygen content of the exhaust gas is continuously monitored by means of an exhaust gas oxygen sensor. The output being fed back to the engine management system which can vary the fuelling to the engine accordingly.

There are also disadvantages associated with the use of current catalyst technology. The first is the requirement to run under stoichiometric conditions. This rules out strategies such as lean burn that would be capable of significantly improving fuel consumption and hence reducing CO_2 emissions. The disadvantages of stoichiometric operation are somewhat lessened when EGR is used to help limit NOx emissions. Under these conditions the catalyst will effectively see exhaust gas corresponding to stoichiometric combustion. The second disadvantage is the need for the catalyst to reach minimum operating temperature, which can take up to one minute, although this time is being reduced very significantly by moving the catalyst closer to the engine.

HC emissions can be very high during the time taken for the catalyst to warm up. The inability of the catalyst to oxidise the HC emissions produced by the engine will be compounded by the fuel enrichment requirement during cold starts and warm-up, which themselves will lead to high hydrocarbon concentrations in the feed-gas to the catalyst. Various strategies have been suggested to help alleviate this problem, most of them attempting to reduce warm-up time by heating the catalyst using alternative means. These include electrically powered heaters, although the power requirements seem prohibitively high, and use of exhaust gas ignition, which can be achieved by adding either air alone or a combination of air and fuel to the exhaust gas prior to entering the catalyst.

Legislation to Control Exhaust Emissions from Automotive Vehicles

The motivation behind much of the current research into IC engines has been the need for manufacturers to meet emissions legislation. It became apparent that, over recent decades, emissions from vehicles have been the primary factor in the deterioration of urban air quality. Legislation in this area, first enforced in Los Angeles in the mid-1960s and relatively scant in nature, has become more detailed with future proposals setting very stringent limits on the main pollutants.

To ensure consistency, there must be some form of pre-defined test that is applied to the vehicle. The contents of such tests vary between countries to reflect the local driving patterns consequently changing the emphasis placed on the different pollutants exhausted to the environment.

Figure 1.18 shows the combined ECE 15 (urban) and EUDC 15 (suburban) test cycle applicable to all new cars sold in the European Community from the beginning of 1993 [Anon (1994)]. Collection of exhaust gases begins 40 seconds after the start of the test, with test and soak temperatures set at 20 °C and 30 °C respectively. The analysis is carried out on a chassis dynamometer without interruption. Table 1-1 shows the limits on average tail-pipe emissions applicable to the test.

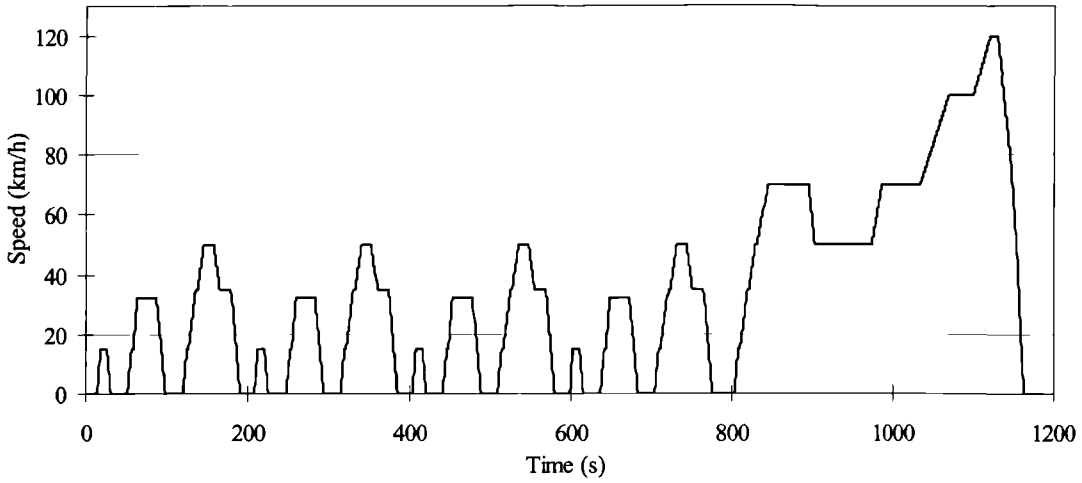

Figure 1.18
The ECE/EUDC test cycle applicable from 1993 in Europe
[Anon. (1994)]

Petrol engined vehicles	1993 (Euro I)	1997 (Euro II)
CO (g/km)	2.72	2.2
HC + NOx (g/km)	0.97	0.5

Table 1-1
Limits on emissions from gasoline engines [Anon. (1994)]

These limits are to be lowered from 1 January 1997 (i.e. 1996 Model Year (MY) onwards) to the values indicated in Table 1-1. Table 1-2 shows the values proposed for the years 2000 and 2005 [Daniels (1996)]. Additional revisions may include a reduced soak temperature of 7 °C, an additional cold start at –7 °C, sampling commencing from cranking, increased durability of emissions equipment, the requirement for on-board diagnostic equipment, and the inclusion of further pollutant categories [Anon (1994), Daniels (1996)]. The last of these may be taken to include hydrogen sulphide, which is known to reduce catalyst efficiency, formaldehyde, and Volatile Organic Compounds (VOC), the best known being benzene. Some VOCs are thought to be carcinogenic.

Petrol engined vehicles	EC2000 (Euro III)	EC2005 (Euro IV)
CO (g/km)	2.3	1.0
HC (g/km)	0.2	0.1
NOx (g/km)	0.15	0.08

Table 1-2
Proposals for future limits on pollutants in Europe
[Daniels (1996)]

The limits applicable in the US are based on the Federal Test Procedure (FTP 75) driving cycle and are shown in Table 1-3 together with the proposals for California. Non-Methane Hydrocarbons (NMHC) are becoming more important (Non-Methane Organic Gases (NMOG)) in California) as it has been suggested that methane evaporates to the upper atmosphere too quickly to have an adverse effect on local air quality [Daniels (1996)]. The legislation in California also limits formaldehyde (HCHO) emissions from methanol-fuelled vehicles.

All values in g/mile	NMHC/ NMOG	CO	NOx	HCHO (Formaldehyde)
Pre-control (1966)	10.6	84	4.1	
Federal				
Tier I (1994)	0.25	3.4	0.4	
Tier II (2003)	0.125	1.7	0.2	
California				
Conventional Vehicles (1993)	0.25	3.4	0.4	
TLEVs (1994)	0.125	3.4	0.4	0.015
LEVs (1997)	0.04	1.7	0.2	0.015
Ultra LEVs (1997)	0.04	1.7	0.2	0.008

Table 1-3
Pollutant limits for California and US
[Daniels (1996)]

Some reporters have suggested that the proposed limits for Europe will be at least as strict as the Californian ULEV standards [Daniels (1996) and Haddad *et al.* (1995)]. Indeed, as reported by Daniels (1996), there is a general feeling that such controls represent the technical limits of what is possible using current technology. He also points out that the benefits of reductions in NOx emissions beyond these levels may start to diminish while costs increase sharply.

1.2.6. Lean Burn and Stratified Charge Engines.

One of the best methods of reducing the levels of harmful emissions (including CO_2) is by use of a mixture leaner than stoichiometric. Such an engine would offer benefits in fuel economy as load can be controlled by changes in AFR, leading to a reduction in pumping losses, as well as lower emissions (particularly NOx) as shown in Figure 1.19. Further benefits, which at first may not be apparent, are the increase in cycle efficiencies brought about by the possibility to use higher compression ratios and the higher ratio of specific heats for leaner mixtures.

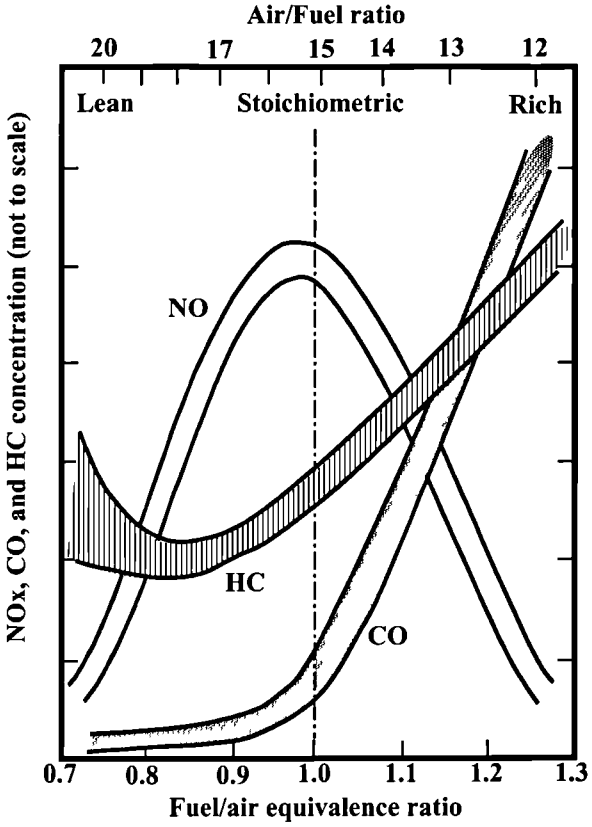

Figure 1.19
Variation in pollutant concentration with air/fuel ratio
[Heywood (1988)]

If the benefits of lean operation are to be fully utilised, a compact combustion chamber allied with a sufficient degree of in-cylinder motion is necessary to prevent an excessive deterioration in combustion. Such a system is described by Horie *et al.* (1992) who use valve deactivation to achieve the required degree of axial swirl. The method of achieving axial swirl and the shape of the combustion chamber are shown in Figure 1.20. The authors reported an improvement in fuel consumption of 8% at low speed and load, and 12% in the highway mode of the Federal Test Procedure.

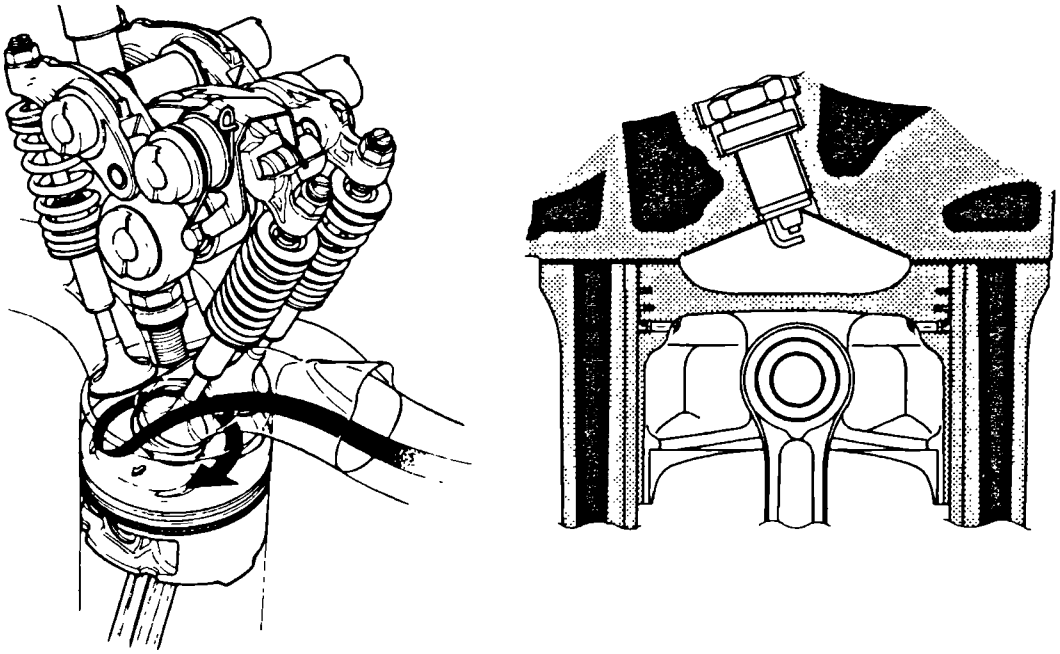

Figure 1.20
Honda VTEC-E combustion system [Horie *et al.* (1992)]

The main obstacle to the adoption of lean burn technology has been the absence of a NOx reduction catalyst capable of operating under the oxygen-rich exhaust conditions [Stokes *et al.* (1994)]. Stokes *et al.* (1994) compare possible combustion strategies for improved emissions and fuel economy performance. A graphical representation of their comparison is shown in Figure 1.21. From their review of current technology, the authors concluded that, in the absence of a lean catalyst, a system capable of operating under extended levels of EGR offers the most promising approach. In particular they suggested that an effective method of producing such a system would be to stratify the charge.

Charge stratification operates on the principle of retaining a combustible mixture in the vicinity of the spark plug and having a weaker mixture, or possibly exhaust gas elsewhere. The key to such a system is an ordered in-cylinder bulk motion combined with a well-targeted and efficient fuel injection system. The in-cylinder motion may be either axial swirl or tumble or a combination of the two. It can be argued that systems using deactivation of ports optimised for tumble are actually employing such a combination of the two flow regimes. The fuel injection system needs to be capable of varying the timing of injection and providing a high flow rate. The latter allows the fuel 'packet' to be accurately placed within the cylinder, which could be achieved by either using port or Direct Injection (DI).

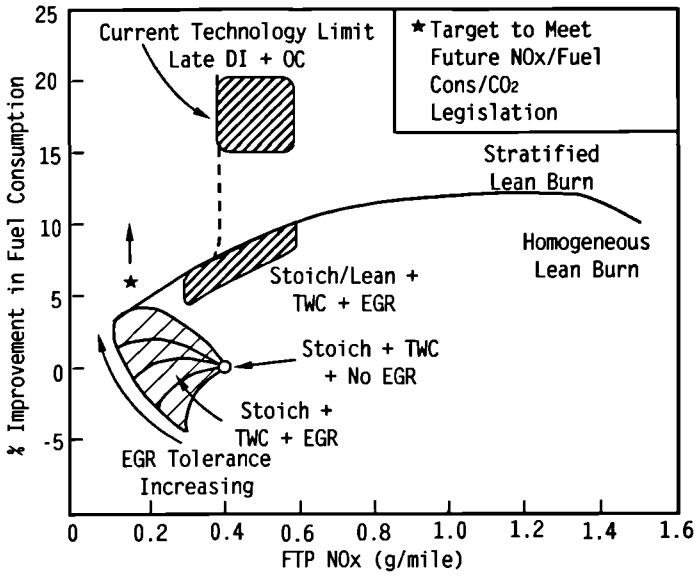

Figure 1.21
Comparison of possible combustion strategies for improved emissions and fuel economy performance [Stokes *et al.* (1994)]

An example of a stratified charge system is described by Stokes *et al.* (1994) (originally presented by Kiyota *et al.* (1992)), employing barrel stratification and using air as the diluent (Figure 1.22). The system is claimed to be capable of operating at air/fuel ratios of up to 30:1. The main disadvantages are the off-centre location of the spark plug and a loss in performance. In general it seems that axial swirl should be the preferred motion as it does not break down in the way tumble is likely to. Additionally, it is difficult to keep the two streams in a tumbling system from mixing.

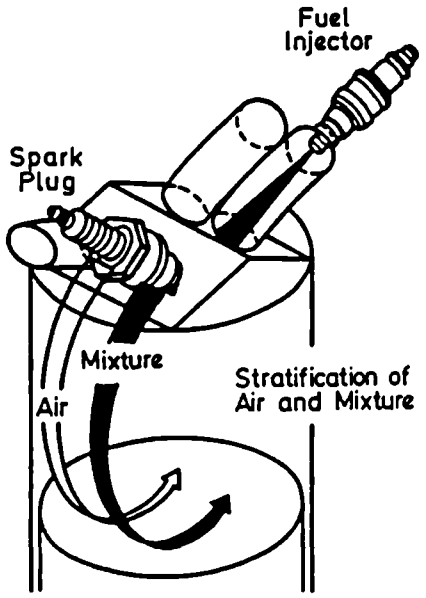

Figure 1.22
Stratified charge using barrel stratification [Stokes *et al.* (1994)]

DI systems are handicapped by their lack of development, and the increased complexity and cost of the high-pressure fuel system. Nevertheless, Mitsubishi are planning to launch a DI based stratified charge engine on the Japanese market in 1996 *(and have done so during the duration of this project [Ando (1996)])*. The engine uses a reverse tumbling flow set up by vertical (in line with the cylinder axis), as opposed to horizontal, intake ports.

1.3. A Review of Variable Valve Actuation

It is apparent that there are a number of possible schemes capable of helping reduce harmful emissions while retaining or enhancing the performance of an SI engine. In the absence of a catalyst capable of operating under lean conditions, it seems probable that the use of a three-way catalyst combined with EGR will form the basis of any such scheme. The problems with such strategies, particularly the tolerance of a combustion system to high levels of charge dilution and limiting engine-out hydrocarbons, may be addressed by adopting techniques that help reduce many of the compromises inherent in current designs. One area showing particular promise is that of Variable Valve Actuation (VVA). This section aims to look at valve timing requirements and the possibilities to influence engine operation by adopting some form of VVA.

1.3.1. How Individual Valve Events Affect Engine Operation

There are two distinct gaseous exchange processes required in a 4-stroke cycle, namely the induction and exhaust strokes. These are normally controlled by poppet valves located in the cylinder head. The valves are operated by either one or two camshafts which may be driven by a belt, chain or gears from the crankshaft. Due to the nature of this arrangement, the timing for the opening and closing of the valves and their lift is normally fixed at some value arrived upon by consideration of the engine's requirements over its full operating range.

In an ideal cycle the induction stroke would begin with the inlet valve opening at TDC and end at BDC in preparation for compression of the fresh charge. Similarly, the exhaust stroke would begin and end at BDC and TDC respectively. This type of operation is only suitable for very low engine speeds and is never used in practice, mainly due to the fact that full-load performance becomes severely reduced at all speeds. The indicated power of an internal combustion engine at a given speed is proportional to the mass flow rate of air. Thus inducting the maximum air mass at WOT, and retaining that mass within the cylinder, is one of the primary aims of the gas exchange process [Heywood (1988)]. For this reason the actual valve opening and closing characteristics become a compromise between idle stability, low speed torque and WOT power. Figure 1.23 shows the timing diagram for a typical SI engine.

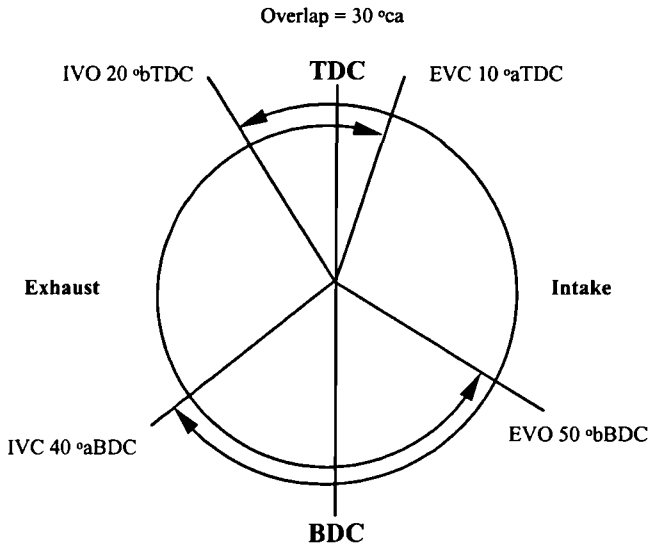

Figure 1.23
Valve timing diagram for an SI engine

The exhaust valve normally opens before BDC on the expansion stroke in order to ensure a good blowdown of the cylinder contents to reduce pumping work especially at higher speeds. The penalty is a loss in expansion work that could have been extracted had the valve remained shut. This loss can be demonstrated with reference to the pressure-volume diagram shown in Figure 1.24.

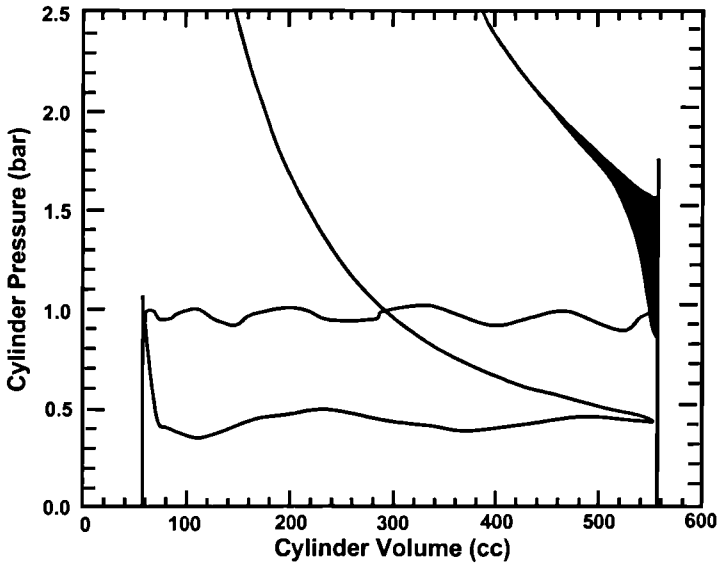

Figure 1.24
Pressure-volume diagram for gas exchange processes
(adapted from Leone *et al.* (1996))

The shaded area represents additional work that could have been extracted from the combustion gases had the expansion been allowed to continue to the bottom of the piston stroke. The early opening of the exhaust valve may also have a bearing on emissions, in particular levels of

unburned hydrocarbons. By allowing further time for post-combustion reactions to take place, particularly at low speeds and light loads when combustion is slowest, the amount of unburned hydrocarbons released into the exhaust can be reduced. Conditions during the later stages of the expansion stroke are especially important if crevice effects are significant since post-combustion oxidation is the only mechanism available within the cylinder.

The inlet valve is opened before TDC to ensure it has attained sufficient lift by the time the piston begins its downward motion, thus maximising volumetric efficiency at high speeds. Consequently, there is an overlap period when both the exhaust and inlet valves are open. When the engine is running at its design point, tuning effects in the exhaust ensure that there is very little, if any flow into the intake port. However, this is not the case under low load and speed conditions. The overlap allows a flow of exhaust gas back into the cylinder and consequently into the intake port which is invariably at a lower pressure. The exhaust residuals, although desirable for emissions control under certain operating conditions, will rarely be at an optimum level. Indeed at idle, where there is a need to reduce the levels of RGF, the situation is worst as this corresponds to the lowest pressure in the intake manifold whilst providing the longest time for the backflow process to occur. Figure 1.25 shows the influence of valve overlap on full load and idle operation.

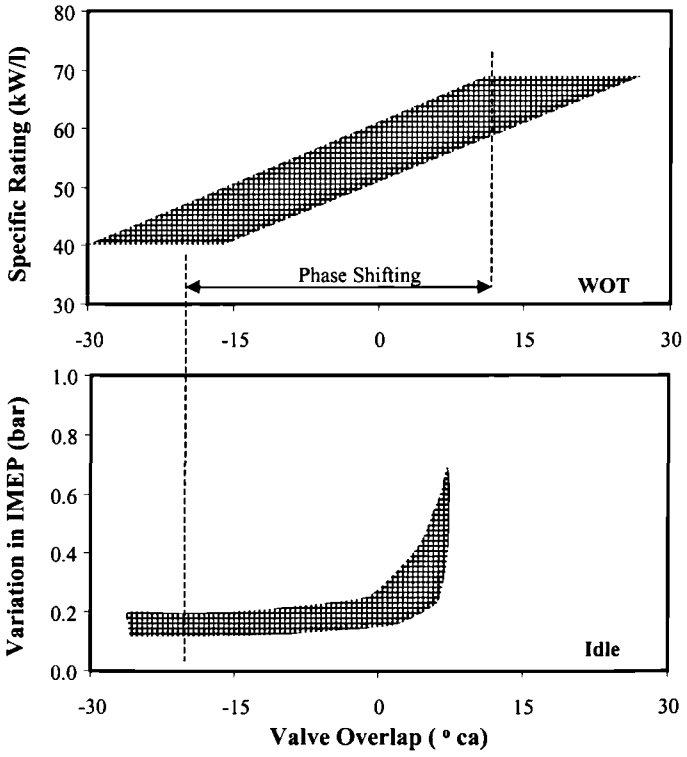

Figure 1.25
Influence of valve overlap on full-load and idle operation of 4-valve engines (adapted from Endres *et al.* (1990))

EVC normally occurs after TDC to take advantage of exhaust tuning effects at higher speeds. At lower speeds, however, exhaust gas is drawn back into the cylinder. The combined timing of IVO and EVC together affects the phasing and duration of the overlap period relative to TDC. The timing of EVC will have a bearing on emissions of unburned hydrocarbons as the HC rich 'tail' of the exhaust gases can be reingested in the backflow.

The inlet valve is closed some time after BDC to increase volumetric efficiency at higher speeds, again due to aftercharging affects. However, at lower speeds, maximum torque is compromised since a part of the fresh charge is effectively pushed back into the intake port as the piston has already commenced its compression stroke. The effective compression ratio will also be lowered as a consequence and this may become very significant if inlet camshaft phasing is used.

1.3.2. The Move to Multi-Valve Engines

In recent years there has been a trend towards multi-valve (more than two valves per cylinder) engines. Historically this technology was limited to high performance engines, but it has now become advantageous to incorporate it into mid-range cars to meet emissions targets. The primary benefit of such engines is the improvement in volumetric efficiency, typically 15% higher than their 2-valve counterparts, and is mainly due to their larger flow cross sections [Endres *et al.* (1990)]. Figure 1.26 shows the results from a comparison between twelve 2-valve engines and ten 4-valve engines.

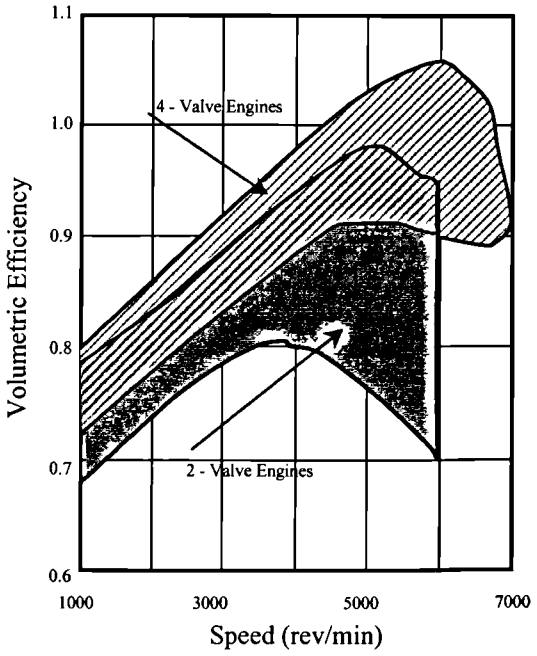

Figure 1.26
Volumetric efficiencies of 2 and 4-valve engines (adapted from Endres *et al.* (1990))

The gains in volumetric efficiency can be achieved with the added benefit that 4-valve engines naturally induce tumble, thus enhancing mixture preparation in the cylinder and speeding up the combustion process itself. The main disadvantages of 4-valve engines are found under low load conditions. The relatively low airflows under these conditions means that both flow velocities and turbulence intensity can be very low, leading to problems with output and idle stability as compared with 2-valve designs.

1.3.3. Potential for Variable Valve Actuation

Variable Valve Actuation offers the potential to alleviate some or all of the drawbacks associated with the conventional valve trains discussed so far. By effectively varying the valves' opening and closing characteristics, it should be possible in theory to achieve the optimum running condition for the engine under any load or speed. This optimum can be defined in terms of performance, emissions or fuel economy, although in practice these goals may be disparate under certain conditions. Figure 1.27 shows the possibilities to influence engine characteristics by means of VVA.

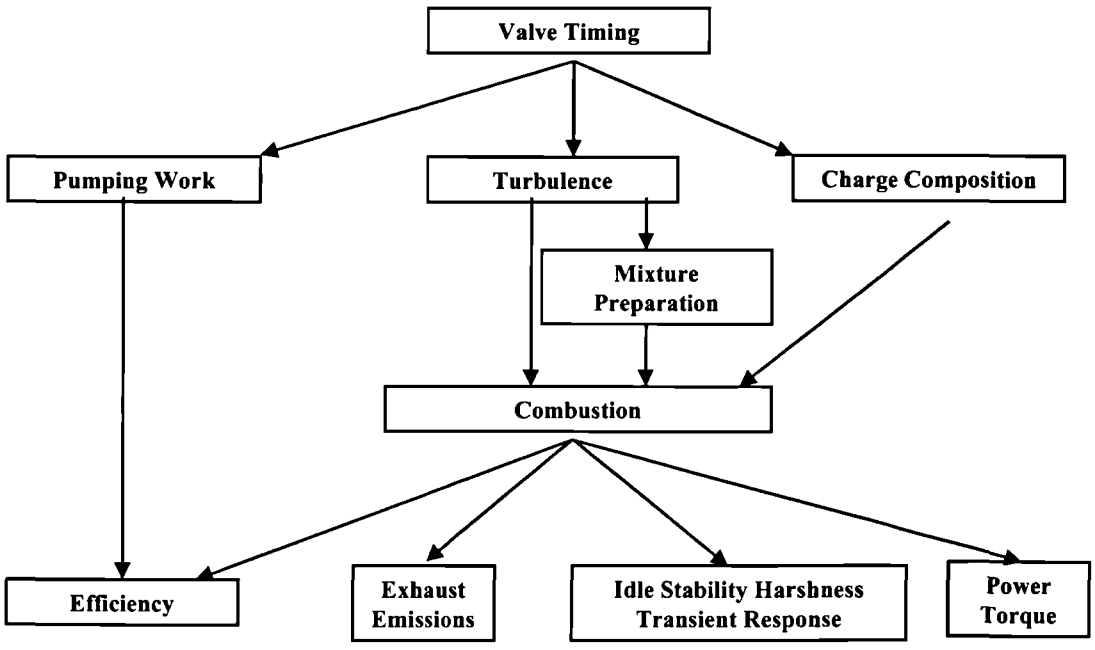

Figure 1.27
Possibilities to influence engine characteristics by means of VVA (adapted from Kreuter *et al.* (1992))

Each of the categories shown in Figure 1.27 will be discussed separately before being brought together to form a coherent strategy for the use of VVA.

Reduction of pumping losses and elimination of the throttle by means of VVA.

The conventional method of controlling engine output is by means of a throttle which drops the pressure in the manifold thus controlling the mass of charge induced. The engine therefore has to do work by taking in gas at a low pressure and exhausting it at atmospheric pressure.

For an engine running at a constant speed, the mechanical losses remain practically constant with varying load. Under low loads however, the portion of the indicated power converted to shaft work falls as the pumping losses increase [Tuttle (1980)] (Figure 1.28). The pumping loss is most significant at idle and low loads, and can account for up to 50% of the indicated power under these conditions [Tuttle (1982)].

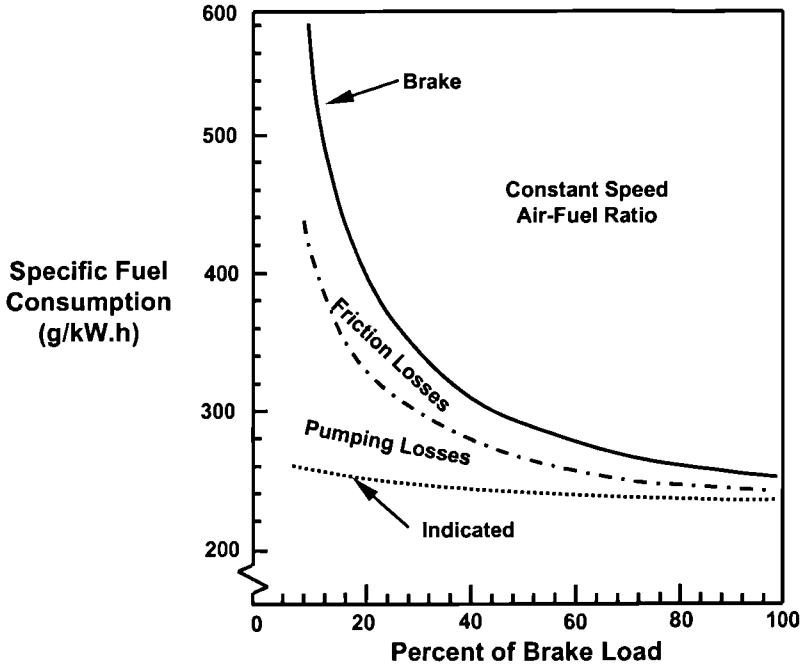

Figure 1.28
Fuel consumption characteristics for an engine with varying load at constant speed (adapted from Tuttle (1980))

It is possible to control engine load by methods based on varying the characteristics of the intake valve events. These are:

- early closing of the intake valve (EIVC)
- late closing of the intake valve (LIVC)
- limiting the lift of the intake valve, effectively using it to take over the throttling process.

The principles of EIVC and LIVC are very similar, namely to control the amount of fresh charge within the cylinder by closing the valve at a point when the cylinder volume is less than the maximum. Ideally, both EIVC and LIVC would allow the pressure in the manifold to remain at

or near atmospheric. In the case of EIVC, the inlet valve is opened as normal, but is closed partway through the induction stroke. The timing of IVC can be varied to induce the required amount of fresh charge at atmospheric pressure. Figure 1.29 compares the difference in pressure-volume characteristics for an EIVC load-controlled, a LIVC load-controlled and a conventional throttle-controlled engine.

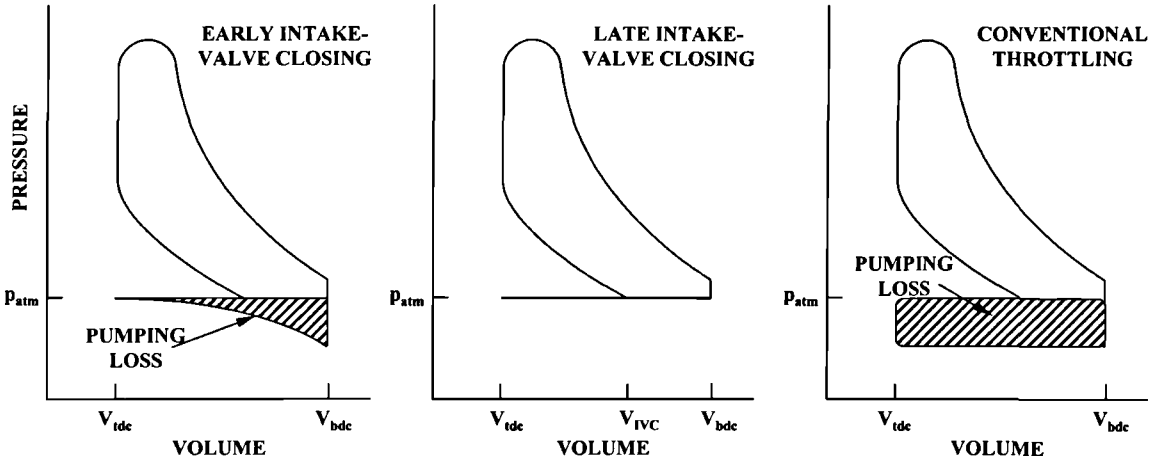

Figure 1.29
Pressure-volume diagrams for an EIVC load-controlled, a LIVC load-controlled and a throttle-controlled engine (adapted from Tuttle (1982))

For EIVC, the fresh charge undergoes an expansion before being compressed. This process serves to alter the condition of the charge by reducing the overall temperatures during the cycle as well as reducing the effective compression ratio. EIVC can also be expected to have an effect on the emissions characteristics, the combustion efficiency and the knock performance of the engine. The lower temperatures will help to bring down NOx levels, although there is some evidence to suggest that this may be reduced in part due to the lower levels of residuals within the cylinder. The lower levels are due to the fact that the intake manifold will be at a higher pressure and consequently the amount of backflow, both from the exhaust into the cylinder and into the intake port, is reduced. The lower effective compression ratio can provide benefits in the knock performance of the engine, although the thermal efficiency of the engine will be reduced. The lower overall temperatures also help the reduction in knock tendency. The increased time between IVC and the start of combustion means that the intensity of any in-cylinder motion may be severely reduced leading to poorer combustion. The lower temperatures will also serve to increase the combustion duration. Urata *et al.* (1993) identified three factors that adversely affect combustion stability, particularly at idle: the cooling of the flame kernel due to lower temperatures, a lower flame propagation speed which was additionally affected by weak in-cylinder motion, and the presence of non-uniform residual gas due to lower backflow levels. In addition, the depression in the manifold, which serves as a useful aid in fuel vaporisation, is

absent and this may be expected to harm the mixture preparation quality of an engine. Kreuter *et al.* (1992) suggests that this problem would have to be compensated by use of increased mixture temperatures, improved atomisation and increased gas velocities during intake.

Figure 1.30 compares the charge exchange losses in terms of IMEP for an engine equipped with a conventional throttle and for one using an EIVC system.

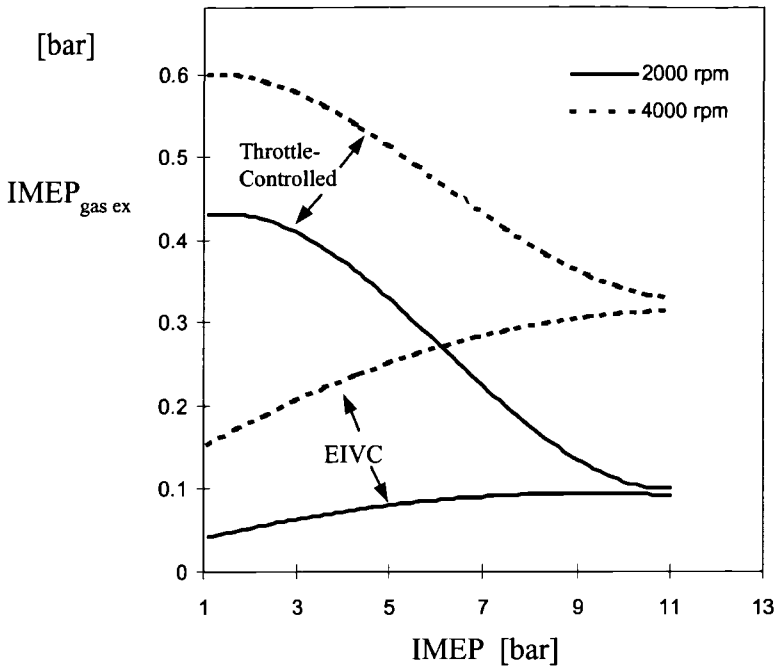

Figure 1.30
Charge exchange losses for EIVC and throttle-controlled engines (adapted from Kreuter *et al.* (1992))

At higher loads and speeds, the difference between the two becomes progressively smaller until at WOT there is no difference, as expected. It must be borne in mind that use of EIVC does not completely eliminate the pumping losses. These remain to some extent because the valve will still have a throttling effect during the opening and closing phases. This is particularly so when the valve is required to close at maximum piston velocity. Urata *et al.* (1993) indicate that the pumping loss reduction may be as high as 80% at low speeds, but falls to only 40% in the medium speed range.

Finally the mechanical challenges of EIVC must also be recognised. Tuttle (1982) recommends that, to be effective, an engine equipped with an EIVC mechanism will require the intake valve duration to be varied by up to 200 crank angle degrees, which is well beyond the capabilities of existing phase shifting mechanisms. It also seems likely that the maximum lift would also need to be varied to avoid excessive valve acceleration for short duration events.

Much of the discussion applicable to EIVC is also relevent to LIVC. However, there are additional issues that need to be addressed. First, the LIVC strategy will inherently suffer from higher flow losses in comparison with EIVC as part of the fresh charge is first inducted and then expelled back into the intake port. Secondly, LIVC at very light loads may require the inlet valve to close after the spark timing [Ma (1988)]. This problem was investigated by Ma (1988) using a harmonic drive mechanism to control the two inlet valves separately, allowing the use of a phase shifting mechanism to close the second valve later in the cycle. The study showed that regulation down to 40% of full load could be achieved without throttling by applying a phase shift of 90°. Beyond this angle, a throttle would be needed if the valve closing time was not to encroach on the spark timing.

There is still a benefit to be gained from LIVC because the amount of throttling required would be less than that in a conventional engine. In fact the degree of throttling required might be less than expected due to the increase in intake charge temperature from the backflow of cylinder gases at the end of the intake stroke. Tuttle (1980) measured the intake charge temperature 15 mm from the intake valve and found that the temperature increased from 55 °C to 103 °C for an increased duration of 96° (Figure 1.31). This temperature rise corresponded to a 13% decrease in intake charge density. In addition, it is reasonable to assume that the increase in intake charge temperature may also have a beneficial effect on mixture preparation, although this aspect was not discussed.

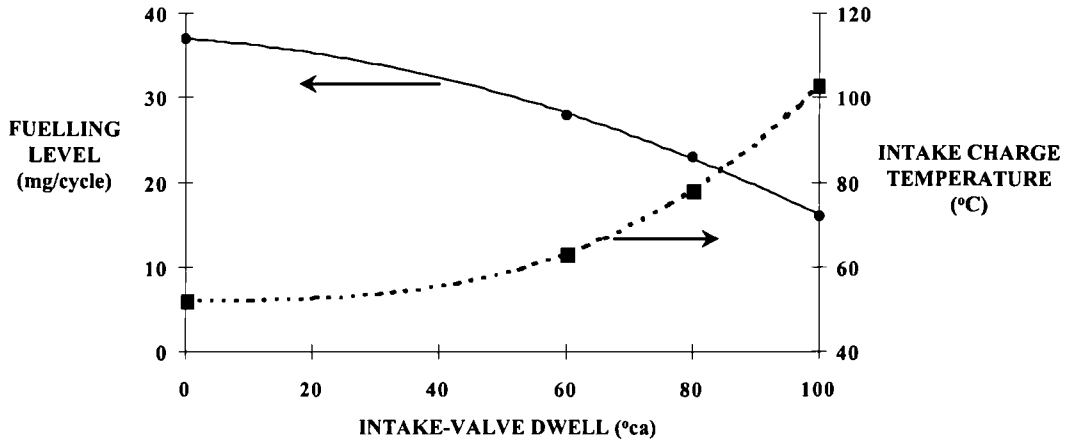

Figure 1.31
Variation of fuelling level and intake charge temperature with intake valve dwell (adapted from Tuttle (1980))

The final method of using the inlet valve to throttle the incoming charge offers the potential for improved mixture preparation although it does not necessarily reduce the pumping losses. Shock waves set up by the sonic conditions at the throat of the valve can be used break up the fuel

droplets entering the cylinder. Stivender (1968) proposed intake valve throttling as a means to enhance in cylinder motion producing turbulent eddies of small length scale. Analysis of cylinder pressure data during combustion indicated a significant increase in the burn rate. It is arguable that it would be preferable to induce a larger scale bulk motion which would persist longer as opposed to these smaller eddies which dissipate their energy very quickly. Stivender found that this increased level of turbulence, if retained under higher part load conditions, was found to give higher levels of harshness. The mechanical problems of intake valve throttling as yet would preclude it as a viable option since it would require very small valve events, which would cause problems in achieving a consistent air distribution between cylinders.

Promotion, uses and control of in-cylinder motion

Suitable in-cylinder motion primarily offers a significant improvement in the rate of combustion with its attendant benefits. VVA can be used to control in-cylinder motion by allowing a greater degree of control over the bulk flow characteristics of the airflow entering the cylinder. In particular, it can allow control over the intensity of the motion by varying the flow velocity. The use of asymmetric valve strategies (opening and closing the inlet valves independently) additionally allows selection of the type of in cylinder motion [Johansson and Soderberg (1996), Wilson *et al.* (1993), Horie *et al.* (1992)].

The use of VVA to increase the intensity of in-cylinder motion is particularly attractive under part load operation. Higher inlet air velocities serve to increase the momentum of the charge entering the cylinder. This can be achieved by limiting the lift of the intake valves, disabling one valve or a combination of both. The subsequent loss of flow coefficient is not a problem at part load as this necessitates a lower pressure drop across the throttle, leading to no change in the pumping work [Stone *et al.* (1993)].

It is generally accepted that engines designed for tumbling air motion regimes can be modified to promote axial swirl by some form of inlet valve or port deactivation system. Port deactivation has been the preferred option due to its relative simplicity. However, Honda have succeeded in producing a production engine capable of inducing axial swirl at low speeds by use of their VTEC mechanism [Horie *et al.* (1992)]. Systems such as these operate by allowing the flow to enter the cylinder tangentially thus promoting axial swirl.

Wilson *et al.* (1993) carried out a study to characterise the type of in-cylinder motion produced by asymmetric strategies and correlated it with engine test data. They used a steady-flow rig in conjunction with swirl meters to measure tumble and axial swirl, and demonstrated how it was

possible to map the tumble, swirl and flow characteristics of a given head and valve strategy. Their steady-flow results are summarised in Figure 1.32 and indicate that the intensity of the in-cylinder motion can be raised by an asymmetric valve strategy in regions where the low flow velocities encountered using a symmetric strategy would prevent the build-up of a strong bulk flow. Asymmetry introduces an axial swirling motion whilst also retaining a tumbling characteristic, in effect, rotating the axis of the motion of the charge within the cylinder. The degree to which each of these flow regimes exist is debatable. A series of steady-flow tests conducted by Baker and Nightingale (1996) indicated that tumble was almost doubled when one valve was deactivated, although no measurements of axial swirl were made. Stone *et al.* (1993) found that for a 4-valve per cylinder engine, valve disablement actually increased the level of tumble whilst additionally generating axial swirl. In a study by Johansson and Soderberg (1996) applying Laser Doppler Velocimetry (LDV) to an optically-accessed combustion chamber, deactivation of one valve led to the presence of swirl although the existence of tumble was not commented upon. Thus, it would seem that tumble is still the dominant motion with axial swirl serving to modify it. This conclusion is borne out to some extent in the steady-flow data presented by Wilson *et al.* (1993) which shows significant peaks in the tumble characteristics in the asymmetric region of operation (Figure 1.32). In their case the steady flow data was used to select seven different strategies to be investigated on a running engine (Table 1-4).

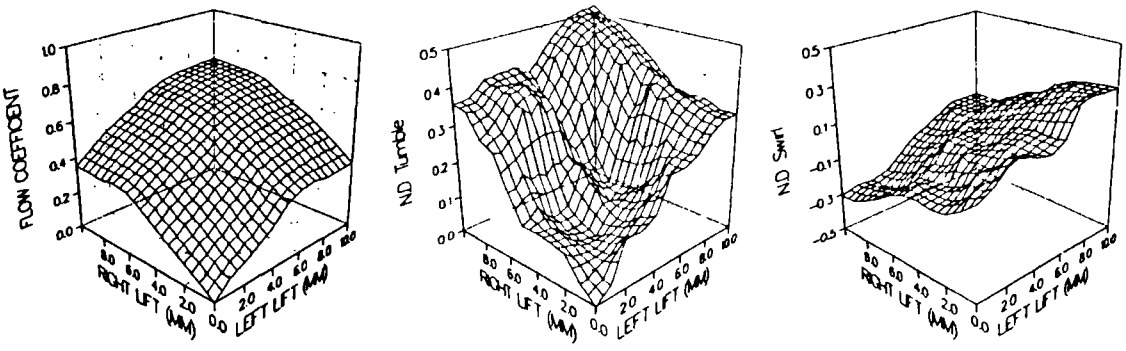

Figure 1.32
The effect of different valve lift combinations on flow coefficient, tumble and axial swirl [Wilson *et al.* (1993)]

The effect of in-cylinder motion was studied through the use of heat release models to estimate ignition delay and burn duration combined with measurements of idle stability. It was found that the most significant factor influencing these parameters was still the mean gas velocity, implying that the intensity of the motion was more important than its type. Axial swirl showed a good correlation with reductions in ignition delay, whilst tumble was found to reduce both the delay and duration of the combustion. Stone *et al.* (1993) found that valve disablement gave on average a 23% shorter ignition delay and burn duration. This reduction was attributed to the

presence of axial swirl. No correlation with tumble was made, even though the intensity of the tumble was found to be nearly twice that for the standard valve configuration.

Strategy	Left Inlet Valve				Right Inlet Valve			
	Lift (mm)	Duration	IVO (bTDC)	IVC (aTDC)	Lift (mm)	Duration	IVO (bTDC)	IVC (aTDC)
I	8.5	235°	10°	45°	8.5	235°	10°	45°
II	8.5	235°	10°	45°	4.4	205°	-20°	45°
III	8.5	235°	10°	45°	4.4	205°	10°	15°
IV	8.5	235°	10°	45°	4.4	205°	5°	30°
V	8.5	235°	10°	45°	0.0	0°	0°	0°
VI	8.5	235°	10°	45°	2.0	135°	-40°	-5°
VII	8.5	235°	10°	45°	2.0	135°	-90°	45°

Table 1-4
Asymmetric valve strategies investigated by Wilson *et al.* (1993)

Johansson and Soderberg (1996) reported that delaying the opening of the single active valve by up to 43° gave very significant improvements in both ignition delay and burn duration. The improvement is not stated quantitatively although their graphs suggest that both are reduced by at least 60%. This dramatic improvement was achieved by the very intense motion caused by the large pressure difference across the valve when it is opened. The improvements in turbulence are shown in Figure 1.33, which also shows the effect of such a strategy on the pumping work. In particular, the authors pointed out that any pumping increase in the cycle was compensated for by a decrease later in the induction stroke. The authors also found that leaner AFRs affected combustion delay and duration to a lesser extent when using valve deactivation.

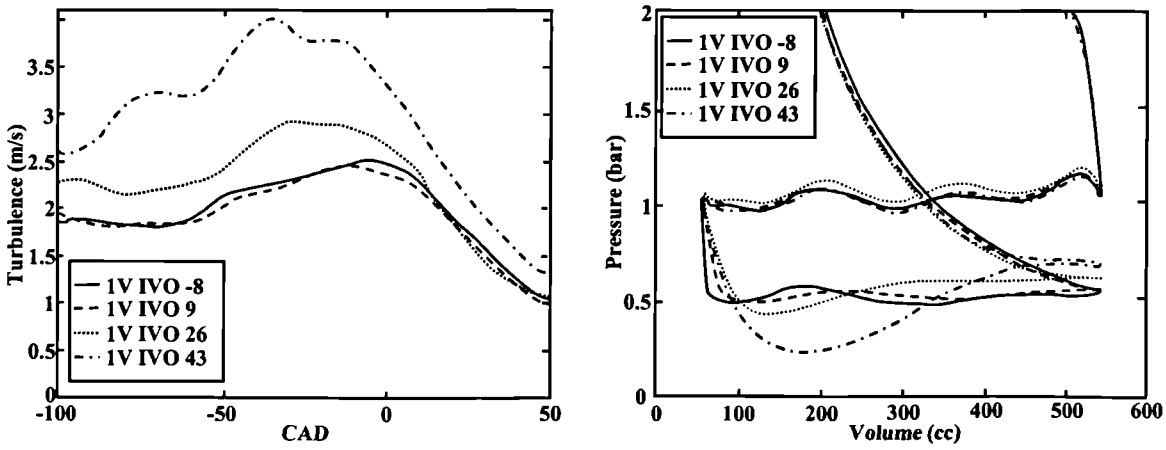

Figure 1.33
Effect of late inlet valve opening on in-cylinder turbulence and pumping work with valve deactivation [Johansson and Soderberg (1996)]

Idle and low load stability is also improved by valve deactivation. Wilson *et al.* (1993) reported that idle stability was improved for all the asymmetric strategies they investigated with the best case being complete valve deactivation. Johansson and Soderberg (1996) and Stone *et al.* (1993) have all found significant idle stability benefits from deactivation. The improvement stems from a combination of three factors. The first is the reduction in effective overlap brought about by an asymmetric strategy tending to reduce the levels of exhaust residuals flowing back into the intake port and hence giving a lower trapped RGF. The second effect is due to the improvement in the 0-10% Mass Fraction Burned (MFB) brought about by the enhanced in-cylinder motion. The shorter delay results in less time being available for the flame kernel to be moved around during the initial stages of combustion. Finally the introduction of axial swirl will tend to stabilise the flame in its early stages [Stone *et al.* (1993)].

Using VVA to control cylinder charge composition.

The cylinder charge in a running engine consists of two parts: the fresh air/fuel mixture drawn through the intake system and a certain amount of exhaust gas. The presence of exhaust gas in the cylinder will be due to the backflow process, and additionally due to any external EGR system employed. Using VVA gives greater control over the RGF eliminating the need for any external EGR system. This is an important consideration as it increases EGR tolerance during transients allowing the engine to be operated closer to its steady-state EGR tolerance level [Leone *et al.* (1996)].

The optimum amount of RGF required varies depending on the engine running conditions. At idle it is important to minimise the level of RGF to maintain stability. Greater stability can also allow a lower idle speed to be set giving subsequent benefits in fuel consumption. The amount of RGF at part load can be raised to minimise NOx emissions. At higher loads, the amount of RGF tolerable is dependent on the knock performance of the engine since the higher gas temperatures will be more likely to induce knock.

The amount of exhaust gas retained within the cylinder is primarily a function of the valve overlap period, its phasing and the pressures in the cylinder and the intake and exhaust ports. Appropriate control of the inlet and exhaust valves will influence some or all of these parameters. VVA can be used to directly vary the overlap duration but can be additionally employed to alter the phasing relative to the piston motion. This effect, although secondary, can become significant when the camshaft phase variation becomes large. By delaying the overlap period into the induction stroke, it is possible to use the piston's downward motion to draw in additional exhaust gas from the exhaust port using the motion of the piston. The amount of

exhaust gas retained will have a bearing on the manifold pressure required to induce the fresh charge for a given engine output. A greater degree of internal EGR necessitates a higher manifold pressure allowing a reduction in pumping losses.

VVA can also be beneficial in reducing emissions of unburned hydrocarbons. Figure 1.34 shows the time resolved hydrocarbon history of the exhaust gases near an exhaust valve for part of one cycle of a typical 4-valve per cylinder SI engine. It can be clearly seen that the 'tail' end of the combustion gases have a significantly higher concentration of unburned hydrocarbons. By arranging for this peak to be reingested as part of the valve strategy, it is possible to limit the unburned hydrocarbons in the exhaust offering an added benefit over an external EGR system.

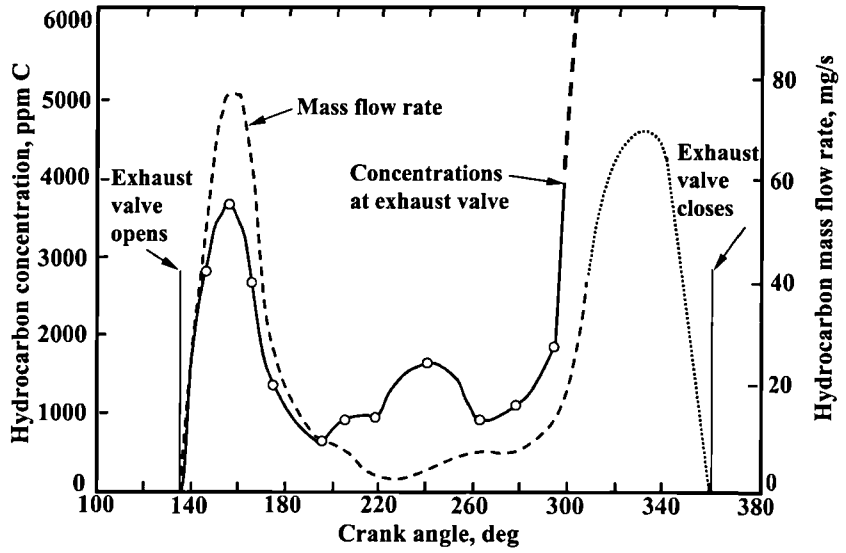

Figure 1.34
Variation of unburned hydrocarbons with crank angle [Heywood (1988)]

1.3.4. Alternatives to VVA

There are two other possibilities to modify the gas exchange processes occurring within the engine in addition to VVA: Variable Intake Systems (VIS) and port throttling. Both of these are potentially more simple in design and easier to implement. They do, however, have the disadvantage that they can only be applied to the intake system and therefore offer less benefit than VVA as an emissions control tool.

Mikulic *et al.* (1990) give a comparison between the merits of VVA (presumably in the form of a phasing system) and VIS. The rudimentary form of the VVA considered (a 2-step switching system) would generally be used where torque optimisation is of greater importance and therefore does not fully reflect the benefits of VVA. VIS may be considered to be of three forms: those which use variation of ram pipe length, those which vary pipe diameter, for example by

port deactivation, and those which vary the resonance volumes. Figure 1.35 assesses each of these as well as a simple 2-step intake-only VVA system.

System	Variation of			Steps	Vol. efficiency in speed range			Performance		Pack-aging	Cost	Application		
	Length	Area	Res. Vol.		Low	Med	High	Part-Load	Idle			IL4	IL6	V6
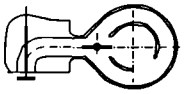	X	(X)	(X)	(2) 3		+	+			--	--	X	X	(X)
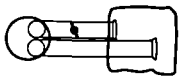	(X)	X		2 (3)	+	+	+	+	+		--	X	X	(X)
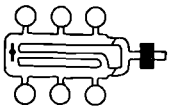			X	(2) 3		+	+			+	+		X	X
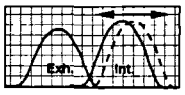				2	+		+		+	+	--	X	X	(X)

Figure 1.35

Relative merits of variable gas exchange devices [Mikulic *et al.* (1990)]

Mikulic *et al.* (1990) argue that varying ram pipe length is a more attractive proposition as port deactivation leads to poor knock performance and partial charge stratification preventing the increase in volumetric efficiency from being completely utilised. The value of a VIS system (as opposed to VVA) is also dependent on the engine speed range. At very low speeds (up to 1500 rev/min) VIS has very little influence due to the very low gas velocities in the port. In this respect VVA offers significant potential for improvement. From 2000 to 4000 rev/min, VIS offers higher volumetric efficiency, although this may not be as important as emissions control. Above these speeds, both systems offer considerable benefits. VIS is particularly suitable for six cylinder engines [Mikulic *et al.* (1990)]. Figure 1.36 compares a 2-step VVA system and a 3-step VIS on a V6 engine with 4-valves per cylinder. The improvement in torque achievable using VIS gives it a more attractive cost/efficiency ratio than VVA [Mikulic *et al.* (1990)].

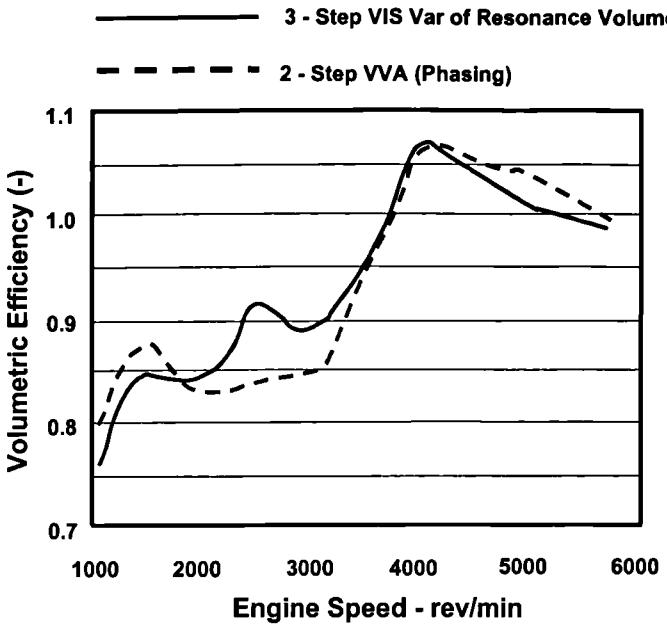

Figure 1.36
Comparison of volumetric efficiency with engine speed for VIS and VVA on a V6 engine [Mikulic *et al.* (1990)]

The principle of port throttling is shown schematically in Figure 1.37. Both butterfly throttles and barrel throttles are suitable for this function. Figure 1.37 also shows the concept of combining port mounted throttles with a conventional plenum throttle. Such a strategy offers the possibility of having a certain degree of control over the backflow process, allowing its use as an emission control system.

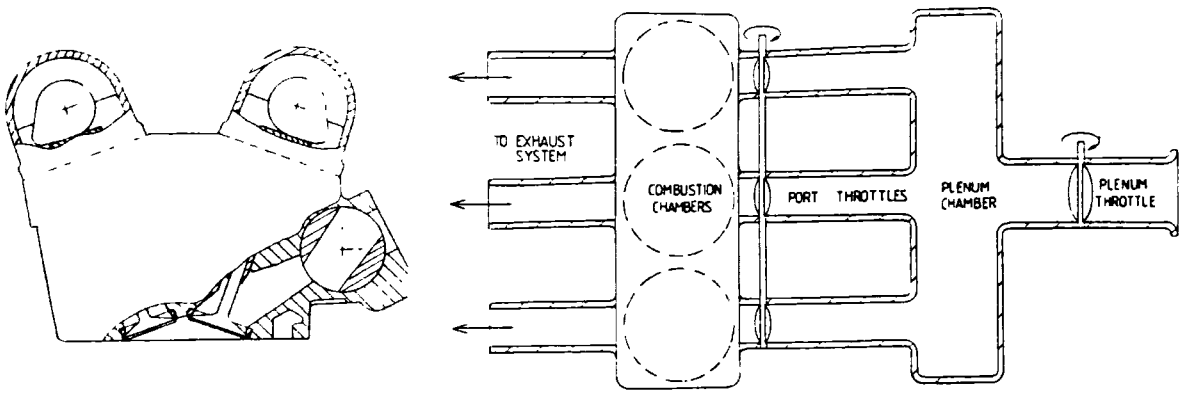

Figure 1.37
Port throttling applied to SI engines [Poole *et al.* (1992)]

Port throttles provide two main benefits. First they allow the use of long duration valve events with extended overlaps to increase maximum power. Combustion stability at low speed is maintained because the port throttle acts as a restriction preventing excess exhaust gas from

travelling up the intake port, which in turn limits charge dilution to an acceptable level. Secondly, they allow reductions in pumping work by means of the port pressure recovery mechanism described by Newman *et al.* (1989). The pressure in the port can rise back to atmospheric pressure whilst the intake valve is closed because of the relatively small port volume. When the inlet valve opens, there is very little pressure difference across the valve leading to a reduction in pumping work during the first part of the induction stroke (Figure 1.38). Newman *et al.* (1989) reported a larger than expected deterioration in burn rate which was attributed to poor mixing between the fresh charge and exhaust gas inside the cylinder. This was despite the fact that the investigation had been carried out on an engine with one intake port per cylinder deactivated. It was suggested that this deterioration was due to the lower gas velocities which were themselves a result of the minimal backflow levels. The authors also acknowledged the problems of obtaining an adequate balance of airflows between individual cylinders. Duckworth and Barker (1996) reporting on a comparison between port-mounted barrel throttles and VVA suggested that barrel throttles could have some role to play in increasing in-cylinder gas motion although this was not quantified.

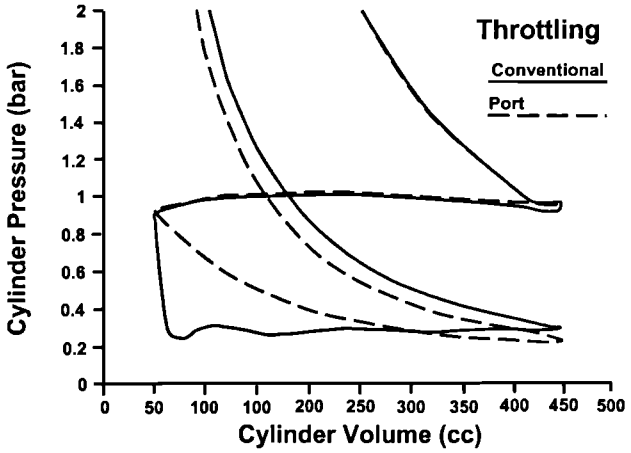

Figure 1.38
Pressure-volume diagram showing port pressure recovery mechanism
[Newman *et al.* (1989)]

Baker (1995) studied the effect of combining port throttles with a plenum throttle to allow full control of internal EGR as well as port deactivation. The filling and emptying effects were modelled by a computer program which also helped demonstrate that port throttling offered the capability of altering the inlet flow versus crank angle characteristic. This modelling indicated that a 25/75% split between the port and plenum throttles could improve in-cylinder motion. Subsequent engine tests showed that such a strategy had a slightly higher tolerance to external EGR. Much of the benefit appeared to be the ability to use long duration camshafts without loss in emissions performance. The author concluded that incorporating deactivation, which had

given the best emissions results, would be one possibility for future low-emission high performance engines.

Both VIS and port throttling give improvements in performance or, to a lesser extent, in emissions. However, it can be argued that neither allows optimisation of the gas exchange process throughout the engine's speed/load envelope. They simply offer a means to exploit possible benefits in one region of operation while circumventing some of the problems this would otherwise cause. In this respect, at least, VVA offers a far greater potential for minimising the need for these trade-offs.

1.3.5. Current Perspectives on VVA Strategies

The majority of VVA arrangements currently available in automotive vehicles are based on camshaft phasing systems (e.g. Jaguar, Mercedes [Grohn (1990)], BMW, Alfa Romeo), although there are a few other types, the VTEC system produced by Honda and the variable duration system developed by Rover being noteworthy examples. The consensus seems to be that intake camshaft phasing, is the most cost-effective method of gaining significant improvements in performance.

Phasing of the intake camshaft provides improvements in idle stability, low speed torque and maximum power. The phasing strategy for achieving these improvements is shown in Figure 1.39. Idle stability is improved by retarding the intake cam reducing the overlap period hence minimising charge dilution. The camshaft can be advanced in the low speed range to prevent fresh charge from being pushed back into the intake port. The increased overlap also increases internal EGR levels helping to control NOx emissions. Finally the cam is again retarded for high speed operation to increase maximum power.

The aim of most VVA systems has been to increase torque throughout the speed range and, until the early 1990's, very little work has been done on optimising camshaft phasing strategies to reduce emissions or fuel consumption [Mikulic *et al.* (1990), Demmelbauer-Ebner *et al.* (1991)]. The primary reason being the lack of understanding of how the different factors, such as valve event phasing and duration, affect emissions levels. Studies seem to fall into two camps: those looking at improving some aspect of the engine's characteristics such as in-cylinder motion, and those which carry out relatively detailed investigations to assess the benefits of one form of VVA, usually based on camshaft phasing. Recent work in the former has already been discussed, this section will aim to review some of the recent work in the latter area with reference to two studies investigating VVA.

Engine Performance Objectives	Required Valve Timing Characteristics
Greater Maximum Power	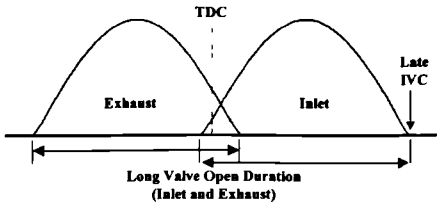
Greater Low-speed Torque	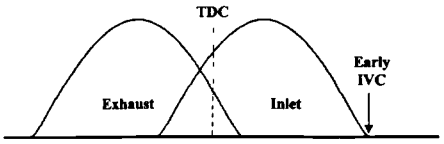
Better Idle Stability	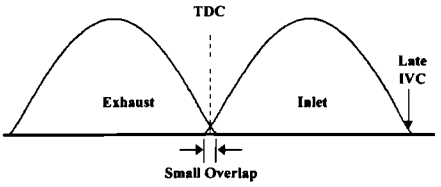

Figure 1.39
Camshaft phasing strategies to improve idle stability, low speed torque and high-speed power (adapted from Maekawa *et al.* (1989))

Duckworth and Barker (1996) carried out a study to assess the relative merits of intake camshaft phasing and port and plenum throttling. The aim was to investigate their use as a means of achieving internal EGR whilst retaining possible improvements in performance. The VVA strategy investigated is shown in Figure 1.40 together with the timing diagram for the camshafts used in the port-throttled variant. Full load performance was increased by both strategies, as expected, although this was also dependent on exhaust tuning which had been optimised and, in the port-throttled case, the longer duration camshafts used. The longer duration camshafts were not fitted to the VVA engine as the authors felt that their use would have required too great a swing to achieve the required degree of overlap at idle. A longer duration cam for the VVA tests would have possibly allowed a fairer comparison, even though the swing required (approximately 52° ca) would have been towards the upper limit of current camshaft phasing systems. By using the same camshafts, the later IVC could have shown reductions in pumping losses as well as an improvement in output power. This may also have reduced or even alleviated the need to optimise the exhaust system for each type. The test results quoted by the authors showed that the port-throttled version gave a higher power output (due to its longer duration camshaft) while the VVA variant gave a flatter WOT torque curve. Results at part throttle conditions suggested that both VVA and port throttling could be used to control internal EGR to an extent that the external EGR circuit could be omitted. However, their work could be criticised

for the paucity of results for the VVA version and for not using camshafts optimised for VVA operation.

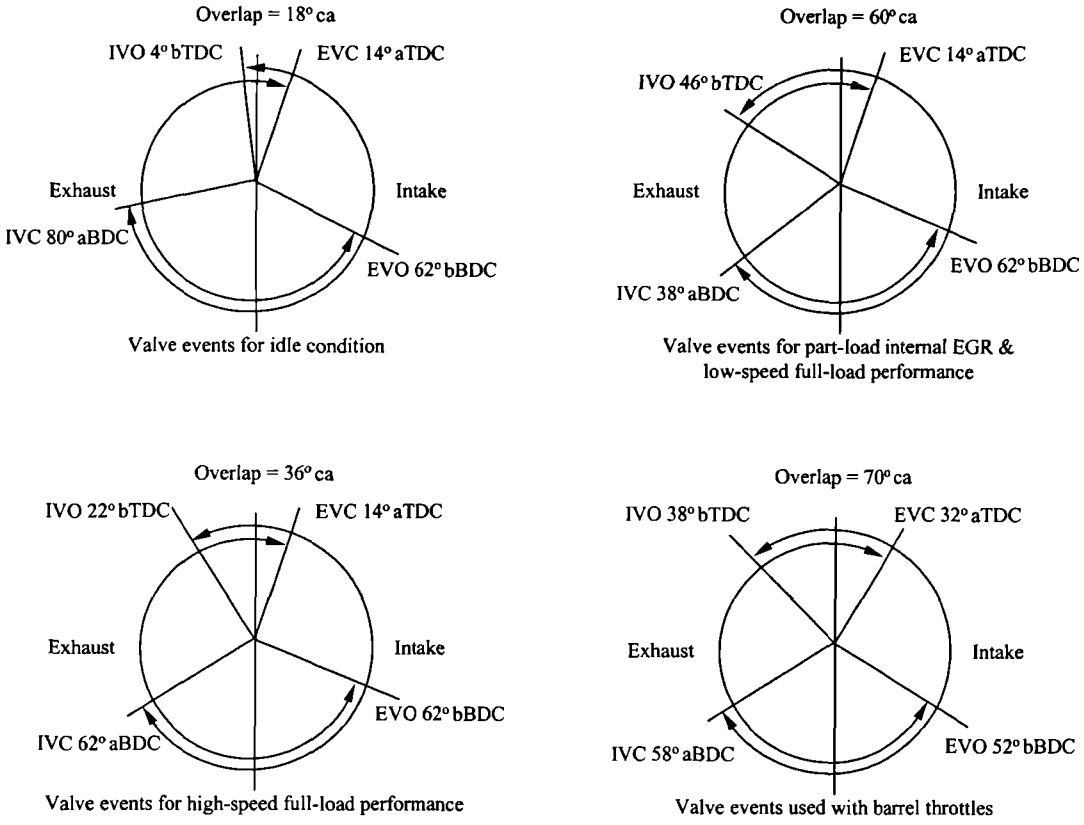

Figure 1.40
Timing diagrams for VVA and port throttle equipped engines studied by Duckworth and Barker (1996)

The port throttled engine used barrel throttles which are known to aid in-cylinder motion leading to increased burn rates. By increasing the internal EGR level, the balance of the throttling shifts from the port to the plenum throttle and the burn rate approaches that of a conventional engine with external EGR and plenum throttling. As expected, the VVA equipped engine gave extremely good idle stability due to lower dilution levels, whilst the port throttled engine demonstrated its ability to maintain stability levels similar to the baseline while using long duration camshafts.

Leone *et al.* (1996) carried out an extensive study to compare four camshaft-phasing strategies:

- varying the phasing of the exhaust camshaft only (exhaust-only)
- varying the phasing of the intake camshaft only (intake-only)
- varying both the exhaust and intake camshafts by the same amount (dual-equal)
- varying the exhaust and intake camshafts independently (dual-independent).

The benefits expected from the first three are summarised in Figure 1.41.

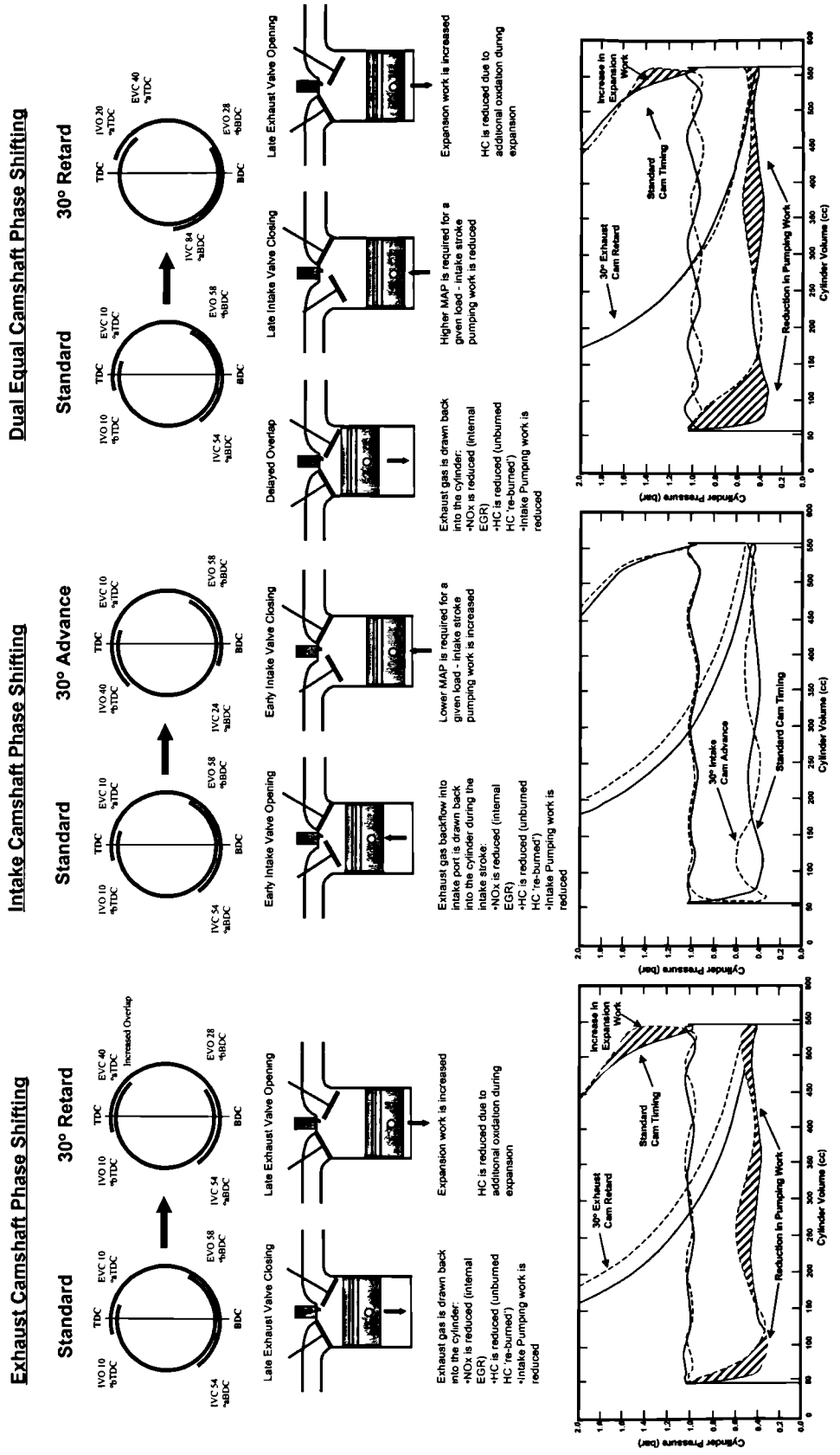

Figure 1.41
Summary of benefits expected from the three camshaft phasing strategies investigated by Leone *et al.* (1996)

Leone *et al.* (1996) stated a number of benefits for control of residual dilution under transient conditions. Internal EGR eliminates the manifold filling and emptying effects associated with external EGR, allowing an engine to operate under increased levels of dilution without sacrificing benefits in emissions of unburned hydrocarbons and BSFC under transient conditions. The comparison between camshaft phasing and external EGR was made at lower NOx levels for the VVA case as it was assumed that an engine operating with such a system would be capable of operating under higher levels of dilution. For example, it was found that compared to 10% external EGR 40° dual-equal retard reduced BSFC by 4.4%, 35° exhaust retard gave a 3.8% reduction whilst 35° intake advance gave an improvement of 3.4%. The exhaust and intake-only strategies were limited by the onset of combustion instability. An estimate of the components giving the benefit in fuel consumption is given in Table 1-5.

	Dual-Equal Retard	Exhaust Retard	Intake Advance
Pumping	**4.5**	**3.1**	**2.5**
Dilution	**0.9**	**1.1**	**0.9**
EVO	**0.6**	**0.6**	**0.0**
HC	**0.2**	**-0.1**	**-0.1**
CO	**-1.3**	**0.3**	**0.2**
Total Calc.	**4.9**	**4.9**	**3.5**
Measured	**4.4**	**3.8**	**3.4**
Corr. For CO	**5.7**	**3.5**	**3.3**

Table 1-5
Estimate of components giving fuel economy benefits (%)
[Leon *et al.* (1996)]

The corrections made for BSCO are based on work performed by the authors on the effect of VVA on air/fuel mixing and burn rates. In particular, it was stated that the changes in measured BSCO values were related to the air/fuel mixing (both in the intake port and in-cylinder), and would depend on the type of engine used. To this end the authors cited work from a previous study [Stein *et al.* (1995)] comparing four different engine configurations including valve masking and ports optimised for axial swirl. The effects of dual-equal camshaft retard on BSCO levels for the four engines are shown in Figure 1.42. It seems that deterioration in the mixing process inside the intake port due to reduced backflow is offset by the higher in-cylinder charge motion levels caused by masking. Tests conducted by the authors using a propane-fuelled engine

indicated that air/fuel mixing is the major factor affecting BSCO levels. It is difficult to say whether in-cylinder motion is the primary factor affecting the mixing process as backflow levels will also be different for engines employing masking. However, the results clearly indicate the benefits of improved air/fuel mixing in minimising BSCO levels.

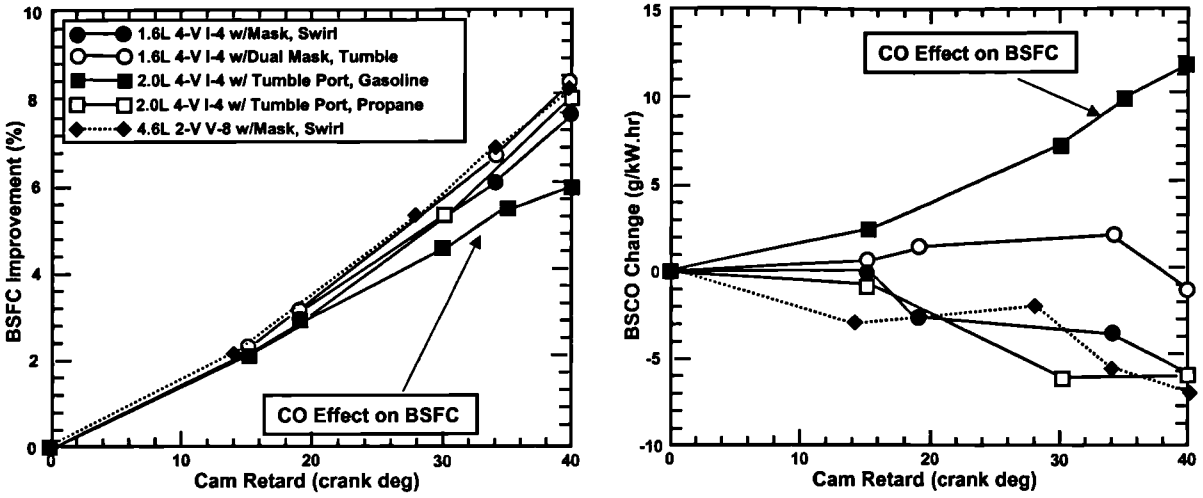

Figure 1.42
Dual-equal camshaft retard for four engines at 1500 rev/min, 2.62 bar BMEP (1200 rev/min for 2-valve)
[Stein *et al.* (1995)]

As all the strategies investigated by Leone *et al.* (1996) were aimed at using internal EGR, the overall gas temperatures at the end of the compression stroke would be expected to be higher, thus increasing the engine's susceptibility to knock. However, where late IVC forms part of the strategy, the lower effective compression ratio will help counteract this trend to some extent. It was found that the dual-equal strategy actually increased the knock margin while the other two were found to reduce it. On their test engine, it was found that the exhaust-only strategy became knock limited at 5 bar BMEP whilst the intake-only was limited at 4 bar BMEP. The NOx and fuel economy benefits for the different strategies are shown in Figure 1.43.

The dual-independent strategy was regarded as an extension of dual-equal. It was postulated that, by independently varying the camshafts, it would be possible to maintain an adequate torque reserve (lower manifold absolute pressure) as opposed to the dual-equal strategy which would lead to an unthrottled engine at medium-high load. The lower manifold pressure would have little effect on pumping losses as the cylinder pressure would not fall as low during the first part of the intake stroke (Figure 1.44).

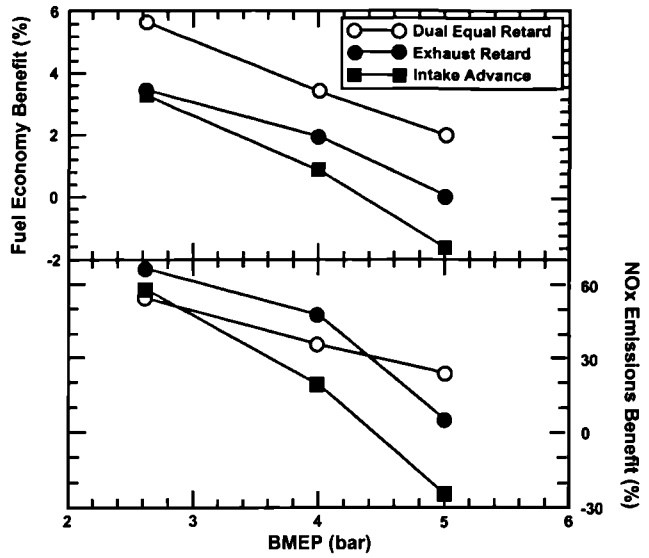

Figure 1.43
NOx and fuel economy benefits of variable camshaft timing at 1500 rev/min [Leone *et al.* (1996)]

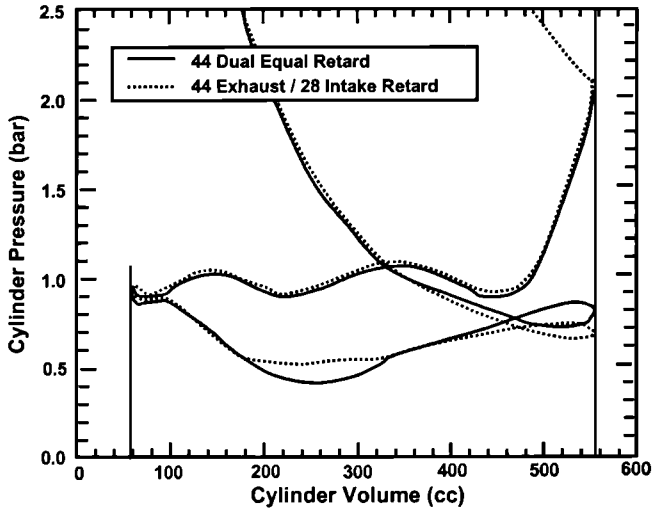

Figure 1.44
Pumping loops for dual-independent and dual-equal strategies at 2500 rev/min, 4.0 bar BMEP [Leone *et al.* (1996)]

From these results the authors argued that, because improvements in fuel economy and NOx emissions decrease with increasing load, VVA would be of greater benefit in less heavily loaded vehicles, i.e. those with large engine displacements in comparison with vehicle weight. The overall conclusion was that the dual-equal strategy was significantly better than the inlet and exhaust-only approaches in terms of part load emissions and fuel consumption, but suffered from lack of torque reserve at medium to high load conditions, which could be overcome by using the dual-independent approach. Much of the improvements attributed to the dual-phasing strategies, however, could also be achieved by using a combination of intake-only phasing and variable intake event duration.

1.3.6. Mechanisms for VVA Systems

Numerous ingenious solutions to the problems of achieving VVA have been proposed and implemented. This section aims to briefly survey some of the systems proposed in terms of their operation and effectiveness. A number of surveys have previously been carried out on VVA systems [Demmelbaur-Ebner *et al.* (1991), Ahmad and Theobald (1989), Dresner and Barkan (1989), Stone and Kwan (1989) and Gray (1988)]. Such systems can be classified by the manner in which each alters the valve opening/closing characteristics:

- those which shift the phase of the camshaft with respect to the crankshaft
- those which alter the duration as well as phase
- those allowing modification of valve lift in addition to the first two.

Phase Shifting Systems

Systems that allow the cam phasing to be altered (either discretely or continuously) have found the greatest success in terms of their adoption in production engines (Jaguar, Alfa Romeo, BMW, Mercedes and Nissan). Their success is probably due to the fact that such systems can be produced economically [Demmelbauer-Ebner *et al.* (1991)] and there is now some understanding of how they can best be controlled. These systems are predominantly based on a helical spline arrangement, although others have been proposed (see Figure 1.45). The greatest problem is achieving the required degree of camshaft swing. For torque optimisation, a helical spline arrangement varying the camshaft through a cam angle of the order of 10^{o} gives torque improvements of between 3 to 10%, which is typical of the systems currently available. A far greater range will be required if such systems are to be truly used for emissions optimisation. An example is that used by Seabrook (1995) which was capable of achieving a swing of 40^{o} ca.

VVA Systems which Modify Duration in addition to Phase.

A major drawback of any phase shifting system is that the IVO point needs to be shifted far less than IVC as engine speed increases. Thus systems which allow some variation in duration offer considerable benefits in minimising this conflict. Unfortunately, the greatest problem seems to be the inability of such systems to capitalise on any efficiency benefits due to them suffering from higher mechanical losses. In his investigation on a harmonic drive system (Figure 1.46), Ma (1988) found that frictional losses alone were enough to make the system unsuitable for practical application.

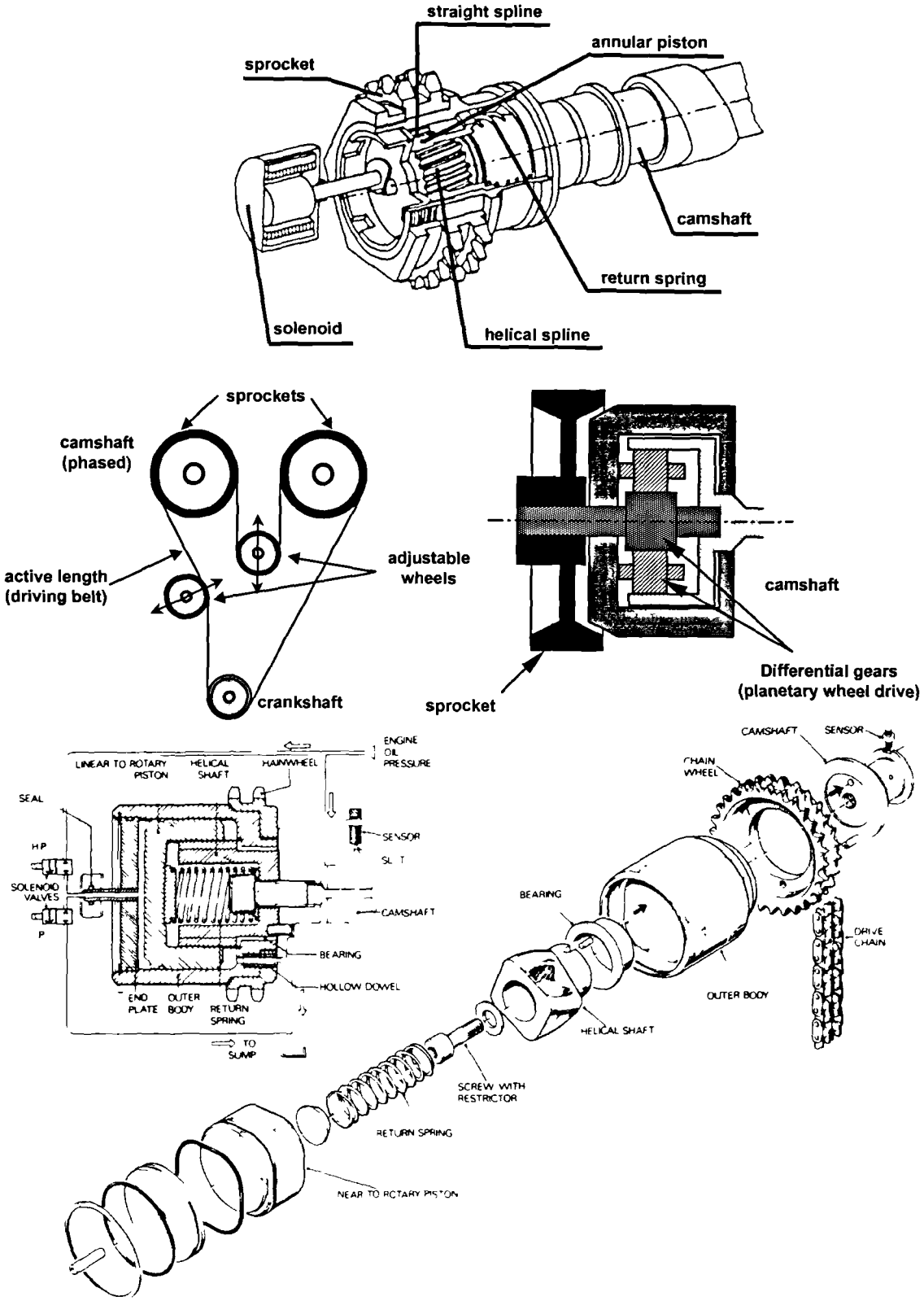

Figure 1.45
Examples of camshaft phasing systems
[Demmelbauer-Ebner *et al.* (1991) and Gray (1988)]

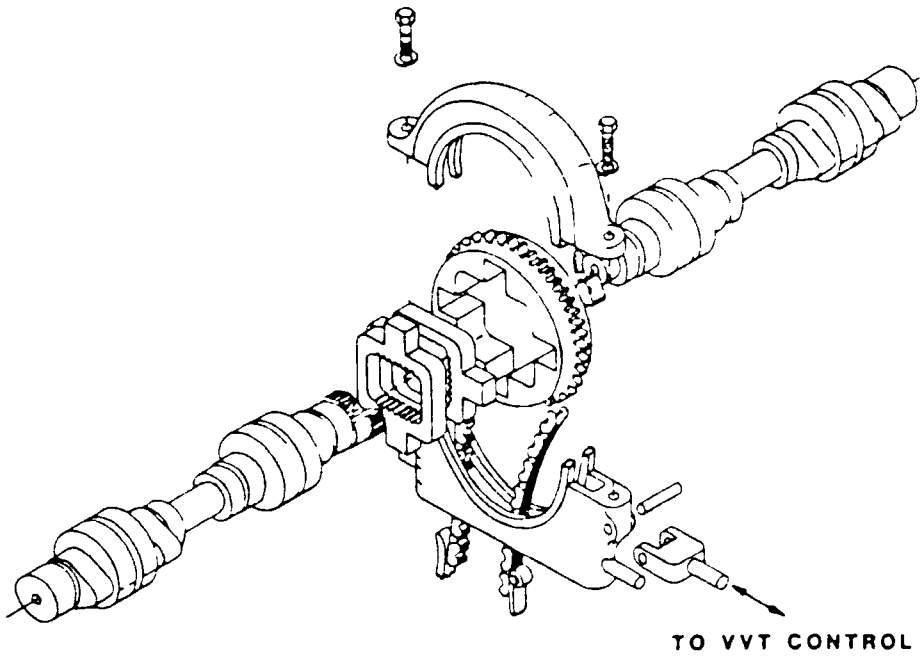

Figure 1.46
Ford harmonic drive system [Gray (1988)]

Systems Capable of Modifying Phase, Duration and Lift.

Systems such as these fall into three possible groups [Ahmad and Theobald (1989)]: those which switch between different cam profiles, those using electromagnetic actuators to operate the valves, and those based on some form of hydraulic system. The most successful of these have been from the first category, as they combine relative simplicity with significant improvements in performance. The Honda VTEC system first described by Inoue *et al.* (1989), and also the VTEC-E system [Horie *et al.* (1992)] switch between two different profiles to improve performance in the first case, and fuel economy (by means of valve deactivation and axial stratification) in the second. Lotus [Dopson and Drake (1991)] also describe a profile switching system, as well as Shibano *et al.* (1992) who advocate the adoption of roller followers to reduce frictional losses. The Honda and Lotus systems are shown in Figure 1.47.

Titolo (1991) describes a three-dimensional cam system for use on the Ferrari V8 engine. By combining axial translation of the camshaft with phasing it allows all valve event parameters to be varied although not independently (Figure 1.48). Ricardo [Norris (1991)] have developed a system capable of independently varying valve events by means of a two camshaft and prism arrangement. Such a system, however, would be difficult to implement on a production engine as it has severe packaging problems due to the proximity of two inlet camshafts.

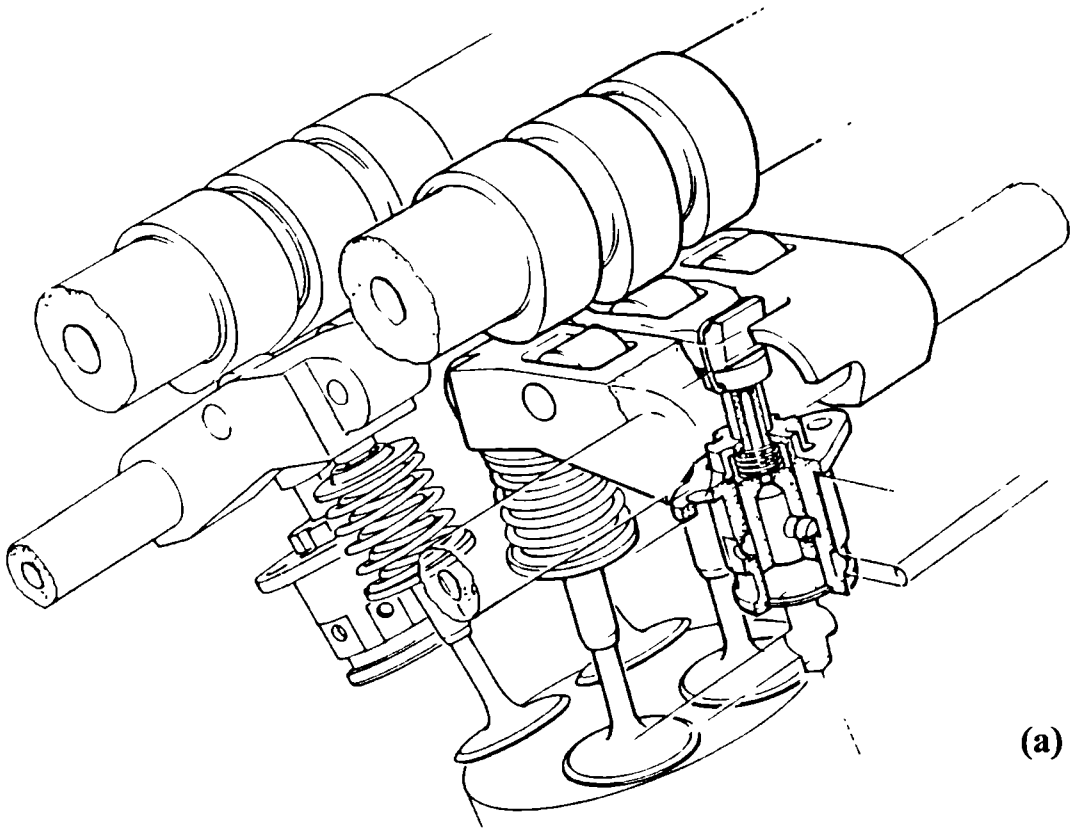

(a)

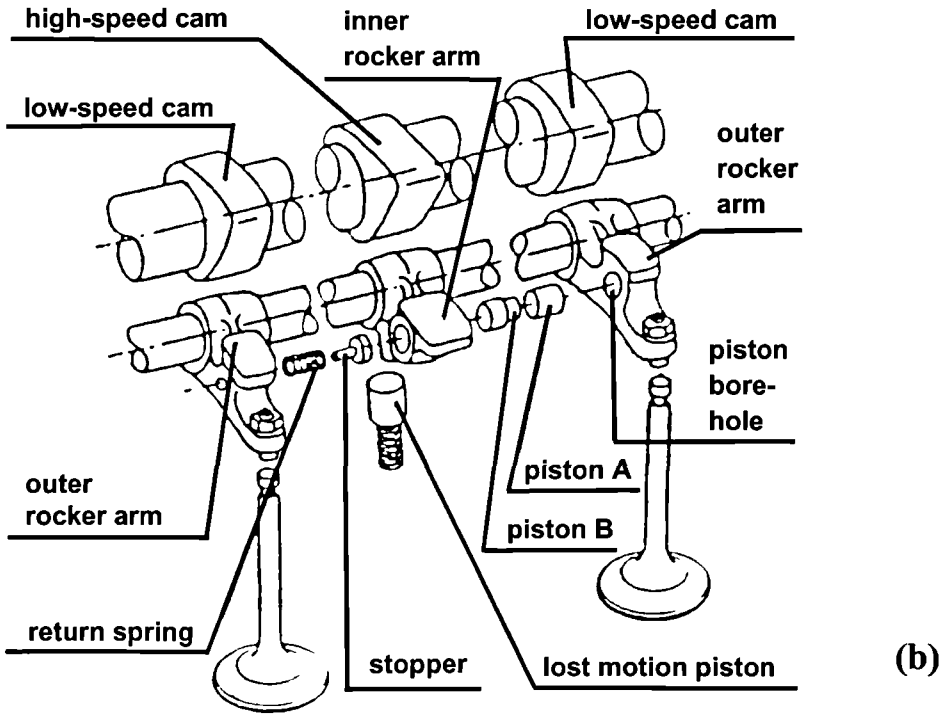

(b)

Figure 1.47
(a) The Lotus camshaft profile switching system [Dopson and Drake (1991)], and (b) the Honda VTEC system [Inoue *et al.* (1989)]

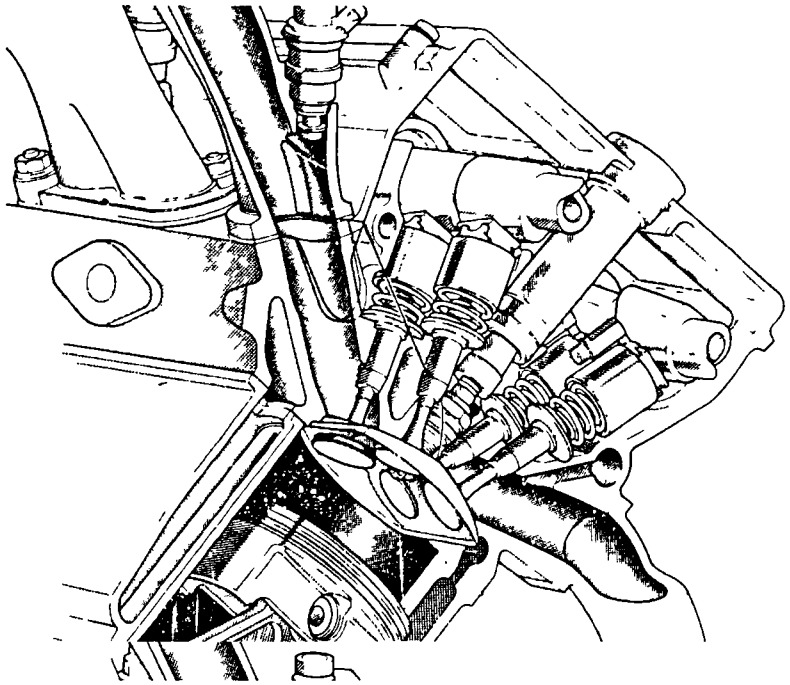

Figure 1.48
Variable valve timing for Ferrari V8 engine [Titolo (1991)]

Systems using electromagnetic actuators are very attractive as they offer the flexibility of control possible from modern engine management systems [Ahmad and Theobald (1989)]. The best known of these is that described by Pischinger and Kreuter (1984) which alternately energises two coils to attract a plate mounted on the valve stem. Although the system allowed lower idle speeds and improvements in fuel consumption, these improvements were not apparent at higher speeds. Indeed the system was only tested up to 2000 rev/min, probably due to the limited valve accelerations achievable rendering it impractical for application on an engine. It is known that companies are still working on systems for the electromagnetic operation of valves, although virtually no details have been published. Success in this area could transform the prospects and potential of VVA.

The final category covers hydraulically-based systems which can either consist of a variable hydraulic mechanism between a conventional cam and valve or hydraulic actuators to operate each valve individually. The latter obviously offers significant flexibility but is also the most difficult to implement. Ahmad and Theobald (1989) list the problems associated with the former as high seating velocities, speed limitations, high cycle-to-cycle variation, temperature sensitivity of the hydraulic system and the high level of complexity. Hydraulic actuators are also subject to many of these problems, but also suffer from the need to have a separate power source and their physically large size. An example is the Active Valve Train (AVT) developed by Lotus [Wilson *et al.* (1992)] shown in Figure 1.49. This system is capable of reproducing typical camshaft

profiles at speeds up to 4000 rev/min which, although relatively high, is still some way from the required maximum speed. The system has, however, proved useful as a research tool to investigate VVA strategies (Wilson *et al.* (1993)).

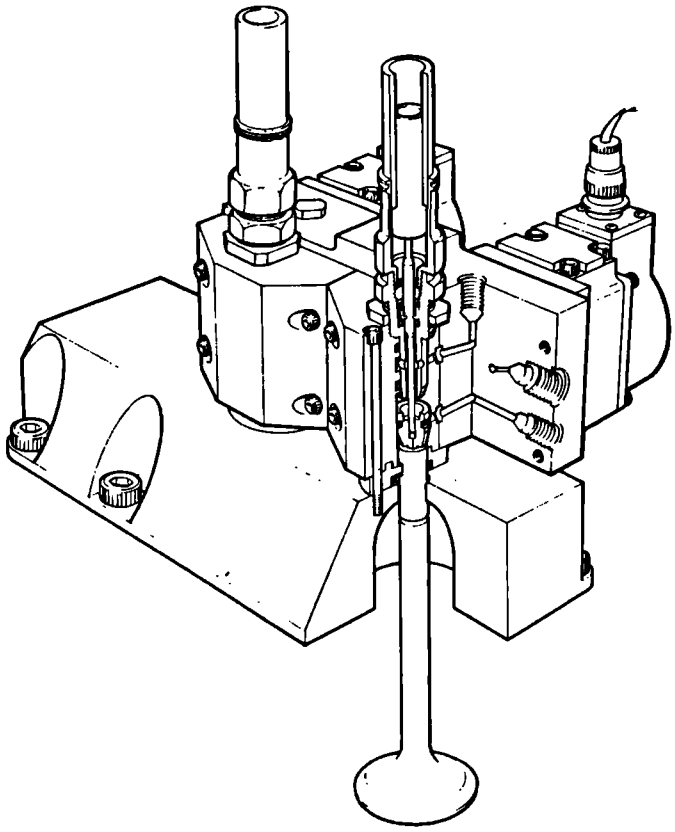

Figure 1.49
Lotus Active Valve Train (AVT) [Wilson *et al.* (1992)]

In general, it seems that systems that allow continuous variation of all valve event parameters can still only be considered as research tools but their flexibility would make them an attractive proposition were they to become feasible for production engines.

1.4. Conclusions

The internal combustion engine looks set to be the primary automotive power source in the medium term at least. This literature survey has shown that there is a great scope for improvement. The wide operating range of automotive engines, means that a great deal of compromise is required. The use of fixed valve timings and the need to use EGR, rather than lean burn, in order to use three-way catalysts demonstrate this. Valve timing, fuel injection, lean burn, stratified charge, EGR and catalyst technologies are all areas where further improvements can be made.

In the absence of a lean catalyst, a combination of stoichiometric fuelling, EGR and a three-way catalyst will form the basis of the emissions control package on conventional SI engines. The inability of current designs to operate with high levels of EGR poses severe limits on this basic strategy. Methods that increase the engine's ability to tolerate high levels of charge dilution must therefore be sought to achieve further NOx reductions. Methods aimed at reducing hydrocarbon emissions usually compromise performance or fuel economy. These problems point to the need to reduce some of the compromises inherent in conventional 4-valve per cylinder engines. In this respect, the case for adopting a VVA strategy is a strong one.

VVA promises gains in performance while simultaneously reducing fuel consumption and emissions, the last two categories are only now being looked at. Much work has been conducted to investigate single aspects of VVA systems, the work on camshaft phasing being a notable example. Intake camshaft phasing systems are already in the marketplace. Their ability to help control the quantity of residuals trapped within the cylinder combined with their potential to improve performance makes such systems very attractive and ensures that they will become more prevalent in the future. Exhaust camshaft phasing, while providing little gain in performance, can help significantly in controlling unburned hydrocarbons as well as NOx. It is feasible for an engine employing a combination of phasing on the two camshafts to operate without any external EGR system.

The benefits of varying valve event timing and lift, including the use of valve deactivation, on in-cylinder motion have also been demonstrated. Use of strategies capable of improving combustion by enhancing in-cylinder motion can allow engines to operate with higher levels of dilution. Such techniques, particularly at part-load, are attractive as they can be used for emissions control as well as improving efficiency and overcoming some of the deficiencies of 4-valve designs.

The case for individual VVA strategies has been made, yet the greatest potential lies in them being brought together. A system capable of individually varying phasing, duration and lift is ultimately desirable. Although this aim cannot be physically achieved on a production engine at present, it is apparent that systems combining two or more of these, albeit to a limited degree, offer far greater potential than the simple phasing systems which have typically found their way into the marketplace. One of the key questions for the more complex VVA systems is undoubtedly that of assessing whether the benefits realised in individual valve strategies, such as phasing and deactivation, remain when such techniques are combined. It is possible that significant interactions exist between such strategies and these may prove to be of great benefit.

The main problem in this area is the lack of knowledge as to what the nature of these interactions may be, and how the large number of variables involved can be selected optimally to meet both the demands of the consumer and emissions legislation. The aim of the work reported in this thesis has been to investigate possible gains from combining strategies, and to gain an understanding of the underlying mechanisms.

Chapter 2

THE EFFECTS OF POPPET VALVES ON GAS FLOW

2. The Effects of Poppet Valves on Gas Flow

2.1. Introduction

Heywood (1988) describes the valves and ports as the most important flow restrictions in the intake and exhaust systems. The primary objective of their design is invariably to minimise the restriction they present to the flow thereby reducing pumping losses. However, the flow pattern set up by the inlet valves is also important and will have a significant influence on the combustion process with a direct effect on efficiency and pollutant formation.

The dependence of flow rate on the continually varying valve open area and on the state of the gas (pressure, temperature, and composition) makes it extremely difficult to record detailed measurements under such conditions. Annand and Roe (1974) argue that much can be learnt from simpler observations, made away from the running engine using a test apparatus under steady flow conditions. In this way the relationships between parameters such as valve lift, pressure drop, flow rate and in-cylinder motion can be investigated at fixed valve lifts.

This chapter describes a series of such tests conducted to quantify both the degree of restriction the valves present to the flow and the intensity of the in-cylinder bulk flow generated by the gas flowing past them. The motivation being to gain an insight into the benefits of adopting different valve event strategies and to help explain results from the engine tests to be conducted later.

2.2. Valve discharge coefficients

Adopting a discharge coefficient allows the average flow rate past the valve at any instant to be related to that of a frictionless nozzle. Discharge coefficients are derived empirically, and typically vary over the range of lifts through which the valves must operate. Annand and Roe (1974) presented details on the behaviour of gas flow past poppet valves, particularly the relationship between discharge coefficient and valve lift and seat geometry.

The aim of this initial testing was to quantify discharge coefficients as a function of valve lift for the Jaguar AJ26 engine, so the data could later be incorporated into a suitable model for the gas exchange process. The development of the model is presented in the following chapter. This section will discuss the experimental work conducted to determine the discharge coefficients.

2.2.1. The nature of discharge coefficients

Two quantities are required to define a discharge coefficient for a given combination of poppet valve geometry. These are a chosen reference area A_r representing the degree of port opening and an effective area, A_e. The discharge coefficient C_D can then be written as:

$$C_D = \frac{A_e}{A_r} \tag{2.1}$$

Annand and Roe (1974) stated that there is no correct choice for geometric area although they, and also Heywood (1988) and Stone (1992), used the valve curtain area, A_c:

$$A_c = \pi D_v L_v \tag{2.2}$$

where D_v is the valve head diameter, and L_v is the axial valve lift. Stone (1992) defined A_e as the outlet area of an ideal frictionless nozzle, which would pass the same flow, with the same pressure drop when drawing from a large constant-pressure reservoir and discharging into a large unrestricted volume:

$$A_e = \frac{\dot{m}}{\rho v_0} \tag{2.3}$$

$\dot{m}$ is the mass flow rate, v_0 is the frictionless velocity, and ρ is the density of the gas upstream of the nozzle. The velocity can be calculated either by using the assumption of incompressible flow or the more complete model accounting for compressibility effects. The equations for the latter are given in Chapter 3. Both Stone (1992) and Annand and Roe (1974) stated that testing is usually performed under conditions of low pressure drop (Δp) across the valves and it is therefore reasonable to use the equation for incompressible flow under these circumstances:

$$v_0 = \sqrt{(2\Delta p / \rho)} \tag{2.4}$$

Thus:

$$C_D = \frac{\dot{m}}{A_c \sqrt{(2\rho \Delta p)}} \tag{2.5}$$

Annand and Roe (1974) gave details of the dependence of the discharge coefficient on factors such as the Reynolds number associated with the flow. Stone (1992) stated that for normal valve lifts (i.e. not extremely small lifts) the effect of Reynolds number on discharge coefficient is negligible. In any case, the results of Annand and Roe (1974) indicated that the Reynolds

number is only influential for small lifts, and the flow rates under such conditions are likely to be very low. The effects of Reynolds number can therefore be neglected with little loss in accuracy.

2.2.2. Steady-flow rigs and test procedure

Discharge coefficients can be measured by means of a steady flow rig designed to draw air past the valves whilst measuring the flow rate and the corresponding pressures and temperatures in the volumes either side of the valves. Although the mean flow of gas in an engine is in the forward direction (into the cylinder for air, and out of the cylinder for exhaust gas), there are significant periods of reverse flow, particularly during the valve overlap period. It is therefore necessary to measure the discharge coefficients for inlet and exhaust valves for both forward and reverse flow.

Figure 2.1 shows a schematic representation of the apparatus used for the tests. The rig consisted of an aluminium 'dummy' cylinder with a bore and stroke identical to the test engine. An aluminium box constructed of plate was used for the lower plenum while the standard manifolds were retained at each of the ports. The valves could be opened or closed by screws acting on the valve stem. Valve lift was calculated from knowledge of the pitch of the thread (1 mm) and the angle through which the screw had been turned. Airflow measurements were made by using the air mass flow meter taken from the test engine. The readings were recorded directly from the engine management system software, which contained the calibration for the meter. It might seem that this approach relied on the accuracy of the original calibration of the airflow meter by its manufacturers. However, the fact that the discharge coefficients were being applied in a program to model the one particular test engine meant that any inaccuracy would not matter in the context of that engine. Airflow predictions by the program would be on the basis of what the airflow meter would have indicated, rather than the absolute value of the airflow rate. Pressure measurements were made by manometers connected to tappings at the locations indicated in Figure 2.1. Gas temperatures were recorded by means of type K thermocouples mounted in each of the plenum chambers. The tests were conducted in the Fuel Systems Test Facility at UCL, which is described in detail by Miller and Nightingale (1990). The vacuum pump fitted inside the plant room was used to draw air through the test rig to create the required conditions.

Baker (1995) had conducted similar tests arguing that it was adequate for them to be carried out with a fixed pressure drop across the valves sufficiently high to ensure turbulent flow. A similar strategy was adopted for the tests described in this chapter with the adoption of a pressure drop of 600 mmH_2O across the valves. Figure 2.2 shows the results in graphical form, with complete details given in Appendix 1

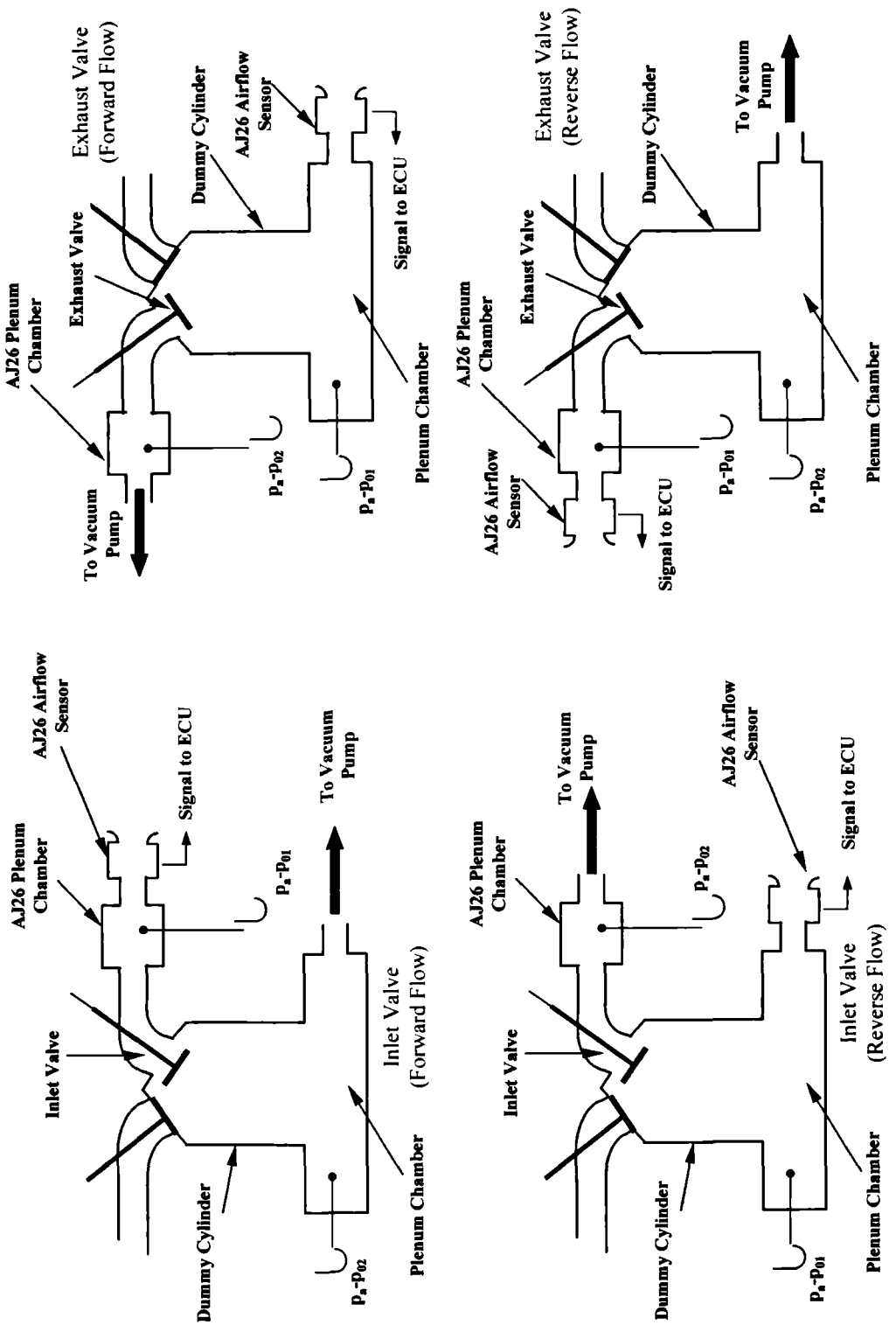

Figure 2.1
Schematic representation of steady-flow rig for measuring discharge coefficients

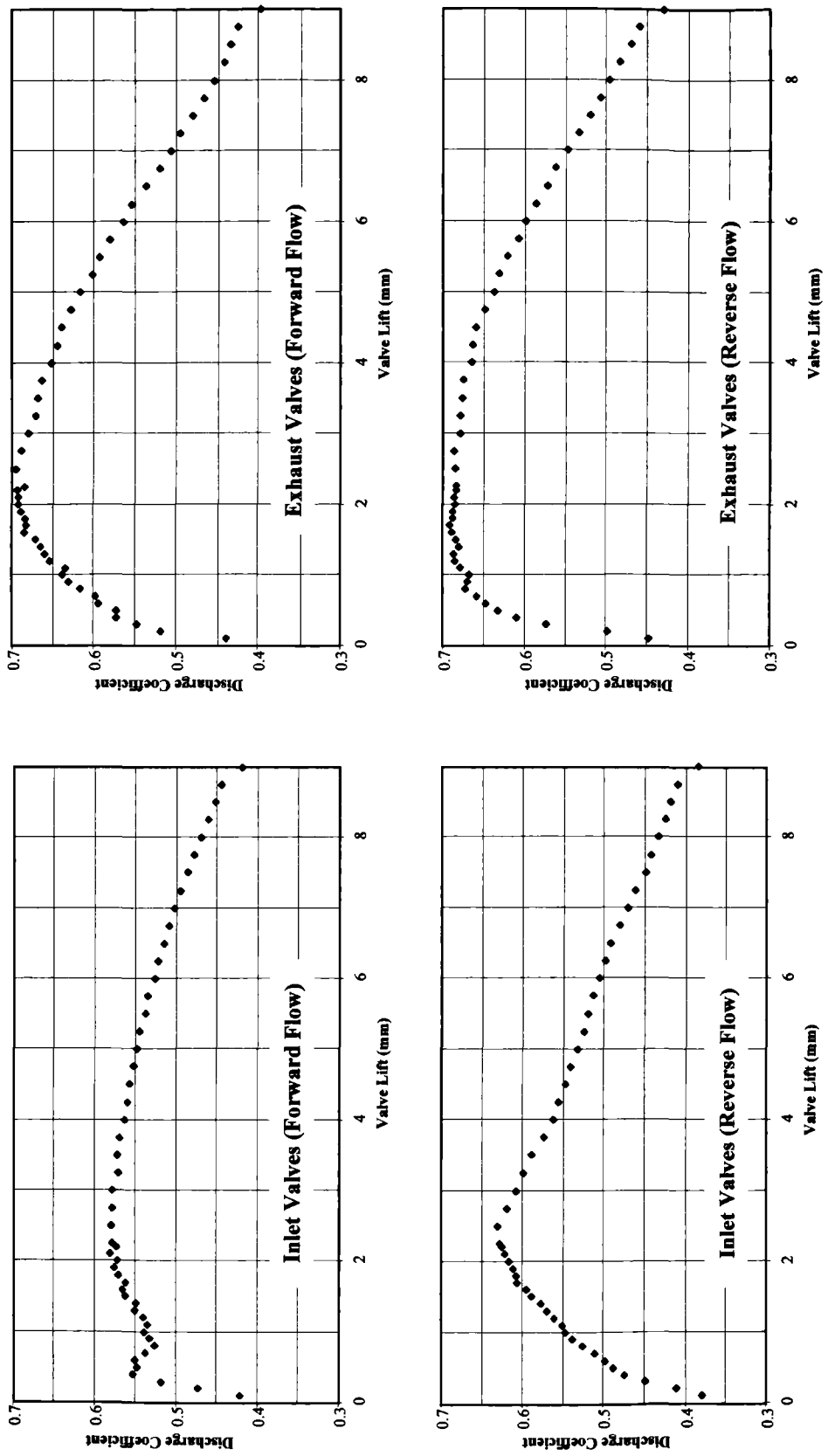

Figure 2.2
Discharge coefficients for inlet and exhaust valves

2.3. Measuring in-cylinder motion

The second aspect of the interaction between valves and gas flow to be studied was the effect of inlet valve lift on in-cylinder motion. As described in Chapter 1, de Boer *et al.* (1990) have discussed two structured forms of motion, namely axial and barrel swirl, and their effects on combustion are discussed in Chapter 1. Barrel swirl (also referred to as tumble) is expected to be the dominant flow structure when a combination of two or more inlet valves per cylinder and a pent roof combustion chamber is used. Opening the inlet valves by a differential amount can lead to an additional axial swirl component being imparted to the flow, this being particularly so if complete valve deactivation is used. The aim of the in-cylinder motion tests was to 'map' the intensity of these two types of flow structure within the cylinder over the entire range of valve lifts.

There is no single industry standard for measuring structured flow although two main types of measuring system prevail. The first is the use of a rotating wheel or vanes placed in the flow stream, the angular velocity of which can be related to the intensity of the motion. Wilson *et al.* (1993) used such a device for measuring both types of motion. The second type is known as an impulse torque meter, which relates the torque exerted on a flow-straightening section placed in the stream to the degree of swirl. Work reported by as Stone *et al.* (1993) and Baker (1995) used this type of meter, although the details of their designs varied from one to the other. The type of apparatus used for this study was based on the design of Baker (1995). Some of the modifications made to Baker's design are discussed in Section 2.3.2.

2.3.1. Defining swirl ratios

The most common method of presenting results from steady flow tests is in the form of non-dimensional ratios. These ratios may also be combined with flow coefficient and lift data over the valve event to give an overall indication of the swirl generating capabilities of a particular valve timing strategy. Stone and Ladommatos (1992) used the Ricardo definition of swirl ratio, which is based on the assumption of a forced vortex with uniform angular velocity. The angular velocity of the flow (ω) can then be related to the moment of momentum flux, which is related to the torque reaction on the flow straightener (T):

$$T = i\omega \tag{2.6}$$

i, the moment of inertia of the flow, in the case of a forced vortex can be written as:

$$i = \frac{\dot{m}}{2}\left(\frac{B}{2}\right)^2 \tag{2.7}$$

where B is the bore. The angular velocity of the vortex can now be converted to a non-dimensional form by dividing it by a representative velocity for the system. Baker (1995) used engine speed in his definition, while Stone *et al.* (1993), used gas velocity at the valve. This latter method was used for the results in this chapter as the final swirl ratio allows conclusions to be drawn about the efficiency with which the incoming momentum is converted into a structured bulk flow. Equation (2.4) can be used to estimate this velocity giving:

$$N_R = \frac{8T}{\dot{m}B v_0} \tag{2.8}$$

N_R is sometimes known as the Ricardo swirl coefficient, and is referred to here as the swirl or tumble ratio (as appropriate). It tends to vary with valve lift. Although numerous methods for calculating such ratios exist, it is worth noting that, particularly for studies such as this where the results are used for comparative purposes only, it is the consistency in the use of a particular definition that is important. Care, however, must be taken when comparing such readings with published data.

2.3.2. The impulse torque meter

A schematic of the 'core' of the impulse meter is shown in Figure 2.3 below.

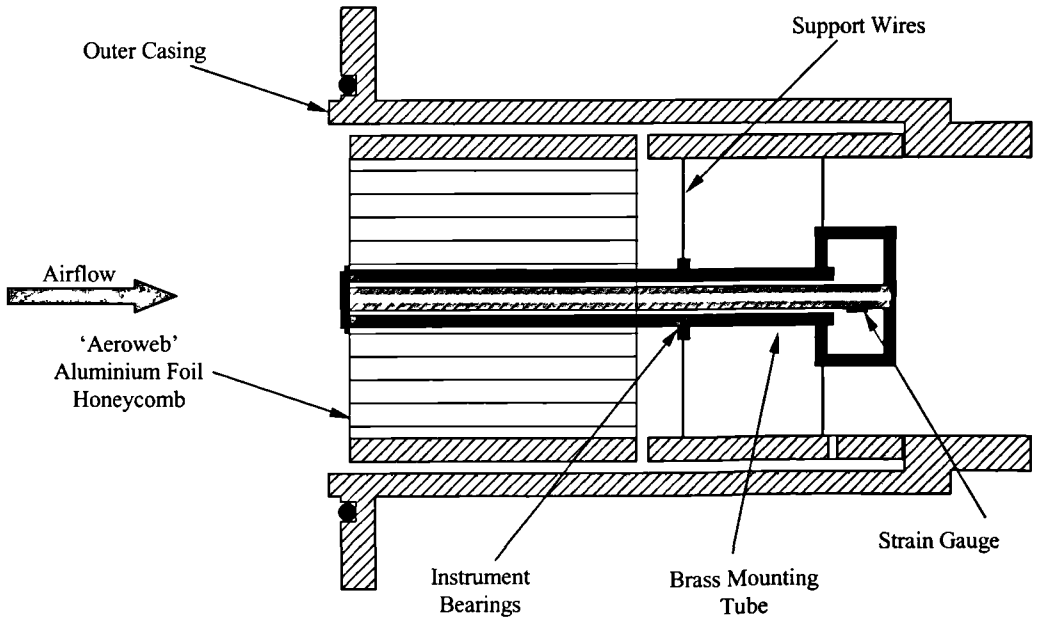

Figure 2.3
Schematic of impulse torque meter

The honeycomb flow straightening section consisted of commercially available 'Aeroweb' aluminium foil with a passage depth of 50 mm and a cell width of 3 mm. This section was mounted by means of a brass tube, itself running in a set of precision instrument bearings. The reaction torque was measured by means of a strain gauge attached to a thin inner aluminium shaft fixed at either end. As the outer tube took up the entire weight of the arrangement, the strain gauge reading directly corresponded to the torque exerted on the honeycomb. A second strain gauge attached at 90° to the first allowed temperature effects to be corrected.

Although the 'core' of the impulse torque meter was that used by Baker (1995), a number of key components of the tumble rig had to be designed from scratch to allow testing to be performed with the Jaguar components. These consisted of the dummy cylinder, false piston, draw-off tubes and the outer casing for the meter itself. There was no previous arrangement for measuring axial swirl at UCL so this was a new design. Schematics for both the swirl and tumble rigs are shown in Figure 2.4.

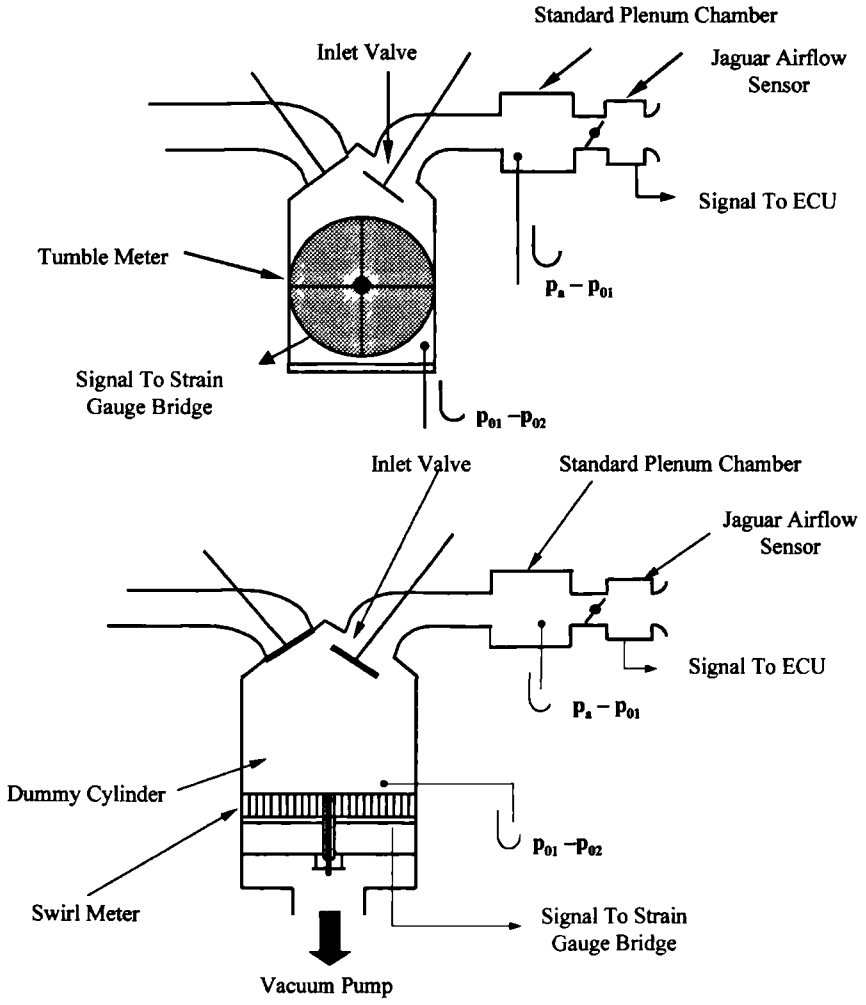

Figure 2.4
Schematic of swirl and tumble rigs

The tumble rig was initially designed to allow air to be drawn off on either side of the dummy cylinder immediately after passing the valves. Tests using such an arrangement indicated that the force on the impulse meter was too small to be accurately measured. This was due in part to the fact that only half the flow of gas was actually passing through the branch containing the meter. The results proved to be inconsistent, and were further compounded by problems with balancing the flows to each branch. Consequently, the secondary branch was blocked off allowing all the air to pass through the honeycomb. This removed the problem of flow balancing and also alleviated the problem of very low strain readings. The only problem with such an arrangement is the possibility of any axial swirl turning through the corner and influencing the tumble readings. The solution to this is discussed in Section 2.3.3. Finally, it is worth noting that the tubes drawing off air were tapered towards the ends. The reason was that the original meter had been designed for an engine with a bore of approximately 80 mm in comparison to 86 mm for the Jaguar engine. The taper was very slight and any losses due to friction would have been negligible.

2.3.3. Test procedure and results

A unique feature of the Fuel Systems Test Facility at UCL is the ability to draw large flow rates of air through the rig while maintaining a representative depression in the manifold. A preliminary test was conducted to determine tumble coefficients with ambient conditions in the plenum and then a repeat test with a depression of 400 mmHg across the throttle. Air was drawn from both sides for these tests, with the flow being balanced only approximately by use of an orifice plate in each branch. The results are shown in Figure 2.5.

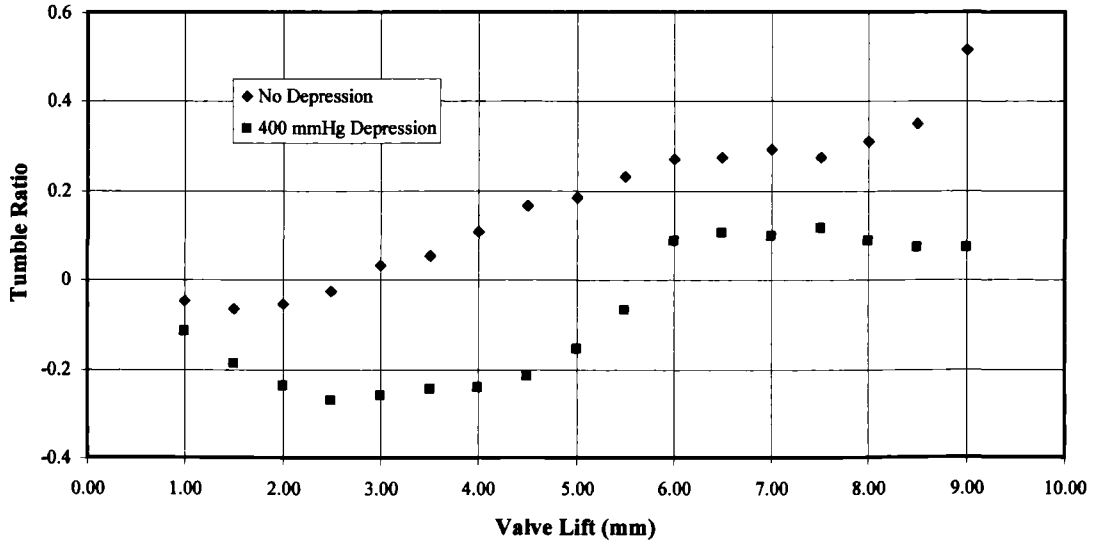

Figure 2.5
Comparison of tumble ratio for two different manifold pressures

The preliminary tests showed a marked dependence on the pressure in the plenum. In addition they indicated the rather surprising results that the vortex rotated in opposite directions for low and high lifts. The effect of reduced manifold pressure will be to reduce the density of the air flowing past the valves. It must therefore flow at a greater velocity past the valves to maintain the same mass flow rate. The tumble ratio takes this effect into account through the velocity term in the denominator. Flows entering with high velocity do have the potential to give higher levels of in-cylinder motion, but a greater proportion of the energy associated with the flow is likely to be lost through friction. This effect is reflected in the results, the case with a lower pressure showing a lower ultimate tumble ratio. The difference in the direction of rotation is a little more difficult to explain. One possible cause could be the close proximity of the inlet valve to the walls of the dummy cylinder for low values of valve lift. The interaction of the flow stream with the walls may lead to a stronger jet being formed nearer the wall helping to establish a vortex rotating in the opposite direction. Whether this effect would be greatly enhanced by the lower plenum pressure is debatable.

It was decided that the detailed tests would be conducted with a depression in the manifold as this was representative of the conditions in the engine at part-load. Again, a depression of 400 mmHg was chosen as this was close to an operating condition of 1500 rev/min, road-load. Problems with balancing flows between the two branches of the tumble rig and the low overall readings from the strain gauge meant that all the air was drawn through the swirl meter, with the secondary branch completely blocked off. The method employed to overcome any dependence of the tumble results on axial swirl was to average two readings, when the valves were opened by different amounts. The first reading was taken with one valve open more than the other. A second reading was then taken with the lift of the two valves reversed, and the two results averaged. The effect of any axial swirl would then be removed, as it would have been in opposing directions for the two readings. The only problem with this approach was that any bias between the two valves could not be distinguished. The tests for axial swirl were conducted after those for tumble and indicated very little difference between the two valves. It was therefore concluded that there was little loss accuracy by adopting such an approach. The results from both the axial swirl and tumble tests were plotted as three-dimensional surfaces and are shown in Figure 2.6 and Figure 2.7 respectively.

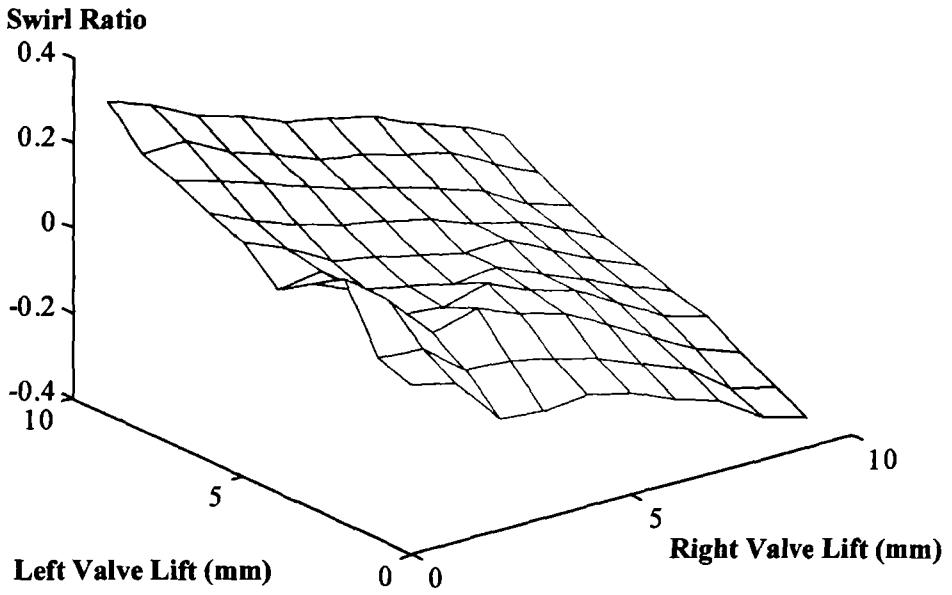

Figure 2.6
Non-dimensional swirl ratio as a function of left and right valve lift

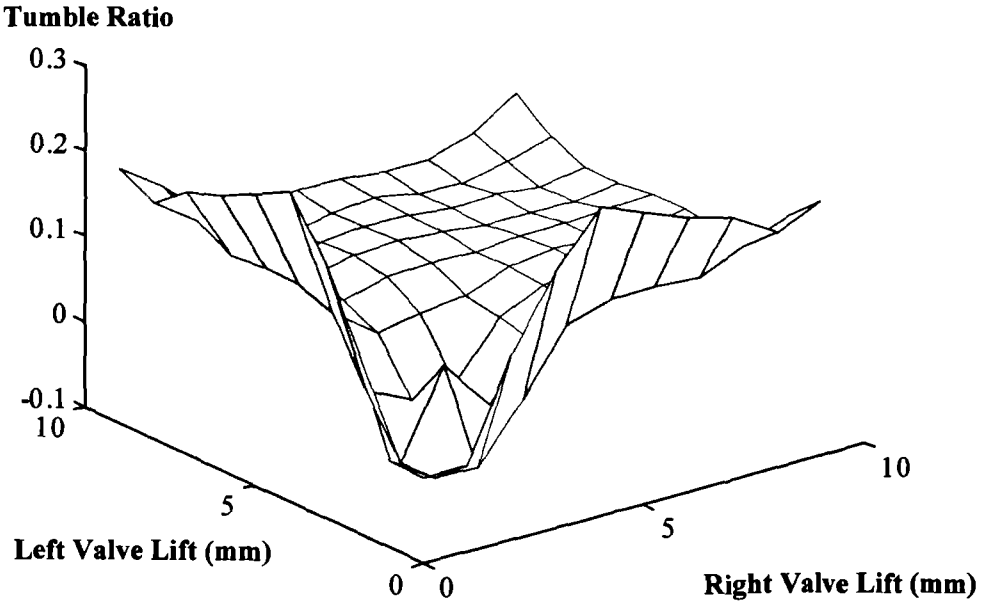

Figure 2.7
Non-dimensional tumble ratio as a function of left and right valve lift

The results shown in Figure 2.6 confirm the need for asymmetric valve lift if an axially swirling component to the airflow is to be established. The direction of the vortex was found to be entirely dependent on which valve was more open. The tumble results indicate that there is a relatively flat region of modest tumble ratio in the middle. The results at high valve lifts indicate that tumble increases when both valves are fully opened. The most promising area, however, is where one of the valves is completely deactivated and the other is opened by a relatively small amount in the 3 – 5 mm region. This region also gives a reasonable degree of axial swirl although the highest levels are to be found with a combination of deactivation and high lift on the primary valve.

The results from the steady-flow tests indicate that there is significant potential to alter the in-cylinder flow structure by optimising valve lift strategy, and this is particularly so in the asymmetric region of operation. The extent to which this can be translated into an improvement in combustion remains to be seen. An approach of particular interest would be to allow efficient combustion with high levels of dilution with exhaust residuals by creating enhanced in-cylinder motion. A vigorous motion would certainly be of benefit in such circumstances. Of course, such valve strategies would also serve to alter levels of residual exhaust gases trapped within the cylinder, and this issue is addressed in the subsequent chapter.

Chapter 3

MODELLING OF GAS FLOWS

3. Modelling of Gas Flows

3.1. Introduction

This chapter describes a program developed to model gas flow into and out of an SI engine. The primary motivation being to gain an insight into the effects of varying an engine's valve event characteristics in order to aid interpretation of the engine test results appearing in subsequent chapters. The responses of particular interest are changes in the Residual Gas Fraction (RGF), pumping work and gas velocities past the inlet valves. The model was developed from the ideas presented by Watson and Janota (1982) and the work of Baker (1995) who developed a computer program to investigate gas flows of port-throttled engines. In addition to giving some insight into results from engine tests, this model was also used as a tool for planning further engine tests.

3.2. Background

The filling and emptying model is based on following the fluid mechanic and thermodynamic processes to which the air and fuel entering the engine are subjected [Watson and Janota (1982)]. It is possible to model the engine as a set of distinct control volumes connected by a series of restrictions, such as a throttle and inlet and exhaust valves. A representation of this is depicted in Figure 3.1. Watson and Janota (1982) argue that the unsteady flows in a real engine can be modelled by assuming them to be quasi-steady in nature. This assumption allows the General Flow Energy Equation (GFEE) to be applied to each of the control volumes shown in Figure 3.1.

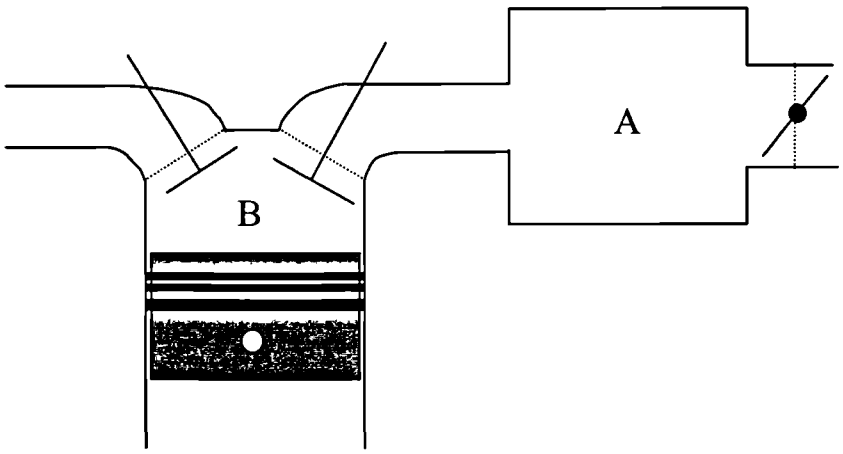

Figure 3.1
Schematic representation of control volumes and restrictions of a typical SI engine

The GFEE is applied in two different forms depending on whether it relates to a control volume or to one of the restrictions. The following sections discuss the individual terms in the equations and how they are combined to produce a suitable model.

3.3. The GFEE applied to control volumes

The GFEE is based on the first law of thermodynamics, relating internal energy within a control volume to mass, heat and work transfer across the control volume boundaries. Watson and Janota (1982) present the GFEE in a form suitable for application to IC engines. For a control volume, such as a cylinder (e.g. control volume B in Figure 3.1), the GFEE can be written as follows:

$$\frac{dU}{dt} = \frac{dQ}{dt} - \frac{dW}{dt} + \sum_j \frac{dH_0}{dt} \tag{3.1}$$

Where U is the internal energy, Q is the heat transfer into the control volume, W the work done, H_0 the enthalpy, and j denotes different entries to the control volume under consideration. Some of the terms in Equation (3.1) can be converted to a specific basis by the introduction of m the mass within the control volume, while others can be expanded to give:

$$m\frac{du}{dt} + u\frac{dm}{dt} = \frac{dQ}{dt} - p\frac{dV}{dt} + \sum_{in} m\frac{dh_0}{dt} - \sum_{out} m\frac{dh_0}{dt} \tag{3.2}$$

It is worth noting that Equation (3.2) neglects the potential energy terms, as their effects will be negligible. Any kinetic energy associated with the flow can be incorporated within the enthalpy terms by using stagnation values h_0.

3.3.1. Modelling procedure

Equation (3.2) allows the changes to the internal energy of the working fluid within a control volume to be estimated knowing the heat transfer, work and enthalpy terms. It relies on knowledge of the internal energy of the gas within the control volume, which will be a function of position, composition, temperature, and the mass and pressure within the control volume. For an SI engine, the volume exhibiting the greatest variation in these would be the cylinder, particularly during combustion. As long as combustion is ignored, it is reasonable to assume a homogeneous composition for the gas within the engine, particularly for a model designed to give information on gas flows during the induction and exhaust strokes. The only useful information which modelling combustion would yield for such an application is the condition of the gas inside the cylinder at the instant the exhaust valve opens. To reduce complexity, it was

decided to avoid modelling combustion, instead utilising experimental data, which could be readily measured. Consequently, the contents of all the control volumes were assumed to be homogeneous. The effects of chemical dissociation, which again are most significant during combustion, were also neglected allowing the model to be simplified further. Under such assumptions, the internal energy is reduced to being a function of only the temperature T, and the equivalence ratio F. Thus:

$$u = u(T, F) \tag{3.3}$$

Where:

$$F = \frac{(m_f/m_a)_{actual}}{(m_f/m_a)_{stoich}} = \frac{f_{actual}}{f_{stoich}} = \frac{m_f}{m_a f_{stoich}} \tag{3.4}$$

This simplification allows the first term in Equation (3.2) to be partially differentiated giving:

$$m\left[\frac{\partial u}{\partial T}\frac{dT}{d\theta} + \frac{\partial u}{\partial F}\frac{dF}{d\theta}\right] + u\frac{dm}{d\theta} = \frac{dQ}{d\theta} - p\frac{dV}{d\theta} + h_{in}\frac{dm_{in}}{d\theta} - h_{out}\frac{dm_{out}}{d\theta} \tag{3.5}$$

The base has been changed from one of time, t, to one of crank angle, θ, as this is more convenient for engine cycle calculations. Equation (3.5) can now be combined with an equation for the conservation of mass (Equation (3.6)) and the ideal gas equation (Equation (3.7)) to allow changes within a series of connected control volumes to be estimated knowing the flow rates between them.

$$\frac{dm}{d\theta} = \sum_{in}\frac{dm}{d\theta} - \sum_{out}\frac{dm}{d\theta} \tag{3.6}$$

$$p = \frac{mRT}{V} \tag{3.7}$$

3.3.2. Estimating properties of the working fluid

The two main types of gas present within an IC engine are the air drawn into the engine, and the exhaust gases produced as a result of the combustion process. Vaporised fuel would also be present in smaller quantities in the port and cylinder, however, the difficulties associated with modelling the behaviour of gasoline in such regions means that fuelling was ignored. Instead, it was assumed that fuel is added directly into the cylinder after the inlet valve has shut. A mixture of air and exhaust gas therefore represented the gas in the port and the cylinder during the

induction, compression and exhaust strokes. The GFEE can only be applied once the properties of the gas within the control volume and of any gas flowing in or out are known. A mixture of exhaust gas ($F = 1$) and air ($F = 0$) can be thought of as the product of burning a mixture leaner than stoichiometric.

Krieger and Borman (1966) presented approximations for the specific gas constant, R, and the specific internal energy, u, as a function of equivalence ratio and temperature.

$$R = 287 + (20F) \quad \text{J/kgK} \tag{3.8}$$

And

$$u = K_1(T) - K_2(T)F \quad \text{J/kg} \tag{3.9}$$

K_1 and K_2 are both functions of temperature only and are given by:

$$K_1 = 692T + 39.17\times10^{-3}T^2 + 59.2\times10^{-6}T^3 - 228.62\times10^{-10}T^4 + 277.58\times10^{-14}T^5$$
$$K_2 = 3049.39\times10^3 - 57T - 9.5\times10^{-2}T^2 + 21.53\times10^{-6}T^3 - 200.26\times10^{-11}T^4$$

Equations (3.8) and (3.9) are both in terms of the original mass of air used to produce the exhaust gas/air mixture. Equation (3.4) can be used to express R and u in terms of the total mass. The total mass must be the sum of the mass of air and burned fuel:

$$m = m_a + m_f \tag{3.10}$$

Knowing F therefore allows the individual components of the mixture to be expressed in terms of the total mass in the control volume:

$$m_a = \frac{m_a}{m}\times m = \frac{m_a m}{m_a + m_f} = \frac{m}{\left[1 + (m_f/m_a)\right]} = \frac{m}{1 + Ff_{stoich}}$$

$$\Rightarrow m_a = \frac{m}{F'} \tag{3.11}$$

Where

$$F' = 1 + Ff_{stoich} \tag{3.12}$$

Similarly

$$m_f = \frac{mFf_{stoich}}{F'} \tag{3.13}$$

Equations (3.11) and (3.13) can now be used to express R and u in terms of the total mass of gas within a control volume.

$$R \times \frac{m_a}{m} = R \times \frac{m_a}{m_a + m_f} = \frac{R \times \frac{m}{F'}}{\frac{m}{F'} + \frac{mFf_{stoich}}{F'}} = \frac{R}{(1 + Ff_{stoich})} = \frac{R}{F'} \tag{3.14}$$

The specific enthalpy of such a gas can be evaluated from the following relationship:

$$h = u + RT \tag{3.15}$$

The last property of the gas that needs to be evaluated is the ratio of the specific heats given by:

$$\gamma = \frac{c_p}{c_v} \tag{3.16}$$

However, c_p and c_v are also related through the specific gas constant:

$$R = c_p - c_v \tag{3.17}$$

The specific heat at constant volume is defined as:

$$c_v = \frac{du}{dT} \tag{3.18}$$

c_v can now be evaluated by differentiating Equation (3.9) with respect to temperature, allowing c_p, and hence γ to be calculated.

All the gas property calculations rely on the equivalence ratio for the gas in the control volume being known. Flows of gas with different F values will serve to alter the value of F within the control volume. The effect of this is included in the GFEE and will therefore need to be computed. Differentiating the right side of Equation (3.4) gives:

$$\frac{dF}{d\theta} = \frac{1}{f_{stoich}}\left\{(m - m_f)\frac{dm_f}{d\theta} - m_f\left(\frac{dm}{d\theta} - \frac{dm_f}{d\theta}\right)\right\}\frac{1}{m_a^2} \tag{3.19}$$

$$\Rightarrow \frac{dF}{d\theta} = \frac{1}{f_{stoich} m_a}\left\{\frac{m}{m_a}\frac{dm_f}{d\theta} - \frac{m_f}{m_a}\frac{dm}{d\theta}\right\} \tag{3.20}$$

Substituting for m_a from Equation (3.11) into Equation (3.20) gives:

$$\frac{dF}{d\theta} = \frac{F'}{m}\left\{\frac{F'}{f_{stoich}}\frac{dm_f}{d\theta} - F\frac{dm}{d\theta}\right\} \tag{3.21}$$

An approximation can be made at this stage:

$$\frac{dm_f}{d\theta} = \left(\frac{dm_f}{d\theta}\right)_{in} - \left(\frac{dm_f}{d\theta}\right)_{out} \tag{3.22}$$

From Equation (3.13):

$$\frac{dm_f}{d\theta} = \frac{F_{in} f_{stoich}}{F_{in}'}\frac{dm_{in}}{d\theta} - \frac{F_{out} f_{stoich}}{F_{out}'}\frac{dm_{out}}{d\theta} \tag{3.23}$$

Thus:

$$\frac{dF}{d\theta} = \frac{F'}{m}\left\{\frac{F'}{f_{stoich}}\left[\frac{F_{in} f_{stoich}}{F_{in}'}\frac{dm_{in}}{d\theta} - \frac{F_{out} f_{stoich}}{F_{out}'}\frac{dm_{out}}{d\theta}\right] - F\frac{dm}{d\theta}\right\} \tag{3.24}$$

Writing Equation (3.24) only in terms of the mass flow rates in and out:

$$\begin{aligned}\frac{dF}{d\theta} &= \frac{F'}{m}\left\{F'\frac{F_{in}}{F_{in}'}\frac{dm_{in}}{d\theta} - F'\frac{F_{out}}{F_{out}'}\frac{dm_{out}}{d\theta} - F\frac{dm_{in}}{d\theta} + F\frac{dm_{out}}{d\theta}\right\} \\ \Rightarrow \frac{dF}{d\theta} &= \frac{F'}{m}\left\{\left(F'\frac{F_{in}}{F_{in}'} - F\right)\frac{dm_{in}}{d\theta} - \left(F'\frac{F_{out}}{F_{out}'} - F\right)\frac{dm_{out}}{d\theta}\right\}\end{aligned} \tag{3.25}$$

3.4. Compressible flow equations

3.4.1. Flow past an orifice

The control volumes used to model an SI engine are connected to each other through two types of restriction; namely the inlet and exhaust valves and the throttle. Knowing conditions on either

side of such a restriction, it is possible to apply equations for the isentropic flow of a compressible fluid past an orifice. The basic flow equations are derived from the application of the GFEE to compressible flow in a duct and a complete derivation can be found in a standard text on thermodynamics such as Rogers and Mayhew (1992). The compressible flow equation for mass transfer past an orifice can be written as:

$$\frac{dm}{dt} = C_d A_2 p_1 \sqrt{\left\{\left(\frac{2\gamma_1}{\gamma_1 - 1}\right)\frac{1}{RT_1}\left[\left(\frac{p_2}{p_1}\right)^{2/\gamma_1} - \left(\frac{p_2}{p_1}\right)^{(\gamma_1+1)/\gamma_1}\right]\right\}} \qquad \textbf{(3.26)}$$

The corresponding equation for the velocity is given by:

$$C_2^{\,2} - C_1^{\,2} = \left[\left(\frac{2\gamma_1}{1-\gamma_1}\right)RT_1\left\{\left(\frac{p_2}{p_1}\right)^{(\gamma_1-1)/\gamma_1} - 1\right\}\right] \qquad \textbf{(3.27)}$$

The subscripts '1' and '2' refer to conditions upstream and at the orifice respectively, and C refers to the velocity. The pressure upstream will be known, the pressure at the orifice, however, may not. At this stage, a simplification is made. It is assumed that the pressure downstream of the restriction is the same as that at the orifice. Watson and Janota (1982) state that this is a common assumption as the turbulent nature of the flow means that there is very little pressure recovery downstream of the restriction. C_d is an empirically-derived discharge coefficient to account for secondary flow effects, boundary layer separation, friction etc. [Watson and Janota (1982)]. The nature of the discharge coefficient for the poppet valves was investigated in the preceding chapter. A model for the throttle will be presented in the following section.

In certain cases the flow past the valves will reach sonic speeds, and become choked. Under such conditions, the mass flow rate and velocity will be independent of the downstream pressure, and more simple equations can be used for calculating them:

$$\frac{dm}{dt} = C_d A_2 p_1 \sqrt{\left[\frac{\gamma_1}{RT_1}\left(\frac{2}{\gamma_1+1}\right)^{(\gamma_1+1)/(\gamma_1-1)}\right]} \qquad \textbf{(3.28)}$$

$$C_2^{\,2} - C_1^{\,2} = \left(\frac{2\gamma_1}{1+\gamma_1}\right)RT_1 \qquad \textbf{(3.29)}$$

The critical pressure ratio is a function of the ratio of the principal specific heats for the gas

under consideration and is given by:

$$\left(\frac{p_2}{p_1}\right)_{crit} = \left(\frac{2}{\gamma_1 + 1}\right)^{\gamma_1/(\gamma_1 - 1)} \tag{3.30}$$

3.4.2. Flow past the throttle

The effective flow area for a throttle can be calculated from a combination of the throttle open area and a discharge coefficient. However, determination of the discharge coefficient for the particular throttle used on the engine is not important for the purposes of a model. Instead, the flow area can be calculated from the angle and geometry of the throttle, the important dimensions for which are shown in Figure 3.2.

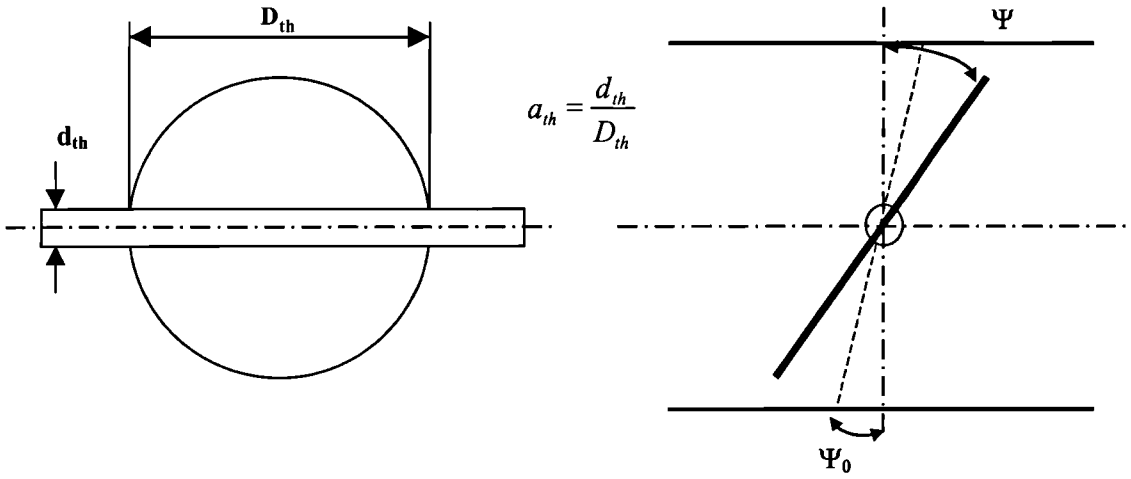

Figure 3.2
Geometry of throttle plate

Heywood (1988) (originally from Harrington and Bolt (1970)), presents the following expression for the throttle open area:

$$A_{th} = \frac{\pi D_{th}^2}{4}\left\{\left(1 - \frac{\cos\psi}{\cos\psi_0}\right) + \frac{2}{\pi}\left[\frac{a_{th}}{\cos\psi}\sqrt{\left(\cos^2\psi - a_{th}^2\cos^2\psi_0\right)}\right.\right.$$
$$\left.\left. + \frac{\cos\psi}{\cos\psi_0}\sin^{-1}\left(\frac{a_{th}\cos\psi_0}{\cos\psi}\right) - a_{th}\sqrt{\left(1 - a_{th}^2\right)} - \sin^{-1}a_{th}\right]\right\} \tag{3.31}$$

The discharge coefficient can be expressed in terms of the throttle angle and the pressure ratio across it [Heywood (1988), originally from DeLosh *et al.* (1981)].

$$C_d = \{0.451 + 2.465\times10^{-2}(\psi-\psi_0) - 6.153\times10^{-4}(\psi-\psi_0)^2 + 7.25\times10^{-6}(\psi-\psi_0)^3 - 2.7\times10^{-8}(\psi-\psi_0)^4\}\left(\frac{p_2}{p_1}\right)^{0.1} \quad (3.32)$$

3.5. Heat transfer to the cylinder walls

The GFEE contains a term to cater for heat transfer across the surfaces of the control volume. Heat transfer will be present to varying extents in different parts of the engine. For example, heat transfer in the port will, in general, be quite small apart from periods of backflow from the cylinder. Heat transfer in the cylinder, however, will be more significant since the wall temperatures will have been raised as a consequence of combustion. Heywood (1988) discusses three types of correlation for heat flux; those intended to predict time-averaged heat flux to the chamber walls, correlations for the instantaneous spatially-averaged heat flux and those for instantaneous local heat fluxes. Of these, a correlation for the instantaneous spatially-averaged heat flux is most suitable for incorporation into a model designed for engine performance analysis. A convective heat transfer coefficient (h_t) can be defined from the equation [Watson and Janota (1982)]:

$$\frac{\dot{Q}}{A_{cyl}} = h_t(T_g - T_{sf}) \quad (3.33)$$

T_g and T_{sf} are the gas and surface temperatures, respectively, and A_{cyl} is the area of the cylinder surfaces. Heywood (1988) uses dimensional analysis to show that h_t can be related to a number of properties for the gas and the physical dimensions of the system under consideration. A relationship between the Nusselt (which incorporates h_t), Prandtl, and Reynolds numbers can be established which is analogous to that for turbulent flow in pipes or over flat plates, and it takes the following form:

$$Nu = a_1 Re^{a_2} Pr^{a_3} \quad (3.34)$$

Where a_1, a_2, and a_3 are constants. Watson and Janota (1982) argue that the variation in Prandtl number is small, allowing it to be omitted with little loss of accuracy.

One of the most common correlations based on this simplified model is that due to Annand (1963) which hides the exact nature of the relationship given in Equation (3.34) by using two further empirically derived constants K_1' and K_2':

$$\frac{\dot{Q}}{A_{cyl}} = K_1' \frac{k}{B}(Re)^{K_2'}(T_g - T_{sf}) \tag{3.35}$$

Annand (1963) found that the value of K_1' varied with engine speed and design, typically lying between 0.35 and 0.8 with K_2' set to 0.7. Baker (1995) found that a value of 0.4 for K_1' and 0.8 for K_2' gave good results for his model, and these were the values adopted for the current program. He also estimated the thermal conductivity k by curve fitting data tabulated by Rogers and Mayhew (1992), in which k could be related to the film temperature, defined as the mean of the gas and surface temperatures. The characteristic velocity used in calculating the Re was the piston speed, the characteristic dimension being B, the cylinder bore.

3.6. Incorporating physical engine data

The GFEE contains a term for the work done by the piston, which in turn, is related to the rate of change of cylinder volume. The heat transfer model requires information about the surface area and piston speed, whilst the ideal gas equation requires information about the cylinder volume. These can all be calculated from the geometry of the crank mechanism. Heywood (1988) gives standard equations for each of these quantities.

3.7. Numerical integration

It can be seen from Equation (3.5) that many of the terms within it can be calculated by expressions given in the preceding sections. The compressible flow equations allow calculation of the mass flows in and out. Knowing the properties of these flows allows calculation of the enthalpies associated with them, together with their effect on the equivalence ratio for the gas within the control volume. Heat transfer can be estimated for the cylinder, by means of the heat transfer model and knowledge of the cylinder area and piston speed. The work term can be estimated from knowledge of the rate of change of cylinder volume. Both heat transfer and work for the port are assumed to be zero. Equation (3.5) therefore allows the rate of change of temperature to be estimated at any particular instant in time, which on integration allows the temperature at a subsequent time to be estimated. Once this has been achieved, Equation (3.6) can be employed to estimate the change in mass for the control volume, finally allowing the ideal gas equation to be used to calculate the pressure.

The method employed to calculate temperature, mass and equivalence ratio at the end of a step

was found to have a significant effect on the stability of the program. Given a starting value $y(x)$, the value at a subsequent point $y(x+h)$ can be expressed as a Taylor series:

$$y(x+h) = y(x) + hy'(x) + \frac{h^2}{2}y''(x) + \ldots\ldots \tag{3.36}$$

For very small values of h, the higher order terms in Equation (3.36) can be neglected leaving:

$$y(x+h) \approx y(x) + hy'(x) \tag{3.37}$$

This scheme is known as the Euler method for numerical integration and is shown graphically in Figure 3.3.

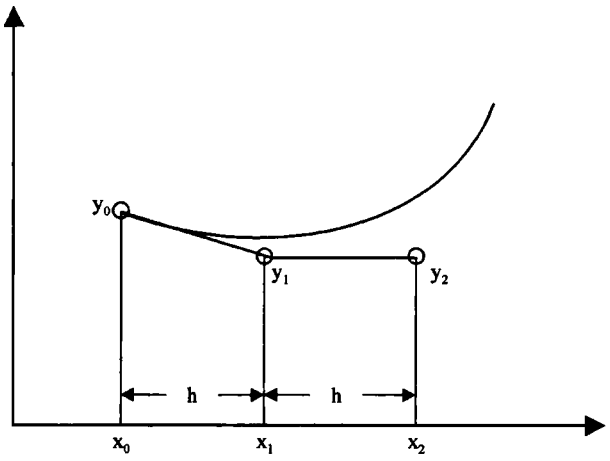

Figure 3.3
Graphical representation of Euler method for numerical integration

In practice, use of the Euler method was found to lead to instability when large gradients were encountered, for example during the valve overlap period. Baker (1995) successfully used the Euler method although he employed a scheme to detect and suppress oscillatory behaviour, accepting the inevitable loss in precision. In fact, it is generally accepted that the Euler method is not suitable for numerical integration and is rarely used [Kreyszig (1993)]. Watson and Janota (1982) recommend the use of either a predictor-corrector method or the fourth order Runge-Kutta method. Press *et al.* (1995) suggest that the Runge-Kutta method is to be preferred for general-purpose applications and that predictor-corrector methods have now been superseded by superior techniques.

A detailed explanation of the Runge-Kutta method can be found in many standard texts on mathematics and numerical techniques, e.g. Kreyszig (1993). The method uses four estimates for the gradient, one at the beginning, two at half the step size ($x+h/2$) and one at the end, k_1, k_2, k_3,

and k_4 respectively. These are termed auxiliary values and are used instead of computing the higher derivatives in Equation (3.36). The Runge-Kutta algorithm can be summarised as:

$$\begin{aligned} k_1 &= hf(x_n, y_n) \\ k_2 &= hf\left(x_n + \tfrac{1}{2}h, y_n + \tfrac{1}{2}k_1\right) \\ k_3 &= hf\left(x_n + \tfrac{1}{2}h, y_n + \tfrac{1}{2}k_2\right) \\ k_4 &= hf(x_n + h, y_n + k_3) \\ x_{n+1} &= x_n + h \\ y_{n+1} &= y_n + \tfrac{1}{6}k_1 + \tfrac{1}{3}k_2 + \tfrac{1}{3}k_3 + \tfrac{1}{6}k_4 \end{aligned} \qquad \textbf{(3.38)}$$

It was decided to adopt such an algorithm to estimate the mass flow rates in and out, the change in equivalence ratio, and the change in temperature over the step. It must be borne in mind that the procedure required the GFEE to be solved four times for every step, therefore increasing the computing overhead. However, it did provide an effective solution to the issue of instability.

When using the Runge-Kutta method to estimate the end values for mass, temperature and F, there will be four estimates for the mass flow rates in and out with their corresponding F values, and similarly for the rate of change of temperature. Thus:

$$\begin{aligned} \frac{dm_{in}}{d\theta} &= \frac{1}{6}\frac{dm_{in}}{d\theta}_1 + \frac{1}{3}\frac{dm_{in}}{d\theta}_2 + \frac{1}{3}\frac{dm_{in}}{d\theta}_3 + \frac{1}{6}\frac{dm_{in}}{d\theta}_4 \\ \frac{dm_{out}}{d\theta} &= \frac{1}{6}\frac{dm_{out}}{d\theta}_1 + \frac{1}{3}\frac{dm_{out}}{d\theta}_2 + \frac{1}{3}\frac{dm_{out}}{d\theta}_3 + \frac{1}{6}\frac{dm_{out}}{d\theta}_4 \\ \frac{dT}{d\theta} &= \frac{1}{6}\frac{dT}{d\theta_1} + \frac{1}{3}\frac{dT}{d\theta_2} + \frac{1}{3}\frac{dT}{d\theta_3} + \frac{1}{6}\frac{dT}{d\theta_4} \end{aligned} \qquad \textbf{(3.39)}$$

These can be used to estimate the equivalence ratio at the end of the step:

$$F_{end} = \frac{1}{f_{stoich}}\left(\frac{m_f}{m_a}\right)_{end} = \frac{1}{f_{stoich}}\left\{\frac{\frac{mFf_{stoich}}{F'} + \frac{F_{in}f_{stoich}}{F'_{in}}\frac{dm_{in}}{d\theta}\Delta\theta - \frac{F_{out}f_{stoich}}{F'_{out}}\frac{dm_{out}}{d\theta}\Delta\theta}{\frac{m}{F'} + \frac{1}{F'_{in}}\frac{dm_{in}}{d\theta}\Delta\theta - \frac{1}{F'_{out}}\frac{dm_{out}}{d\theta}\Delta\theta}\right\}$$

$$\Rightarrow F_{end} = \left\{ \frac{\frac{mF}{F'} + \left(\frac{F_{in}}{F'_{in}} \frac{dm_{in}}{d\theta} - \frac{F_{out}}{F'_{out}} \frac{dm_{out}}{d\theta} \right) \Delta\theta}{\frac{m}{F'} + \left(\frac{1}{F'_{in}} \frac{dm_{in}}{d\theta} - \frac{1}{F'_{out}} \frac{dm_{out}}{d\theta} \right) \Delta\theta} \right\} \tag{3.40}$$

Where:

$$\frac{F_{in}}{F'_{in}} \frac{dm_{in}}{d\theta} = \left\{ \frac{1}{6} \left(\frac{F_{in}}{F'_{in}} \frac{dm_{in}}{d\theta} \right)_1 + \frac{1}{3} \left(\frac{F_{in}}{F'_{in}} \frac{dm_{in}}{d\theta} \right)_2 + \frac{1}{3} \left(\frac{F_{in}}{F'_{in}} \frac{dm_{in}}{d\theta} \right)_3 + \frac{1}{6} \left(\frac{F_{in}}{F'_{in}} \frac{dm_{in}}{d\theta} \right)_4 \right\}$$

$$\frac{F_{out}}{F'_{out}} \frac{dm_{out}}{d\theta} = \left\{ \frac{1}{6} \left(\frac{F_{out}}{F'_{out}} \frac{dm_{out}}{d\theta} \right)_1 + \frac{1}{3} \left(\frac{F_{out}}{F'_{out}} \frac{dm_{out}}{d\theta} \right)_2 + \frac{1}{3} \left(\frac{F_{out}}{F'_{out}} \frac{dm_{out}}{d\theta} \right)_3 + \frac{1}{6} \left(\frac{F_{out}}{F'_{out}} \frac{dm_{out}}{d\theta} \right)_4 \right\}$$

$$\frac{1}{F'_{in}} \frac{dm_{in}}{d\theta} = \left\{ \frac{1}{6} \left(\frac{1}{F'_{in}} \frac{dm_{in}}{d\theta} \right)_1 + \frac{1}{3} \left(\frac{1}{F'_{in}} \frac{dm_{in}}{d\theta} \right)_2 + \frac{1}{3} \left(\frac{1}{F'_{in}} \frac{dm_{in}}{d\theta} \right)_3 + \frac{1}{6} \left(\frac{1}{F'_{in}} \frac{dm_{in}}{d\theta} \right)_4 \right\}$$

$$\frac{1}{F'_{out}} \frac{dm_{out}}{d\theta} = \left\{ \frac{1}{6} \left(\frac{1}{F'_{out}} \frac{dm_{out}}{d\theta} \right)_1 + \frac{1}{3} \left(\frac{1}{F'_{out}} \frac{dm_{out}}{d\theta} \right)_2 + \frac{1}{3} \left(\frac{1}{F'_{out}} \frac{dm_{out}}{d\theta} \right)_3 + \frac{1}{6} \left(\frac{1}{F'_{out}} \frac{dm_{out}}{d\theta} \right)_4 \right\}$$

and $\Delta\theta$ is the step size in degrees crank angle.

3.8. **Modelling a multi-cylinder engine**

A model of a complete engine has to cater for the filling and emptying effect produced by the presence of other cylinders. This will normally manifest itself through changes in the pressure, temperature and composition of the gas in the plenum. There are two possible ways to model the effect of other cylinders. The first is to model every cylinder as a separate control volume, for which the GFEE can be solved. However, the results for each cylinder would be identical once the model has converged. An alternative approach was adopted for this program. The GFEE was applied to only one cylinder and a record of the properties for the plenum and cylinder together with a record for the flow rates from one to the other were kept. The effect of the other cylinders was modelled by using data calculated at an earlier crank angle. This principle can be demonstrated by using the case of a two-cylinder engine as an example. If it is assumed that the cylinders fire with equal spacing, the cylinders will effectively be 360° out of phase with each other. To estimate the effect of the additional cylinder, the flow into or out of the cylinder being modelled 360° earlier is used to represent conditions in the other cylinder. The effect is to add extra mass and enthalpy terms and a term for changes in composition to the GFEE for the

plenum. For the engine under consideration, such a scheme was extended to account for the seven other cylinders of its V8 configuration.

3.9. The complete model

The previous discussions have shown how, given the conditions within a series of control volumes at some instant in time, it is possible to estimate the conditions at a later point. All that remains is to provide information on the initial conditions within the control volume.

The model was designed to start at EVO and run through a complete engine cycle of 720°. Although combustion is ignored, modelling of the cylinder is continued to cater for the possibility of adding a heat release model later. For the first cycle only, the conditions in the cylinder at EVO need to be given by setting a pressure and temperature for the exhaust gas in the cylinder. As the model is designed to simulate operation with closed-loop fuelling, the equivalence ratio for the gas is known together with the cylinder volume. Application of the ideal gas equation allows the mass in the cylinder to be estimated. Similarly, the plenum pressure and temperature together with an initial throttle angle are set. The exact values are not important, providing they are realistic, as the model will soon converge to the correct settings. Subsequent cycles only require the pressure in the cylinder at EVO to be set. The only other information that the model requires is the target mass flow rate, which it attempts to match by adjusting the throttle.

The model was implemented in three parts. The main algorithm presented so far was written in C++. The program made full use of Object Oriented Programming (OOP) techniques, which allowed the control volumes and restrictions to be coded as individual components that could then be assembled into a representation of the engine. A pre-processing routine was written in MATLAB, which converted the camshaft profile and valve discharge coefficient data into an appropriately sized array dependent on the number of steps per degree crank angle. Finally, another MATLAB routine was used to convert the model output files into useful predictions of RGF, pumping work and properties of the gases within each control volume. This post-processing routine also calculated flow velocities, mass flow rates and the momentum associated with the gas flow past the inlet valves. The operation of the model can best be explained by means of a flow diagram, which is shown in Figure 3.4.

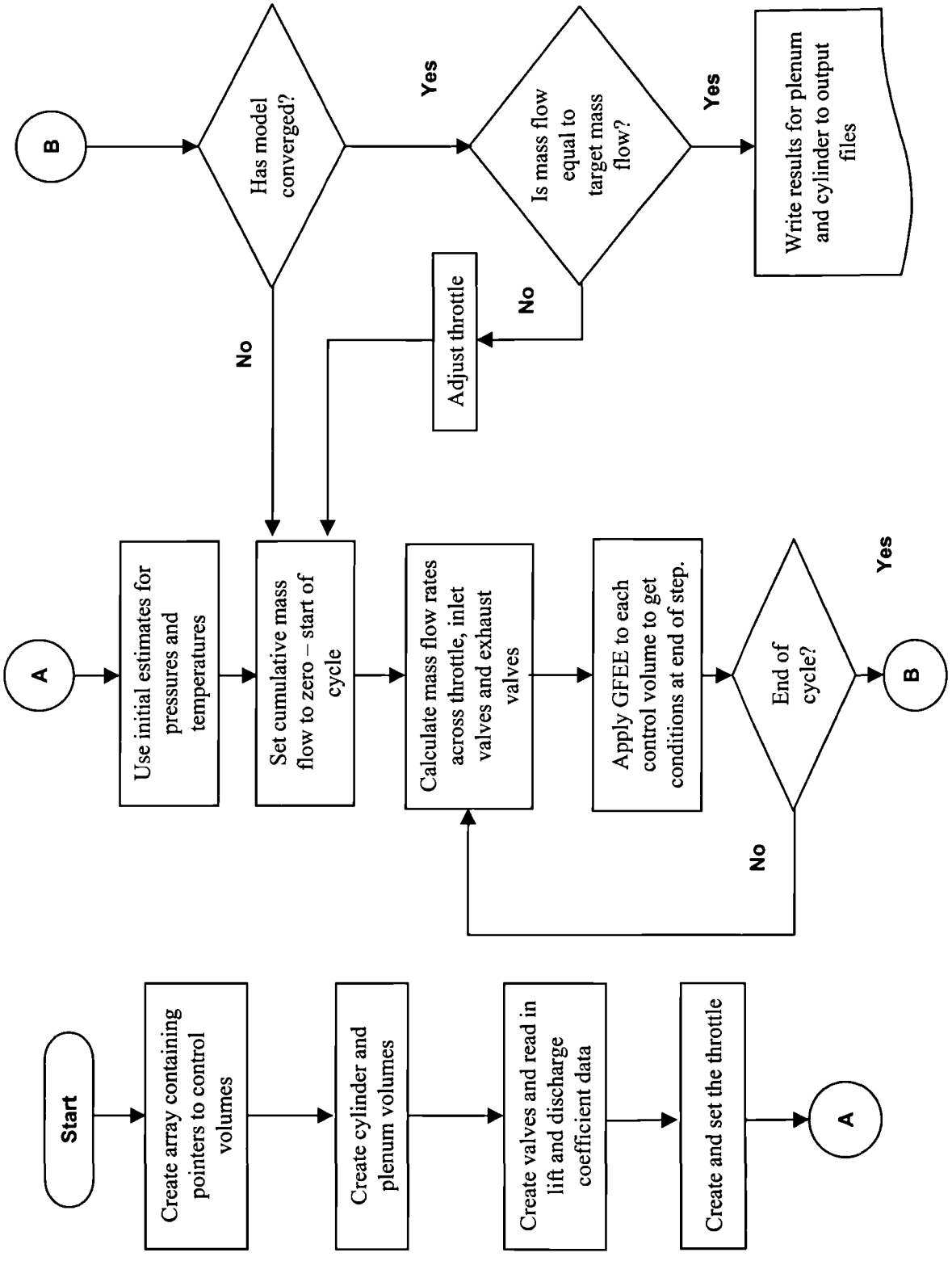

Figure 3.4
Schematic representation showing operation of model

3.10. Initial results

The model was to be applied to the majority of tests conducted during the research program. Consequently, most of the results are presented in the appropriate chapters. This section presents the results for two camshaft settings, taken from the first series of engine tests, to demonstrate the type of information produced. The tests were run to simulate an engine condition of 1500 rev/min, 2.62 bar BMEP. The target mass flow was determined from the reading taken from the engine airflow sensor. The remaining values, such as exhaust gas temperature, were also taken from experimental data. Table 3-1 gives details of the valve event settings discussed in this section.

Setting No.	EVO (° bBDC)	IVO (° bTDC)	EVC (° aTDC)	IVC (° aTDC)	RGF (%)	PMEP (bar)
1	35	27.5	15	217.5	33.5	0.44
2	35	-2.5	15	247.5	19.3	0.52

Table 3-1
Valve event settings used for demonstration of results

3.10.1. Predicting residual levels

The equivalence ratio at the end of the induction stroke represents a mixture of exhaust gas and air. The quantity of exhaust gas determines the residual gas fraction trapped within the cylinder and can be calculated by using Equation (3.41).

$$RGF = 100 \times \frac{F(1 + f_{stoich})}{F'} \tag{3.41}$$

The RGF for each test condition is calculated by the post-processing routine and is recorded as a single value. The predicted RGF values for the two strategies are also given in Table 3-1.

3.10.2. Pumping work

The work, which the engine expends in inducing fresh charge and expelling exhaust gases will depend on the valve timing strategy employed. Figure 3.5 shows the pumping section of pressure-volume diagram for the two valve event settings.

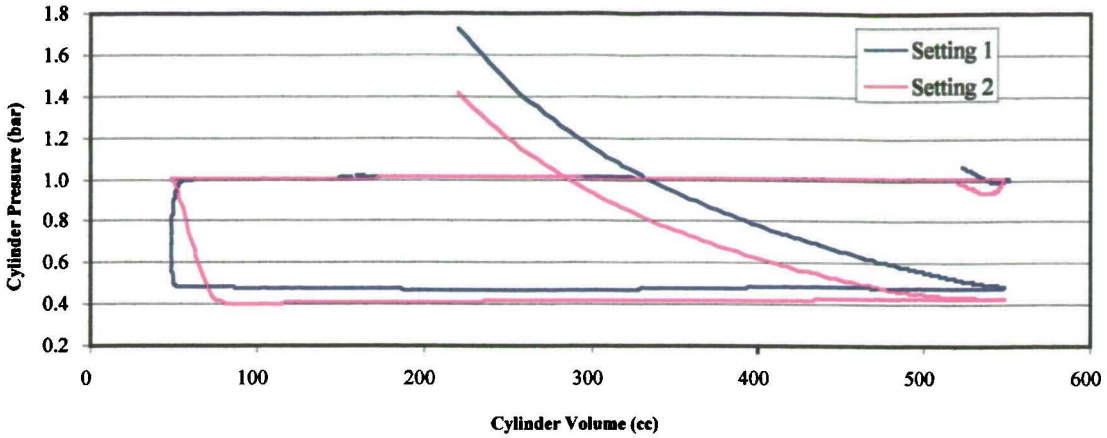

Figure 3.5
Pumping loop predictions

The post-processing routine also integrates the area under the curve between BDC on the exhaust stroke and BDC on the induction stroke. The value is then converted into a mean effective pressure before being recorded. Table 3-1 gives the PMEP values for the two settings. It is apparent that a greater overlap period leads to higher residual levels, which in turn, necessitate a higher plenum pressure and hence reduced pumping work.

3.10.3. Gas velocity, flow rate and momentum

Equations (3.26) to (3.29) can be employed to estimate the mass flow rate and velocity of the gas flowing past the inlet valve. These are shown in Figure 3.6 and Figure 3.7 respectively.

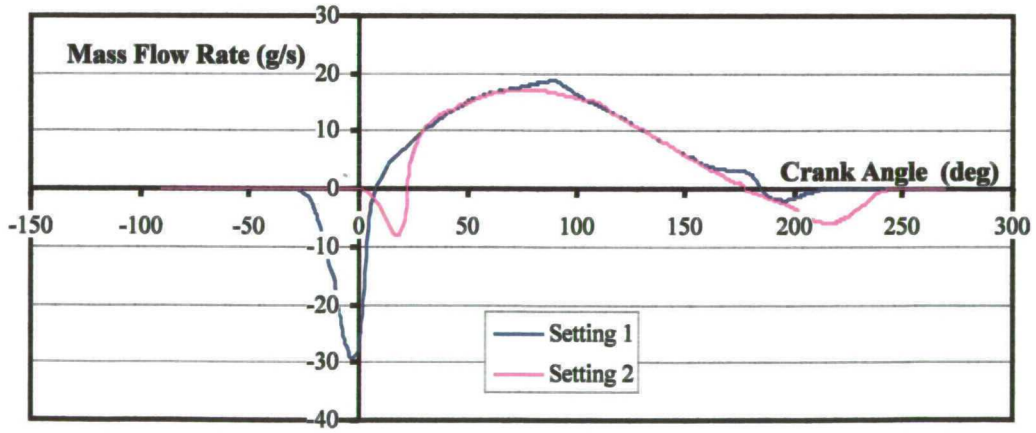

Figure 3.6
Comparison of mass flow rate/crank angle characteristics for two valve event settings

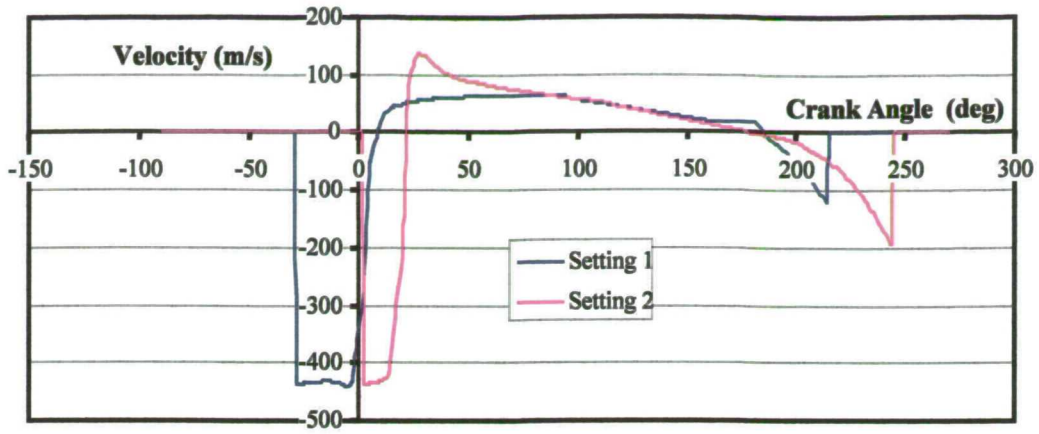

Figure 3.7
Comparison of velocity/crank angle characteristics for two valve event settings

The product of gas velocity and flow rate represents the momentum associated with the flow and has a direct influence on the intensity of the in-cylinder turbulence generated (Figure 3.8). Differences in flow/crank angle histories may be influential in determining the usefulness of the momentum in creating such in-cylinder motion, as higher levels towards the end of the induction stroke are thought to be beneficial [Baker (1995)].

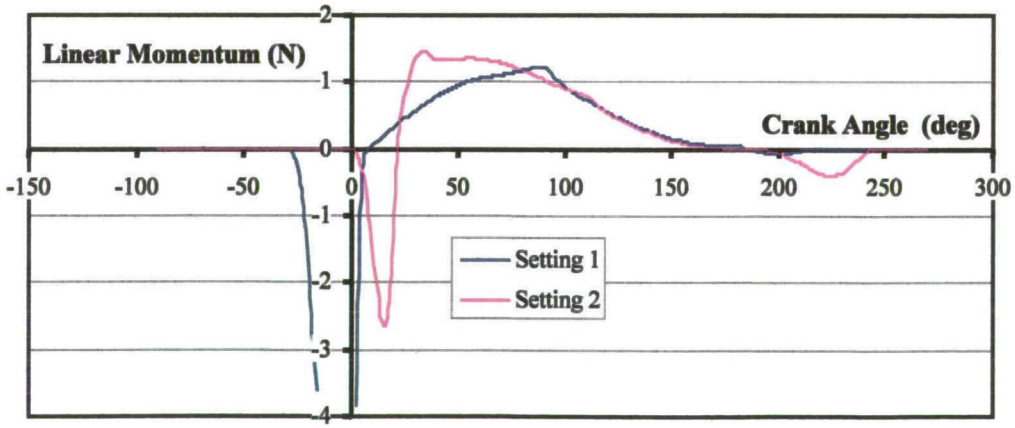

Figure 3.8
Comparison of flow momentum/crank angle characteristics for two valve event settings

3.11. Other methods for modelling intake port flows and mixing

The model described in this chapter assumes perfect mixing of backflow gases with the gas in the plenum. In reality, there will be some turbulent mixing in the port, although its effect would not be significant in the plenum itself. Before writing the current program, two other approaches to the modelling of backflow were attempted. The first was to assume 'plug flow' for the

exhaust gas travelling back up the port. This meant the creation and destruction of a third control volume representing the exhaust gas in the port. Although the program functioned reasonably for most of the cycle, it had problems with stability as the control volume was destroyed. This was because the gas properties were markedly different for the exhaust gas and the bulk of gas in the plenum. It should be mentioned that, at that time, the simple Euler method of integration was being employed, and it may be possible to overcome the stability problem using the Runge-Kutta method.

The second method adopted a more sophisticated technique. The port volume was divided into a number of smaller volumes, each of which contained a homogenous mixture of gases. The mixing effect could then be modelled by allowing these smaller volumes to contain gas of different compositions. A schematic for these port volumes is shown in Figure 3.9

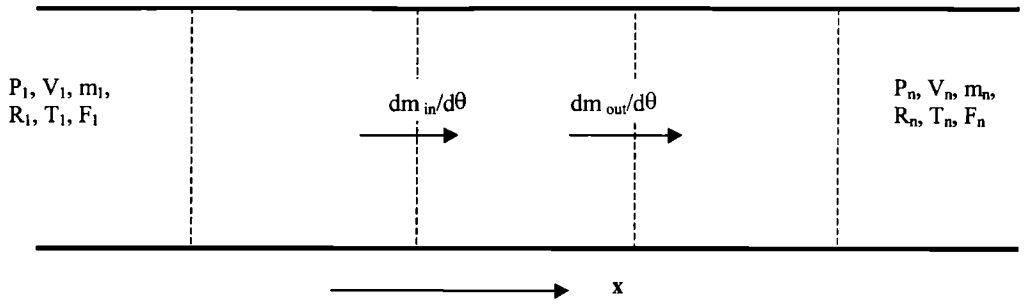

Figure 3.9
Schematic representation of port volumes

The program required information on the mass transfers between these control volumes to allow the GFEE to be solved for each. It was decided to assume that the pressure rise in all the volumes was the same, allowing a series of simultaneous equations to be established. These could then be solved by matrix inversion to give the mass flows between the volumes. For this method to work, the direction of the flows needed to be known before the simultaneous equations could be set up. An iterative scheme was devised which took an initial guess at the flow directions, solved the resulting equations to see if the guess and the results agreed, and then adjusted them accordingly. It was found that during backflow, the iterative scheme could not converge and would simply switch from one combination of flow directions to the other. A solution for this problem was not found and the scheme was consequently abandoned. Appendix 2 gives details of the method employed to establish the simultaneous equations.

3.12. Concluding comments

The assumption of perfect mixing between the backflow gases and gases in the plenum means that the model predictions of RGF within the cylinder have some error in their absolute values. This, in turn, affects the absolute values of pumping work for the gas exchange processes. However, the model should be accurate in revealing trends for the variation of RGF and pumping work with changes in valve events, and it should still be capable of aiding the interpretation of the engine test results. These limitations of the model should be borne in mind when it is applied to the engine test conditions described in chapters 6 and 7.

Chapter 4

DESIGN OF EXPERIMENTS

4. Design of Experiments

4.1. Introduction

The potential for improving engine efficiency and reducing emissions by adopting VVA was discussed in Chapter 1. The lack of understanding of how the various methods would interact together to alter an engine's performance makes it difficult to suggest a particular strategy for any given purpose. There is an obvious need to further knowledge in this area by investigating such interactions and quantifying the potential advantages and disadvantages. The potentially large number of variables makes it necessary to use formal experimental design procedures to help reduce the number of tests. This chapter discusses some of the background to the design of experiments and their application to the VVA tests on the Jaguar AJ26 engine.

4.2. Background to statistical design of experiments

Formal methods for the design of experiments date back to the early years of the 20th century when researchers in the subject came to realise that some of the new methods being developed, such as analysis of variance, were intimately related to the problem of experimental design [Fisher (1935)]. The main focus of the statistical methods at the time was in the field of agriculture where the time taken for each test, and indeed the time between trials, meant that it was extremely important to maximise the information from a single experiment. Fisher (1935) and Yates (1935) wrote some of the earliest publications devoted to the subject.

The 1940's saw an extension of the subject to include fractional designs [Finney (1945)], commonly used in the industrial environment today. By this time the subject had found greater acceptance in other areas of the biological sciences as well as agriculture. However, one of the most significant developments came from the chemicals industry, which needed a slightly different approach to problem solving. Their problem was one of determining the conditions of such factors as temperature and concentration for giving the highest yield, or purity, or least cost [Davies (1954)]. Box and Wilson (1951) published the first paper on response surface methodology, which attempted to model empirically the underlying laws governing chemical systems. The method gained wide favour in the chemicals industry with some acceptance outside.

The most recent phase in the development of experimental methods began in the 1980's when work by Taguchi (1987) and others helped establish their use in the production environment as companies strived to improve the quality of the products they manufactured. However, there has also been a resurgence in the conventional experimental design methods, particularly for investigations in the areas of research and development (Pilley *et al.* (1994), Seabrook (1995)) as the methods originally developed by Box continue to gain wider acceptance.

A recent development has been the application of Bayesian statistics to engine experimentation as demonstrated by Mowll *et al.* (1996). The mathematics have their roots in the 18th century, and a basic requirement is some prior knowledge of the responses to be modelled. This approach was in its infancy, at least in its applications to engines, at the start of this work. The main problem in applying it to this work would be that the tests would be using combinations of variables for which little or no prior knowledge existed. It is considered to be an interesting development, but one that could not be easily applied to the proposed programme of tests.

4.3. Basic ideas relating to experimental design

Diamond (1989) suggested four major steps involved in establishing guidelines for decision making using experimental data:

- Stating the two alternative decisions.
- Defining the acceptable risks for selecting the wrong alternative.
- Establishing an objective criterion between the alternative decisions.
- Computing the requisite sample size.

The aim of the investigator is to estimate the magnitude of a particular response and calculate an interval within which the true value almost certainly lies [Box *et al.* (1978)]. Such an interval is known as a confidence interval and depends on the confidence with which the experimenter can accept one of two mutually exclusive hypotheses. These are applied to some characteristic of the data, for example, the mean value of the response μ[1].

The null hypothesis states that a change in variable A say, has no effect on the value of μ for two different populations:

$$H_0 : \mu_1 = \mu_2 \qquad \textbf{(4.1)}$$

[1] Although the mean of the data is used here for illustrative purposes, the ideas presented are equally applicable to other characteristics of the data, for example, the variance.

The alternative hypothesis states that an increase in variable A will affect the mean of the response:

$$H_a : \mu_1 \neq \mu_2 \tag{4.2}$$

This hypothesis is double-sided, the experimenter has no commitment to either population. The alternative hypothesis can also be written in a single-sided form where the primary focus is on one of the populations:

$$H_a : \mu_2 > \mu_1 \tag{4.3}$$

The experimenter will only have a limited amount of data from which to infer the correct decision. The risk of accepting the wrong hypothesis can be controlled by proper selection of the sample size. Two types of risk can be defined:

- The alternative hypothesis is accepted, whereas the null hypothesis is actually true. This is known as an alpha error (α).
- The null hypothesis is accepted, whereas the alternative hypothesis is actually true. This is known as a beta error (β).

The experimenter can be (1-α).100% confident that the null hypothesis is correct if it has been accepted, or (1-β).100% that the alternative hypothesis is the right one if it has been selected. These confidence levels are correct provided that the sample size (N) for the experiment has been computed appropriately.

The experimenter can define the minimum change in the response that is regarded as significant (δ). This allows an objective criterion to be established, against which one of the two alternative hypotheses can be accepted. The exact form of the criterion depends on the type of experiment and is explained further in Diamond (1989).

Once a value for δ has been selected, the required sample size can be calculated:

$$N = \left(U_\alpha + U_\beta\right)^2 \left(\frac{\sigma}{\delta}\right)^2 \tag{4.4}$$

U_α and U_β are the normal deviates for a given α and β error, σ^2 is the population variance. In many instances the variance of the population will not be known. In this case, δ is normally expressed as a function of σ and the Student's t distribution is used to estimate the deviates.

4.4. Factorial and fractional designs

In practice, most problems are likely to be dependent on a number of variables, and the researcher is interested in modelling, or possibly optimising, some response of the system to changes in those variables. The most widely used approach, particularly for an optimisation problem, is to adopt a 'change one variable at a time' method, whereby one of the variables is adjusted whilst holding the others constant in order to find the best response. Once this has been found, the variable is fixed at its optimum level, and the procedure is repeated with the next variable. Diamond (1989) and Seabrook (1995) demonstrated the problems associated with such an approach. Figure 4.1 (adapted from Diamond (1989)), depicts the experimental space for a three-variable experiment at two levels (-1 and +1). Typically, the experimenter may decide to maintain variables B and C at their low values whilst testing at levels -1 and +1 for variable A. This test may be repeated an appropriate number of times to satisfy the decision making criteria discussed in Section 4.3.

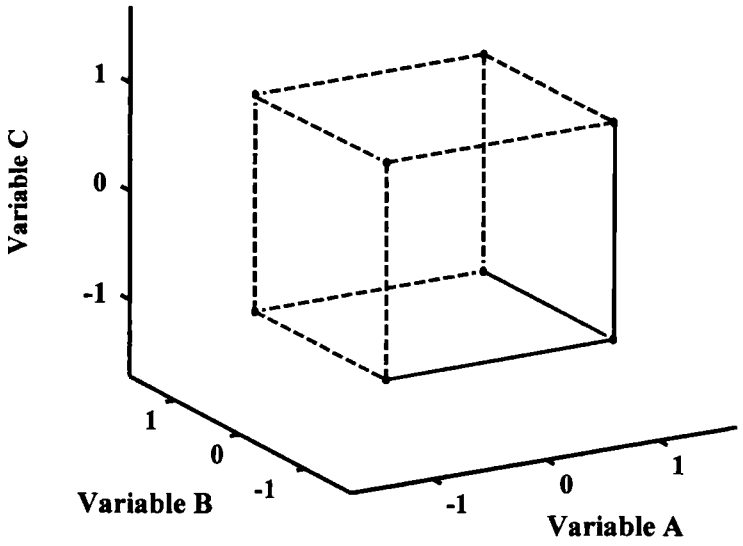

Figure 4.1
Experimental space for a three-variable experiment at two levels depicting path taken for 'change one variable at a time' approach in red (adapted from Diamond (1989))

For such an experiment, it may transpire that the results indicate that a high value of A gives a better response than a low one. The experimenter therefore decides to fix A at its higher value and repeats the tests, this time altering the value of variable B. This may indicate that a low value of B is to be preferred. Finally the experimenter applies the same reasoning to C to find that a high value of C is best. The experimental path that has been taken is shown in red in Figure 4.1. Say the computed sample size had been four, the experimenter has carried out twenty-four tests, four at each of the levels of each variable. However, the experimenter is able to say nothing of

the response to the combinations represented by the other vertices of the cube, unless it is assumed that no interaction exists between the variables. The experimenter will only be able to interpolate between the points visited, but cannot draw any conclusions about the rest of the volume enclosed by the cube. For example it may be that a low value of variable A, together with high values for variables B and C, gives an even better response due to an interaction between the variables, than that achieved by the experimenter who would be oblivious to this. Ideally the experiment would be performed in such a manner as to allow conclusions to be drawn about the response within the entire volume enclosed by the cube, as this represents the entire range of values possible for the variables. This can be achieved by testing at all the vertices of the cube, in effect testing every combination of the variables, giving a full factorial experimental design. The question is how many times must the test at each point be repeated to ensure that the results are within the appropriate confidence limits? In this case, it has been assumed that four samples at each of the levels is sufficient to satisfy this criterion. However, this does not mean that each trial is to be repeated four times, simply that the effect of variable A, say, needs to be measured four times at a high value and four times at a low value. This is satisfied if the experimenter were to carry out a single test at each point on the cube as four of the results will be for high A and four for low A. In addition, the same tests give information about high B versus low B and similarly for C. Thus, an experiment with eight trials has given information about all the possible combinations of the three variables and, in addition, this information allows the response to be estimated anywhere within the cube, if it is assumed that the response is a linear function of the variables. The condition for linearity arises due to the fact that only two levels are used. The information will, however, take into account any interaction between the variables.

A full factorial experiment is only suitable when a relatively small number of variables at a few levels are involved. For example, a three variable experiment at two levels requires 8 trials, whereas one with 4 variables at 5 levels requires 625. With such a potentially large number of trials, it is understandable why the experimenter may consider adopting the 'change one variable at a time' strategy. However, factorial experiments, particularly at two or three levels, can be used to form the building blocks for many other experimental designs. Testing at two levels allows a straight line fit using linear regression, which will be discussed later in the chapter. The design for a three variable experiment at two levels (±1) is shown in Table 4-1, and can be thought of as a cube in three dimensions (see Figure 4.1). The design allows estimation of interactions between all the variables, which are represented by columns 4 to 7 in Table 4-1. Diamond (1989) demonstrated the uses of such a design for estimating the response of interest.

Trial No.	A	B	C	AB	AC	BC	ABC
1	-1	-1	-1	+1	+1	+1	-1
2	+1	-1	-1	-1	-1	+1	+1
3	-1	+1	-1	-1	+1	-1	+1
4	+1	+1	-1	+1	-1	-1	-1
5	-1	-1	+1	+1	-1	-1	+1
6	+1	-1	+1	-1	+1	-1	-1
7	-1	+1	+1	-1	-1	+1	-1
8	+1	+1	+1	+1	+1	+1	+1

Table 4-1
Experimental design for a three-variable experiment at two levels

Whilst two-level full factorial designs allow all interactions between variables to be estimated, in practice, higher (greater than three or four) order interactions are relatively small and may in fact be neglected. This is similar to neglecting the higher order terms in a Taylor series (upon which the modelled response is likely to be based), and in most cases it gives a reasonable representation of the true response [Box *et al.* (1978)]. One reason for this is that high order interactions are often so small in magnitude that they are indistinguishable from the noise present in the experimental data. The experimenter is required to make a judgement as to what degree of accuracy is needed. Consequently, the high order interaction columns (referred to as contrast columns) in a full factorial design can be used to model the main and low order effects of additional variables, forming a fractional design. Replacing the ABCD interaction in a four-variable experiment with a fifth variable (E) gives a half fraction design.

There is one limitation of such a design, namely the presence of an effect known as confounding. Confounding refers to a situation where the effects of two different factors[2] are indistinguishable from each other. In the case above, for example, ABCD is confounded with E. Replacing ABCD with E does not mean that the four-variable interaction is not present, rather that its effect is sufficiently small to allow any changes in that column to be attributed to E without much loss in accuracy. If, in actual fact, there were a significant ABCD interaction, the experimenter would only be able to conclude that any change in response was a function of either ABCD or E or both. A half fraction, five-variable, design has confounding between main effects and fourth order interactions, and between second and third order interactions; this is known as a resolution V design. Resolution refers to the 'quality' of the information available from the design. A resolution V design allows all two variable interactions to be estimated provided higher order interactions are negligible. A resolution IV design has confounding between two variable

[2] It is important to distinguish between variables and factors. Factors represent both variable main effects and interactions, e.g., A, B, AB are all factors, whereas only A and B are variables.

interactions so can only estimate the effects of groups of these. A resolution III design has confounding between main effects and second-order interactions. Thus, main effects can only be estimated in the absence of interactions.

An extension to the above approach is to use a spare high-order contrast column to split the experiment into two orthogonal blocks. For example, if the total number of trials is too large for the experiment to be completed in one day, the experiment can be divided into two blocks, one for each day. This is a significant problem if it is expected that something beyond the experimenter's control, atmospheric pressure for example, is likely to change over this period and influence the test results. Returning to the four-variable experiment, the contrast column for the ABCD interaction can be used to cater for this effect. If all the tests with a minus sign in the ABCD contrast column are conducted on the first day, and those with a plus on the second, any effect due to the different days will be confounded with ABCD. However, it is now possible to view the two days as two levels of a variable, the effect of which can be modelled and removed. So, although the mean response may have changed due to the different days, the effect of the main variables on the response can still be modelled. This technique is known as blocking, and is widely used to remove the effect of variables beyond the experimenter's control.

4.5. Composite designs

The discussion so far has concentrated on experimental designs using only two levels for each variable. Whilst such designs may be adequate for some problems, their main disadvantage is the inability to model non-linear behaviour. A statistically-designed experiment, when used to model a response surface, attempts to fit some form of graduating function such as a polynomial to model the response [Box and Draper (1987)]. Thus, in a two level experiment, the graduating function is a linear equation relating the change in response to changes in the variables. Using a greater number of levels allows more complex graduating functions to be used, allowing non-linear behaviour to be modelled. In general, the graduating function will be a polynomial of relatively low order in all the variables of interest. Use of higher order polynomials will necessitate an increase in the number of levels with marked increase in the number of trials needed.

A composite design is one which augments a factorial or fractional factorial design with additional points to help estimate curvature in the response surface. A particularly efficient design is the Central Composite Rotatable Design (CCRD), which uses star and centre points in addition to the two-level factorial cube. Figure 4.2 shows this for the case of three variables.

Such a design effectively requires the variables to be at five levels[3]. The star points are located at extreme values ($\pm\psi$) whilst the others are set to their centre point values. The combination of star and centre points allows a quadratic polynomial to be used as the graduating function for the modelled response. Two criteria are used to decide on the number of centre points and the value for ψ. These are related to the properties of orthogonality and rotatability of the design matrix.

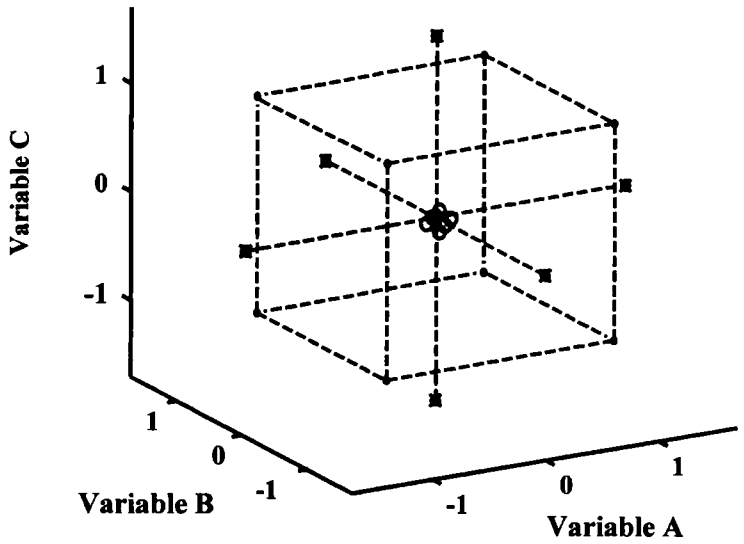

Figure 4.2
A Central Composite Rotatable Design for three variables at five levels

Orthogonality allows the effects of one variable to be estimated without distortion by the others. In a two-variable (A and B) experiment, for example, orthogonality would allow a response surface to be drawn in three dimensions with the axes perpendicular to each other. It is possible to estimate the effect of varying A whilst holding B constant. Lack of orthogonality would mean that the axes were no longer perpendicular. Making an estimation of the effects of A would also require B to be varied. Box *et al.* (1978) showed that for orthogonality:

$$\psi^2 = k\frac{\left(1+\frac{n_{s0}}{n_s}\right)}{\left(1+\frac{n_{F0}}{n_F}\right)} \qquad (4.5)$$

Where k is the number of independent variables, n_s and n_F are the number of star and factorial points, and n_{s0} and n_{F0} are the associated centre points. It can be seen that a blocked design

[3] Although the variables are at five levels, many authors would define this as a three level experiment, however, this discussion will refer to such as a five level design.

would alter this value as the blocking columns effectively behave as extra variables.

Box and Draper (1987) described rotatability as a logical extension of orthogonality. Rotatability in a design means that the variance is only a function of the distance from the centre points. A rotatable design helps ensure a spherical distribution of data [Box and Draper (1987)]. For rotatability, the following condition must be satisfied [Box *et al.* (1978)]:

$$\psi = \left(\frac{2kn_F}{n_s} \right) \tag{4.6}$$

A variation on the CCRD is one in which the star points are brought into the middle of the cube (ψ=1), reducing the number of levels to three. However, this loses the advantage of a rotatable design.

4.6. Analysis of experimental data

So far much has been said about the design of experiments with little being devoted to the issue of analysing experimental data and, in particular, checking the adequacy of the fitted model. A more complete description of parameter estimation in multiple linear regression using the method of least squares can be found in numerous standard texts on the subject. Myers and Montgomery (1995) gave a description in the context of response surface methods. Linear regression allows a suitable equation to be used to model the experimental data. However, it is always necessary to examine the fitted data to ensure that it provides an adequate approximation to the true response [Myers and Montgomery (1995)]. This section deals with several checks used to judge the adequacy of a model.

Measuring goodness of fit

The most common measure of goodness of fit is the coefficient of multiple determination R^2, which can be defined as:

$$R^2 = 1 - \frac{\sum_{i=1}^{n} (y_i - \hat{y}_i)^2}{\sum_{i=1}^{n} (y_i - \bar{y})^2} \tag{4.7}$$

where y_i and $\hat{y}_i$ are the ith observed and estimated responses respectively, and $\bar{y}$ is the mean of the response. Myers and Montgomery (1995) described this value as a measure of the amount of

reduction in the variability of y obtained by using the regressor variables in the model. An alternative is to view it as the amount of variability in the response that is explained by adoption of the model. The value for R^2 is model dependent as its value always increases with the inclusion of extra terms in the regression model. It should therefore only be used as a rough guide. Myers and Montgomery (1995) presented an adjusted version of this parameter that can be used to judge the merit of adding extra terms into the regression equation. Only the simple value of R^2, as given by Equation (4.7), was used in the experimental analysis during this study.

Residual Analysis

A second-order polynomial equation for a two variable CCRD experiment may be written as:

$$y = \beta_0 + \beta_1 x_1 + \beta_2 x_2 + \beta_{11} x_1^2 + \beta_{22} x_2^2 + \beta_{12} x_1 x_2 + \varepsilon \qquad \textbf{(4.8)}$$

Any single observation y_i can be expressed in terms of the model parameters given in Equation (4.8) with the variables set at their corresponding values:

$$y_i = \beta_0 + \beta_1 x_{i1} + \beta_2 x_{i2} + \beta_{11} x_{i1}^2 + \beta_{22} x_{i2}^2 + \beta_{12} x_{i1} x_{i2} + \varepsilon_i \qquad \textbf{(4.9)}$$

The value ε_i is known as a residual and represents the variability in the data that is not accounted for by the fitted model. Residuals play an important role in assessing the quality of the fitted model. For example, they are often plotted against the predicted response to judge whether the variance in the original observations is constant, as is assumed. Residuals are also plotted against case number, or in chronological order, to look for non-random trends that would indicate model inadequacy. Residual values that appear excessive would indicate outliers in the results. Seabrook (1995) discussed some of the trends that may be apparent in experimental data with the same regression statistics.

Testing for significance of individual factors

The use of hypothesis tests to judge the usefulness of individual model parameters is an important aspect of response surface methods. In particular, it can be useful to plot the relative significance of all the factors used in the regression model. Using the hypothesis tests presented in Section 4.3, and information about the variance of the data, it is possible to assign a confidence level above which a factor can be regarded as significant. Appendix 3 presents the method used for estimating the variance and calculating the test statistic for significance.

4.7. Experimental design applied to IC engines

While statistically-designed experiments have found a place in the automotive production environment, their role as a research tool in the field of IC engines has been limited [Pilley *et al.* (1994)]. However, one notable study directly related to this investigation is that carried out by Seabrook (1995). The purpose of the study was to investigate optimisation of emissions on an engine incorporating continuous phasing on the inlet and exhaust camshafts and a swirl control valve in the inlet port. The study used a four-variable, blocked, Central Composite Rotatable Design to model HC, NOx and fuel consumption as the main responses. In particular, the investigation was divided into three phases, an initial phase utilising the entire domain of the variables, a definition phase to investigate further regions of particular interest, and a confirmation phase to judge the efficacy of the modelled responses. It was pointed out that the latter phase was not strictly necessary, as the data from the definition tests was sufficient to provide the necessary information about the accuracy of the model. It can be argued that one of the primary aims of the study was to demonstrate application of the method to IC engines, and in this respect, the confirmation phase helped to prove the applicability. One aspect of experimental design, which was not brought out very clearly by Seabrook (1995), is the importance of considering the system to be modelled when designing the experiment; this will be covered in the following section.

4.8. Design options for investigating VVA on the Jaguar AJ26 Engine

The application of statistically-designed experiments to investigate VVA raised a number of issues that needed to be resolved before deciding upon a final design. An initial proposal for the choice of variables was to use phasing, lift and duration for the inlet valve, while using phase and duration for the exhaust valve, with the possibility of including spark timing to judge robustness (see later in the section) of the response at each test point. Splitting these variables into smaller groups was thought to be a potentially dangerous strategy, as the results would allow no inferences to be drawn about interactions across the groups. For example, an initial proposal from the sponsor (Jaguar Cars), suggesting a two-phase study separating lift and duration into two investigations, would have provided no information about a lift/duration interaction. It is possible, although unlikely, that no such interaction exists, but it would have been preferable to know one way or the other.

Box and Draper (1987) argued that the process of learning by experiment is an iterative one. Ideally, a well designed experiment would include a screening phase utilising a lower resolution

design, at two levels perhaps. This would help to formulate a more detailed study which, in turn, could lead to further investigations. Screening experiments can be used to estimate where the most influential factors and interactions lie, helping to optimise the selection of variables for the subsequent experiments.

For this study the main variables were those already mentioned. Even with this limited number, a factorial design would have become prohibitively large, so there was an incentive to eliminate one of the variables. Exhaust event duration was chosen for elimination as it was expected to be the least influential, phasing being of greater benefit for both HC and NOx reductions. In addition, it was thought likely that manufacturers would be reluctant to incorporate variable duration technology on both inlet and exhaust valves on the basis of cost. The reduction of variables to five meant that it was feasible to use a half-fractional scheme as the basis of the design. However, as the lead time for manufacturing the camshafts was so long, it was preferable to move to a composite design, as it would yield detailed information more quickly and would prove more useful in deciding on the parameters for the second phase of the project. A design such as the CCRD had the added benefit of allowing the factorial portion to be conducted first, permitting the possibility to assess the validity of the interim results. The only remaining issue was the possible inclusion of spark timing.

The accepted method for judging robustness of a response at a particular point is to include the variable by which robustness is to be judged in the design. Figure 4.3 demonstrates the difference between a robust optimal response and one that is higher but less stable.

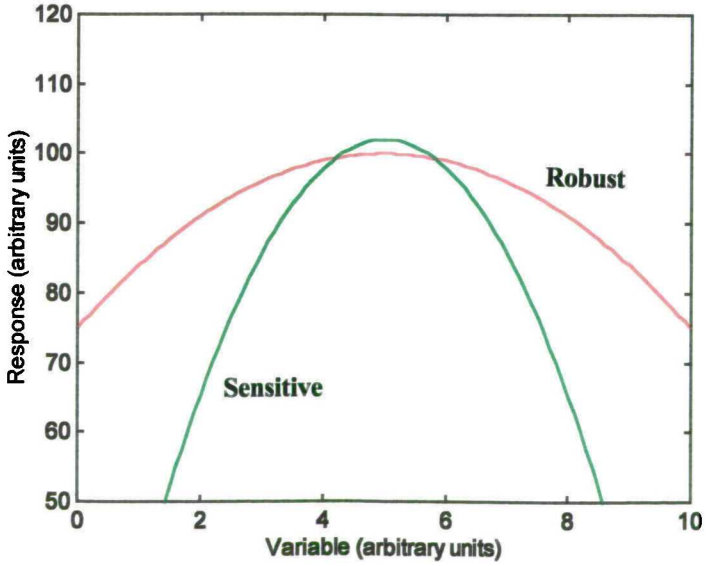

Figure 4.3
Comparison between a robust optimal response and one sensitive to variations

Variations in the variable cause little change in the response for the first system, whereas a small change in the second causes a larger change in the response, bringing it below that of the first system. Since the aim of the engine manufacturer would usually be to set spark timing to MBT in order to maintain fuel economy, it was concluded that MBT spark timing could be viewed as a response. The conventional method of finding MBT is to carry out an 'ignition sweep', producing curves similar to those in Figure 4.3. It would therefore be possible to assess the robustness of the responses, at least in the regions near the test points, by looking at the shape of the ignition sweep curves. Spark timing was thus removed as a potential variable. However, as is discussed in Chapter 6, it later became necessary to include it for the idle tests. A design including spark timing will also be discussed later.

One advantage of the CCRD design is the augmentation of a two-level design with star and centre points. These allow an estimation of curvature of the responses by adding quadratic terms to the regression model. The definition of variables plays an important role in the experimental design. A number of options were considered, and these will be discussed individually with reference to a five-variable CCRD design originally proposed by Winterbottom (1996) for this project, and the four-variable design used by Seabrook (1995). The choice of variable definitions becomes important because of the fact that higher order interactions cannot be estimated, and indeed may be confounded with one and two variable effects. A suitable example is that of valve overlap, which has an affect on the RGF trapped in the cylinder. Other potential variables such as valve lift, pressures and temperatures in the ports, and piston velocity may also have an effect. Selection of inlet valve event phasing and duration and exhaust event phasing as variables means that the NOx response may largely be dependent on factors which are a combination of these. Any non-linear response will manifest itself as an interaction between these, making the prospect of distinguishing it from an interaction between overlap and some other variable (spark timing for example) extremely unlikely. If, instead, overlap angle is selected as one of the variables, any non-linear dependence on it (for example, the area under the valve lift curves) will only affect the curvature and would still allow an interaction with a second variable to be distinguished. It is therefore advantageous to define variables in a manner that reduces unnecessary interactions such that a potentially high order interaction is reduced to a lower order one. This process is known as transformation, and is advocated by Box and Draper (1987) whenever there is theoretical or empirical evidence to suggest that model simplification may occur as a result.

Reducing high order interactions to lower ones can be a problem in terms of increasing experimentation time and costs. This is demonstrated by considering the following two CCRD designs.

4.8.1. Using intake event phasing and duration, exhaust event phasing, inlet lift and spark timing as variables

Table 4-2 shows a potential scheme when using the above variables. The range of these variables was based on the following criteria:

- The IVO point could not be advanced further than 35° bTDC otherwise there would be contact between the inlet valves and the piston.
- It was assumed that EVC could not be retarded further than 35° aTDC to prevent possible exhaust valve and piston contact.
- The phasing range of the AJ26 was 30° but systems in the near future would probably extend this to beyond 60°. A 60° range was therefore chosen.
- The longest duration for the inlet event was set to 260° as longer values would have resulted in excessive overlap at some test points. In addition, this was the longest duration profile that could be produced from a standard camshaft casting.
- It was assumed that the lowest lift capable of allowing the engine to run at the highest load point of 2500 rev/min/5.5 bar BMEP was 3mm.
- The maximum lift of interest was approximately 8.6mm. Lifts higher than this did not significantly influence flow coefficients according to the data presented by Barraclough (1996).
- The range of duration was chosen to be as wide as possible as this should be one of the aims during the initial phases of such a project.

SparkTiming (°bTDC)	Intake MOP (°aTDC)	Exhaust MOP (°bTDC)	Intake Duration (°ca)	Inlet Valve Lift (mm)
10	95	130	215	7.2
30	95	130	215	4.4
10	125	130	215	4.4
30	125	130	215	7.2
10	95	100	215	4.4
30	95	100	215	7.2
10	125	100	215	7.2
30	125	100	215	4.4
10	95	130	245	4.4
30	95	130	245	7.2
10	125	130	245	7.2
30	125	130	245	4.4
10	95	100	245	7.2
30	95	100	245	4.4
10	125	100	245	4.4
30	125	100	245	7.2
0	110	115	230	5.8
40	110	115	230	5.8
20	80	115	230	5.8
20	140	115	230	5.8
20	110	145	230	5.8
20	110	85	230	5.8
20	110	115	200	5.8
20	110	115	260	5.8
20	110	115	230	3.0
20	110	115	230	8.6
20	110	115	230	5.8

Table 4-2
Experimental design for a five-variable CCRD experiment with a half fraction factorial cube. Note: Last row represents centre point.

The total number of camshafts needed for this design was nine. Although it is advisable to explore as large a range as possible for screening purposes, the likelihood of any of the camshafts being useful for subsequent testing was reduced. For this reason, extreme ranges were avoided. In addition, it was not advisable to use too broad a range if the response surface was to be modelled by a second order fit, as the probability of a cubic term appearing in the true response was increased. There were two main advantages to this design:

- the relatively small number of camshafts needed.
- the possibility to visit more than one test point in a day, when a cam change was not required.

The main disadvantage of this design was the confounding of the results with higher order interactions, in particular the interactions affecting overlap angle and hence NOx levels. However, such a scheme would still have provided a valuable insight into which factors were the most influential. It was possible that a significant two-variable interaction was in fact caused by the three-variable one with which it was confounded. It was felt that there was some scope for judgement to be made on this by applying available knowledge to assess whether the three-variable interaction was a feasible one. For example, the results may have indicated that NOx levels were significantly affected by a lift/spark timing interaction, which was confounded by an intake phase/exhaust phase/intake duration interaction. Using background knowledge in such a situation would help to decide whether the two-variable interaction or the three-variable interaction was the cause. In addition, first analysis of the experimental results might show one of the variables (e.g. lift) to have a negligible effect on one of the responses (e.g. NOx). In this situation, the two-level portion of the design could be regarded as a full factorial experiment for NOx in terms of the other four variables, with no confounding in the results. The three-way interaction affecting overlap (inlet phasing, inlet duration, exhaust phasing) would then be revealed. It should be noted that this design could be modified for four variables by removing spark timing, and viewing it as a response instead, giving a similar advantage. A design modified in this way could be regarded as that originally used by Seabrook (1995).

4.8.2. Using inlet valve opening angle, inlet valve closing angle, exhaust valve closing angle and inlet valve lift as variables

Table 4-3 shows the layout for this scheme. The criteria for selection of the ranges were similar to those mentioned previously. The IVC angle is determined through the phasing and duration. The main disadvantage is that the setting for phasing is no longer de-coupled from the settings for duration. This design increased the number of camshafts required to eleven with an attendant increase in testing time. In addition, the engine would need a cam change at practically every test

point. Although there are these disadvantages for the test procedure, there were also significant benefits to be gained. In particular some of the higher order interactions would be reduced. Whereas the first scheme would have revealed an interaction between phasing and duration for a response dependent on IVC, for example, this arrangement would reveal it directly, allowing interactions between IVC and the other variables to be studied.

IVO (°bTDC)	EVC (°aTDC)	IVC (°aTDC)	Intake Lift (mm)
20	0	210	4.4
0	0	210	4.4
20	20	210	4.4
0	20	210	4.4
20	0	230	4.4
0	0	230	4.4
20	20	230	4.4
0	20	230	4.4
20	0	210	7.2
0	0	210	7.2
20	20	210	7.2
0	20	210	7.2
20	0	230	7.2
0	0	230	7.2
20	20	230	7.2
0	20	230	7.2
30	10	220	5.8
-10	10	220	5.8
10	-10	220	5.8
10	30	220	5.8
10	10	200	5.8
10	10	240	5.8
10	10	220	3.0
10	10	220	8.6
10	10	220	5.8

Table 4-3
Experimental design for a four-variable CCRD experiment using valve opening and closing angles. Note: Last row represents centre point.

4.8.3. Selection of design

The CCRD appeared to offer the most efficient design for the first phase of testing. The inclusion of most of the variables of interest meant that it could potentially offer great insight into the significance of each on the responses of interest, and help plan a way forward for the second phase of engine tests. The two schemes shown, and some of the others investigated, had their individual merits. The selection of one was dependent on the trade-off between the number, and hence cost, of camshafts required and the quality of information obtained. The first phase of the work could be viewed as a detailed screening experiment, for which design 1 would be sufficient. It would allow second order interactions to be modelled in the absence of significant third order interactions. It would give a good indication of the variables that should be included in phase 2. It was felt, however, that more information would be available from the first phase if the four-variable option based on design 1, eliminating spark timing, was used. The advantage of this was that it retained the simplicity of the design, and the lower number of camshafts, whilst giving a full factorial design at two levels to improve understanding of the higher order

interactions. The four-variable version of design 1 was finally chosen as it offered the best compromise between number of camshafts and quality of information. The chosen design is shown in Table 4-4.

Intake MOP (°aTDC)	Exhaust MOP (°bTDC)	Intake Duration (°ca)	Inlet Valve Lift (mm)
95	130	215	7.2
125	130	215	4.4
95	100	215	4.4
125	100	215	7.2
95	130	245	4.4
125	130	245	7.2
95	100	245	7.2
125	100	245	4.4
95	130	215	4.4
125	130	215	7.2
95	100	215	7.2
125	100	215	4.4
95	130	245	7.2
125	130	245	4.4
95	100	245	4.4
125	100	245	7.2
80	115	230	5.8
140	115	230	5.8
110	145	230	5.8
110	85	230	5.8
110	115	200	5.8
110	115	260	5.8
110	115	230	3.0
110	115	230	8.6
110	115	230	5.8

Table 4-4
Experimental design for chosen four-variable CCRD experiment.
Note: Last row represents centre point.

4.8.4. Implications for testing time

Whichever design was selected, it was inevitable that there would be a large number of camshaft changes. This meant that it would be difficult to visit more than one, or possibly two, test points in any one day. Blocking was therefore impossible and the best strategy appeared to be one where a reading at the centre point was taken before a camshaft was changed for the test point. This meant that there would be extra readings for the centre points that could be additionally used to judge any discrepancies from day to day. However, it became clear during testing that even this would be impractical, and a standard scheme involving randomly spaced centre points was finally used.

Chapter 5

ENGINE HARDWARE AND INSTRUMENTATION

5. Engine Hardware and Instrumentation

5.1. Description of engine

The engine used for the testing was a development version of the Jaguar AJ26 unit. It had a swept volume of four litres in a 90° V8 configuration and employed pent-roof combustion chambers with four-valves-per-cylinder. Chain-driven overhead camshafts directly acted upon 'bucket' type tappets using hardened steel shims to set the valve clearances. The engine also employed precision cooling technology to reduce warm-up time and minimise cylinder-to-cylinder temperature variation. A sectioned view is presented in Figure 5.1 and engine details are given in Table 5-1. A full description of the technical details and the development of the engine is given by Joyce *et al.* (1996). There are, however, some important features of the test engine pertinent to the present study and these will be touched upon briefly in the following sections.

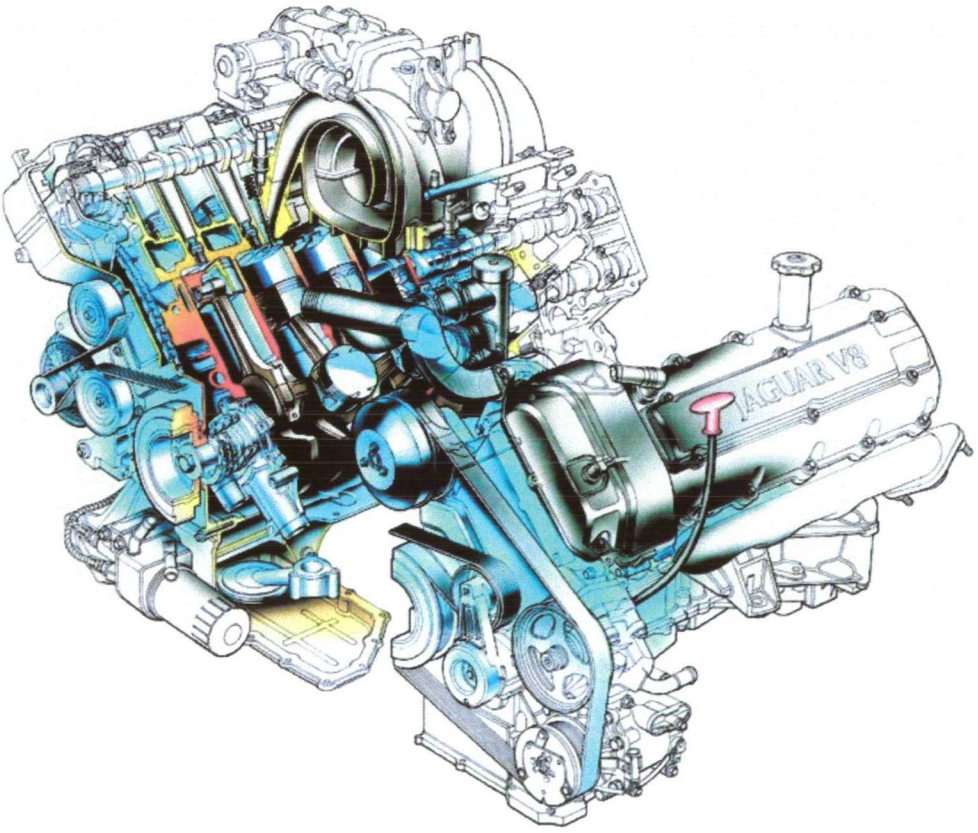

Figure 5.1
Sectioned view of Jaguar AJ26 V8 engine
[reproduced from Jaguar Intranet, images website]

Configuration	90° V8, 4 valves per cylinder, dohc
Swept volume	3997 cc
Bore	86 mm
Stroke	86 mm
Compression ratio	10.75:1
Combustion chamber	Pent-roof
Camshaft duration (std.)	230° Exhaust, 240° Intake
Intake MOP (std. retarded)	125° aTDC
Intake phasing range (std.)	30° ca
Exhaust MOP (std.)	115° bTDC
Included valve angle	28° 24′
Engine Management	Nippon Denso
Fuel injectors	Denso twin-spray side-feed
Ignition	Plug-mounted coils (Denso)
Coolant	50/50 ethylene glycol/water
Lubricant	Gulf Protech Super 10W/40 semi-synthetic

Table 5-1
Details of Jaguar AJ26 V8 engine

5.1.1. Variable valve timing

In its standard form, the AJ26 is fitted with a two-position phasing system on the intake camshafts. The system is based on a piston-helical spline arrangement giving a 30° variation in camshaft phasing. It was found to be more convenient to remove the phasing units for the test programmes as they delayed the frequent changing of camshafts. Instead, ordinary sprockets were used making it possible to change camshafts without removal of the front timing chain cover, resulting in a significant saving in the time required to perform camshaft changes.

5.1.2. Engine management system

A schematic representation of the Engine Management System (EMS) in its standard configuration is shown in Figure 5.2. The Engine Control Unit (ECU) was connected by means of a serial cable to a personal computer running the appropriate version of the Development Aid (Devaid) software. The only changes that were made to the hardware for the initial tests (Phase 1) were the substitution of the 'drive-by-wire' throttle with one actuated by a stepper motor and disablement of the EGR valve. Modifications to the throttle arrangement are discussed in the following section. The EGR valve was disabled by insertion of a blanking plate between it and the plenum. In addition the EGR map in the EMS was modified, so that no external EGR was applied over the range of speed/load conditions investigated. The second phase of testing required inlet valve deactivation and the further modifications are discussed in Chapter 7.

1. Intake air temperature (IAT) sensor
2. Mass air flow (MAF) sensor
3. Air assist control (AAC) valve
4. Throttle position (TP) sensor
5. Throttle motor
6. Accelerator pedal position (APP) sensor
7. Fuel injectors
8. Camshaft position (CMP) sensors
9. Engine coolant temperature (ECT) sensor
10. Knock sensors
11. Coil-on-plug ignition modules
12. VVT oil control valve
13. Upstream linear heated oxygen (HO2) sensors
14. Downstream heated oxygen (HO2) sensors
15. Crankshaft position (CKP) sensor
16. Engine oil temperature (EOT) sensor

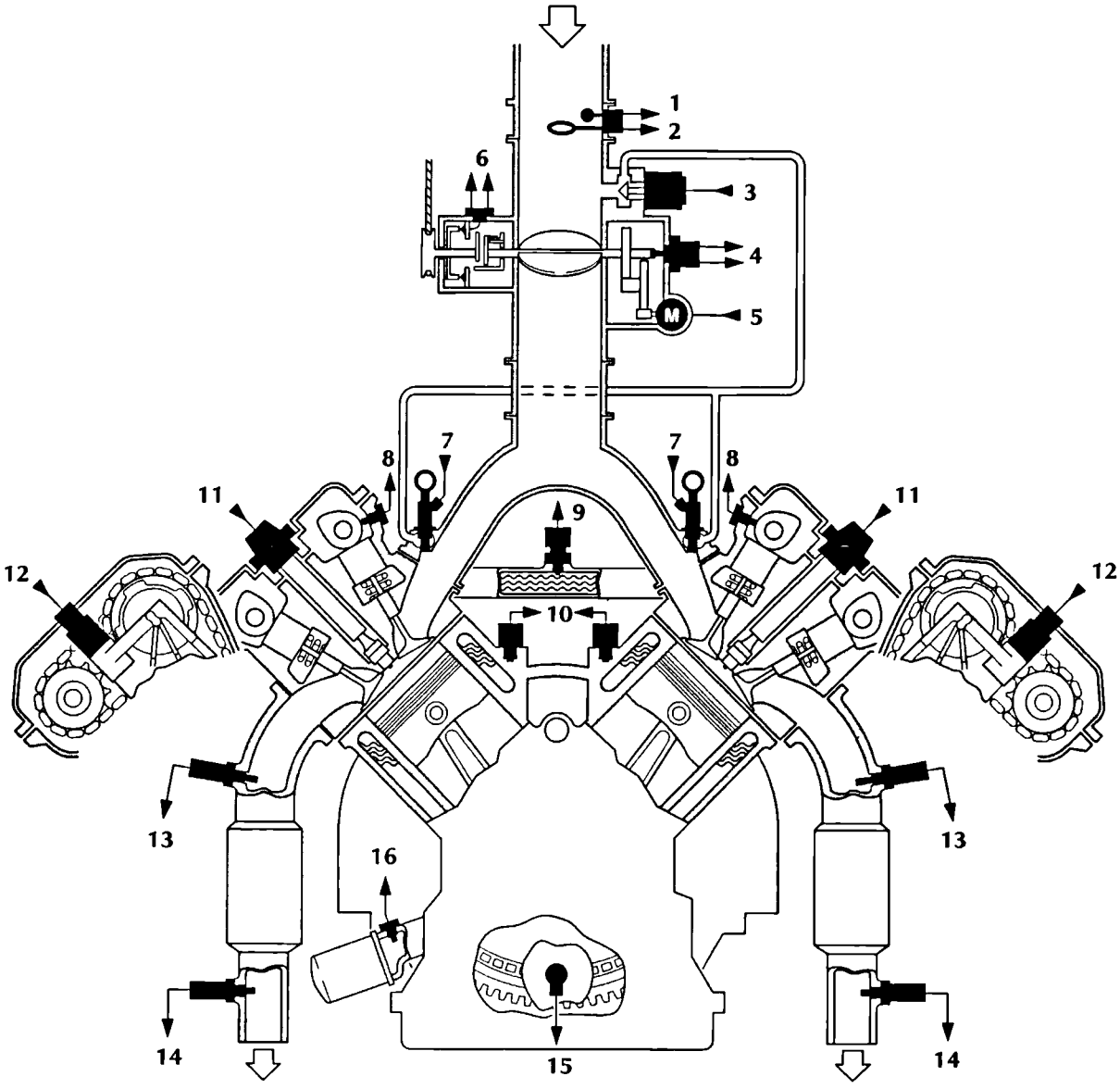

Figure 5.2
Schematic representation of engine management system
[reproduced from Jaguar Technical Guide]

Spark timing

Spark timing was adjusted by appropriate modifications to the base ignition map. This defines ignition advance in terms of engine speed and the mass flow rate of air. Care was taken to ensure that all values in the region of operation were set to the required value thus removing any changes caused by small perturbations in engine speed or load.

Fuelling

For the majority of the tests, fuelling was under closed-loop control with feedback from the Heated Exhaust Gas Oxygen (HEGO) sensors mounted in the exhaust system before the catalysts. However, modification to the throttle arrangement meant that there was a possibility of the engine entering its full-load fuelling regime, which in turn would cause the EMS to switch to open–loop operation with fuel enrichment. To avoid this, the throttle angle at which full-load fuelling would commence was increased to 80°. The fuelling strategies adopted for the tests at idle are discussed in the relevant chapters.

Knock sensing

The knock sensing system is based on two piezo-electric accelerometers mounted in the cylinder block on the inboard side of each bank. Whenever knock is detected, the EMS retards the timing of the spark of the affected cylinders. It was decided to disable the knock sensing system by setting the maximum allowable retard to 0° in the appropriate map in order to avoid the ignition timing being changed inadvertently

Adaptions (i.e. modifications to basic maps)

Fuelling and ignition adaptions were disabled by setting the coolant temperature at which they would begin to a value in excess of normal operating conditions. The motivation being to prevent a drift in the experimental results.

5.1.3. Electronic throttle

On the standard engine, the electronic throttle carries out all air control functions including basic throttling, idle speed control, starting air, cruise control and power limitation [Joyce *et al.* (1996)]. This is achieved by means of a dc motor connected to the throttle blade via a reduction gearbox and operated under closed-loop control of the EMS. One of the consequences of using this type of control system is the continuous movement of the throttle blade about its mean position. It was decided that this movement would present an unacceptable source of variation for the steady-flow tests, and it was therefore decided that the entire throttle assembly would be

replaced with one operated by a stepper motor. This was achieved by modifying the housing of an existing throttle body to accept the new motor.

5.2. Camshaft Design

Camshaft profiles for both phases of the engine tests were designed using the routines developed by the sponsor (Jaguar Cars). The program uses a series of polynomial equations to simulate the valve acceleration, which is then integrated twice to give the valve lift. Other programs were then applied to calculate oil film thickness and contact stresses amongst others in order to judge the suitability of any profile designed.

The strategy used for designing the Phase 2 profiles is discussed in Chapter 7. For the Phase 1 tests, nine profiles were required of differing duration and lift. The methodology used was to design a 'family' of profiles such that any profile could be thought of as being a scaled version of a base profile. This scaling could be in terms of the lift, duration (Figure 5.3) or both. The base profile was based on the camshaft requiring the largest lift in relation to duration, as this would imply the greatest valve acceleration. The ramps were identical for all the profiles.

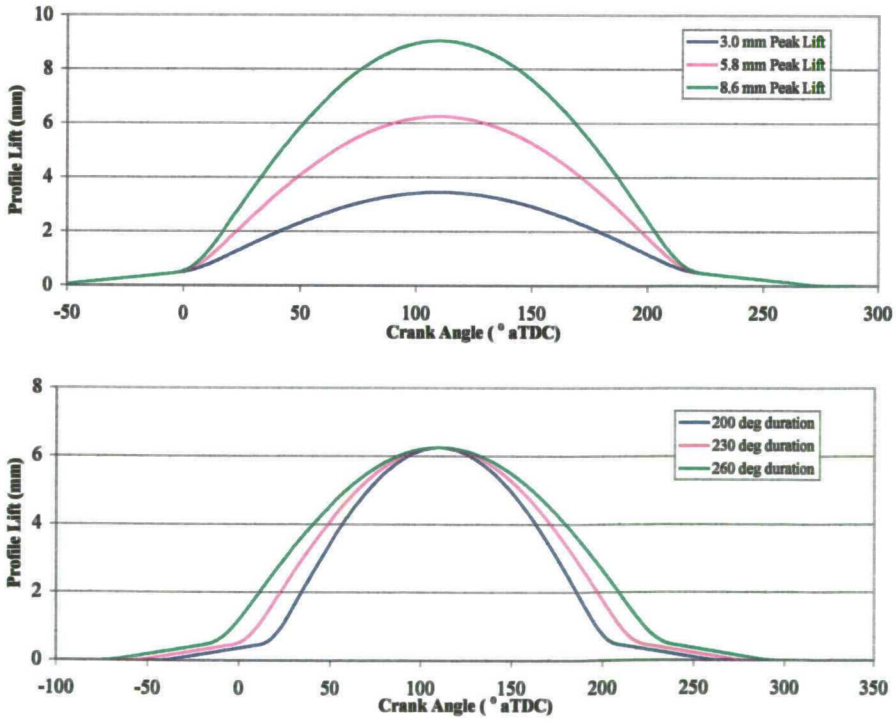

Figure 5.3
Scaling applied to camshaft profiles of different duration and lifts

5.3. Test Cell

The engine was fitted in the Environmental Test Chamber at UCL, with the dynamometer located outside. Tsatsami (1987) gives details of the test facility. The AJ26 was larger than the prototype six-cylinder engine fitted previously by Seabrook (1995), which itself had posed problems in terms of physical size and capacity of the cooling and refrigeration systems. For the AJ26, the extra heat dissipation made it impossible to control ambient conditions by means of the refrigeration equipment. Instead, the chamber door was left open and laboratory air was blown over the engine by the chamber fans. The passage of the exhaust pipes through the chamber wall posed additional problems, particularly at higher speeds and loads. The heat shielding arrangement, although uprated, proved unsatisfactory, and a fan was used to blow cold air over the exhaust pipes.

5.4. Instrumentation

A complete listing of all the instrumentation used during the two phases of engine tests may be found in Appendix 4

5.4.1. Engine load

The load on the engine was applied by a Heenan and Froude water-cooled eddy-current dynamometer fitted with a spring-balance to measure engine torque. The original control circuits for the field coils were inoperative and a regulated power supply was used to supply the current to the field coils. Engine speed was monitored by means of the Devaid software running on a personal computer

5.4.2. Emissions analysis equipment

Hydrocarbon and NOx emissions were measured from gas samples drawn separately from each cylinder bank. Tappings were made at the 'swan neck', towards the rear of each exhaust manifold. Samples from the two banks could be isolated by means of two high-temperature ball valves allowing emissions from each bank to be measured individually. All pipework and fittings were constructed from 316 stainless steel. A schematic of this arrangement is shown in Figure 5.4. A Signal Instruments thermostatically controlled heated sample line transmitted the exhaust gas samples to the exhaust gas analysis equipment.

Hydrocarbons were measured by a Signal Instruments 3000HM heated Flame Ionisation Detector (FID), and NOx emissions by a Signal Instruments 4000VM heated

Chemiluminescense analyser (CLA). The first phase of tests also employed a bank of older Beckman exhaust gas analysis equipment described by Seabrook (1995). These analysers were not heated, and consequently required sample gas that had first been cooled and dried. The results from this second set of apparatus allowed a check on the results from the heated analysers, although the Beckman analysers typically indicated higher emission levels due to the absence of water in the sample. The readings from the unheated analysers are not presented in this work.

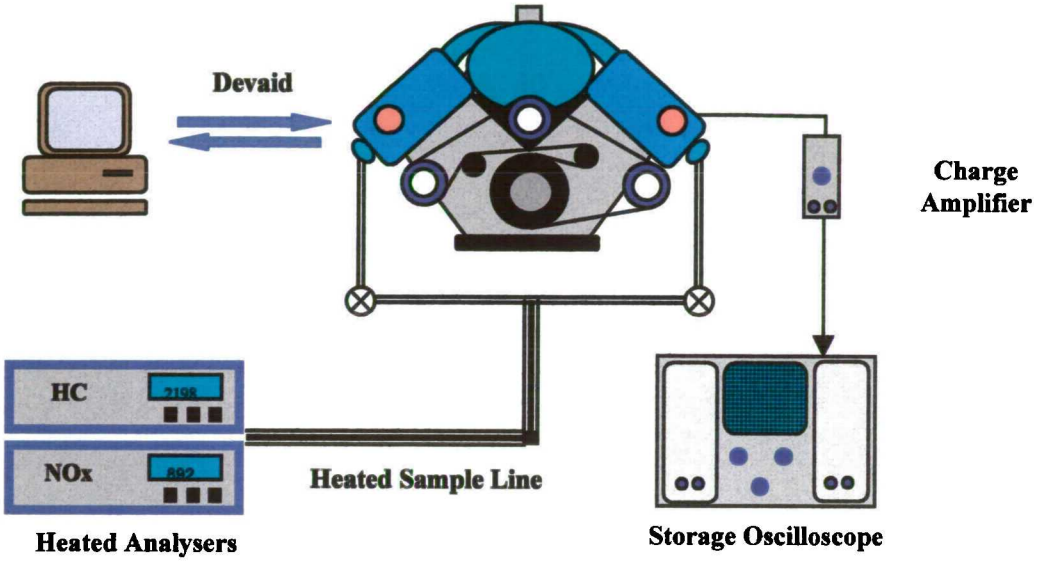

Figure 5.4
Schematic showing engine test-bed

Carbon monoxide levels were monitored by a Horiba MEXA-3231E Non-Dispersive Infra-Red absorption (NDIR) analyser for diagnostic purposes only. The results were not subjected to statistical analysis, as the accuracy of the instrument was not sufficiently great to detect the small changes observed with stoichiometric fuelling. The NDIR also had the facility to measure hydrocarbons, and this was used as a check on hydrocarbon readings from the heated FID for the Phase 2 tests.

5.4.3. Fuel and fuel consumption

Throughout the test programme particular care was taken to ensure a consistent supply of fuel. The large quantities of fuel consumed by the V8 engine meant that it was impossible to obtain and store enough fuel from a single batch. Instead three separate batches of fuel were used, two for the Phase 1 tests, and one for the Phase 2 ones. The experimental design for the Phase 1 was blocked allowing any effects due to fuel type to be removed from the analysis.

An AVL 730 dynamic gravimetric balance measured the rate of fuel flow to the engine. This was set to give a reading in g/min. Some of the problems experienced in measuring fuel consumption are discussed in Chapter 6.

5.4.4. Pressure measurements

Cylinder pressure

The cylinder head on the B bank of the engine was machined to accept a pressure transducer in each combustion chamber. Cylinder 2 was fitted with a Kistler 6121 piezo-electric pressure transducer. Blanking plugs, identical in physical dimensions to the transducer, were used to seal off the tappings on the other cylinders. The signal from the transducer was transmitted to a charge amplifier that converted the signal to a voltage that was recorded on a storage oscilloscope (see section 5.4.6).

Plenum pressure

The pressure inside the plenum was measured by means of a Druck PDCR 910 transducer mounted in the induction elbow below the throttle. The transducer operates by means of an integrated silicon strain gauge bridge fed with an electrical supply of 10V. The signal from the transducer was amplified by means of a differential amplifier (described by Taylor (1998)) and monitored on a Digital Volt Meter (DVM). The entire measuring chain was calibrated by means of a dead-weight tester both prior to and after the series of engine tests.

Ambient pressure

Ambient pressure was recorded by means of a Prosser digital barometer.

5.4.5. Temperature measurements

All temperatures, apart from engine coolant, were measured by means of type K thermocouples that were connected to a Comark, microprocessor-controlled, thermocouple meter.

The temperatures of the exhaust gases were measured at the 'swan neck' towards the rear end of each exhaust manifold. This was also the point from which the exhaust gas sample was withdrawn. The thermocouples used were suitably selected to withstand the expected high gas temperatures. The temperature of the air entering the engine was measured at the box housing the air filter. Engine air was drawn from outside the facility and consequently changed little in temperature during the duration of a test. Oil temperature was recorded by means of a thermocouple fitted to the sump plug bolt. Fuel temperature was monitored at the point where the

high-pressure fuel supply connected to the fuel rail. A thermocouple inside the test chamber was used to monitor the ambient temperature around the engine. Finally, coolant temperature was measured through interrogation of the EMS Devaid software, which uses the engine's coolant sensor as the input.

5.4.6. Data acquisition

Cylinder pressure was recorded on a Nicolet four-channel, 12-bit, digital storage oscilloscope. In addition signals from the engine's crank and cam sensors were also recorded to give crank angle data. Other major parameters such as engine speed, airflow rate, spark timing, fuelling, and coolant temperature were logged by the EMS Devaid software.

Chapter 6

PHASE 1 ENGINE TESTS

6. Phase 1 Engine Tests

6.1. Introduction

The Central Composite Rotatable Design (CCRD) discussed in Chapter 4 was used to investigate emissions and fuel consumption from a Jaguar AJ26 engine in response to changes in valve event phasing, and intake event duration and lift. The tests were conducted at idle, 1000 rev/min 1.0 bar BMEP, 1500 rev/min 2.62 bar BMEP, and 2500 rev/min 5.5 bar BMEP. Statistical analysis of the results allowed the responses to be modelled over the range of the variables investigated. Comparisons were made with results from gas flow modelling (Chapter 3) and steady flow tests to measure in-cylinder motion (Chapter 2) and these are discussed.

6.2. Experimental details

Valve event settings were altered by using a series of intake camshafts with different lift/duration combinations. Nine different camshaft profiles were employed for the tests. Phasing for both intake and exhaust camshafts was adjusted using a series of hardened setting blocks located against a flat towards the front end of each camshaft, this being the normal method used by engine builders at Jaguar. The engine uses conventional 'bucket' tappets with steel shims on top to set the valve clearances. Care was taken to ensure that these clearances were set to their recommended values (0.20 mm for intake and 0.25 mm for exhaust) when the engine was cold. A separate set of tappets was used for each camshaft, to reduce the need for re-shimming each time the camshaft was fitted.

Table 6-1 gives the valve events for each test condition at the three part-load speeds. The idle tests used a narrower range of phasing to avoid excessive overlap values. Appendix 5 gives details of all the experimental settings.

Prior to a test, the engine was run through a simple conditioning cycle. After starting, the engine was allowed to idle for approximately 30 seconds and then run at 1500 rev/min, 3 bar BMEP, until the coolant temperature had stabilised. As oil temperature was dependent on engine speed and load, the engine was then run at the required test condition until the oil temperature had stabilised for at least five minutes. The ignition timing during this period was set to the corresponding value in the base ignition map of the ECU.

An ignition sweep was conducted once conditions had settled. The curve of engine torque versus ignition advance was plotted to determine the timing corresponding to a one-percent reduction in maximum torque, to which the engine was set. The engine was then run at this condition until the oil temperature had again stabilised.

Test Case No.	EVO (°ca bBDC)	IVO (°ca bTDC)	EVC (°ca aTDC)	IVC (°ca aTDC)	Peak Lift (mm)
1	65.0	12.5	-15.0	202.5	4.4
2	35.0	12.5	15.0	202.5	4.4
3	65.0	-17.5	-15.0	232.5	4.4
4	35.0	-17.5	15.0	232.5	4.4
5	65.0	27.5	-15.0	217.5	4.4
6	35.0	27.5	15.0	217.5	4.4
7	65.0	-2.5	-15.0	247.5	4.4
8	35.0	-2.5	15.0	247.5	4.4
9	65.0	12.5	-15.0	202.5	7.2
10	35.0	12.5	15.0	202.5	7.2
11	65.0	-17.5	-15.0	232.5	7.2
12	35.0	-17.5	15.0	232.5	7.2
13	65.0	27.5	-15.0	217.5	7.2
14	35.0	27.5	15.0	217.5	7.2
15	65.0	-2.5	-15.0	247.5	7.2
16	35.0	-2.5	15.0	247.5	7.2
17	80.0	5.0	-30.0	225.0	5.8
18	20.0	5.0	30.0	225.0	5.8
19	50.0	35.0	0.0	195.0	5.8
20	50.0	-25.0	0.0	255.0	5.8
21	50.0	20.0	0.0	240.0	5.8
22	50.0	-10.0	0.0	210.0	5.8
23	50.0	5.0	0.0	225.0	3.0
24	50.0	5.0	0.0	225.0	8.6
25	50.0	5.0	0.0	225.0	5.8

Table 6-1
Valve event settings for Phase 1 tests. Test No. 25 corresponds to the centre point setting and was repeated 7 times.

The tests at idle were conducted in a different manner. The AJ26 uses spark advance for idle speed control. Consequently, the engine was calibrated to operate with a retarded timing, because engine speed is more sensitive to changes in spark timing when retarded. A typical calibration value was 10° bTDC when the transmission system was in its 'drive' setting. Since ignition timing was a variable, spark control of idle speed was disabled but this led to unstable operation because the throttle alone was incapable of maintaining a consistent speed. The engine running closed loop, which also caused fluctuations in speed, further exacerbated this problem. It was decided to disable idle speed and closed loop AFR control since it was not the aim of the study to

investigate the manner in which the control strategies would respond to valve event changes. A throttle assembly from a Ford Zetec engine was substituted allowing idle speed to be set manually. An initial test using a calibrated lambda sensor was conducted to determine the appropriate setting for the injector calibration constant (KGCK) in the ECU consistent with stoichiometric operation, with valve events set at their centre point values. This constant was used by the EMS to calculate injector pulsewidth from the air mass flow rate.

Emissions readings for the two banks were recorded separately and subsequently averaged. The majority of results presented in this chapter are those for average readings between the banks. Results for individual banks are discussed where significant differences were apparent. Two sets of gas analysis equipment were used. A set of heated analysers were supplied sample gas via a heated sample line, whilst a second, unheated set, were supplied with sample gas which had been cooled and dried (see Chapter 5). For brevity, the results presented are from the heated analysers.

6.3. Filling and emptying model

The filling and emptying model was described in Chapter 3, however, since its development, an important issue had emerged with respect to the predictions made by it. For the original runs, exhaust event phasing had not been correctly applied and an overlap period existed for all the settings. The results presented in Chapter 3 have been corrected for this error. Subsequent runs with the correct exhaust phasing revealed large predicted values for RGF when the exhaust valve closed before TDC, particularly in the absence of overlap. All lift profile data used for the program had, up until this point, excluded the ramps. It was postulated that if the true lift profile was modified to contain the ramps, the RGF predictions might be altered. A series of runs was conducted with the profile starting at different points on the ramp. This was achieved by changing the valve clearance setting for the input data to the program. A set of results was produced assuming that the valve clearances remained at their 'cold' value (0.20 mm for inlet and 0.25 mm for exhaust). These were compared with those for a set assuming that differential expansion increased the cold clearance by 0.1 mm, and a further set assuming that the full ramp height (0.45 mm) provided the clearance. Figure 6.1 shows a comparison of RGF and pumping work predictions for six different valve event settings with the three clearances. The effect of valve clearances can be explained with reference to the predicted cylinder pressure-volume diagram for test number 1 in Figure 6.1. The pumping loop for this test is shown for two different valve clearances in Figure 6.2. EVC for this test is at 15° bTDC whilst IVO is at 12.5° bTDC (measured from the top of the ramp). The early closure of the exhaust valve leads to extra exhaust gas being trapped within the cylinder. A larger valve clearance means that the valve

appears to close earlier accentuating this effect. As it was difficult to ascertain the actual valve clearances, it was decided to use the 'cold' clearance setting in the model.

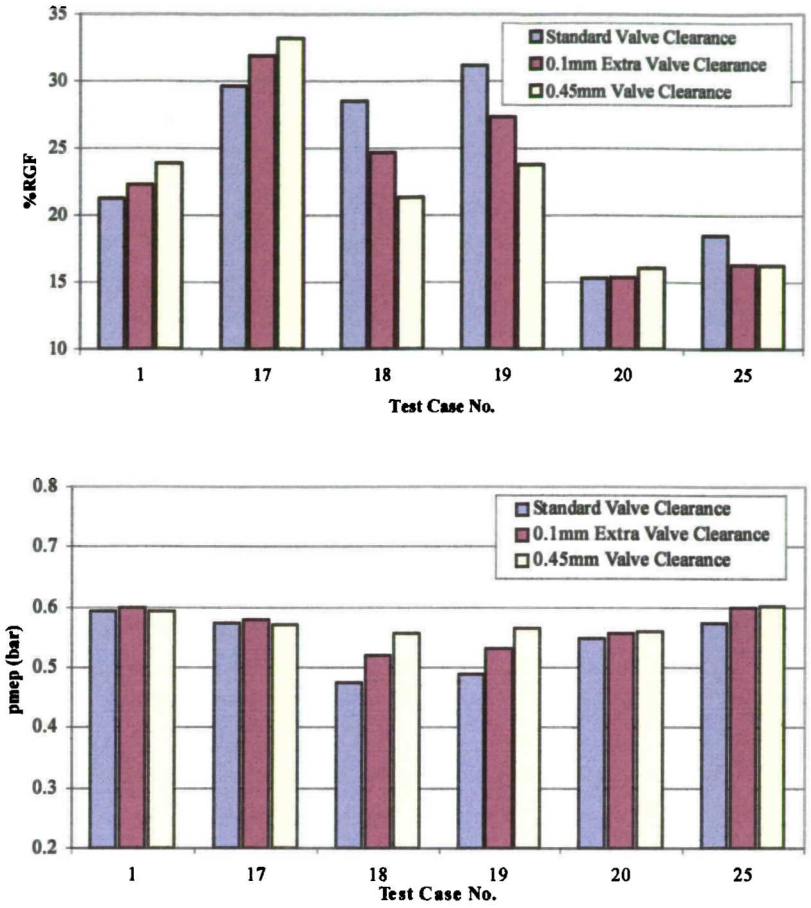

Figure 6.1
Examples of model predictions for RGF and pumping work with three different valve clearances

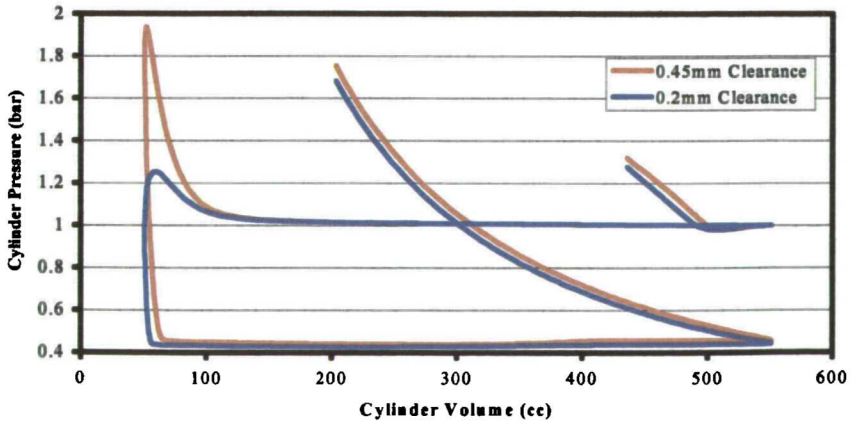

Figure 6.2
Model predictions for pumping loop for two different valve clearances (Test Case No. 1)

6.4. Presentation and analysis of results

The following sections discuss the main features of the experimental results with reference to each of the responses investigated. A full set of results is contained in Appendix 5. The majority of the analysis relied on the use of statistics to determine the most significant factors affecting each response. The results obtained at idle, consisting of a five-variable experiment, were found difficult to model for many of the responses. This was probably due to a combination of the broad range of the variables and the complex nature of the responses. Fitting of a second-order model under these conditions showed a significant lack of fit, and examination of the residuals indicated that the statistics were failing to model the results adequately. However, there were consistent indications that the effect of lift was negligible. Therefore, a decision was taken to remove it as a variable from the analysis, and treat the experiment as one in four variables. Care was needed in interpreting such results so a series of scatter plots were also used to confirm the main features of any trends present. The results for fuel consumption, however, did lend themselves to a more complete analysis and they are discussed.

6.4.1. Oxides of nitrogen

Mean NOx levels were nearly two orders of magnitude greater at 2500 rev/min than at idle. Figure 6.3 shows the factors found to be most influential at each of the part load sites investigated. The two factors that consistently appeared as most important were phasing of the intake and exhaust valve events. Advancing the intake camshaft leads to a longer valve overlap period with an attendant increase in the RGF. Exhaust phasing behaved in a similar fashion when it was retarded, but it consistently appeared as an **AA** term indicating the presence of curvature in the response. NOx levels were lower for a retarded exhaust event, rising as it was advanced towards the middle of the range and then falling again as the valve event was further advanced. This trend was brought about by the exhaust valve closing before the piston reached TDC and was consistent with the changes in RGF predicted by the filling and emptying model.

Figure 6.4 shows a response surface created for RGF predictions from the filling and emptying model (greatest overlap in the bottom left-hand corner), indicating the effect of early EVT to be almost as significant as that due to valve overlap. Exhaust gas residuals within the cylinder act as a 'thermal sink' reducing peak pressures and temperatures during combustion, thereby limiting NOx production [Heywood (1988)]. Figure 6.5 shows the correlation between model predictions for the RGF and NOx levels at the 1500 rev/min test condition, clearly reinforcing the link between the two. RGF is also a function of intake event duration, as it too contributes to overlap, and this is confirmed by the experimental results showing it to be the next most influential factor after intake and exhaust event phasing.

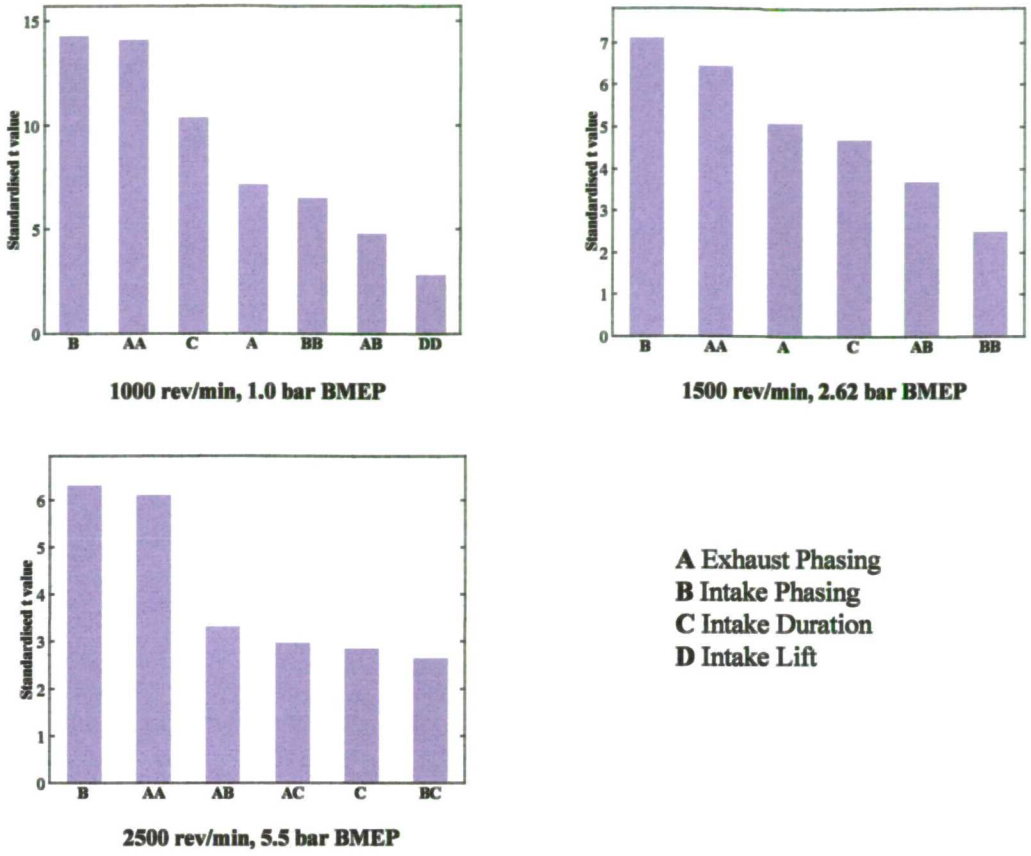

Figure 6.3
Factors influencing NOx emissions

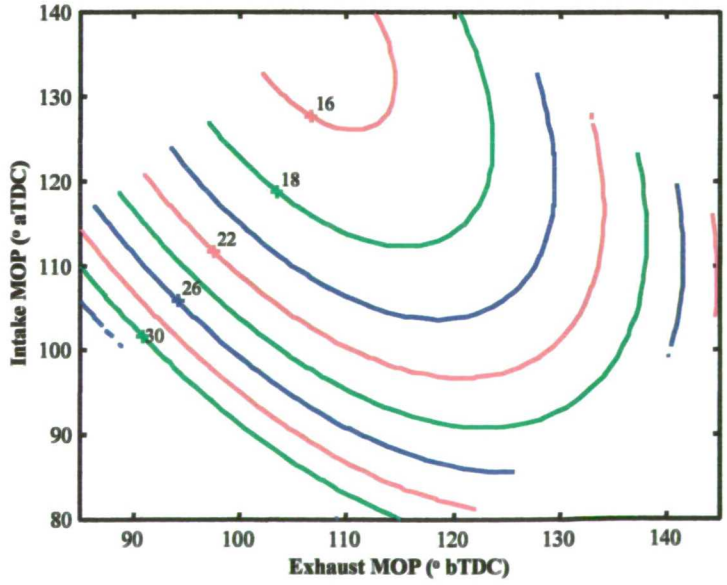

Figure 6.4
Model predictions for RGF (percentage values)
as a function of camshaft phasing at 1500 rev/min, 2.62 bar BMEP

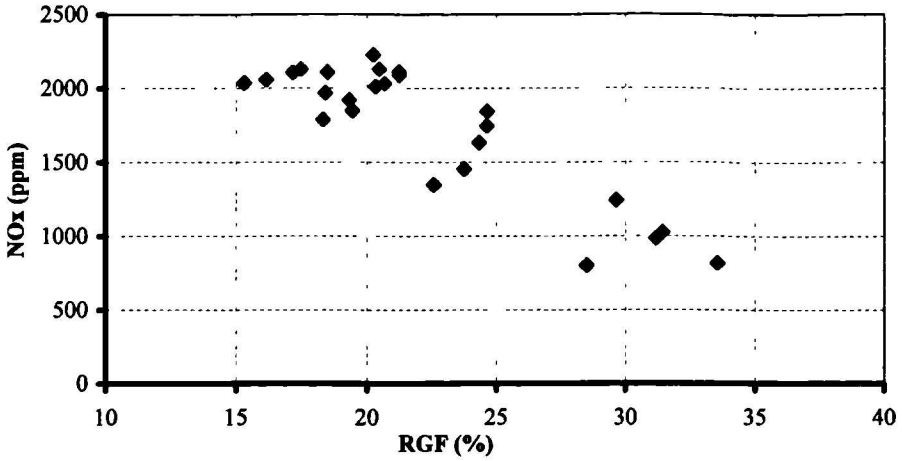

Figure 6.5
Correlation between model predictions for RGF and NOx levels at 1500 rev/min, 2.62 bar BMEP

Figure 6.6 displays the variation in NOx levels at 1500 rev/min as intake and exhaust event phasing are altered, with lines of constant overlap superimposed. Moving along such a line indicates the effect of shifting the overlap period with respect to TDC – equivalent to the dual-equal strategy adopted by Leone *et al.* (1996).

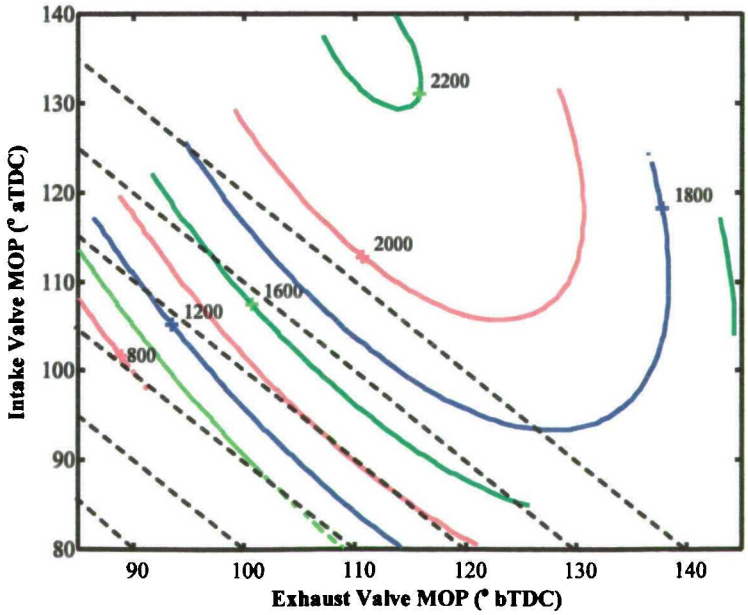

Figure 6.6
Effects of valve event phasing on NOx levels (Vppm) at 1500 rev/min, 2.62 bar BMEP

It is apparent that, for significant degrees of overlap, retarding both events lowered NOx values. The resulting lower compression ratio would have aided in this reduction. However, Figure 6.7 showing NOx variation with intake camshaft phasing and duration for a fixed IVO and overlap,

indicates that changes in duration (and hence, compression ratio) had a relatively modest effect. A second mechanism affecting the results may have been changes in burn rate, due to increased residuals as the events were retarded. The piston may have assisted in drawing gas in from the exhaust port as it began its descent. Advancing the valve overlap would conspire to give the opposite effect. The filling and emptying model predicted this dependence to be insignificant, however, the burn rate data in Figure 6.8 does indeed indicate that the overall burn angle was extended for dual-equal retard.

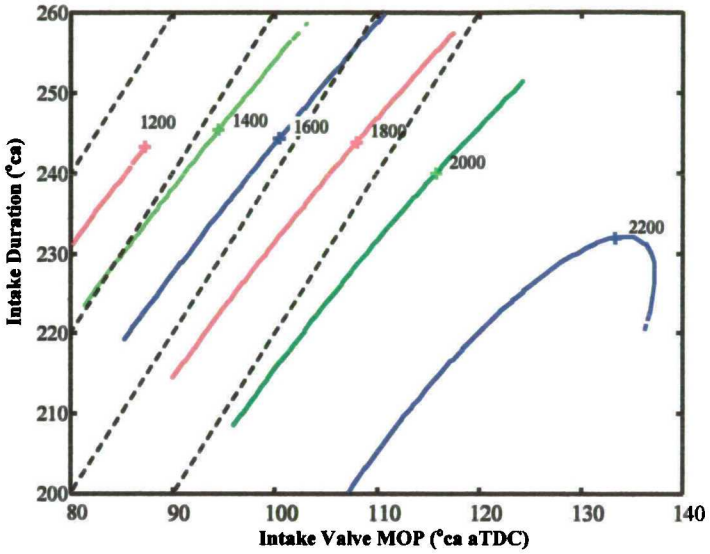

Figure 6.7
Effects of intake event phasing and intake event duration on NOx levels (Vppm) at 1500 rev/min, 2.62 bar BMEP

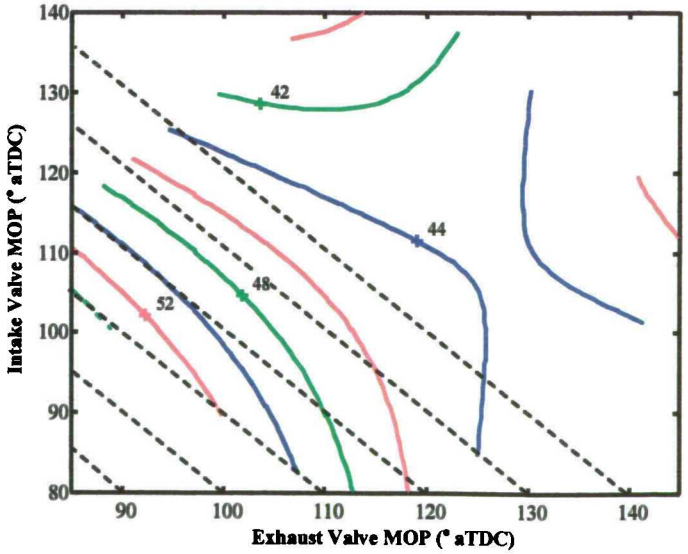

Figure 6.8
The effect of event phasing on 0 – 80% MFB burn duration (° ca) at 1500 rev/min, 2.62 bar BMEP

Under all the conditions investigated, valve lift, and any interactions with it, appeared to be relatively insignificant. This result was surprising since it was expected that a reduced valve lift would help promote in-cylinder turbulence levels and burn rate, with an inevitable effect on NOx levels. Possible reasons for this insensitivity are discussed later in the chapter.

The effects discussed so far relate to NOx levels if equal quantities of exhaust gas from each bank had been combined prior to measurement by the gas analysis equipment. As such, they represent emissions from the engine as a whole. Individual sampling of the two banks consistently indicated a difference between the relative significance of intake and exhaust camshaft phasing at 1000 and 1500 rev/min. The significance plots for the two banks indicated that for the 'A' bank, exhaust event phasing was more significant than intake. Closer inspection revealed the significance of intake camshaft phasing at any particular speed/load condition to be similar in magnitude between the banks, whereas the **AA** effect was less significant for the 'B' bank. The exhaust camshafts fitted to both banks had identical profiles, but, the cylinder heads themselves were from two different periods of development and this may have contributed to this difference. Any differences in valve clearances between the banks may also have had an effect, but this is unlikely, as clearances were set individually for each camshaft. These differences do not alter the conclusion that RGF is the strongest influence on NOx levels at any particular load. The engine was knock limited for the majority of tests at 2500 rev/min. The results at this speed, with retarded ignition timing (relative to MBT), appear to follow the trends already presented.

At idle, NOx levels were relatively low although they too fell with increasing RGF (Figure 6.9). The effect of raising the residual gas level on hydrocarbon emissions was substantial and this would prevent a high RGF strategy from being adopted at this condition unless some mechanism for abating these high HC levels is found. One point worth noting is the apparent fall in NOx with ignition advance when combined with early IVT. This reduction may have been due to the higher RGF levels, caused by the lower plenum pressure which, in turn would be brought about by the lower airflow requirement with an advanced ignition timing. The model predictions for RGF at idle appeared to be very high. It was felt that this might be because of the assumption of perfect mixing of backflow and fresh air in the plenum. Further work to investigate the significance of this effect was conducted by modifying the filling and emptying model to include a separate port volume. The method used was that discussed at the end of Chapter 3 and also in Appendix 2. The results, however, were not convincing although they did predict lower levels of trapped residuals. One reason for this was the tendency for the temperature in the plenum volume to fall rapidly whilst that in the port rose excessively. Time considerations during the latter part of the study precluded further investigation so the original model was used. It was felt, however,

that, because the trend in RGF was plausible even if the absolute values were in error, the model would still be of use for predicting trends in the results.

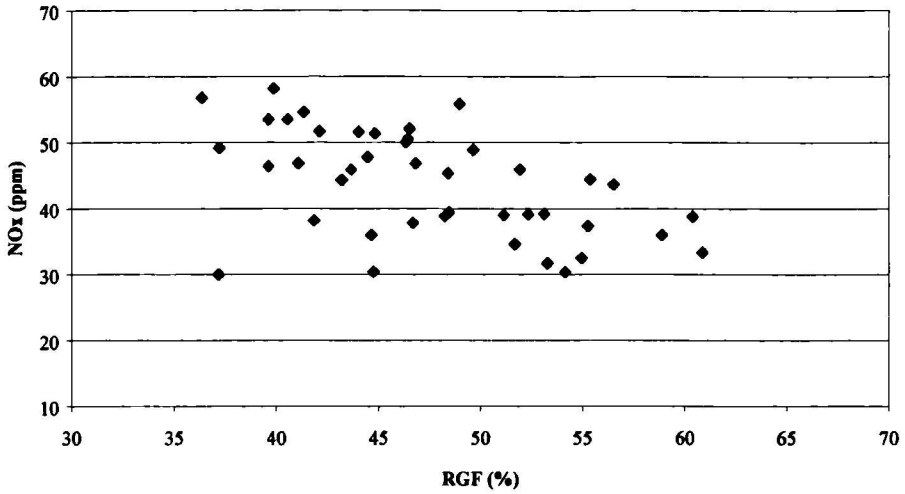

Figure 6.9
Correlation between model predictions for RGF and NOx levels at idle

6.4.2. Unburned hydrocarbons

Unburned hydrocarbon levels are a strong function of exhaust temperature. As load and speed are increased, the higher combustion temperatures serve to promote post-flame oxidation, thus lowering HC levels. The highest levels encountered were during the idle tests, where some of the readings were so high that the engine could be regarded as partially misfiring. Figure 6.10 and Figure 6.11 show the significant factors for unburned hydrocarbons averaged over the two banks. The only variable consistently significant at all speeds was exhaust event phasing, although its effect was different at idle and 1000 rev/min than at the two higher speeds.

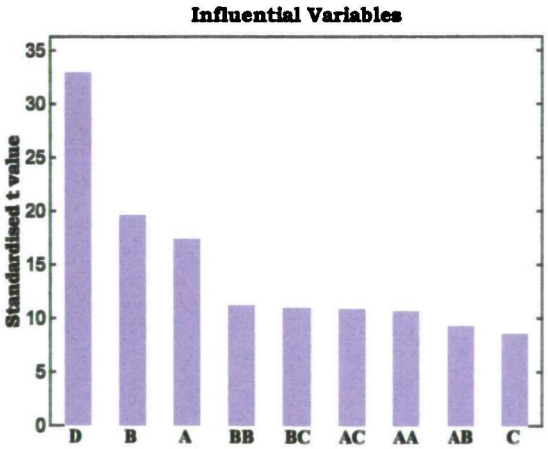

A Exhaust Phasing
B Intake Phasing
C Intake Duration
D Spark Timing

Figure 6.10
Factors influencing HC emissions at idle (ignoring lift)

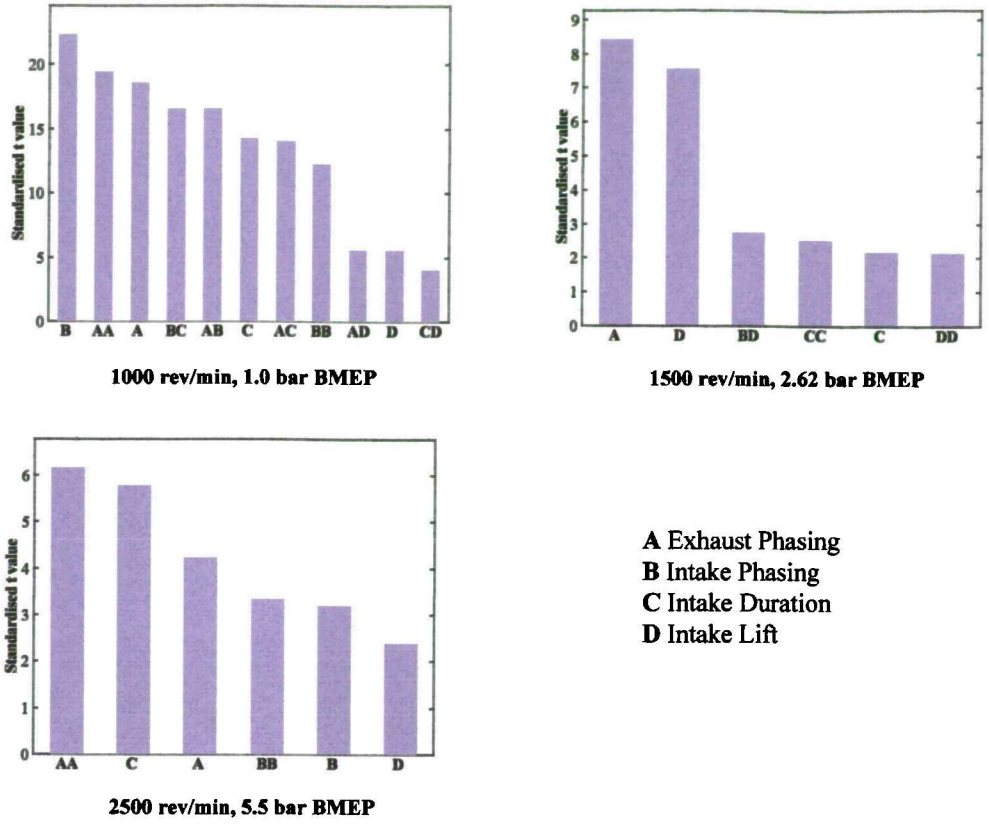

Figure 6.11
Factors influencing HC emissions

The main mechanisms thought to be responsible for lowering HC are high temperatures during the latter part of the combustion process, possibly combined with a longer in-cylinder residence time, and the re-ingestion of the HC-rich gas towards the end of the exhaust stroke [Seabrook (1995)]. The influence of the latter will depend significantly on valve overlap and can be related to the RGF. At idle, spark timing was most influential in controlling HC levels through its effect on exhaust gas temperature (Figure 6.12). The response plots for HC emissions at idle and 1000 rev/min generally followed a trend opposite to that for NOx, again implying a strong dependence on RGF. The curvature with respect to EVT may have been due to the longer residence time for HC prior to EVO and the modest overlap allowing re-induction of the crevice gases. As overlap was increased further, the relatively low combustion temperature would have made bulk quenching more dominant in abating the rate of post-combustion oxidation causing HC to rise. Curvature with respect to IVT and interactions between EVT, IVT and duration, appeared to be far more significant for HC than for NOx. The interactions were caused by the insensitivity of HC to changes in intake and exhaust camshaft phasing and intake duration, when there was little or no overlap as opposed to the sharp rise in HC emissions when overlap was present. HC levels rose when the intake camshaft was significantly retarded.

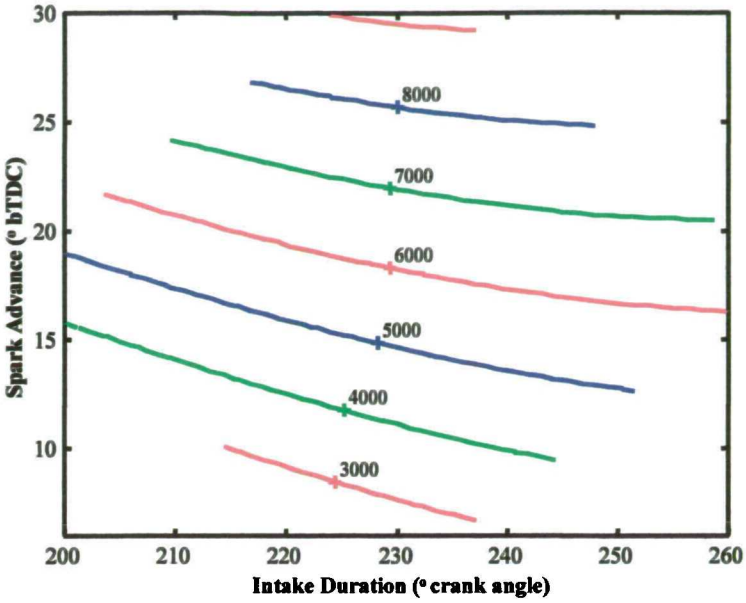

Figure 6.12
The effect of spark advance on HC emissions (Vppm) at idle

At 1500 rev/min, combustion was stable over the range of each variable and only modest differences in HC were observed. The small magnitude of the changes in comparison with the variability in the centre point readings helps to explain the weak significance of the factors. Exhaust event phasing remained an important variable (Figure 6.13), although its effect was to reduce HC levels when retarded. The lack of significance of intake event phasing or duration indicates that late EVO rather than overlap, was the primary influence.

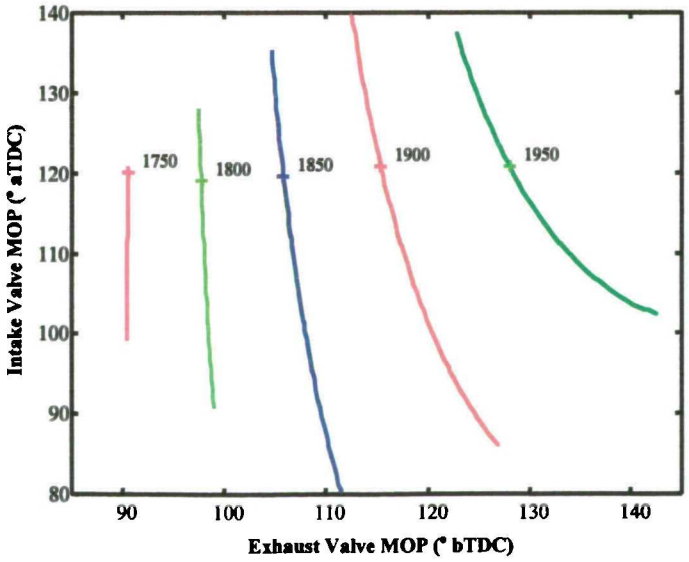

Figure 6.13
Effects of valve event phasing on HC levels (Vppm)
at 1500 rev/min, 2.62 bar BMEP

The results at 2500 rev/min were distorted by the knock-limited ignition timing, helping to explain the lower HC levels for early EVT. Retarding EVT, increasing duration, and to a lesser extent advancing IVT, also appeared to be beneficial probably due to re-ingestion of crevice gases rather than oxidation as exhaust gas temperature was relatively stable for large overlaps (Figure 6.14).

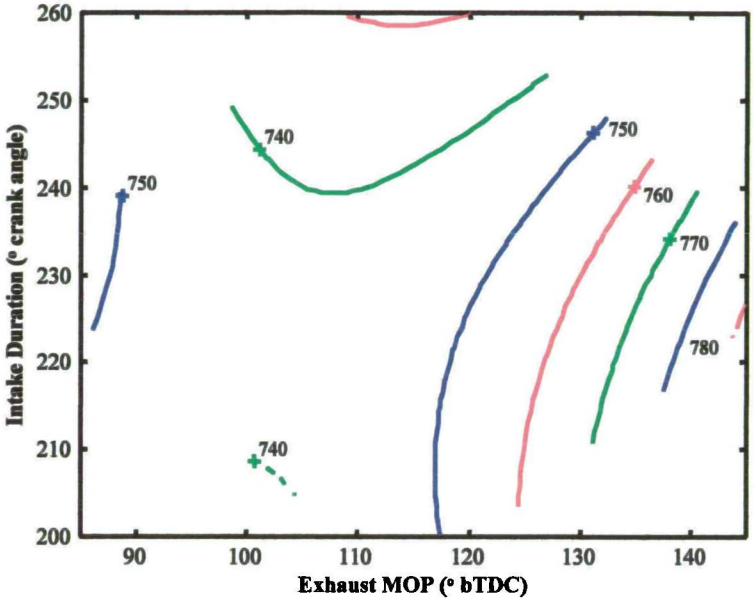

Figure 6.14
The effect of exhaust event phasing and intake event duration on exhaust gas temperature (°C) at 2500 rev/min, 5.5 bar BMEP

6.4.3. Exhaust gas temperature

Exhaust gas temperature at idle and 1000 rev/min is very important in determining the period required for catalyst light-off. At all speeds, a high exhaust gas temperature is expected to aid oxidation of HC. Retarded spark timing and lower burn rates are known to raise exhaust temperature, as combustion continues later into the cycle. Figure 6.15 demonstrates the strong dependence of exhaust temperature on spark advance at idle. At 1000 and 1500 rev/min early EVT dramatically reduced exhaust gas temperature (Figure 6.16). The reverse was true at 2500 rev/min (see Figure 6.14).

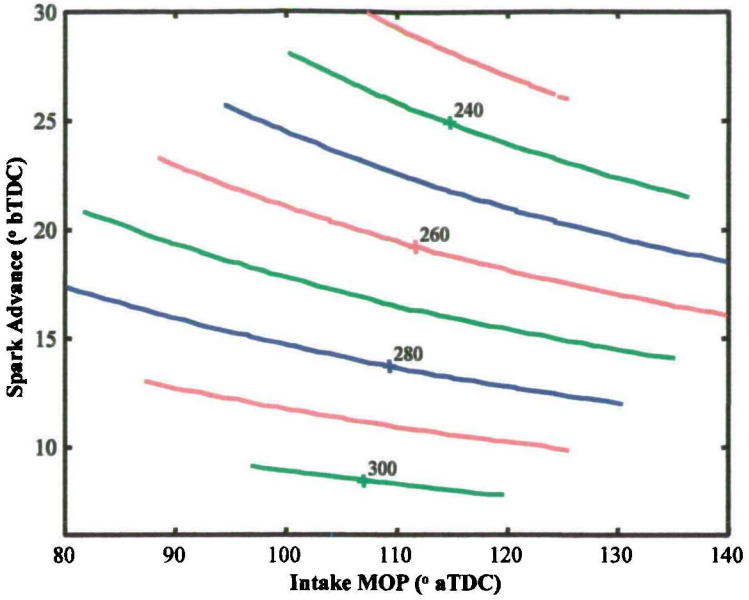

Figure 6.15
The effect of spark advance on exhaust gas temperature (°C) at idle

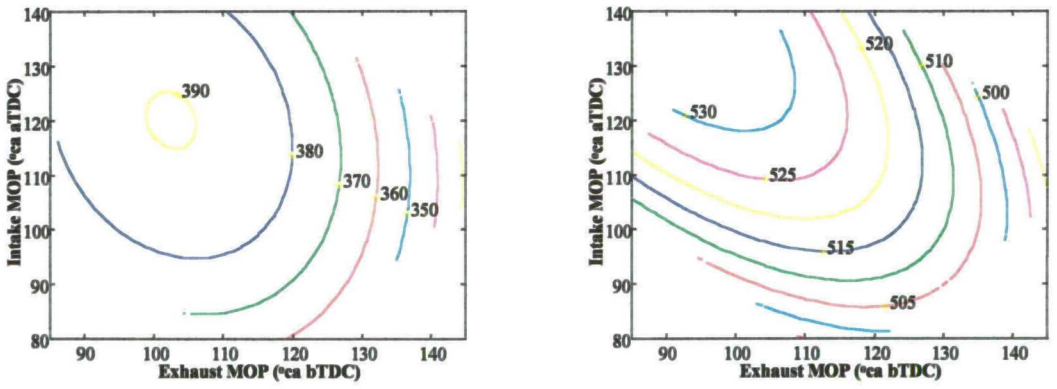

1000 rev/min, 1.0 bar BMEP **1500 rev/min, 2.62 bar BMEP**

Figure 6.16
Effects of valve event phasing on exhaust gas temperature (°C)

Figure 6.17 shows how MBT spark timing varied for the three speeds. At 2500 rev/min, an advanced exhaust event setting reduced the maximum allowable spark advance due to the earlier onset of knock consequently raising exhaust temperature. At the lower speeds, the engine required more ignition advance as the exhaust events were advanced past the middle of their range. The burn duration data for 1500 rev/min (see next section) indicates little change at these settings. It is therefore reasonable to conclude that the lower temperatures were due to the advanced spark timing, allowing more work to be extracted from the expanding gases.

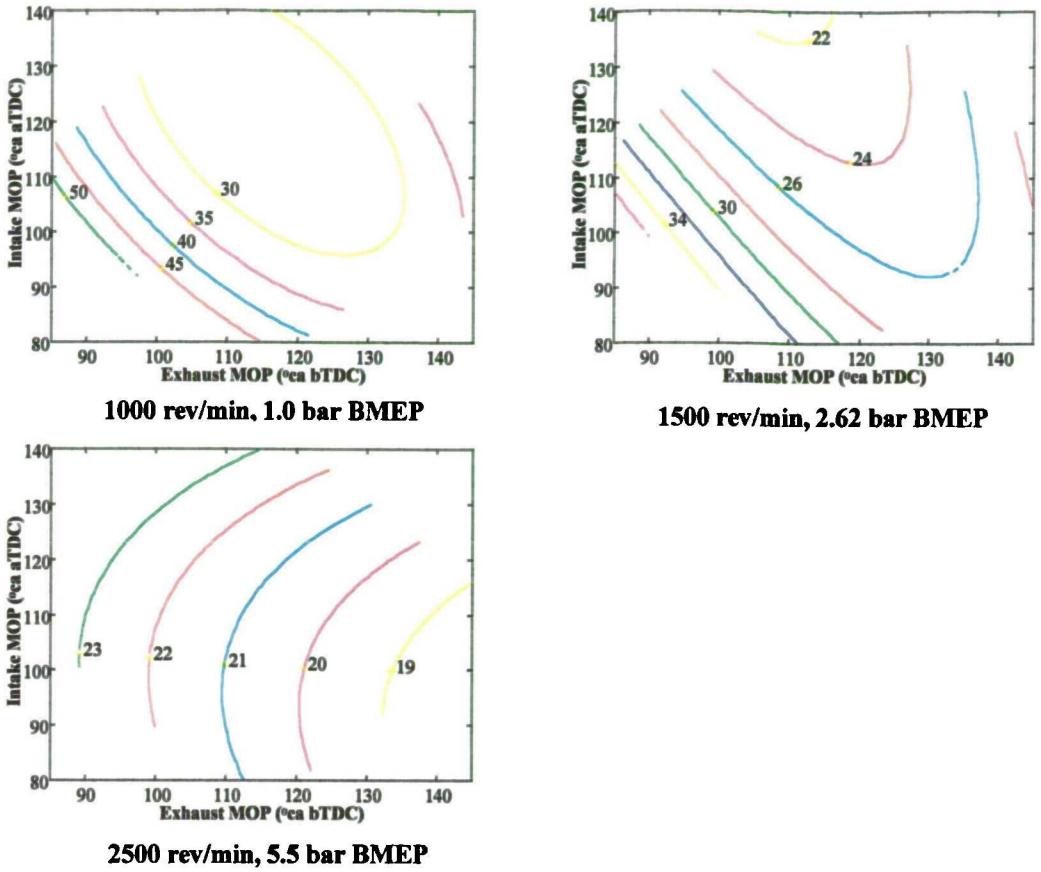

1000 rev/min, 1.0 bar BMEP

1500 rev/min, 2.62 bar BMEP

2500 rev/min, 5.5 bar BMEP

Figure 6.17
The effect of event phasing on MBT spark timing (° ca)

6.4.4. Burn duration at 1500 rev/min and idle

Burn rates were calculated from cylinder pressure data averaged over a period of 30 seconds at 1500 rev/min (375 cycles) and one minute (300 cycles) at idle. A simplified first-law analysis was adopted as it was consistent with that used by the AVL system at Jaguar. The analysis was for comparative purposes only, so heat transfer to and from the cylinder walls was ignored, as it would have been similar in magnitude between the tests. The burn rate data was used to construct cumulative heat release plots from which the crank angle corresponding to 80% of the Mass Fraction Burned (MFB) was estimated. Since the crank angle corresponding to the minimum in the heat release curve was difficult to determine precisely, spark timing was used as the angle for 0% for heat release.

Influential factors at idle and 1500 rev/min are shown in Figure 6.18. The significance levels at 1500 rev/min were relatively low with no single factor being dominant. Again, the implication was that burn duration at both speeds varied with factors affecting the levels of RGF. However, at 1500 rev/min, a comparison with RGF predictions demonstrates that other factors may have been just as important.

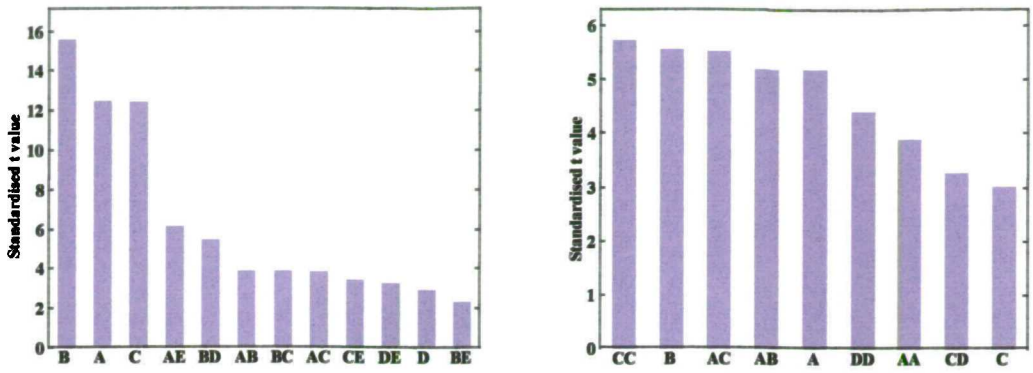

Idle **1500 rev/min, 2.62 bar BMEP**

A Exhaust Phasing **B** Intake Phasing
C Intake Duration **D** Intake Lift
E Spark Timing (idle only)

Figure 6.18
Factors influencing 0 – 80% MFB burn duration

Figure 6.19(a) shows the response of burn duration to changes in intake event duration and phasing, with lines of constant overlap superimposed. Moving along these lines represents changes in the angle of intake valve closure. Figure 6.19(b) shows a similar plot for predicted RGF.

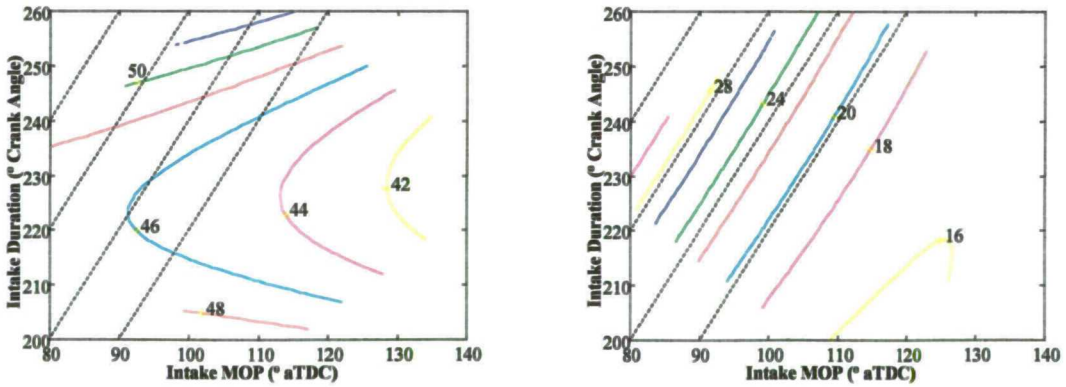

(a) **(b)**

Figure 6.19
The effect of intake event phasing and duration on (a) 0-80% MFB burn duration (° ca) and (b) model predictions for RGF (%) at 1500 rev/min, 2.62 bar BMEP

While the model predictions show the RGF contours following lines of constant overlap (where it exists), the burn duration plots at both speeds indicate that burn angle was lengthened as IVC was retarded. One possibility is that turbulence levels may have been adversely affected by extending the period of reverse flow into the intake port at the end of the induction stroke. The level of turbulence was not expected to be great at idle so this can only be a partial explanation.

The discussion on NOx levels and model predictions at 1500 rev/min indicated that RGF levels were high for an advanced exhaust event, but the plot for burn duration did not show a corresponding rise (Figure 6.8). Spark timing was advanced for these settings, although not to the extent required when large overlaps were present. The exhaust gas temperature was also lower indicating that combustion was completed earlier. It is conceivable that the higher temperature of the RGF trapped, and partially compressed due to early EVT, helped in maintaining burn rate, whilst the temperature of that due to overlap would have been lower due to backflow into the intake port.

The effect of spark angle on burn duration at idle was more pronounced for retarded ignition settings (Figure 6.20). Changes in the engine's air consumption were greater for these settings. As the spark was advanced, airflow into the engine fell as efficiency was improved. The resulting reduction in manifold pressure led to increased residual levels, and both would have raised burn duration angles. There is no clear reason for changes in burn duration in the absence of overlap.

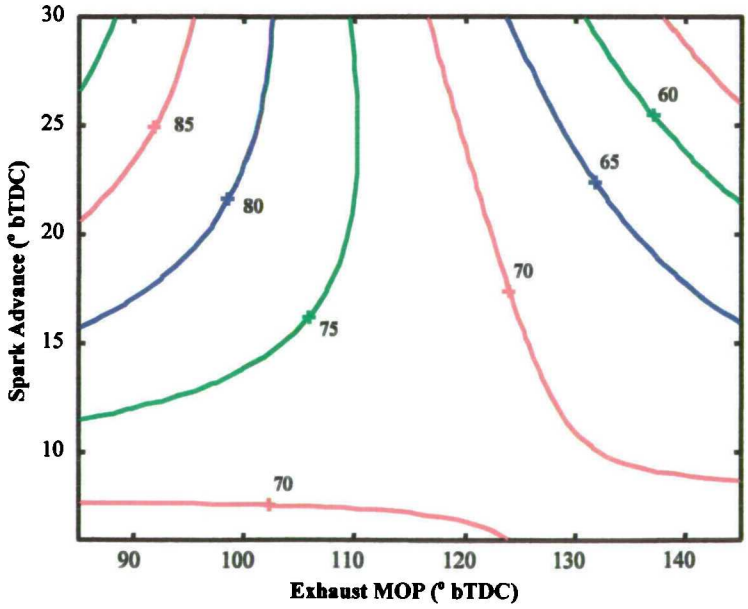

Figure 6.20
The effect of exhaust event phasing and spark advance on 0-80% MFB burn duration (° ca) at idle

6.4.5. Fuel consumption

The significance tests for brake specific fuel consumption at part load conditions, shown in Figure 6.21, indicated very few factors to be influential. This result was due in part to the changes in the modelled response being small in magnitude. More importantly, the relatively large variation in the fuel consumption readings for the centre points produced a large value for the estimated variance of the data. In addition to representing random variation in engine

behaviour, the estimate of variance also includes the effects of human error and variability in instrumentation. The dynamic fuel balance used for measuring fuel flow rate was located inside the test chamber with a considerable portion of the fuel system exposed to the elevated temperatures present during the tests. Vaporisation due to heat transfer to fuel in the return line is believed to have intermittently disrupted the return flow from the fuel rail regulator to the balance giving inconsistent readings in fuel consumption. This problem is thought to be the primary cause of the large variations in fuel consumption. The idle tests were conducted separately. As temperatures were lower and attempts at alleviating the problem had been made, the results were not significantly affected by fuel vaporisation.

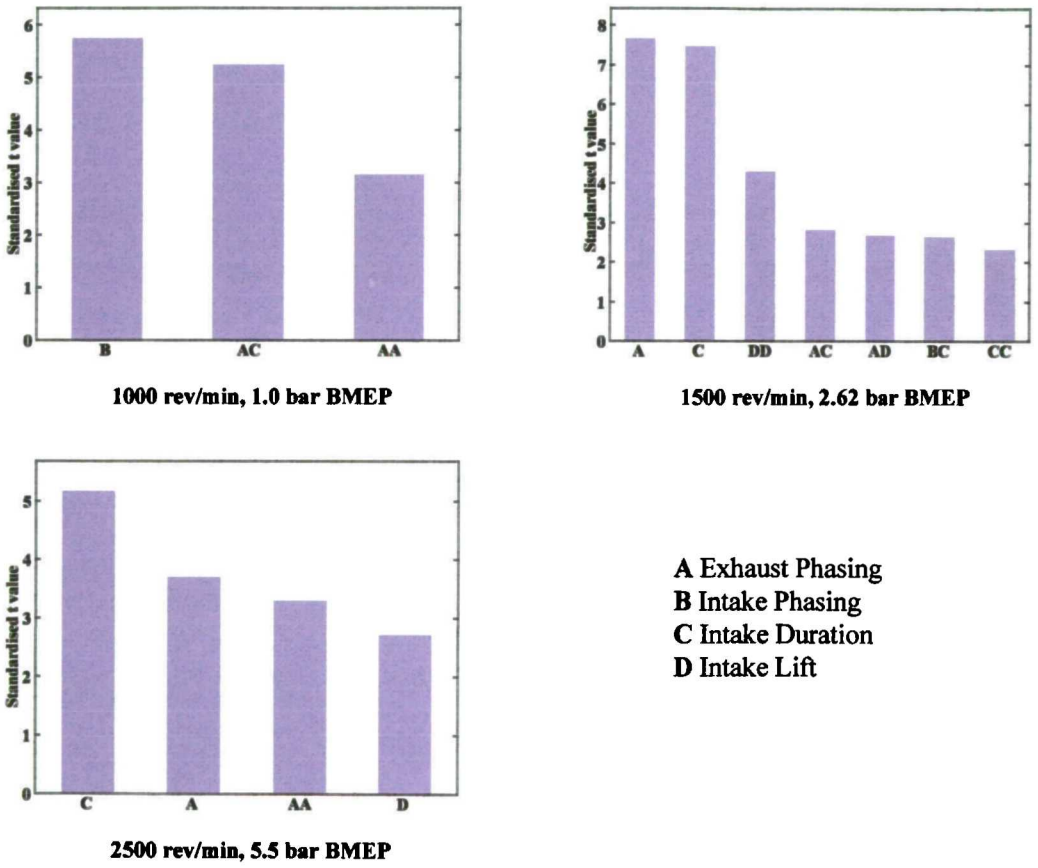

Figure 6.21
Factors influencing brake specific fuel consumption at part-load

Figure 6.22 shows the manner in which fuel consumption varied with changes in EVT, IVT, and duration at 1000 rev/min. Factors that raised RGF levels increased fuel consumption because of the associated deterioration in combustion. Curvature of the response with EVT, and the interaction between EVT and duration, may have been due to a combination of the loss in expansion work and the effect of early exhaust timing on RGF. Figure 6.23 shows how fuel consumption varied with changes in EVT, IVT, and duration at the 1500 rev/min test condition.

The engine was more tolerant of residuals as higher turbulence levels helped in maintaining combustion. Late EVT could therefore be used to extract more work during expansion without the penalty of deterioration in combustion caused by the longer overlap. Reductions in pumping work for high residual levels would also have contributed to improvements in fuel consumption.

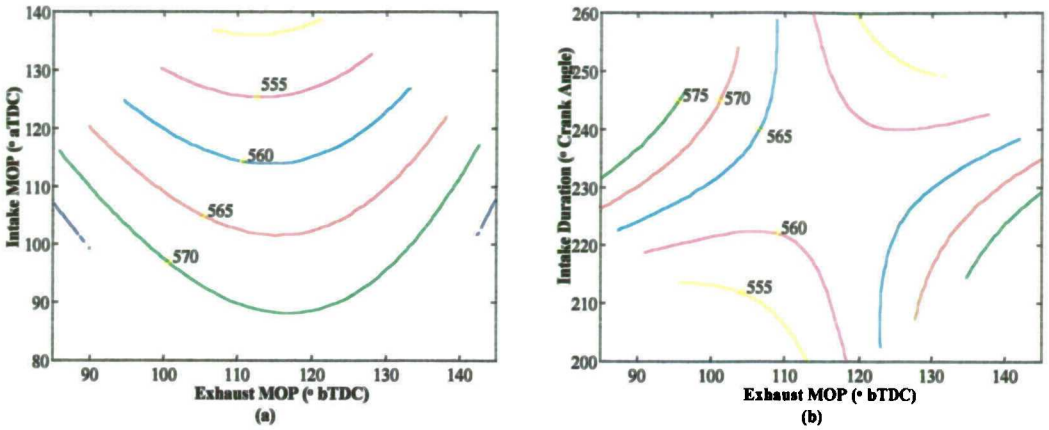

Figure 6.22
The effect of exhaust event phasing with (a) intake event phasing and (b) intake event duration on brake specific fuel consumption (g/kWh) at 1000 rev/min, 1.0 bar BMEP

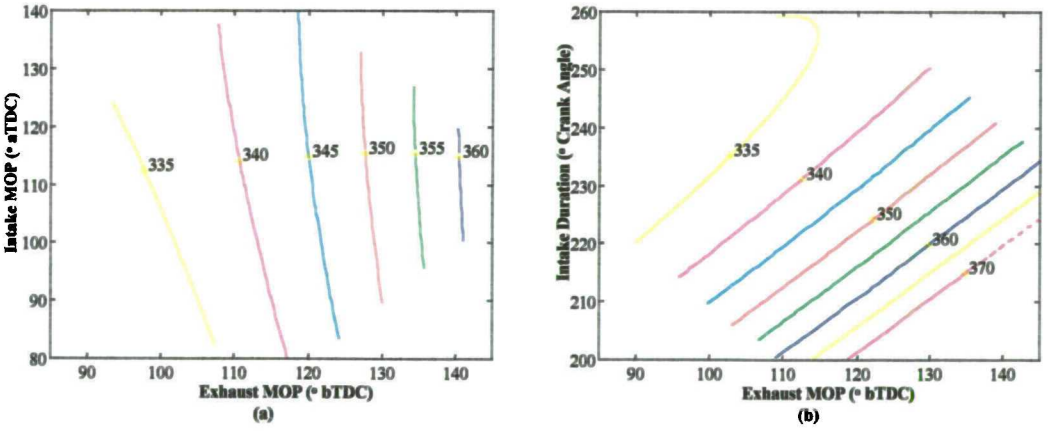

Figure 6.23
The effect of exhaust event phasing with (a) intake event phasing and (b) intake event duration on brake specific fuel consumption (g/kWh) at 1500 rev/min, 2.62 bar BMEP

Figure 6.24 relates model predictions for pumping work to those for RGF. Higher levels of charge dilution necessitate a higher plenum pressure to maintain the flow rate of air into the engine. This leads to a decrease in pumping work due to the reduction in area of the pumping loop on the pressure/volume plot. This benefit is lost if early EVT is used to increase the RGF as the resulting increase in pumping work may well offset any benefit from the higher plenum

pressure needed. This explanation is also supported by the fuel consumption results, which indicate early EVT strategies had the highest fuel consumption.

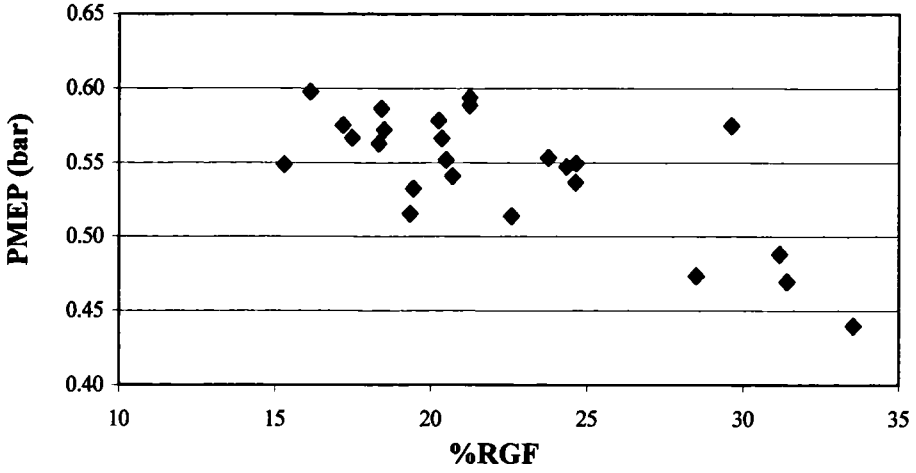

Figure 6.24
Correlation between model predictions for pumping work and residual levels at 1500 rev/min, 2.62 bar BMEP

At 2500 rev/min, the duration of the intake valve event became the most significant factor and the effects of peak lift were more pronounced. Superimposing lines of constant IVO on the response plot for duration against IVT (Figure 6.25) indicated that fuel consumption was insensitive to IVO, but further study shows that BSFC fell as IVC was retarded. This result implied that any improvement in efficiency due to raising the compression ratio was counterbalanced by an effect in the opposing direction. One factor may have been the onset of knock, which limited ignition advance, thereby increasing fuel consumption. Figure 6.26 however, shows that spark timing, and therefore knock was not significantly affected by intake event duration with the effects of lift and EVT being more influential. It is difficult to suggest any other effects to explain this trend. Given the relatively low significance of the results, it is not worthy of further comment. Lift, which appeared as the most significant effect in the spark timing response, also affected fuel consumption. Changes in spark timing were not well modelled as a function of lift with both star points (3.0mm and 8.6mm) being outliers. It would be reasonable, however, to conclude that lower peak lifts encouraged the onset of knock, perversely by raising burn rates, therefore limiting ignition advance. Consequently, fuel consumption was seen to rise slightly for lower values of lift.

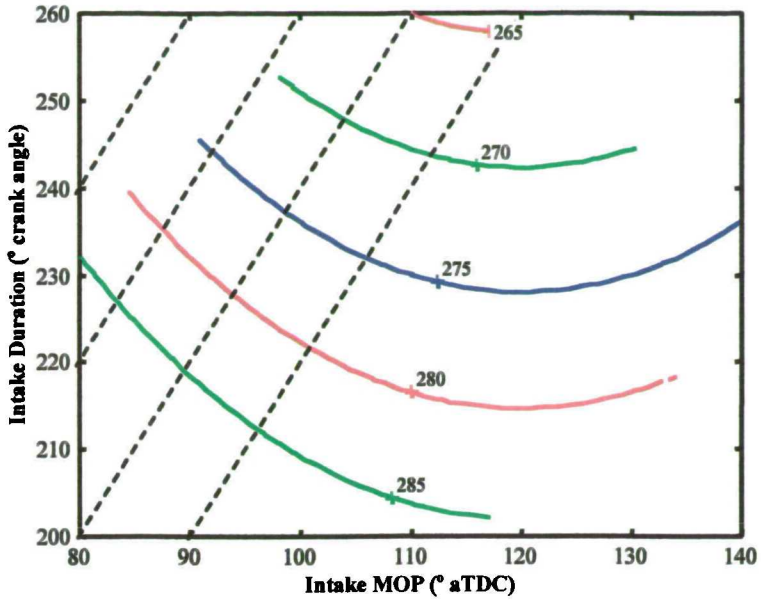

Figure 6.25
The effect of intake event phasing and duration on brake specific fuel consumption (g/kWh) at 2500 rev/min, 5.5 bar BMEP

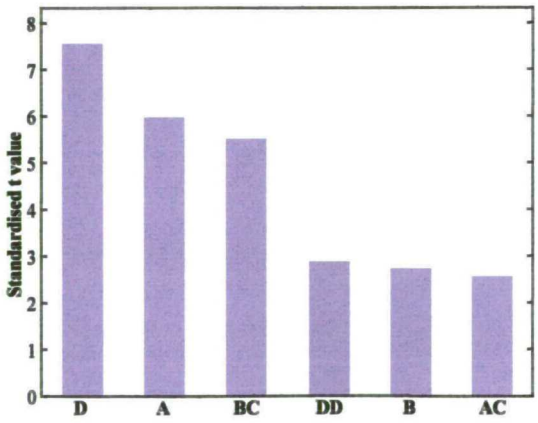

A Exhaust Phasing
B Intake Phasing
C Intake Duration
D Intake Lift

Figure 6.26
Factors influencing spark timing at 2500 rev/min, 5.5 bar BMEP

Analysis of the residual plot for the idle tests revealed that lift was not well modelled. The significance tests indicated that lift was the least influential of the variables so it was removed to give an equivalent four-variable experiment. The resulting analysis produced an improved residual plot, which is compared with the original in Figure 6.27. Comparison of the significance tests between the two methods of analysis showed that the same factors appeared to be significant (apart from those involving lift) producing response surfaces almost identical in nature. It was therefore decided that the five-variable analysis was valid provided no conclusions were drawn about the effect of intake valve lift.

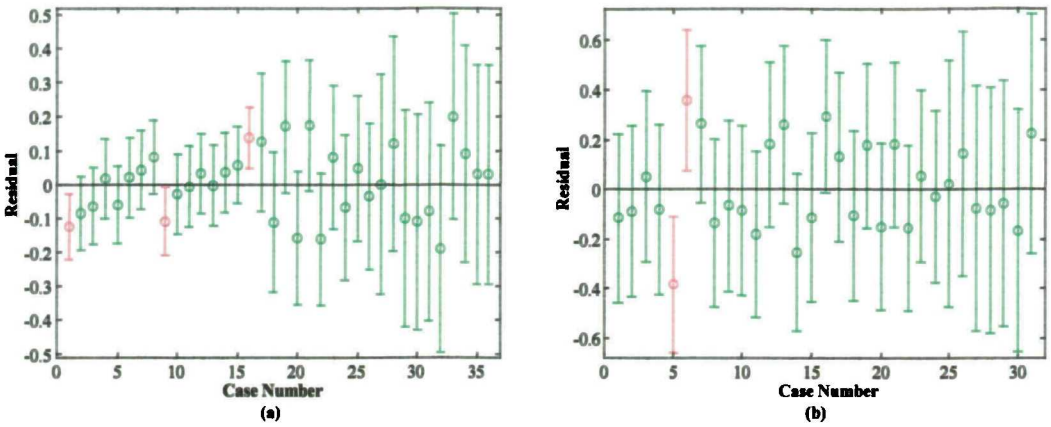

Figure 6.27
Comparison of residual plots for BSFC at idle with (a) all five variables and (b) four variables (lift removed)

Fuel consumption at idle was predominantly determined by spark timing (Figure 6.28). The range of values used was retarded significantly from typical MBT values, as explained in Section 6.2 so that any advancement in timing would inevitably improve efficiency. The effect of increasing overlap was to raise fuel consumption due to the rapid deterioration in combustion. In fact, the extremely high levels of unburned HC measured for some of the test conditions would account for much of this increase.

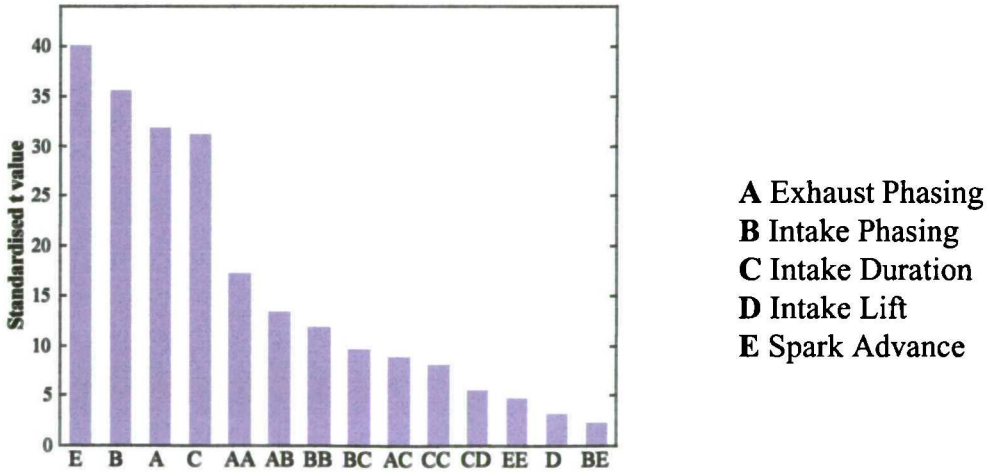

Figure 6.28
Factors influencing fuel consumption at idle

6.5. The effects of changes in peak intake valve lift

Of all the experimental variables, lift proved the least influential for most of the responses. Figure 6.29 shows the effect of lift and intake camshaft phasing on 0-80% MFB at 1500 rev/min.

Both high and low values of lift were beneficial in enhancing combustion while peak lifts in the middle of the range gave the poorest performance. This trend was characteristic of the manner in which many of the responses behaved to changes in lift.

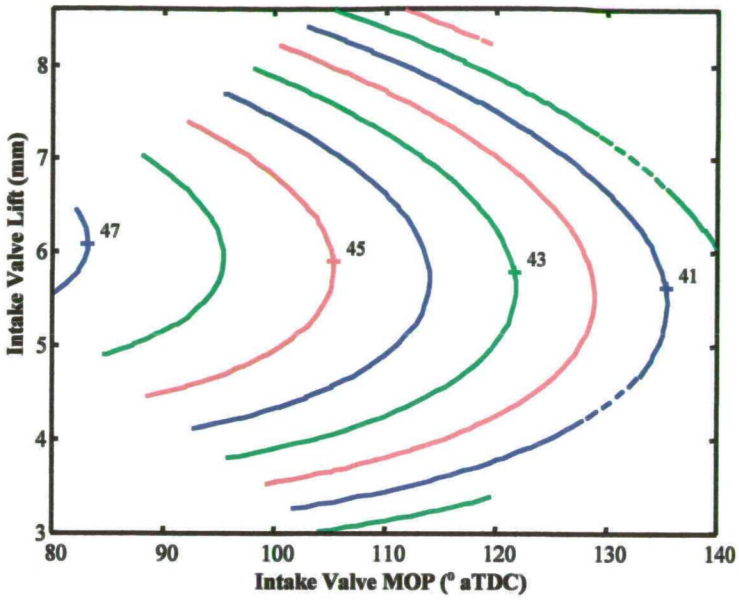

Figure 6.29
The effect of intake event phasing and intake valve lift on 0 – 80% MFB burn duration (° ca) at 1500 rev/min, 2.62 bar BMEP

Valve lift was expected to influence in-cylinder motion by enhancing velocities past the intake valve when lift was reduced. Figure 6.30 compares model predictions for velocity, mass flow and momentum against crank-angle for three camshafts of identical phasing and duration with lifts of 3.0, 5.8, and 8.6 mm at 1500 rev/min, 2.62 bar BMEP. A high valve lift imparts the least momentum to the gas entering the cylinder. The momentum only increases significantly when the lift is substantially reduced. There is very little difference in the characteristics for 8.6 mm and 5.8 mm lift camshafts.

The advantage of a higher lift was demonstrated by the series of steady-flow tumble tests described in Chapter 2, which showed that a high lift was necessary to establish a structured tumbling motion within the cylinder. Whereas tumble is expected to persist well into the compression stroke, the higher velocities and chaotic nature of the flow generated by small valve lifts has a greater potential for energy to be dissipated early. The medium lift strategies may have suffered from a combination of low velocities and the lack of tumble showing them to be the least effective in enhancing combustion.

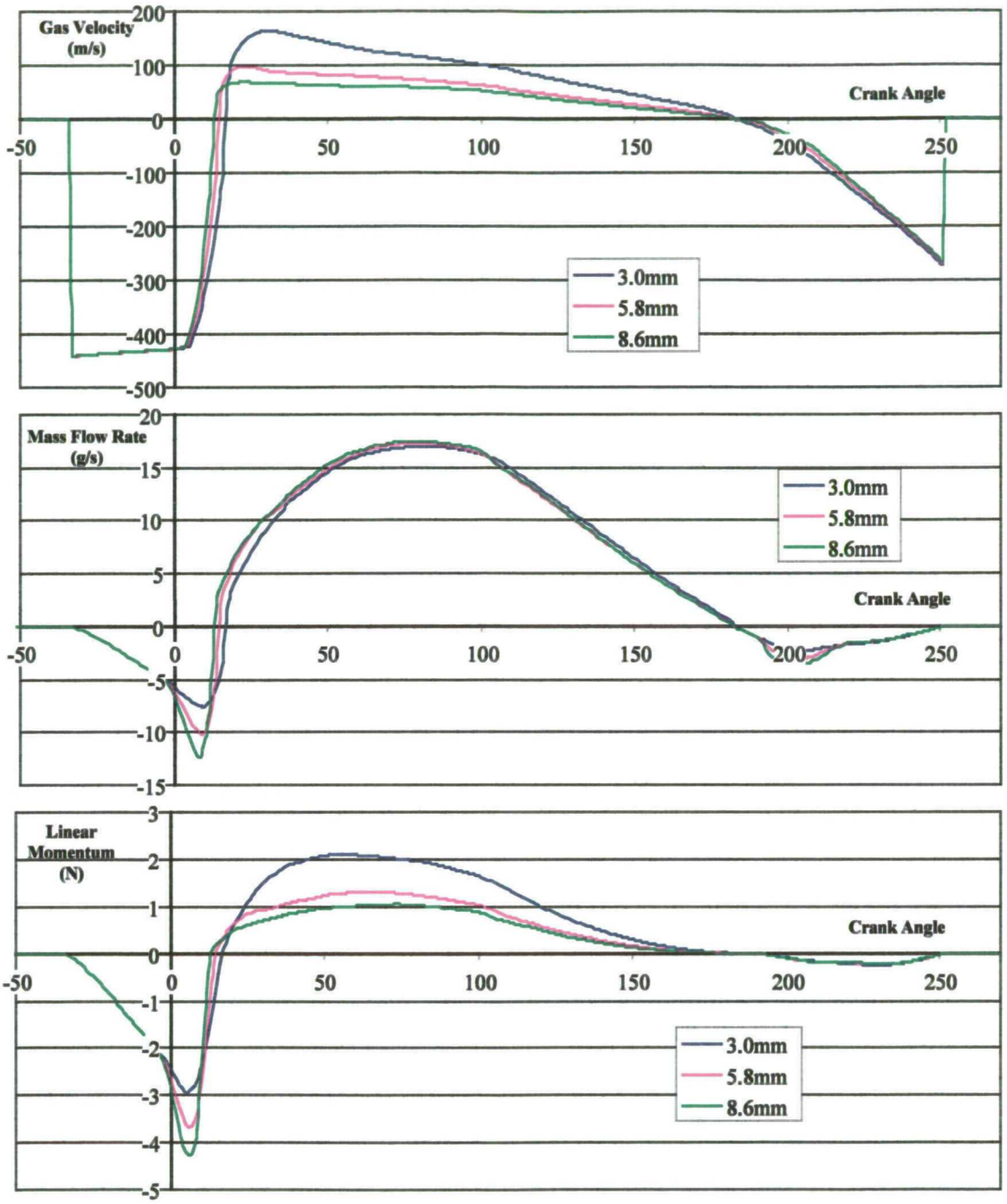

Figure 6.30
Model predictions for gas velocity, mass flow and momentum past the inlet valve for three different values of peak lift at a simulated condition of 1500 rev/min, 2.62 bar BMEP

6.6. A way forward

The results presented in this chapter testify to the importance of using exhaust residuals to their best advantage at part load. The potential for reducing NOx was present for all the conditions investigated. HC emissions could also be improved provided combustion did not deteriorate

significantly. At idle, HC levels dictated the need for reduced overlap. The engine's ability to tolerate large quantities of RGF was not greatly extended by any of the strategies investigated, and the potential for improvements due to reductions in lift was not apparent. It is valid to conclude that there is little value in continually varying valve lift at the part-load conditions investigated. There was an indication that the disappointing response to lift is a result of loss of structured flow within the cylinder (i.e. tumble) at low lifts. However, there was some indication that reduced lifts may enhance momentum of the gas entering the cylinder, although it could be dissipated very quickly due to the chaotic nature of the flow. Therefore, a strategy combining the benefits of higher gas velocities together with a structured in-cylinder motion capable of persisting well into the compression stroke should prove advantageous. For this reason, Phase 2 of the project was based around the application of valve deactivation, with a reduction in lift of the primary valve to 3.3 mm. This could be expected to combine high gas velocities with a strong axially swirling motion. One aim would be to maximise residuals so exhaust event phasing would be removed as a variable and instead be set to its most retarded setting for all tests apart from idle. The two remaining variables, intake event phasing and duration, could then be explored in a full factorial experiment at five levels.

Chapter 7

PHASE 2 – AN INVESTIGATION INTO THE BENEFITS OF VALVE DEACTIVATION

7. Phase 2 – An Investigation into the Benefits of Valve Deactivation

7.1. Introduction

This chapter presents results from engine tests conducted to investigate the effects of changes in two valve-event variables whilst operating only one intake valve per cylinder. The two variables selected were the durations of the valve overlap period and of the intake event. Limiting the lift of the active valve to 3.3 mm further enhanced the effects of valve deactivation. The combination of valve deactivation and low lift was chosen because the swirl and tumble measurements reported in Chapter 2 showed that these conditions led to particularly vigorous in-cylinder gas motion. It was hoped that this enhanced motion could be utilised to allow combustion to take place with high levels of residual exhaust gas in order to reduce NOx emissions. Overlap was selected as a variable due to its relatively direct linkage with residual gas concentration. Inlet valve duration was chosen as the second variable because the results of Phase 1 testing had suggested possible benefits from optimising the point of IVC. It was decided to investigate these variables over wide ranges in order to appreciate their full significance. The extreme nature of some of the settings meant that there was a possibility the engine would not be able to operate satisfactorily. A full factorial experimental design was consequently chosen, as it was better able to cater for missing data.

7.2. Design of experiment and selection of camshaft profiles

The use of only two variables for the investigation made it feasible to employ a full factorial experiment. It was decided to investigate each variable at five levels as this offered a good compromise by allowing the use of a higher order regression model whilst maintaining a manageable number of tests points. Another advantage of such a design was the relative immunity to test points at which the engine might fail to run satisfactorily. The test condition in the middle of the experimental space was repeated up to five times, allowing variability to be quantified as with the CCRD experiment used for Phase 1 testing.

The method chosen for designing the family of camshafts was slightly different from the Phase 1 tests. The two main areas of interest were overlap and IVC, and so it was felt that the camshaft profile should be as similar as possible in these areas. It was therefore decided to add a constant

lift section in the middle of the profile. The duration of this constant lift section could then be adjusted to set the overall period of the intake event, allowing the opening and closing portions of the profile to be identical. Inclusion of a constant lift section required modification to the camshaft design program to allow both valve acceleration and velocity to reach a value of zero before entering the constant lift section. Previously the design program only required zero jerk in the transition from the opening to closing part of the profile. Figure 7.1 shows profiles of two different periods.

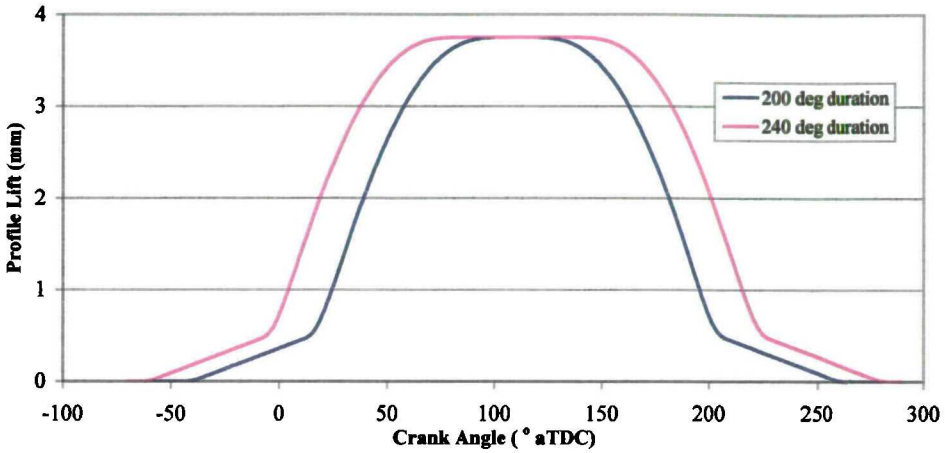

Figure 7.1
Comparison of camshaft profiles of two different periods

Constraints such as maximum valve acceleration and velocity set a limit on the minimum duration that could be used for a given lift whilst the amount of material available on the camshaft blanks set the maximum. The upper limit for overlap duration was determined by the risk of valve/valve and valve/piston interference, with the result that IVO could not occur before 35° bTDC and EVC not later than 35° aTDC. Phase 1 results had indicated that overlap values greater than 30° gave the greatest potential at 1500 and 2500 rev/min, whilst the rapid rise of hydrocarbons at 1000 rev/min and idle limited the potential for overlap values much greater than this. The tests were therefore divided into two sets, and different ranges of overlap were selected for the pairs of engine operating conditions. The ranges chosen are shown in Table 7-1.

	Exhaust MOP	Overlap	Intake duration
1000 rev/min and idle	115° bTDC	-25° ca to 35° ca	200° ca to 280° ca
1500 and 2500 rev/min	80° bTDC	30° ca to 70° ca	200° ca to 280° ca

Table 7-1
Experimental ranges chosen for overlap period and intake event duration at four speed/load test conditions

7.3. Engine modifications to achieve valve deactivation

There were two aspects of the engine hardware requiring modification to allow consistent operation under deactivated conditions. The first was the disablement of one of the two intake valves per cylinder, which was simply achieved by removal of one of the 'bucket' tappets. The two camshaft lobes for each cylinder were machined to be identical, and the low lift (3.3 mm) ensured that there was no danger of interference between the camshaft lobe and the top of the valve stem of the deactivated valve. The second modification involved changes to the injector targeting to avoid fuel collecting in the deactivated port. Honda [Horie *et al.* (1992)] overcame this problem by opening the deactivated valve by a small amount. The steady flow tests, however, indicated that such a strategy would result in much of the advantage of complete deactivation, namely the high swirl and tumble levels observed, being lost. An alternative strategy of targeting the injector spray only down the active port would have required extensive reworking of the plenum, which had an integral fuel rail housing the injectors. This method was therefore rejected as a potential option. The AJ26 engine was fitted with twin-spray injectors, targeting fuel jets individually down each port. A single pintle-type needle metered the fuel and a cap fitted to the end of the injector formed the two jets. Blocking of one of the holes in the end cap ensured that all the fuel was supplied by a single jet targeted in the direction of the active valve, allowing the engine to be operated with complete valve deactivation. Finally, care was taken to ensure that the injection timing remained identical for all the tests by appropriate modification to the maps in the ECU. A brief investigation was conducted to ascertain the effects of injection timing on hydrocarbon levels, but the results proved inconclusive, generally showing little dependence.

7.4. Test details

The tests at the 1500 and 2500 rev/min conditions were performed before the 1000 rev/min and idle tests. The procedure for determining ignition timing was identical to that used for the earlier series of tests. As previously, the spark timing at 2500 rev/min was entirely knock-limited and was consequently retarded 2° from the onset of audible knock. Ignition timing was again included as a variable at idle.

Initial idle tests were conducted under open loop fuelling and with the propeller shaft disconnected, but the engine was very unstable. It was felt that this instability was more a function of the manner in which airflow was measured and fuelling calculated rather than an inherent instability in the combustion process. No solution could be found for the problem and it

was therefore decided to conduct the tests with the propeller shaft connected as the combination of its inertia and that of the dynamometer helped to reduce the problem. During this period it was decided that injection pulsewidth should be fixed at each test point to reduce variability due to changes in fuelling. The pulsewidth could be determined by observing the output voltage from the two HEGO sensors and setting them so that they were in the middle of their range, this corresponding to stoichiometric operation. It was estimated that, typically, pulsewidth could be set to within 10 μs of the pulsewidth corresponding to stoichiometric fuelling using this method. It was later discovered that more stable running resulted when this approach was applied to the fuelling constant instead of pulsewidth. For Phase 1, this fuelling constant had remained fixed at a value determined from the centre points using a calibrated lambda sensor. Adjusting this constant to a setting where the engine's HEGO sensors indicated stoichiometric operation appeared to give the best performance. The last half of the tests at idle were conducted using the latter method. Time, and more importantly fuel limitations, precluded a return to the earlier test points, and so the regression model for the idle results was modified to include an additional variable representing fuelling strategy.

7.5. Test Results at Part-Load

Results from the engine tests were used to construct a series of regression models for each of the responses of interest. It was not initially known whether a second-order polynomial, as had been applied to the results of the CCRD experiment, would be suitable for identifying the main trends. Inspection of the residuals for the second-order model indicated a satisfactory fit and it was therefore decided to use this model for the analysis. In addition, a quadratic model had the advantage of being consistent with the method used for analysing results from the CCRD tests. As before, the regression model was used to identify the influential factors and to plot contours for each response. A full set of results is included in Appendix 6.

7.5.1. Oxides of nitrogen

The aim of using large values of overlap was to minimise NOx production. The first phase of engine tests had confirmed the potential for achieving very significant reductions by employing such a strategy. Figure 7.2 shows the factors found to be most influential in determining NOx emissions with the corresponding contour plots at the three part-load speeds investigated. Overlap remained the most influential variable even though the compression ratio was much reduced for some of the test points. The effects of changes in compression ratio were isolated by superimposing vertical lines onto the contour plots (not shown). With overlap fixed, changes in

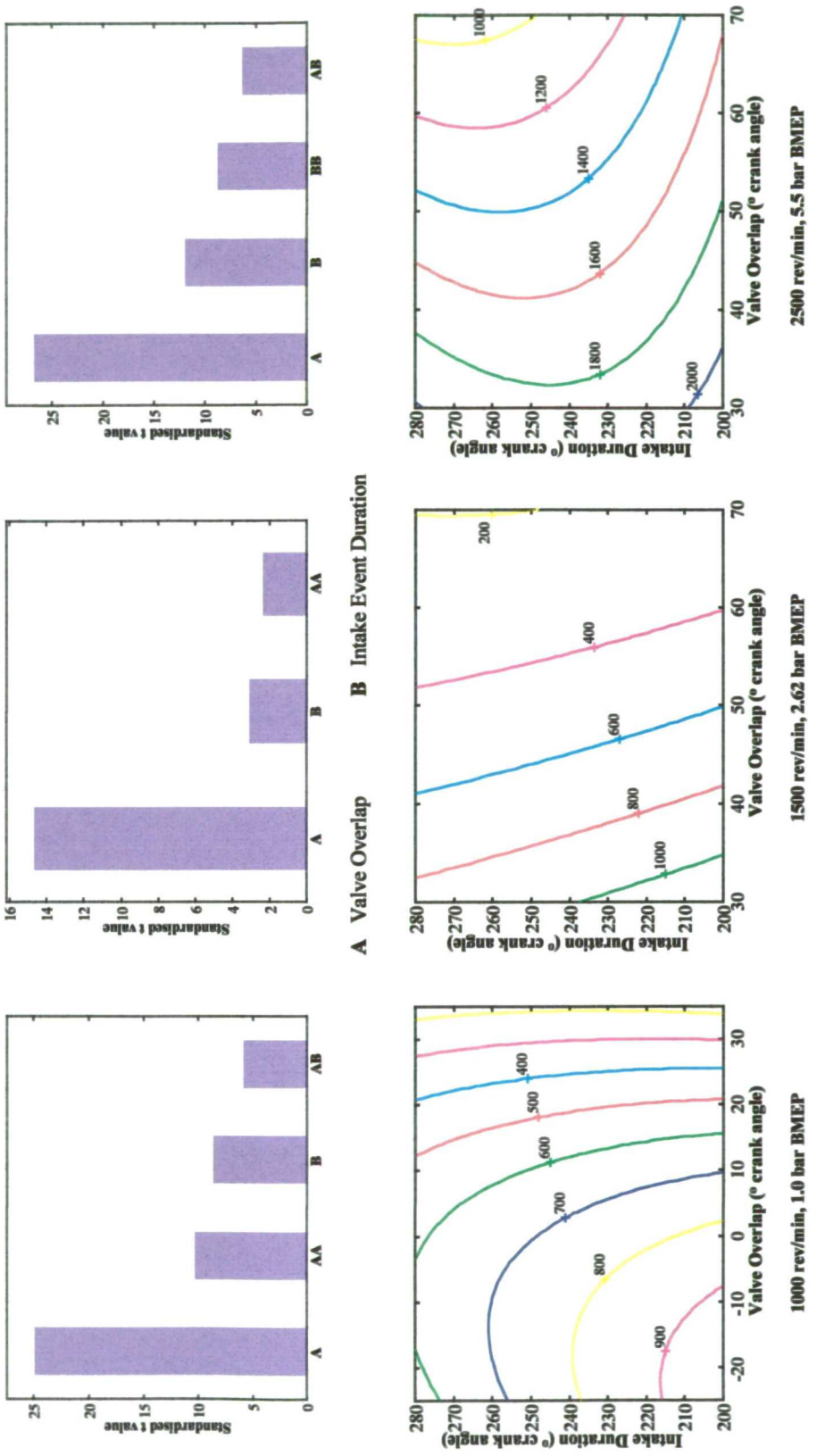

Figure 7.2
Results for NOx emissions (Vppm) with valve deactivation at part-load

the duration of the intake event directly translate into a change in IVC, and therefore compression ratio. At 1000 rev/min the lack of any overlap for half of the experimental space gave rise to a significant difference in response for the two regions. The NOx levels appeared to be only a function of duration where there was absence of overlap. In general, NOx values were slightly higher at the 1000 rev/min condition when using deactivation, in comparison to the results from Phase 1, probably due to the higher burn rates leading to higher peak temperatures and pressures. The results at 1500 rev/min clearly show the relative influence of overlap and compression ratio on NOx levels to be, in general, lower than the results from Phase 1.

At 2500 rev/min, the influence of spark timing distorted the response for short duration events. The contour plot for spark timing at this condition is shown in Figure 7.3 with superimposed lines representing constant angles of intake valve closure. Advancing IVC appears to delay the onset of knock allowing ignition timing to be further advanced. This result is somewhat contradictory to the conventional understanding that higher compression ratios increase the engine's propensity to knock. The most obvious counterbalancing factor in this respect is the faster burn rate, giving less time for the end gas to ignite spontaneously and also leading to lower gas temperatures. Figure 7.4 shows how the mean plenum pressure varied over the experimental region and it is apparent that the engine became unthrottled for combinations of large overlaps and intake events of short duration. Higher plenum pressure leads to a lower RGF and a reduced opportunity for backflow towards the end of the induction stroke with a consequent tendency for a lower temperature in the port. In addition, early closure of the intake valve, particularly before BDC, may give rise to higher gas velocities in turn raising burn rates.

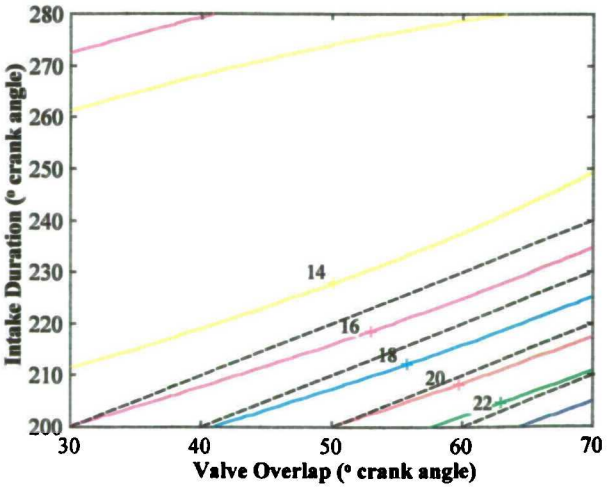

Figure 7.3
The effects of overlap and intake event duration on spark timing (° bTDC) at 2500 rev/min, 5.5 bar BMEP

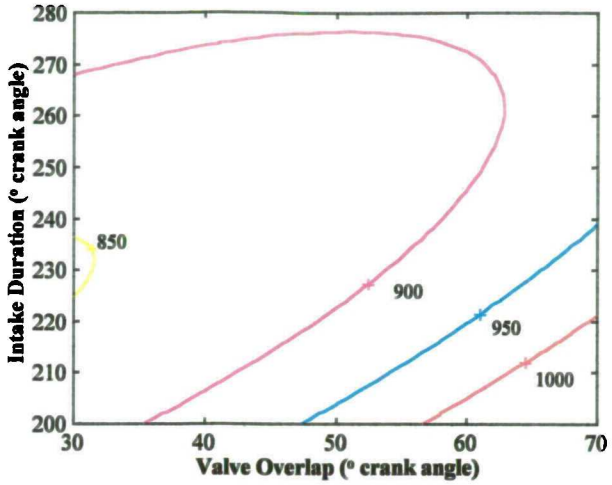

Figure 7.4
The effects of overlap and intake event duration on manifold pressure (mbar) at 2500 rev/min, 5.5 bar BMEP

7.5.2. Unburned Hydrocarbons

One consequence of operating with very high levels of charge dilution is an increase in hydrocarbon levels. The aim of using a valve deactivation strategy was to investigate whether the region of efficient combustion could be extended to any significant degree. Figure 7.5 shows the influential factors affecting levels of unburned hydrocarbons and the modelled response at the three part-load conditions. As for the CCRD tests, hydrocarbon levels remain relatively flat over a significant area of the experimental space. The results do also indicate the extent to which overlap can be tolerated before leading to a substantial rise in hydrocarbon levels. In particular, the results at 1500 rev/min show that overlap values greater than 50° result in a marked rise in hydrocarbons. Some understanding of the trade-off between overlap and hydrocarbons can be gained by plotting hydrocarbons against NOx emissions for each setting. Such a graph is shown in Figure 7.6, which also includes results from the first phase of engine tests using the CCRD experiment. By arbitrarily setting an upper limit of 2000 ppm for hydrocarbons, these results show that the rapid rise in hydrocarbons would set 500 ppm as a practical lower limit to NOx emissions. Unfortunately the results from the CCRD experiment do not enter into this area and it is not possible to comment on whether the region of efficient combustion has indeed been extended. The results at 1000 rev/min do overlap but appear to indicate that deactivation does not provide any benefit, and may even be slightly detrimental. This is due in part to the fact that the fixed exhaust timing (exhaust valve closing at TDC) was probably too early and some retardation would have been beneficial in allowing the post flame oxidation reactions to continue prior to EVO. An exhaust timing somewhere between the two used in this study would probably be the best compromise. There also seems to be an indication that NOx levels at 1000 rev/min were

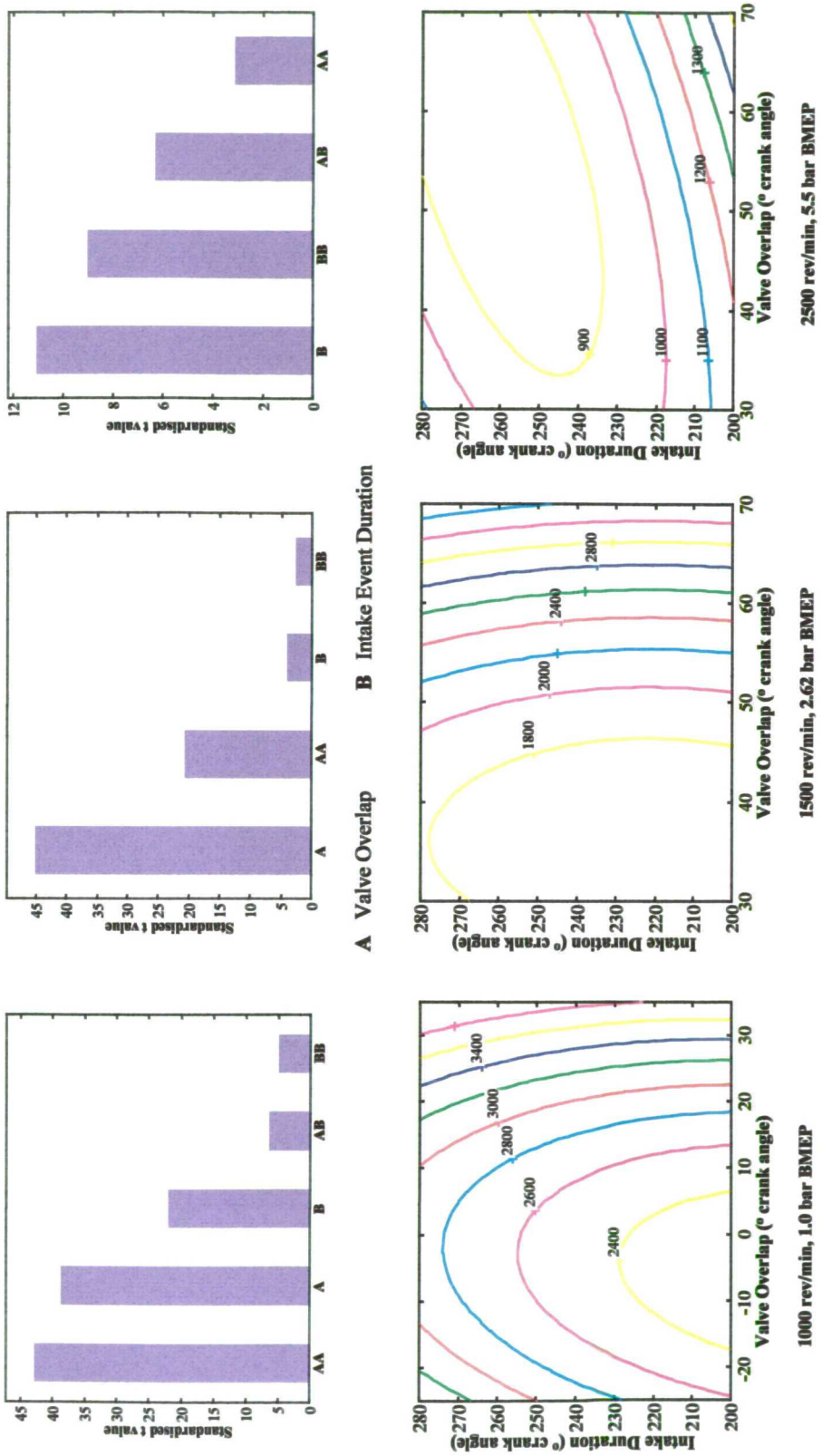

Figure 7.5
Results for HC emissions (Vppm) with valve deactivation at part-load

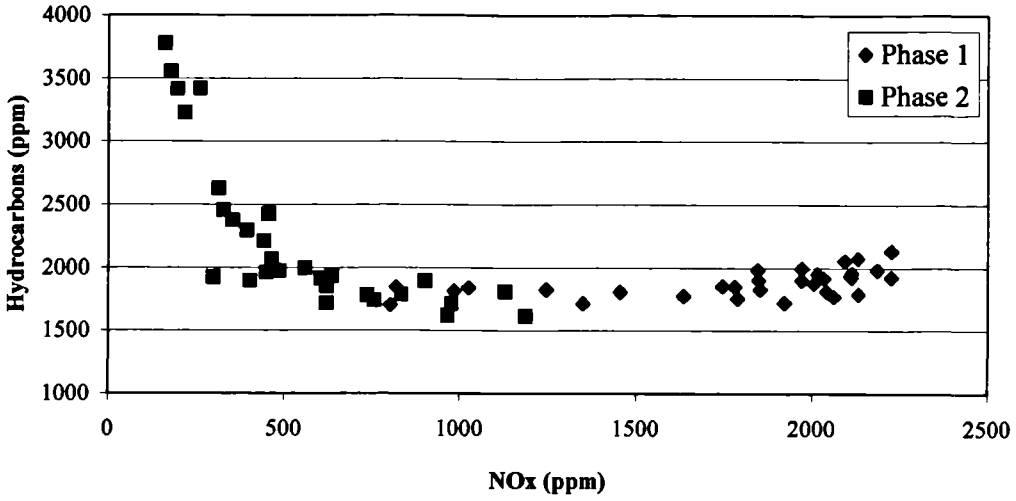

Figure 7.6
Unburned hydrocarbons as a function of NOx emissions at 1500 rev/min, 2.62 bar BMEP

higher for the Phase 2 tests than for Phase 1. The range of overlap values explored in the two phases was similar, although larger values were visited in the first series of tests. Hydrocarbon levels in the region where the intake valve is closed very late do not rise as sharply as they do when overlap is introduced. Conditions in the intake port will be significantly different as fresh charge is returned from the cylinder. A combination of the increased residence time and higher temperatures would certainly assist in mixture preparation and may also help is raising temperatures over the combustion period. Tuttle (1980) had found that the temperature near the intake valve was nearly doubled if IVC was retarded by 96°, this range being similar in magnitude to that employed in the present investigation. One final observation is the marked similarity between the response plots for hydrocarbons and exhaust gas temperature.

At 2500 rev/min, no upturn in hydrocarbons is apparent when overlap is increased. The deactivated strategy continues to show improvements in both NOx and unburned hydrocarbons. This result is probably due to the retarded ignition timings used. The implication of this on fuel consumption is discussed later.

7.5.3. Heat release characteristics with deactivation

Analysis of the 0-80% MFB burn duration at 1500 rev/min (Figure 7.7) confirms the expected dependence on overlap. In comparison with the results from Phase 1, the range of variation appears to be larger, but this is due to the very long periods of overlap employed. Whereas 35 °ca of overlap would typically have resulted in a burn angle of 52° in Phase 1, the results with

deactivation indicate a burn angle value of approximately 47°, a reduction of 10%. However, comparison of burn duration and peak heat release rate as a function of model predictions for RGF (Figure 7.8) indicates the somewhat surprising result that there is little difference between the two sets of tests, implying that deactivation has provided no enhancement in this respect.

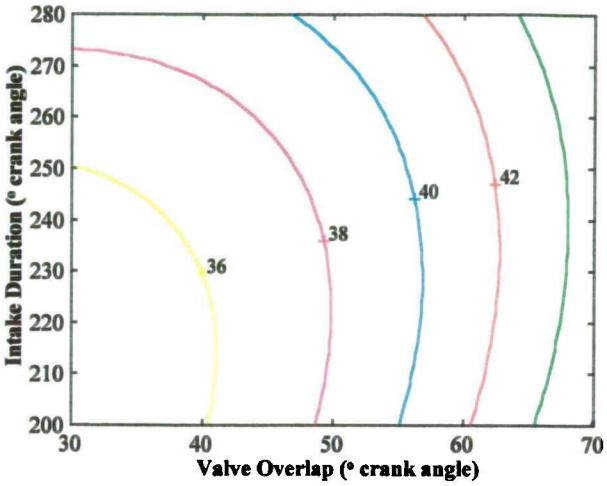

Figure 7.7
0 – 80% MFB (° crank angle) as a function of overlap and intake event duration at 1500 rev/min, 2.62 bar BMEP

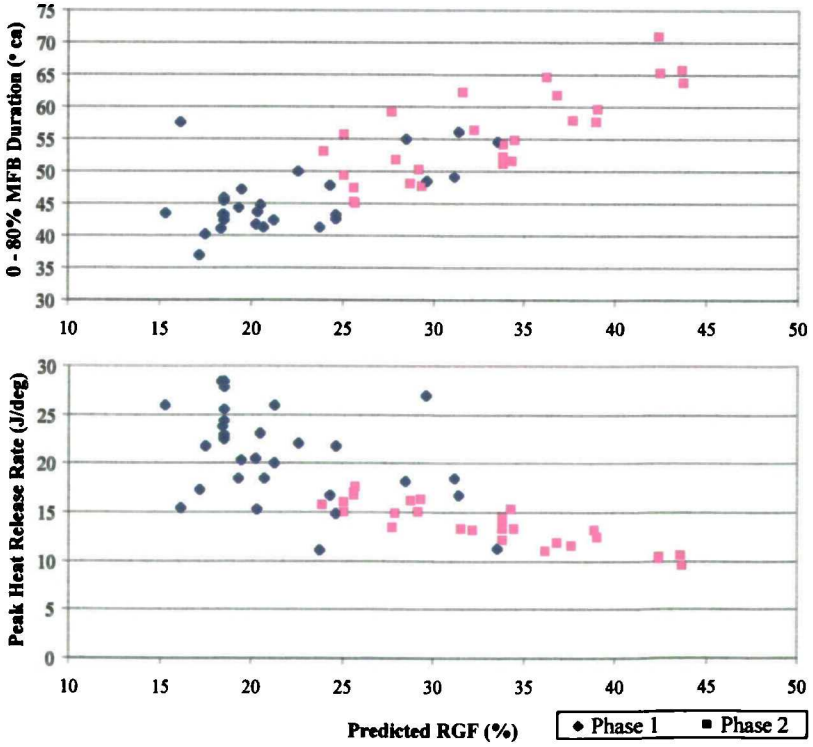

Figure 7.8
Correlation between burn angle, peak rate of heat release and predicted RGF for Phases 1 and 2

Very late intake valve closure angles appear to result in an increase in burn duration. This observation was also made for the phase 1 results where it was suggested that in-cylinder turbulence levels might be reduced as backflow into the port at the end of the induction stroke is increased. The effects of such backflow on in-cylinder motion should be small in comparison to those from deactivation. Given that there is no discernible difference between the two valve strategies, as indicated by Figure 7.8, it seems improbable that such a secondary effect would be so visible. Of course, the reduced temperatures and pressures brought about by a lower effective compression ratio would also lead to a reduction in burn rate, and this may be the predominant influence.

7.5.4. Fuel consumption

It was expected that the main improvement in fuel consumption would be achieved by reductions in pumping work brought about by operation with a higher plenum pressure. The two mechanisms responsible for this being high levels of charge dilution and late intake valve closure leading to some of the cylinder charge being pushed back into the intake port.

The problems experienced with consistency of fuel flow readings in Phase 1 had been redressed and essentially solved. However, the regression coefficients still show relatively low significance levels, indicating the small degree of change observed. Overall, it would seem that both sets of tests imply that potential savings in fuel consumption are relatively small in percentage terms. This is particularly so when compared to the amount of variation observed in the emission responses. The results are shown in Figure 7.9

At 1000 rev/min, fuel consumption is relatively stable for settings combining modest values of intake event duration with little or no overlap. The benefits from both the introduction of overlap and LIVC are individually visible. The improvement due to overlap is smaller than that achievable by changes in IVC, probably because of the narrower range of overlap values explored. As the intake event duration is increased, particularly when combined with retarded event timing, the effects of LIVC become apparent. This change is three to four times greater than that due to overlap, leading to duration appearing as the most influential factor. The practical limit to employing LIVC is the encroachment of the valve closure angle on MBT spark timing. The most retarded setting investigated corresponded to a valve closure angle of 55° bTDC. The corresponding spark advance timing used was 28.7°. The results at this condition suggest that MBT spark timing occurs closer to TDC as IVC is retarded. In fact, retarded, short duration events appear to result in the smallest ignition advance requirement, so there may be a potential for further retardation of IVC.

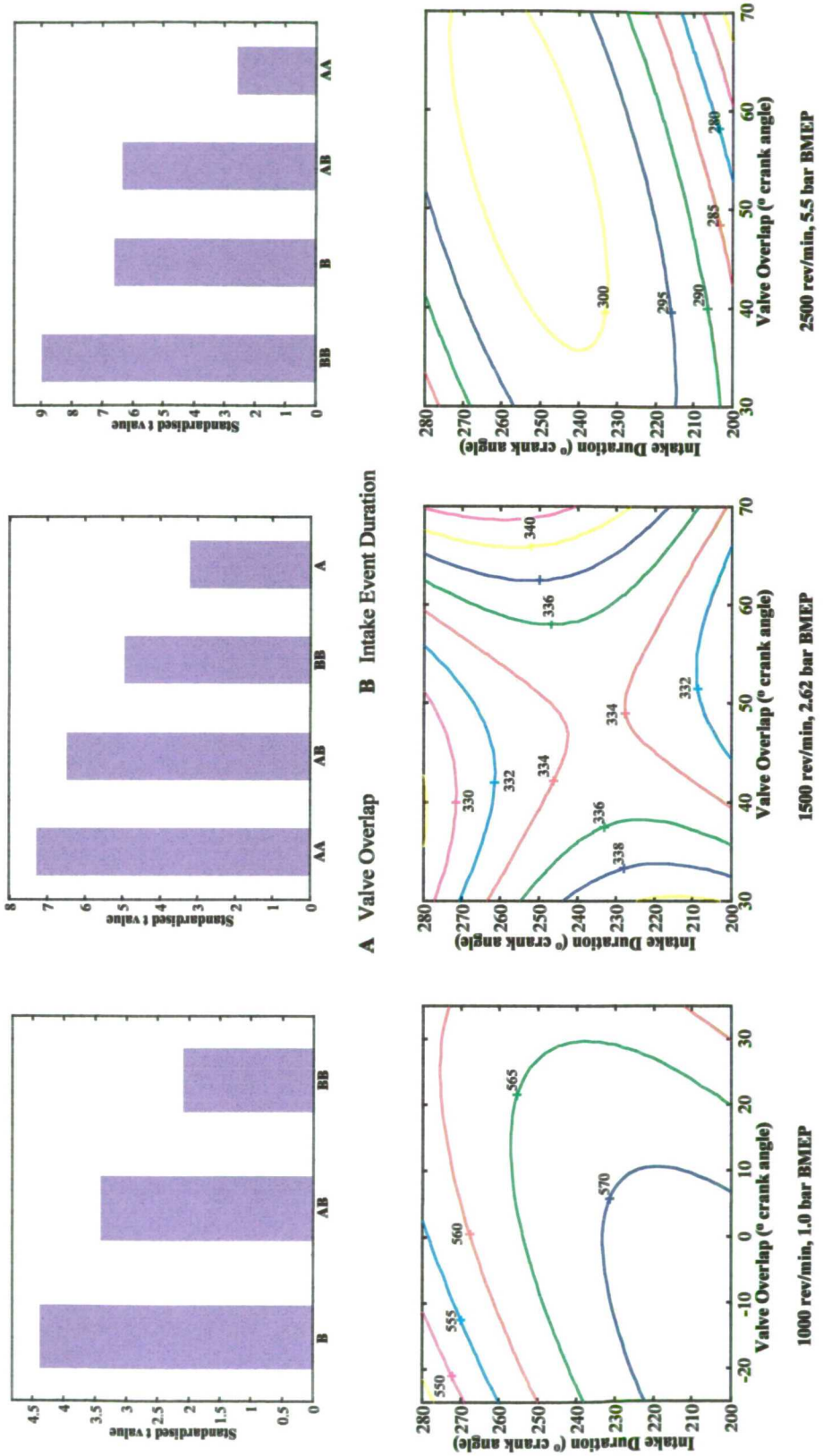

Figure 7.9
Results for BSFC (g/kWh) at part-load

The results at 1500 rev/min show the influence of conflicting trends. Increasing overlap is beneficial, until the engine is unable to tolerate the high levels of dilution. The rise in fuel consumption in this region is probably due to a combination of rapidly rising hydrocarbon levels and a loss in the thermodynamic cycle efficiency as burn duration is significantly increased. The use of a long duration induction event leads to additional improvements from LIVC. The variation in these results over the experimental range is smaller than that seen in Phase 1 and indications are that fuel consumption is slightly better.

As with the other responses, fuel consumption at 2500 rev/min is mainly determined by the susceptibility of a particular setting to the onset of knock. The three most influential factors are the same as for spark timing, they even show similar significance levels. The only area of difference is for a combination of small overlap and a short intake event period where fuel consumption is slightly lower than the spark timing results would imply.

7.6. Results at idle

Spark timing was included as a variable for the tests at idle. The primary motive for this was the observed effect in Phase 1 of changes in spark timing on RGF caused by changes in plenum pressure. It was therefore felt that there was a potential for interaction between spark timing and the two other variables. Four spark angle settings were used between 0 and 30° bTDC inclusive. Engine operation at some settings was too unstable to warrant readings being taken so the experimental design used was a full-factorial one with some data points missing. This was not a problem since only a quadratic model was applied and the number of data points was more than adequate for this application.

As mentioned in Section 7.4, the fuelling strategy used was included in the regression model by representing it as two levels of a dummy variable. The model assumed that no interaction between this qualitative variable and the remaining quantitative ones existed. This meant that the fuelling method would only alter the mean response, and its effect could therefore be removed. Myers and Montgomery (1995) discuss further the inclusion of qualitative variables in regression models.

7.6.1. Oxides of nitrogen

The results for oxides of nitrogen are shown in Figure 7.10. The inclusion of spark timing still does not detract from the fact that overlap remains the dominant variable. In fact, the relatively low significance of spark timing may have been due to the counterbalancing effect of higher

residuals as spark timing was advanced. The effect of intake event duration appears to diminish with increasing overlap leading to a significant interaction between the two variables. This interaction is probably due to the relationship between IVC and compression ratio. The only other interaction is between ignition timing and intake duration with NOx levels being more sensitive to change in spark timing when combined with a long intake event duration and a retarded spark setting.

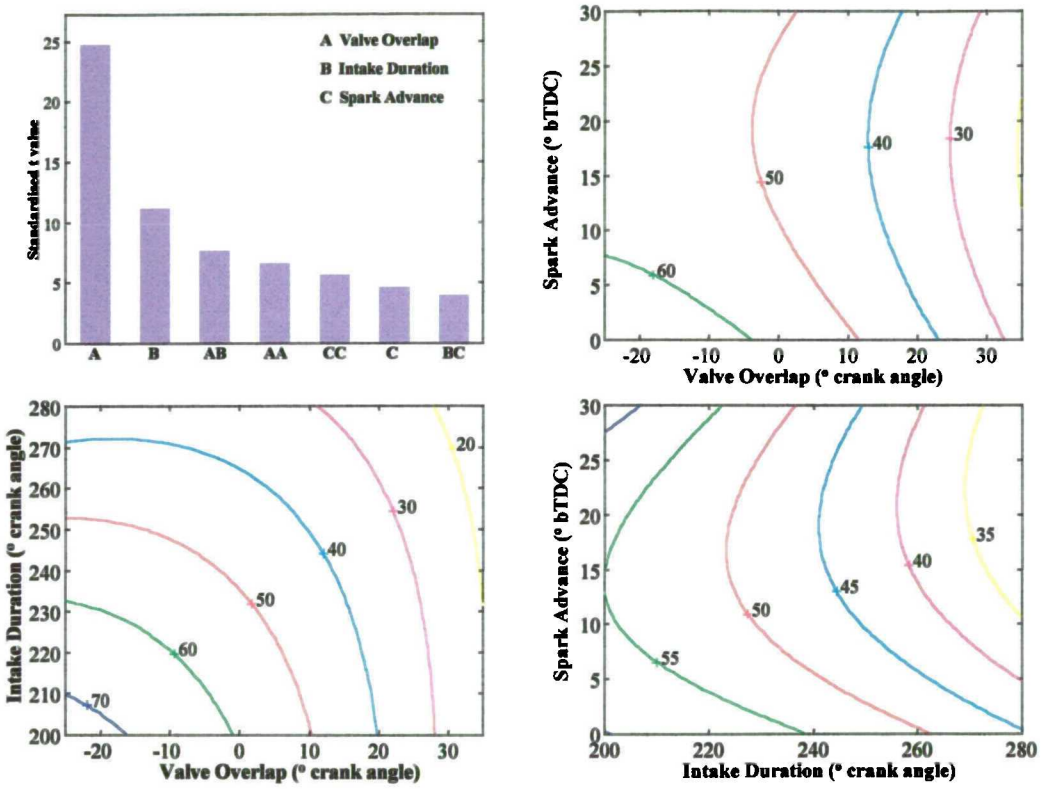

Figure 7.10
Results for NOx emissions (Vppm) at idle

7.6.2. Unburned hydrocarbons

The influence of valve overlap on hydrocarbon emissions proved as significant with valve deactivation as for the Phase 1 tests. Figure 7.11 shows the results, which again confirm the very strong influences of spark timing and valve overlap. The effect of changes in inlet valve event duration appears to be minimal. There is, however, some indication that hydrocarbon levels are more sensitive to changes in spark timing when a long duration event is employed. This would have obvious implications for idle speed control strategies reliant on varying spark timing. The results for exhaust gas temperature (Figure 7.12) also show a similar dependence on long duration intake events, although spark timing and overlap remain the dominant factors. The most plausible explanation for this dependence is probably some lengthening of the overall combustion period as IVC is retarded.

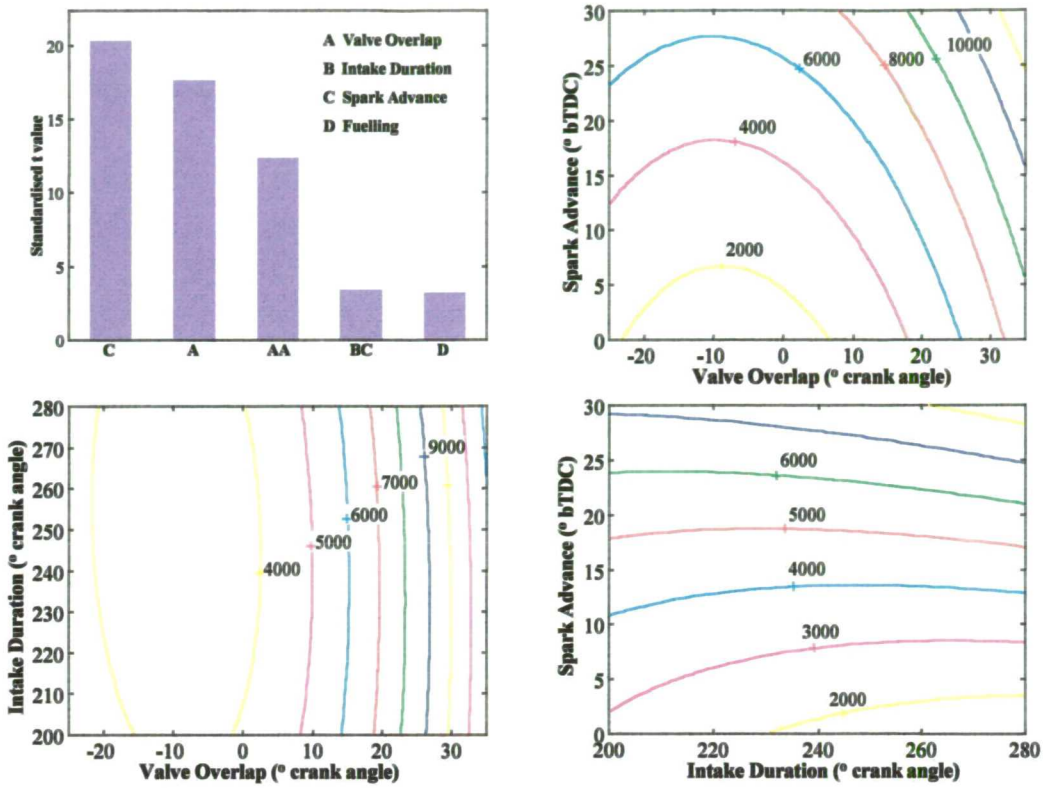

Figure 7.11
Results for hydrocarbon emissions (Vppm) at idle

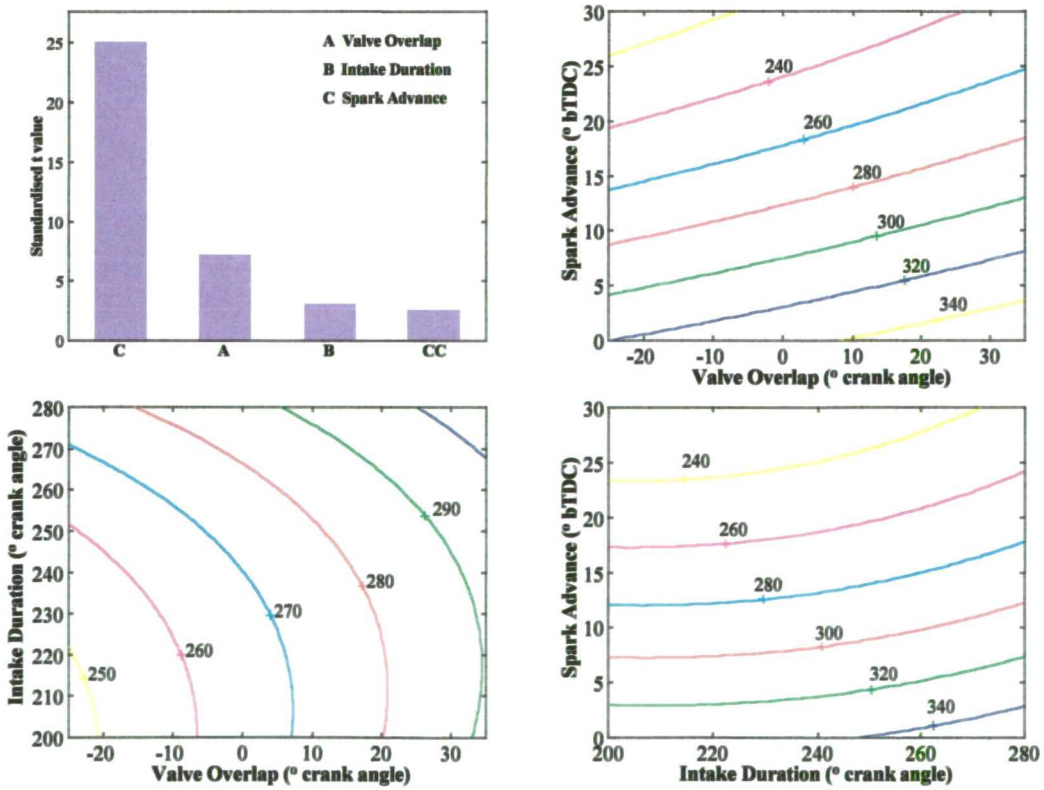

Figure 7.12
Exhaust gas temperature (° C) at idle

7.6.3. Fuel consumption

The fuel consumption results (Figure 7.13) reinforce the dominance of spark timing and overlap over intake event duration. The strong response to changes in spark angle is predictable given the retarded range of values used in the tests. The deterioration in combustion brought about by introducing overlap leads to a significant fuel consumption penalty. This is compounded by the fact that greater overlap, and hence higher levels of charge dilution, would necessitate a greater spark advance in order to maintain the same efficiency due to reduction in flame speed. The relatively strong presence of an interaction term between the two factors testifies to this effect.

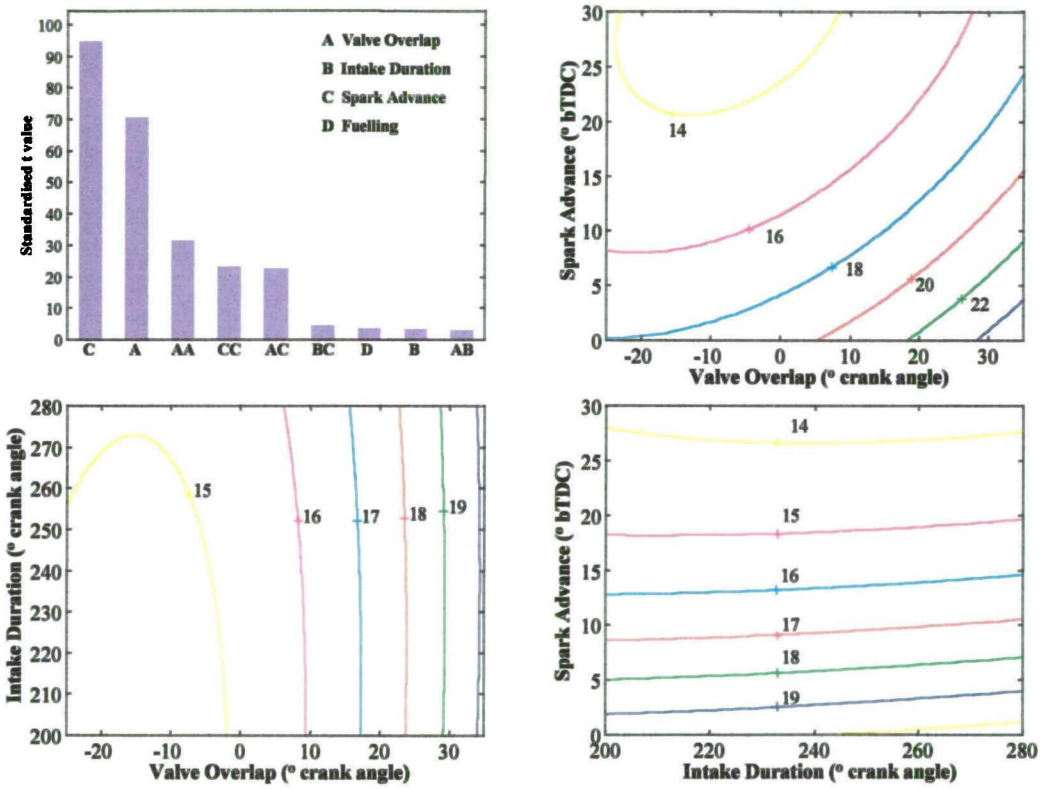

Figure 7.13
Results for fuel consumption at idle (g/min)

Chapter 8

CONCLUSIONS

8. Conclusions

8.1. Conclusions from engine tests

A Central Composite Rotatable Design (CCRD) of experiment was successfully applied to investigate the effects of changes in valve event parameters on emissions, fuel consumption and burn characteristics over a range of speed-load conditions. The design proved effective in giving information over the relatively broad range of each of the variables, allowing the main effects and interactions to be modelled satisfactorily. The range chosen for the variables was larger than any previously investigated, and would appear to represent the limit for modelling with a second-order quadratic function. The use of a quadratic polynomial also proved appropriate for investigating the effects of intake event phasing and duration under valve deactivation.

Consideration was given to the manner in which the variables were selected and defined. Phasing and duration of the valve events, and peak inlet valve lift, were selected rather than valve opening and closing angles. Use of contour plots allowed the effects of the closing and opening events to be studied in isolation to an acceptable degree.

Prior to the engine tests, some assessment had been made of the effects of valve lift on in-cylinder motion through use of a steady-flow impulse swirl meter. In addition, tests to measure discharge coefficients had allowed a filling and emptying model to be developed allowing pumping work, and more importantly, RGF to be estimated for different valve event strategies. A good degree of correlation between these and the results from the engine tests allowed many important conclusions to be drawn.

The Phase 1 tests (i.e. those without valve deactivation) confirmed the dominant role of valve event phasing on emissions, with duration and peak inlet valve lift appearing to be less influential. NOx emissions were primarily influenced by factors affecting the valve overlap period, exhaust camshaft phasing being the more effective than phasing of the intake event. Changes in intake event duration lowered NOx through changes in overlap and compression ratio. Contour plots allowed the effects of changes in IVC and phasing of the overlap period with respect to TDC to be isolated and compared. It was concluded that the latter was at least as influential in determining NOx emissions as changes in compression ratio.

Emissions of unburned hydrocarbons were found to be most influenced by changes in exhaust event phasing. Retarding the exhaust event later into the cycle led, in general, to a reduction in hydrocarbons. The relatively smaller influence of intake event phasing indicated that the reduction in hydrocarbons was primarily due to the longer residence time of the exhaust gases prior to EVO rather than reingestion of hydrocarbons during overlap. Hydrocarbon levels at 1000 rev/min and at idle rose sharply with increasing overlap. The results at 1500 rev/min showed little change while those at 2500 rev/min were found to be distorted by the retarded spark timing needed to avoid knock.

Late IVC appeared to raise hydrocarbon emissions with evidence of a lengthening in burn duration under such conditions, possibly due to a combination of a reduction in turbulence levels and lower combustion temperatures brought about by the reduced compression ratio.

Under all conditions, the effects of peak inlet valve lift on NOx, and to some extent hydrocarbon, emissions were negligible. The steady-flow data from the tumble and swirl rig measurements indicated that a high value of inlet valve lift was required to generate a structured tumbling regime inside the cylinder. This result implied that such motion was predominantly established by the geometry of the port, and the presence of the valves only served to disrupt it. It was therefore concluded that there would be little point in adopting a strategy capable of continually varying valve lift. It was also recognised that, although low values of valve lift did not appear to generate tumble, they would nonetheless lead to a more vigorous gas motion inside the cylinder. The chaotic nature of such a flow meant that the energy associated with it would be dissipated quickly so a valve strategy allowing a structured motion to be retained would appear to be a better approach.

The fuel consumption results proved disappointing largely due to the high variability in the data. However, it would seem that the potential for reductions in fuel consumption were small and this was confirmed by the second phase of engine tests (with valve deactivation) indicating a maximum improvement of the order of 4-5%.

Heat release analysis showed a good correlation with Residual Gas Fraction (RGF) predictions from the filling and emptying model. There was also, in turn, the expected correlation between NOx level and RGF.

The strategy for the phase 2 testing evolved from a combination of the three areas explored previously, namely the steady-flow work, the modelling and Phase 1 engine tests. These were used to select a strategy employing intake valve deactivation with reduced lift of the active valve

in a combination shown by the swirl tests to give a relatively high degree of structured flow within the cylinder.

Phase 2 tests demonstrated the potential for very significant NOx reduction at 1500 and 2500 rev/min. Graphs comparing the trade-off between hydrocarbons and NOx confirmed that a combination of valve deactivation, reduced lift and large overlap can lead to very low NOx values while limiting the rise in hydrocarbon emissions. At 1500 rev/min, the engine was able to tolerate approximately 50° of overlap without a significant penalty in hydrocarbon emissions.

The trend towards longer burn duration with increasing residuals established in the Phase 1 tests was found to continue with Phase 2. It is possible that deactivation allowed the engine to continue operating, albeit with extended burn times, into a region of extremely high levels of RGF where the Phase 1 strategies would have faltered. It seems unlikely that there was no improvement in combustion with deactivation. Unfortunately, no conclusive statement can be made in this regard as the Phase 1 tests did not continue into the very high overlap regions that were investigated during Phase 2.

At 1000 rev/min the benefits of LIVC can be seen in terms of reduced fuel consumption. These benefits are more significant than those due to overlap. A combination of shorter duration events and late phasing leads to a smaller ignition advance requirement giving further potential for LIVC. Some method for counteracting the lower temperatures caused by reduced compression ratio would be needed to prevent a rise in hydrocarbon emissions. A combination of large overlap and short intake event duration led to unthrottled operation at 2500 rev/min. This also corresponded to the lowest specific fuel consumption and the greatest permissible degree of spark advance.

For both phases of testing, NOx values at idle fell with increasing spark advance due to an increase in backflow brought about by a lower pressure in the plenum.

Overall, it can be concluded that the results from both phases of testing indicated that each strategy had considerable potential for reduced emissions levels, without the need for external exhaust gas recirculation. It can be argued that the second strategy (using deactivation) is superior because it achieved its results using fewer variables. Indeed, it may well have further potential for operating at still higher levels of RGF if efforts are made to optimise the port design for a deactivation strategy, rather than just rely on an existing conventional design. It was disappointing that only modest reductions in brake specific fuel consumption were observed as the variation of valve events can lead to reduced pumping work. However, it was apparent that

counteracting factors were often influencing performance, such as longer burn duration negating the reduced pumping loop work. Once again, port design optimised for deactivation should help to unlock the potential for improvement.

8.2. Original aspects of the work

Statistically-designed experiments have been used to conduct the first comprehensive investigation into the effects of changes in exhaust valve event phasing, intake event phasing and duration, and changes in peak intake valve lift. The range of each of these variables has been sufficient to cover most camshaft settings currently found on production engines. The results have been correlated with steady-flow tests quantifying the intensity of axial swirl and tumble within the cylinder, and predictions from a filling and emptying model. The results from the first phase of tests have provided valuable information on the relative importance of phasing and valve event duration, and also on the effects of peak inlet valve lift. In addition, the significance of altering the phasing of the overlap period with respect to crank angle has also been discussed in comparison to changes in IVC.

Previous work had been far more limited in its scope. It had either concentrated on a few settings in isolation from others, or investigated a range of settings with a reduced number of variables (e.g. not including lift or duration). The complexity of the investigation resulting from the increased number of variables cannot be understated, yet knowledge of the many interactions is necessary if engine performance is to be optimised.

The work on combining intake valve deactivation with reduced active valve lift is believed to be original. In particular, the author is not aware of any work reported on investigating such a valve strategy with changes in valve overlap and intake event duration. The second phase of testing has provided an insight into the real potential for such strategies and their relative merit in comparison to conventional means of altering valve events.

The recognition of the importance of valve clearances on emissions and engine efficiency is also believed to be original. It is hoped that this knowledge of the potential influences of valve clearances will spur engine manufacturers to perform sensitivity analyses on their particular designs of valve trains and, where necessary, make detailed changes in design that will result in a more consistent engine performance.

8.3. Recommendations for further work

The results from the second phase of engine tests have provided a valuable insight into the practical benefits of late IVC, however, lack of time precluded an investigation into the potential for early intake valve closure. The obvious motivation for previous researchers concentrating on late rather than early IVC was the ability to avoid excessive valve accelerations. Using a low lift/deactivation strategy removes this obstacle. The poor combustion observed with late valve closure angles may not be present for an early closing strategy, giving it an obvious advantage. There is potential for work to be performed to compare the characteristics (burn rate, etc) between early and late IVC. Any investigation should also look at possible measures to enhance combustion when LIVC is applied.

The filling and emptying model assumed perfect mixing of the backflow gases with those in the plenum. Although it proved valuable in revealing trends, some form of mixing model would certainly help in estimating residuals and pumping work. This is particularly important for very light loads where the perfect mixing assumption appeared to be the most inadequate. The alternative model discussed in Appendix 2 was designed to cater for such mixing by localising the exhaust gas to the volumes in the port region and allowing for mixing between volumes in the port. It may yet be possible to use the scheme for such work.

Reference has been made to the likelihood that deactivation, with or without low lift on the active valve, is only likely to show its full benefit if the intake port design is optimised for this strategy. It follows that a natural extension to the work described here would include intake port design as a variable. How much of the investigation should be performed through initial rig testing and how much through a statistically-designed experiment should be given careful consideration. However, it is likely to be an area of future work that promises to lead to further refinement in the ever-improving SI engine.

Appendix 1

RESULTS FROM STEADY FLOW TESTS TO MEASURE DISCHARGE COEFFICIENTS

Lift (mm)	Mass Flow (g/s)	p_{01} (mmH_2O)	T_{01} (°C)	p_{01}-p_2 (mmH_2O)	T_2 (°C)	T_{amb} (°C)	p_{01} (Pa)	T_{01} (K)	p_2 (Pa)	T_2 (K)	T_{amb} (K)	p_{01}-p_2 (Pa)	Lv/Dv	Density (kg/m^3)	A_{eff} (mm^2)	A_{et} (mm^2)	C_D
0.10	1.0	0.0	25.0	600	24.9	25.1	101700	298.2	95814	298	298	5886	0.0031	1.1885	8.454	20.074	0.421
0.20	2.3	0.0	25.3	600	24.9	25.0	101700	298.5	95814	298	298	5886	0.0063	1.1873	19.032	40.147	0.474
0.30	3.7	0.0	25.2	600	24.9	25.0	101700	298.4	95814	298	298	5886	0.0094	1.1877	31.291	60.221	0.520
0.40	5.3	0.0	25.2	600	24.9	25.0	101700	298.4	95814	298	298	5886	0.0125	1.1877	44.399	80.294	0.553
0.50	6.5	0.0	25.2	600	24.9	24.9	101700	298.4	95814	298	298	5886	0.0157	1.1877	54.971	100.368	0.548
0.60	7.9	0.0	25.2	600	24.9	25.0	101700	298.4	95814	298	298	5886	0.0188	1.1877	66.388	120.441	0.551
0.70	9.0	0.0	25.1	600	25.0	25.0	101700	298.3	95814	298	298	5886	0.0219	1.1881	75.678	140.515	0.539
0.80	10.0	0.0	25.1	600	25.0	25.1	101700	298.3	95814	298	298	5886	0.0250	1.1881	84.556	160.588	0.527
0.90	11.4	0.0	25.1	600	25.0	25.1	101700	298.3	95814	298	298	5886	0.0282	1.1881	96.394	180.662	0.534
1.00	12.8	0.0	25.0	600	25.0	25.1	101700	298.2	95814	298	298	5886	0.0313	1.1885	108.214	200.735	0.539
1.10	14.0	1.0	25.0	600	25.0	25.1	101690	298.2	95804	298	298	5886	0.0344	1.1884	118.365	220.809	0.536
1.20	15.4	1.0	25.0	600	25.0	25.1	101690	298.2	95804	298	298	5886	0.0376	1.1884	130.201	240.882	0.541
1.30	17.0	1.0	24.9	600	24.9	25.1	101690	298.1	95804	298	298	5886	0.0407	1.1888	143.704	260.956	0.551
1.40	18.3	1.5	24.9	600	24.9	25.3	101685	298.1	95799	298	298	5886	0.0438	1.1887	154.275	281.029	0.549
1.50	20.0	1.5	24.9	600	24.9	25.3	101685	298.1	95799	298	298	5886	0.0470	1.1887	169.068	301.103	0.561
1.60	21.5	1.8	24.9	600	24.9	25.4	101683	298.1	95797	298	299	5886	0.0501	1.1887	181.750	321.176	0.566
1.70	22.7	2.0	24.9	600	24.9	25.4	101680	298.1	95794	298	299	5886	0.0532	1.1887	191.897	341.250	0.562
1.80	24.4	2.1	24.8	600	24.9	25.3	101679	298.0	95793	298	298	5886	0.0563	1.1891	206.234	361.323	0.571
1.90	26.0	2.3	24.8	600	24.9	25.3	101678	298.0	95792	298	298	5886	0.0595	1.1891	219.759	381.397	0.576
2.00	27.2	2.5	24.8	600	24.9	25.3	101675	298.0	95789	298	298	5886	0.0626	1.1890	229.905	401.470	0.573
2.10	29.0	3.0	24.8	600	24.9	25.2	101671	298.0	95785	298	298	5886	0.0657	1.1890	245.125	421.544	0.581
2.20	30.0	3.5	24.8	600	24.9	25.2	101666	298.0	95780	298	298	5886	0.0689	1.1889	253.584	441.617	0.574
2.25	30.9	3.5	24.6	600	24.4	24.9	101666	297.8	95780	298	298	5886	0.0704	1.1897	261.104	451.654	0.578
2.50	34.4	4.7	24.6	600	24.5	24.9	101654	297.8	95768	298	298	5886	0.0783	1.1896	290.695	501.838	0.579
2.75	37.8	6.0	24.6	600	24.5	25.0	101641	297.8	95755	298	298	5886	0.0861	1.1894	319.447	552.022	0.579

Results for forward flow past the inlet valves (0.10 to 2.75 mm valve lift)

Lift (mm)	Mass Flow (g/s)	p_{01} (mmH_2O)	T_{01} (°C)	p_{01}-p_2 (mmH_2O)	T_2 (°C)	T_{amb} (°C)	p_{01} (Pa)	T_{01} (K)	p_2 (Pa)	T_2 (K)	T_{amb} (K)	p_{01}-p_2 (Pa)	Lv/Dv	Density (kg/m^3)	Aeff (mm^2)	Act (mm^2)	C_D
3.00	41.2	6.7	24.7	600	24.5	25.0	101634	297.9	95748	298	298	5886	0.0939	1.1889	348.250	602.206	0.578
3.25	44.1	8.0	24.8	600	24.6	25.0	101622	298.0	95736	298	298	5886	0.1017	1.1884	372.849	652.389	0.572
3.50	47.5	9.5	24.8	600	24.6	25.0	101607	298.0	95721	298	298	5886	0.1096	1.1882	401.624	702.573	0.572
3.75	50.7	10.5	24.7	600	24.6	25.0	101597	297.9	95711	298	298	5886	0.1174	1.1885	428.630	752.757	0.569
4.00	53.5	12.0	24.6	600	24.6	24.9	101582	297.8	95696	298	298	5886	0.1252	1.1887	452.258	802.941	0.563
4.25	56.5	13.5	24.6	600	24.6	24.9	101568	297.8	95682	298	298	5886	0.1330	1.1886	477.653	853.125	0.560
4.50	59.5	15.0	24.7	600	24.6	25.0	101553	297.9	95667	298	298	5886	0.1409	1.1880	503.136	903.309	0.557
4.75	62.2	16.5	24.8	600	24.7	25.0	101538	298.0	95652	298	298	5886	0.1487	1.1874	526.094	953.492	0.552
5.00	65.0	18.5	24.8	600	24.7	25.1	101519	298.0	95633	298	298	5886	0.1565	1.1872	549.830	1003.676	0.548
5.25	68.0	20.0	24.8	600	24.7	25.1	101504	298.0	95618	298	298	5886	0.1643	1.1870	575.248	1053.860	0.546
5.50	70.2	21.0	24.8	600	24.7	25.2	101494	298.0	95608	298	298	5886	0.1722	1.1869	593.888	1104.044	0.538
5.75	73.0	23.0	24.9	600	24.8	25.2	101474	298.1	95588	298	298	5886	0.1800	1.1863	617.739	1154.228	0.535
6.00	75.0	24.5	24.9	600	24.8	25.2	101460	298.1	95574	298	298	5886	0.1878	1.1861	634.709	1204.411	0.527
6.25	77.5	26.0	24.7	600	24.7	25.2	101445	297.9	95559	298	298	5886	0.1956	1.1867	655.694	1254.595	0.523
6.50	79.5	27.5	24.7	600	24.7	25.2	101430	297.9	95544	298	298	5886	0.2035	1.1866	672.664	1304.779	0.516
6.75	81.5	28.5	24.7	600	24.7	25.1	101420	297.9	95534	298	298	5886	0.2113	1.1864	689.620	1354.963	0.509
7.00	83.5	30.0	24.7	600	24.7	25.1	101406	297.9	95520	298	298	5886	0.2191	1.1863	706.594	1405.147	0.503
7.25	85.0	31.0	24.7	600	24.7	25.1	101396	297.9	95510	298	298	5886	0.2269	1.1862	719.322	1455.330	0.494
7.50	86.5	32.0	24.8	600	24.7	25.1	101386	298.0	95500	298	298	5886	0.2348	1.1856	732.174	1505.514	0.486
7.75	87.9	33.5	24.9	600	24.8	25.2	101371	298.1	95485	298	298	5886	0.2426	1.1851	744.203	1555.698	0.478
8.00	89.0	34.5	25.0	600	24.9	25.3	101362	298.2	95476	298	298	5886	0.2504	1.1846	753.679	1605.882	0.469
8.25	90.0	35.5	25.1	600	24.9	25.4	101352	298.3	95466	298	299	5886	0.2582	1.1840	762.312	1656.066	0.460
8.50	91.0	36.0	25.0	600	24.9	25.4	101347	298.2	95461	298	299	5886	0.2661	1.1844	770.672	1706.249	0.452
8.75	92.1	37.0	25.0	600	24.9	25.3	101337	298.2	95451	298	298	5886	0.2739	1.1843	780.025	1756.433	0.444
9.00	93.5	38.0	25.0	600	24.9	25.4	101327	298.2	95441	298	299	5886	0.2817	1.1842	791.921	1806.617	0.438

Results for forward flow past the inlet valves (3.00 to 9.00 mm valve lift)

Lift (mm)	Mass Flow (g/s)	p_{01} (mmH_2O)	T_{01} (°C)	p_{01}-p_2 (mmH_2O)	T_2 (°C)	T_{amb} (°C)	p_{01} (Pa)	T_{01} (K)	p_2 (Pa)	T_2 (K)	T_{amb} (K)	p_{01}-p_2 (Pa)	Lv/Dv	Density (kg/m^3)	A_{eff} (mm^2)	A_{ct} (mm^2)	C_D
0.10	0.9	0.0	25.0	600	24.9	25.1	101700	298.2	95814	298.1	298.3	5886	0.0031	1.1885	7.609	20.074	0.379
0.20	2.0	0.0	25.1	600	24.9	25.1	101700	298.3	95814	298.1	298.3	5886	0.0063	1.1881	16.488	40.147	0.411
0.30	3.2	0.0	25.1	600	24.9	25.0	101700	298.3	95814	298.1	298.2	5886	0.0094	1.1881	27.058	60.221	0.449
0.40	4.5	0.0	25.2	600	24.9	25.0	101700	298.4	95814	298.1	298.2	5886	0.0125	1.1877	38.057	80.294	0.474
0.50	5.8	0.2	25.1	600	24.9	25.0	101698	298.3	95812	298.1	298.2	5886	0.0157	1.1881	49.043	100.368	0.489
0.60	7.1	0.3	25.1	600	24.8	24.9	101697	298.3	95811	298.0	298.1	5886	0.0188	1.1881	60.036	120.441	0.498
0.70	8.5	0.5	25.1	600	24.8	24.9	101695	298.3	95809	298.0	298.1	5886	0.0219	1.1881	71.875	140.515	0.512
0.80	10.0	0.7	25.1	600	24.8	25.0	101693	298.3	95807	298.0	298.2	5886	0.0250	1.1880	84.559	160.588	0.527
0.90	11.5	0.9	25.1	600	24.8	25.0	101691	298.3	95805	298.0	298.2	5886	0.0282	1.1880	97.244	180.662	0.538
1.00	13.0	1.1	25.1	600	24.8	25.0	101689	298.3	95803	298.0	298.2	5886	0.0313	1.1880	109.929	200.735	0.548
1.10	14.4	1.3	25.0	600	24.7	25.0	101687	298.2	95801	297.9	298.2	5886	0.0344	1.1884	121.748	220.809	0.551
1.20	16.0	1.5	25.0	600	24.7	25.0	101685	298.2	95799	297.9	298.2	5886	0.0376	1.1883	135.277	240.882	0.562
1.30	17.6	1.7	24.9	600	24.7	25.0	101683	298.1	95797	297.9	298.2	5886	0.0407	1.1887	148.781	260.956	0.570
1.40	19.2	2.0	24.9	600	24.7	25.0	101680	298.1	95794	297.9	298.2	5886	0.0438	1.1887	162.309	281.029	0.578
1.50	21.0	2.0	24.9	600	24.7	25.0	101680	298.1	95794	297.9	298.2	5886	0.0470	1.1887	177.526	301.103	0.590
1.60	22.6	2.2	24.9	600	24.7	25.0	101678	298.1	95792	297.9	298.2	5886	0.0501	1.1887	191.053	321.176	0.595
1.70	24.5	2.5	24.8	600	24.7	25.1	101675	298.0	95789	297.9	298.3	5886	0.0532	1.1890	207.083	341.250	0.607
1.80	26.0	2.9	24.8	600	24.7	25.1	101672	298.0	95786	297.9	298.3	5886	0.0563	1.1890	219.766	361.323	0.608
1.90	27.6	3.3	24.8	600	24.6	25.1	101668	298.0	95782	297.8	298.3	5886	0.0595	1.1889	233.295	381.397	0.612
2.00	29.3	3.7	24.8	600	24.6	25.0	101664	298.0	95778	297.8	298.2	5886	0.0626	1.1889	247.669	401.470	0.617
2.10	31.0	4.2	24.7	600	24.6	25.0	101659	297.9	95773	297.8	298.2	5886	0.0657	1.1892	262.002	421.544	0.622
2.20	32.7	5.0	24.7	600	24.5	25.0	101651	297.9	95765	297.7	298.2	5886	0.0689	1.1891	276.380	441.617	0.626
2.25	33.6	5.2	24.5	600	24.4	24.7	101649	297.7	95763	297.6	297.9	5886	0.0704	1.1899	283.894	451.654	0.629
2.50	37.5	6.5	24.4	600	24.3	24.7	101636	297.6	95750	297.5	297.9	5886	0.0783	1.1902	316.813	501.838	0.631
2.75	40.5	8.0	24.4	600	24.3	24.7	101622	297.6	95736	297.5	297.9	5886	0.0861	1.1900	342.183	552.022	0.620

Results for reverse flow past the inlet valves (0.10 to 2.75 mm valve lift)

Lift (mm)	Mass Flow (g/s)	p_{01} (mmH_2O)	T_{01} (°C)	p_{01}-p_2 (mmH_2O)	T_2 (°C)	T_{amb} (°C)	p_{01} (Pa)	T_{01} (K)	p_2 (Pa)	T_2 (K)	T_{amb} (K)	p_{01}-p_2 (Pa)	Lv/Dv	Density (kg/m^3)	A_{eff} (mm^2)	A_{ct} (mm^2)	C_D
3.00	43.3	9.0	24.4	600	24.3	24.7	101612	297.6	95726	297.5	297.9	5886	0.0939	1.1899	365.857	602.206	0.608
3.25	46.3	10.0	24.4	600	24.3	24.7	101602	297.6	95716	297.5	297.9	5886	0.1017	1.1898	391.224	652.389	0.600
3.50	49.0	11.5	24.4	600	24.3	24.8	101587	297.6	95701	297.5	298.0	5886	0.1096	1.1896	414.069	702.573	0.589
3.75	51.1	13.0	24.4	600	24.3	24.8	101572	297.6	95686	297.5	298.0	5886	0.1174	1.1894	431.846	752.757	0.574
4.00	53.5	14.0	24.4	600	24.3	24.8	101563	297.6	95677	297.5	298.0	5886	0.1252	1.1893	452.150	802.941	0.563
4.25	56.2	15.5	24.3	600	24.2	24.7	101548	297.5	95662	297.4	297.9	5886	0.1330	1.1895	474.923	853.125	0.557
4.50	58.5	17.2	24.3	600	24.2	24.8	101531	297.5	95645	297.4	298.0	5886	0.1409	1.1893	494.400	903.309	0.547
4.75	61.0	18.5	24.3	600	24.2	24.7	101519	297.5	95633	297.4	297.9	5886	0.1487	1.1892	515.561	953.492	0.541
5.00	63.2	20.0	24.4	600	24.3	24.8	101504	297.6	95618	297.5	298.0	5886	0.1565	1.1886	534.283	1003.676	0.532
5.25	65.4	21.5	24.4	600	24.3	24.8	101489	297.6	95603	297.5	298.0	5886	0.1643	1.1884	552.922	1053.860	0.525
5.50	67.8	23.0	24.3	600	24.2	24.7	101474	297.5	95588	297.4	297.9	5886	0.1722	1.1887	573.158	1104.044	0.519
5.75	70.0	25.0	24.3	600	24.2	24.8	101455	297.5	95569	297.4	298.0	5886	0.1800	1.1884	591.813	1154.228	0.513
6.00	72.0	26.5	24.3	600	24.2	24.7	101440	297.5	95554	297.4	297.9	5886	0.1878	1.1883	608.766	1204.411	0.505
6.25	73.9	27.5	24.4	600	24.4	24.8	101430	297.6	95544	297.6	298.0	5886	0.1956	1.1878	624.966	1254.595	0.498
6.50	75.8	29.5	24.3	600	24.3	24.7	101411	297.5	95525	297.5	297.9	5886	0.2035	1.1879	640.989	1304.779	0.491
6.75	77.0	30.5	24.4	600	24.3	24.8	101401	297.6	95515	297.5	298.0	5886	0.2113	1.1874	651.277	1354.963	0.481
7.00	78.1	31.0	24.3	600	24.3	24.8	101396	297.5	95510	297.5	298.0	5886	0.2191	1.1877	660.486	1405.147	0.470
7.25	79.4	32.5	24.3	600	24.2	24.8	101381	297.5	95495	297.4	298.0	5886	0.2269	1.1876	671.529	1455.330	0.461
7.50	80.0	33.0	24.4	600	24.2	24.8	101376	297.6	95490	297.4	298.0	5886	0.2348	1.1871	676.733	1505.514	0.450
7.75	81.5	34.5	24.3	600	24.2	24.8	101362	297.5	95476	297.4	298.0	5886	0.2426	1.1873	689.356	1555.698	0.443
8.00	82.4	35.0	24.3	600	24.2	24.8	101357	297.5	95471	297.4	298.0	5886	0.2504	1.1873	696.986	1605.882	0.434
8.25	83.2	35.5	24.3	600	24.2	24.9	101352	297.5	95466	297.4	298.1	5886	0.2582	1.1872	703.770	1656.066	0.425
8.50	84.4	36.2	24.3	600	24.2	24.9	101345	297.5	95459	297.4	298.1	5886	0.2661	1.1872	713.944	1706.249	0.418
8.75	85.0	37.0	24.3	600	24.2	24.9	101337	297.5	95451	297.4	298.1	5886	0.2739	1.1871	719.048	1756.433	0.409
9.00	85.6	38.0	24.3	600	24.2	24.9	101327	297.5	95441	297.4	298.1	5886	0.2817	1.1869	724.158	1806.617	0.401

Results for reverse flow past the inlet valves (3.00 to 9.00 mm valve lift)

Lift (mm)	Mass Flow (g/s)	p_{01} (mmH_2O)	T_{01} (°C)	p_{01}-p_2 (mmH_2O)	T_2 (°C)	T_{amb} (°C)	p_{01} (Pa)	T_{01} (K)	p_2 (Pa)	T_2 (K)	T_{amb} (K)	p_{01}-p_2 (Pa)	Lv/Dv	Density (kg/m^3)	A_{eff} (mm^2)	A_{ct} (mm^2)	C_D
0.10	0.9	0.0	24.8	600	25.4	25.0	101700	298.0	95814	298.6	298.2	5886	0.0037	1.1893	7.437	20.074	0.370
0.20	2.1	0.0	24.8	600	25.4	25.0	101700	298.0	95814	298.6	298.2	5886	0.0074	1.1893	17.579	40.147	0.438
0.30	3.3	0.2	24.8	600	25.3	25.0	101698	298.0	95812	298.5	298.2	5886	0.0111	1.1893	27.890	60.221	0.463
0.40	4.6	0.4	24.8	600	25.2	25.0	101696	298.0	95810	298.4	298.2	5886	0.0148	1.1893	38.877	80.294	0.484
0.50	5.8	0.6	24.8	600	25.2	24.9	101694	298.0	95808	298.4	298.1	5886	0.0185	1.1892	48.597	100.368	0.484
0.60	7.2	0.7	24.8	600	25.1	24.9	101693	298.0	95807	298.3	298.1	5886	0.0222	1.1892	60.429	120.441	0.502
0.70	8.4	0.8	24.8	600	25.1	24.9	101692	298.0	95806	298.3	298.1	5886	0.0259	1.1892	70.994	140.515	0.505
0.80	9.9	0.9	24.7	600	25.0	24.9	101691	297.9	95805	298.2	298.1	5886	0.0296	1.1896	83.658	160.588	0.521
0.90	11.4	1.0	24.7	600	25.0	24.9	101690	297.9	95804	298.2	298.1	5886	0.0333	1.1896	96.334	180.662	0.533
1.00	12.8	1.2	24.7	600	24.9	24.9	101688	297.9	95802	298.1	298.1	5886	0.0370	1.1896	108.166	200.735	0.539
1.10	14.0	1.4	24.7	600	24.9	24.8	101686	297.9	95800	298.1	298.0	5886	0.0407	1.1896	118.307	220.809	0.536
1.20	15.8	1.6	24.7	600	24.8	24.9	101684	297.9	95798	298.0	298.1	5886	0.0444	1.1895	133.097	240.882	0.553
1.30	17.2	1.9	24.6	600	24.8	24.9	101681	297.8	95795	298.0	298.1	5886	0.0481	1.1899	145.328	260.956	0.557
1.40	18.7	2.1	24.6	600	24.8	24.9	101679	297.8	95793	298.0	298.1	5886	0.0519	1.1899	158.004	281.029	0.562
1.50	20.2	2.5	24.6	600	24.7	24.8	101675	297.8	95789	297.9	298.0	5886	0.0556	1.1898	170.681	301.103	0.567
1.60	22.0	2.9	24.6	600	24.7	24.8	101672	297.8	95786	297.9	298.0	5886	0.0593	1.1898	185.894	321.176	0.579
1.70	23.3	3.2	24.6	600	24.7	24.9	101669	297.8	95783	297.9	298.1	5886	0.0630	1.1897	196.881	341.250	0.577
1.80	24.7	3.5	24.5	600	24.6	24.8	101666	297.7	95780	297.8	298.0	5886	0.0667	1.1901	208.679	361.323	0.578
1.90	26.3	4.0	24.5	600	24.6	24.8	101661	297.7	95775	297.8	298.0	5886	0.0704	1.1901	221.779	381.397	0.581
2.00	27.8	4.4	24.5	600	24.6	24.9	101657	297.7	95771	297.8	298.1	5886	0.0741	1.1900	234.880	401.470	0.585
2.10	29.2	4.9	24.5	600	24.6	24.9	101652	297.7	95766	297.8	298.1	5886	0.0778	1.1899	246.714	421.544	0.585
2.20	30.7	5.5	24.5	600	24.6	24.8	101646	297.7	95760	297.8	298.0	5886	0.0815	1.1899	259.395	441.617	0.587
2.25	31.0	4.5	23.9	600	23.8	24.3	101656	297.1	95770	297.0	297.5	5886	0.0833	1.1924	261.653	451.654	0.579
2.50	34.9	5.5	23.9	600	23.8	24.4	101646	297.1	95760	297.0	297.6	5886	0.0926	1.1923	294.585	501.838	0.587
2.75	38.1	7.0	23.9	600	23.8	24.3	101631	297.1	95745	297.0	297.5	5886	0.1019	1.1921	321.619	552.022	0.583

Results for forward flow past the exhaust valves (0 to 2.75 mm valve lift)

Lift (mm)	Mass Flow (g/s)	p_{01} (mmH_2O)	T_{01} (°C)	p_{01}-p_2 (mmH_2O)	T_2 (°C)	T_{amb} (°C)	p_{01} (Pa)	T_{01} (K)	p_2 (Pa)	T_2 (K)	T_{amb} (K)	p_{01}-p_2 (Pa)	Lv/Dv	Density (kg/m^3)	A_{eff} (mm^2)	A_{ct} (mm^2)	C_D
3.00	41.0	7.7	24.0	600	23.8	24.4	101624	297.2	95738	297.0	297.6	5886	0.1111	1.1916	346.169	602.206	0.575
3.25	43.8	9.0	23.9	600	23.8	24.3	101612	297.1	95726	297.0	297.5	5886	0.1204	1.1919	369.771	652.389	0.567
3.50	47.0	10.5	23.9	600	23.8	24.3	101597	297.1	95711	297.0	297.5	5886	0.1296	1.1917	396.815	702.573	0.565
3.75	50.0	11.5	23.9	600	23.8	24.3	101587	297.1	95701	297.0	297.5	5886	0.1389	1.1916	422.164	752.757	0.561
4.00	52.4	13.0	24.1	600	24.0	24.4	101572	297.3	95686	297.2	297.6	5886	0.1481	1.1906	442.609	802.941	0.551
4.25	55.0	14.5	24.1	600	24.0	24.5	101558	297.3	95672	297.2	297.7	5886	0.1574	1.1904	464.604	853.125	0.545
4.50	57.8	16.0	24.1	600	24.0	24.5	101543	297.3	95657	297.2	297.7	5886	0.1667	1.1903	488.292	903.309	0.541
4.75	59.9	17.5	24.1	600	24.0	24.5	101528	297.3	95642	297.2	297.7	5886	0.1759	1.1901	506.069	953.492	0.531
5.00	62.0	18.5	24.2	600	24.1	24.5	101519	297.4	95633	297.3	297.7	5886	0.1852	1.1896	523.925	1003.676	0.522
5.25	63.5	19.5	24.2	600	24.1	24.6	101509	297.4	95623	297.3	297.8	5886	0.1944	1.1895	536.626	1053.860	0.509
5.50	65.5	21.0	24.2	600	24.1	24.6	101494	297.4	95608	297.3	297.8	5886	0.2037	1.1893	553.568	1104.044	0.501
5.75	67.0	22.0	24.3	600	24.1	24.7	101484	297.5	95598	297.3	297.9	5886	0.2130	1.1888	566.368	1154.228	0.491
6.00	68.0	23.0	24.3	600	24.1	24.6	101474	297.5	95588	297.3	297.8	5886	0.2222	1.1887	574.849	1204.411	0.477
6.25	69.5	23.5	24.3	600	24.1	24.7	101469	297.5	95583	297.3	297.9	5886	0.2315	1.1886	587.543	1254.595	0.468
6.50	70.0	23.5	24.3	600	24.1	24.7	101469	297.5	95583	297.3	297.9	5886	0.2407	1.1886	591.770	1304.779	0.454
6.75	70.5	24.0	24.4	600	24.3	24.7	101465	297.6	95579	297.5	297.9	5886	0.2500	1.1882	596.112	1354.963	0.440
7.00	71.2	25.0	24.4	600	24.2	24.7	101455	297.6	95569	297.4	297.9	5886	0.2593	1.1880	602.060	1405.147	0.428
7.25	72.0	25.5	24.5	600	24.2	24.7	101450	297.7	95564	297.4	297.9	5886	0.2685	1.1876	608.941	1455.330	0.418
7.50	72.3	25.5	24.5	600	24.3	24.7	101450	297.7	95564	297.5	297.9	5886	0.2778	1.1876	611.479	1505.514	0.406
7.75	72.5	26.0	24.4	600	24.3	24.7	101445	297.6	95559	297.5	297.9	5886	0.2870	1.1879	613.082	1555.698	0.394
8.00	72.8	26.5	24.4	600	24.3	24.7	101440	297.6	95554	297.5	297.9	5886	0.2963	1.1879	615.634	1605.882	0.383
8.25	73.0	26.5	24.5	600	24.4	24.8	101440	297.7	95554	297.6	298.0	5886	0.3056	1.1875	617.429	1656.066	0.373
8.50	73.9	27.0	24.6	600	24.4	24.8	101435	297.8	95549	297.6	298.0	5886	0.3148	1.1870	625.161	1706.249	0.366
8.75	74.5	27.0	24.5	600	24.3	24.8	101435	297.7	95549	297.5	298.0	5886	0.3241	1.1874	630.131	1756.433	0.359
9.00	74.8	27.5	24.4	600	24.3	24.8	101430	297.6	95544	297.5	298.0	5886	0.3333	1.1878	632.577	1806.617	0.350

Results for forward flow past the exhaust valves (3.00 to 9.00 mm valve lift)

Lift (mm)	Mass Flow (g/s)	p_{01} (mmH_2O)	T_{01} (°C)	p_{01}-p_2 (mmH_2O)	T_2 (°C)	T_{amb} (°C)	p_{01} (Pa)	T_{01} (K)	p_2 (Pa)	T_2 (K)	T_{amb} (K)	p_{01}-p_2 (Pa)	Lv/Dv	Density (kg/m^3)	A_{eff} (mm^2)	A_{ct} (mm^2)	C_D
0.00	0.0	0.0	25.1	600	24.7	25.0	101700	298.3	95814	297.9	298.2	5886	0.0000	1.1881	0.000	0.000	0.000
0.10	0.9	0.0	25.1	600	24.7	25.0	101700	298.3	95814	297.9	298.2	5886	0.0037	1.1881	7.610	20.074	0.379
0.20	2.0	0.0	25.0	600	24.7	24.9	101700	298.2	95814	297.9	298.1	5886	0.0074	1.1885	16.908	40.147	0.421
0.30	3.5	0.5	24.9	600	24.7	24.9	101695	298.1	95809	297.9	298.1	5886	0.0111	1.1889	29.163	60.221	0.484
0.40	4.9	0.6	24.8	600	24.7	24.9	101694	298.0	95808	297.9	298.1	5886	0.0148	1.1892	41.413	80.294	0.516
0.50	6.4	0.8	24.7	600	24.7	24.9	101693	297.9	95807	297.9	298.1	5886	0.0185	1.1896	53.659	100.368	0.535
0.60	7.8	1.0	24.7	600	24.7	24.8	101690	297.9	95804	297.9	298.0	5886	0.0222	1.1896	65.913	120.441	0.547
0.70	9.3	1.3	24.7	600	24.7	24.9	101688	297.9	95802	297.9	298.1	5886	0.0259	1.1896	78.167	140.515	0.556
0.80	10.8	1.5	24.7	600	24.7	24.9	101685	297.9	95799	297.9	298.1	5886	0.0296	1.1895	91.266	160.588	0.568
0.90	12.1	2.0	24.6	600	24.7	24.9	101680	297.8	95794	297.9	298.1	5886	0.0333	1.1899	102.237	180.662	0.566
1.00	13.4	2.4	24.6	600	24.7	24.9	101676	297.8	95790	297.9	298.1	5886	0.0370	1.1898	113.223	200.735	0.564
1.10	15.0	2.8	24.6	600	24.7	24.9	101673	297.8	95787	297.9	298.1	5886	0.0407	1.1898	126.745	220.809	0.574
1.20	16.5	3.5	24.6	600	24.7	25.0	101666	297.8	95780	297.9	298.2	5886	0.0444	1.1897	139.424	240.882	0.579
1.30	17.9	4.0	24.7	600	24.7	25.0	101661	297.9	95775	297.9	298.2	5886	0.0481	1.1893	151.283	260.956	0.580
1.40	19.1	4.5	24.6	600	24.7	25.0	101656	297.8	95770	297.9	298.2	5886	0.0519	1.1896	161.402	281.029	0.574
1.50	20.6	5.2	24.7	600	24.7	25.1	101649	297.9	95763	297.9	298.3	5886	0.0556	1.1891	174.113	301.103	0.578
1.60	22.1	6.1	24.7	600	24.7	25.1	101640	297.9	95754	297.9	298.3	5886	0.0593	1.1890	186.799	321.176	0.582
1.70	23.6	6.6	24.6	600	24.7	25.1	101635	297.8	95749	297.9	298.3	5886	0.0630	1.1894	199.449	341.250	0.584
1.80	24.9	7.5	24.6	600	24.7	25.1	101626	297.8	95740	297.9	298.3	5886	0.0667	1.1892	210.022	361.323	0.581
1.90	26.2	8.3	24.6	600	24.7	25.1	101619	297.8	95733	297.9	298.3	5886	0.0704	1.1892	221.440	381.397	0.581
2.00	27.5	9.0	24.6	600	24.7	25.1	101612	297.8	95726	297.9	298.3	5886	0.0741	1.1891	232.436	401.470	0.579
2.10	28.9	9.5	24.6	600	24.6	25.1	101607	297.8	95721	297.8	298.3	5886	0.0778	1.1890	244.275	421.544	0.579
2.20	30.3	10.5	24.6	600	24.6	25.1	101597	297.8	95711	297.8	298.3	5886	0.0815	1.1889	256.120	441.617	0.580
2.25	31.0	10.0	23.7	600	22.2	24.0	101602	296.9	95716	295.4	297.2	5886	0.0833	1.1926	261.635	451.654	0.579
2.50	34.5	12.5	23.5	600	22.4	24.0	101577	296.7	95691	295.6	297.2	5886	0.0926	1.1931	291.111	501.838	0.580
2.75	38.0	15.0	23.6	600	22.5	24.0	101553	296.8	95667	295.7	297.2	5886	0.1019	1.1924	320.737	552.022	0.581

Results for reverse flow past the exhaust valves (0.10 to 2.75 mm valve lift)

Lift (mm)	Mass Flow (g/s)	p_{01} (mmH_2O)	T_{01} (°C)	p_{01}-p_2 (mmH_2O)	T_2 (°C)	T_{amb} (°C)	p_{01} (Pa)	T_{01} (K)	p_2 (Pa)	T_2 (K)	T_{amb} (K)	p_{01}-p_2 (Pa)	Lv/Dv	Density (kg/m^3)	A_{eff} (mm^2)	A_{ct} (mm^2)	C_D
3.00	41.0	18.0	23.6	600	22.6	24.1	101523	296.8	95637	295.8	297.3	5886	0.1111	1.1920	346.108	602.206	0.575
3.25	44.4	21.0	23.4	600	22.6	24.1	101494	296.6	95608	295.8	297.3	5886	0.1204	1.1925	374.738	652.389	0.574
3.50	47.6	24.5	23.6	600	22.8	24.0	101460	296.8	95574	296.0	297.2	5886	0.1296	1.1913	401.949	702.573	0.572
3.75	50.9	28.0	23.6	600	22.8	24.0	101425	296.8	95539	296.0	297.2	5886	0.1389	1.1909	429.888	752.757	0.571
4.00	53.5	31.5	23.7	600	22.9	24.0	101391	296.9	95505	296.1	297.2	5886	0.1481	1.1901	452.000	802.941	0.563
4.25	56.7	35.0	23.7	600	23.1	24.0	101357	296.9	95471	296.3	297.2	5886	0.1574	1.1897	479.117	853.125	0.562
4.50	59.6	39.0	23.6	600	23.1	24.0	101317	296.8	95431	296.3	297.2	5886	0.1667	1.1896	503.634	903.309	0.558
4.75	61.9	42.5	23.6	600	23.2	24.0	101283	296.8	95397	296.4	297.2	5886	0.1759	1.1892	523.159	953.492	0.549
5.00	64.0	45.5	23.7	600	23.3	24.0	101254	296.9	95368	296.5	297.2	5886	0.1852	1.1885	541.077	1003.676	0.539
5.25	66.5	48.5	23.8	600	23.3	24.0	101224	297.0	95338	296.5	297.2	5886	0.1944	1.1877	562.389	1053.860	0.534
5.50	68.6	52.0	23.8	600	23.4	24.1	101190	297.0	95304	296.6	297.3	5886	0.2037	1.1873	580.247	1104.044	0.526
5.75	70.1	55.0	23.8	600	23.4	24.2	101160	297.0	95274	296.6	297.4	5886	0.2130	1.1870	593.021	1154.228	0.514
6.00	72.0	58.0	23.9	600	23.5	24.2	101131	297.1	95245	296.7	297.4	5886	0.2222	1.1862	609.286	1204.411	0.506
6.25	73.5	60.5	23.9	600	23.5	24.3	101106	297.1	95220	296.7	297.5	5886	0.2315	1.1860	622.054	1254.595	0.496
6.50	74.5	62.5	23.9	600	23.5	24.3	101087	297.1	95201	296.7	297.5	5886	0.2407	1.1857	630.579	1304.779	0.483
6.75	76.0	64.5	24.0	600	23.6	24.3	101067	297.2	95181	296.8	297.5	5886	0.2500	1.1851	643.446	1354.963	0.475
7.00	76.8	66.0	24.0	600	23.6	24.3	101053	297.2	95167	296.8	297.5	5886	0.2593	1.1849	650.266	1405.147	0.463
7.25	77.5	67.5	23.9	600	23.6	24.3	101038	297.1	95152	296.8	297.5	5886	0.2685	1.1851	656.131	1455.330	0.451
7.50	78.1	68.5	23.8	600	23.6	24.3	101028	297.0	95142	296.8	297.5	5886	0.2778	1.1854	661.131	1505.514	0.439
7.75	78.8	69.5	23.8	600	23.6	24.3	101018	297.0	95132	296.8	297.5	5886	0.2870	1.1853	667.089	1555.698	0.429
8.00	79.5	70.5	23.9	600	23.7	24.3	101008	297.1	95122	296.9	297.5	5886	0.2963	1.1848	673.161	1605.882	0.419
8.25	79.8	71.0	23.8	600	23.7	24.3	101003	297.0	95117	296.9	297.5	5886	0.3056	1.1851	675.604	1656.066	0.408
8.50	80.0	71.5	23.8	600	23.7	24.2	100999	297.0	95113	296.9	297.4	5886	0.3148	1.1851	677.314	1706.249	0.397
8.75	80.5	72.0	23.7	600	23.7	24.2	100994	296.9	95108	296.9	297.4	5886	0.3241	1.1854	681.449	1756.433	0.388
9.00	80.9	73.0	23.8	600	23.7	24.2	100984	297.0	95098	296.9	297.4	5886	0.3333	1.1849	684.983	1806.617	0.379

Results for reverse flow past the exhaust valves (3.00 to 9.00 mm valve lift)

Appendix 2

A METHOD FOR MODELLING INTAKE PORT FLOWS AND MIXING USING FINITE PORT VOLUMES

A2. A method for modelling intake port flows and mixing using finite port volumes

A2.1. Applying the General Flow Energy Equation

For a single control volume (fixed volume), the ideal gas equation can be applied to the contents. Thus:

$$\frac{dp}{d\theta} = \frac{1}{V}\left\{mR\frac{dT}{d\theta} + mT\frac{dR}{d\theta} + RT\frac{dm}{d\theta}\right\} \qquad \textbf{(A2.1)}$$

Take a series of such control volumes in a length of pipe (the intake port for example) as shown below:

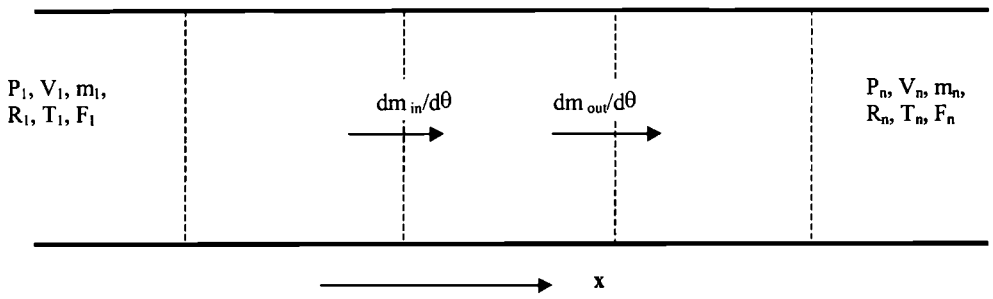

Figure A2.1
Schematic representation of port volumes

If it is assumed that the rate of pressure change as given by Equation (A2.1) is the same for all control volumes, and that this change in pressure is achieved by the appropriate flow of mass from one control volume to the next, a series of simultaneous equations can be written for the control volumes.

$$\begin{aligned}
\frac{dp}{d\theta} &= \frac{1}{V_1}\left\{m_1R_1\frac{dT_1}{d\theta} + m_1T_1\frac{dR_1}{d\theta} + R_1T_1\frac{dm_1}{d\theta}\right\} \\
\frac{dp}{d\theta} &= \frac{1}{V_2}\left\{m_2R_2\frac{dT_2}{d\theta} + m_2T_2\frac{dR_2}{d\theta} + R_2T_2\frac{dm_2}{d\theta}\right\} \\
&\bullet \\
&\bullet \\
\frac{dp}{d\theta} &= \frac{1}{V_n}\left\{m_nR_n\frac{dT_n}{d\theta} + m_nT_n\frac{dR_n}{d\theta} + R_nT_n\frac{dm_n}{d\theta}\right\}
\end{aligned} \qquad \textbf{(A2.2)}$$

There are many unknowns in these equations, however, as the following will show these can all

be expressed in terms of the flow rates into and out of each of the control volumes. The General Flow Energy Equation (GFEE) can be written as follows:

$$m\frac{du}{d\theta}+u\frac{dm}{d\theta}=\frac{dQ}{d\theta}-p\frac{dV}{d\theta}+h_{in}\frac{dm_{in}}{d\theta}-h_{out}\frac{dm_{out}}{d\theta} \qquad \textbf{(A2.3)}$$

In this case, there is no change in volume, and heat transfer can be estimated using some suitable empirical model, thus leaving terms involving mass flow rates and $du/d\theta$. Equation (A2.3) can be expanded to give:

$$m\left[\frac{\partial u}{\partial T}\frac{dT}{d\theta}+\frac{\partial u}{\partial F}\frac{dF}{d\theta}\right]+u\frac{dm}{d\theta}=\frac{dQ}{d\theta}-p\frac{dV}{d\theta}+h_{in}\frac{dm_{in}}{d\theta}-h_{out}\frac{dm_{out}}{d\theta} \qquad \textbf{(A2.4)}$$

Using the principle of conservation of mass:

$$\frac{dm}{d\theta}=\frac{dm_{in}}{d\theta}-\frac{dm_{out}}{d\theta} \qquad \textbf{(A2.5)}$$

Equation (A2.4) can be rearranged to give:

$$\frac{dT}{d\theta}=\left\{-\frac{\partial u}{\partial F}\frac{dF}{d\theta}+\frac{1}{m}\left[\frac{dQ}{d\theta}+h_{in}\frac{dm_{in}}{d\theta}-h_{out}\frac{dm_{out}}{d\theta}-u\frac{dm_{in}}{d\theta}+u\frac{dm_{out}}{d\theta}\right]\right\}\Big/\frac{\partial u}{\partial T} \qquad \textbf{(A2.6)}$$

Now $dF/d\theta$ can be estimated using the following procedure:

First F is defined as;

$$F=\frac{(m_f/m_a)_{actual}}{(m_f/m_a)_{stoich}}=\frac{f_{actual}}{f_{stoich}}=\frac{m_f}{m_a f_{stoich}} \qquad \textbf{(A2.7)}$$

If it is assumed that all the fuel is added in the cylinder, then m_f represents the mass of burned fuel present in the mixture. Since only air and exhaust gas are present, the total mass must be the sum of these:

$$m=m_a+m_f \qquad \textbf{(A2.8)}$$

Knowing F therefore allows the individual components of the mixture to be expressed in terms of the total mass in the control volume:

$$m_a=\frac{m_a}{m}\times m=\frac{m_a m}{m_a+m_f}=\frac{m}{\left[1+(m_f/m_a)\right]}=\frac{m}{1+Ff_{stoich}} \qquad \textbf{(A2.9)}$$

or:

$$m_a = \frac{m}{F'} \tag{A2.10}$$

where:

$$F' = 1 + Ff_{stoich} \tag{A2.11}$$

Similarly

$$m_f = \frac{mFf_{stoich}}{F'} \tag{A2.12}$$

Differentiating the right side of Equation (A2.7) gives:

$$\frac{dF}{d\theta} = \frac{1}{f_{stoich}}\left\{(m - m_f)\frac{dm_f}{d\theta} - m_f\left(\frac{dm}{d\theta} - \frac{dm_f}{d\theta}\right)\right\}\frac{1}{m_a^2}$$

$$\Rightarrow \frac{dF}{d\theta} = \frac{1}{f_{stoich}m_a}\left\{\frac{m}{m_a}\frac{dm_f}{d\theta} - \frac{m_f}{m_a}\frac{dm}{d\theta}\right\} \tag{A2.13}$$

Substituting for m_a from Equation (A2.10) into Equation (A2.13) gives:

$$\frac{dF}{d\theta} = \frac{F'}{m}\left\{\frac{F'}{f_{stoich}}\frac{dm_f}{d\theta} - F\frac{dm}{d\theta}\right\} \tag{A2.14}$$

but

$$\frac{dm_f}{d\theta} = \left(\frac{dm_f}{d\theta}\right)_{in} - \left(\frac{dm_f}{d\theta}\right)_{out} - M\left(\frac{dF}{dx}\right)_{in} + M\left(\frac{dF}{dx}\right)_{out} \tag{A2.15}$$

where M is a mixing coefficient, which, for the moment can be assumed to be a function of concentration gradient only (as in Fick's Law).

From Equation (A2.12):

$$\frac{dm_f}{d\theta} = \frac{F_{in}f_{stoich}}{F_{in}'}\frac{dm_{in}}{d\theta} - \frac{F_{out}f_{stoich}}{F_{out}'}\frac{dm_{out}}{d\theta} - M\left(\frac{dF}{dx}\right)_{in} + M\left(\frac{dF}{dx}\right)_{out} \tag{A2.16}$$

Thus:

$$\frac{dF}{d\theta} = \frac{F'}{m}\left\{\frac{F'}{f_{stoich}}\left[\frac{F_{in}f_{stoich}}{F_{in}'}\frac{dm_{in}}{d\theta} - \frac{F_{out}f_{stoich}}{F_{out}'}\frac{dm_{out}}{d\theta} - M\left(\frac{dF}{dx}\right)_{in} + M\left(\frac{dF}{dx}\right)_{out}\right] - F\frac{dm}{d\theta}\right\} \tag{A2.17}$$

writing this only in terms of the mass flow rates in and out:

$$\frac{dF}{d\theta}=\frac{F'}{m}\left\{F'\frac{F_{in}}{F_{in}'}\frac{dm_{in}}{d\theta}-F'\frac{F_{out}}{F_{out}'}\frac{dm_{out}}{d\theta}-F\frac{dm_{in}}{d\theta}+F\frac{dm_{out}}{d\theta}-M\frac{F'}{f_{stoich}}\frac{dF_{in}}{dx}+M\frac{F'}{f_{stoich}}\frac{dF_{out}}{dx}\right\} \quad \textbf{(A2.18)}$$

$$\frac{dF}{d\theta}=\frac{1}{m}\left\{\left(F'^2\frac{F_{in}}{F_{in}'}-FF'\right)\frac{dm_{in}}{d\theta}-\left(F'^2\frac{F_{out}}{F_{out}'}-FF'\right)\frac{dm_{out}}{d\theta}-M\frac{F'^2}{f_{stoich}}\frac{dF_{in}}{dx}+M\frac{F'^2}{f_{stoich}}\frac{dF_{out}}{dx}\right\}$$

Equation (A2.18) can now be substituted into Equation (A2.6):

$$\frac{dT}{d\theta}=\frac{1}{m}\left\{\left[h_{in}-u-\frac{\partial u}{\partial F}\left(F'^2\frac{F_{in}}{F_{in}'}-FF'\right)\right]\frac{dm_{in}}{d\theta}-\left[h_{out}-u-\frac{\partial u}{\partial F}\left(F'^2\frac{F_{out}}{F_{out}'}-FF'\right)\right]\frac{dm_{out}}{d\theta}\right. \quad \textbf{(A2.19)}$$
$$\left.+\frac{dQ}{d\theta}+M\frac{F'^2}{f_{stoich}}\frac{\partial u}{\partial F}\frac{dF_{in}}{dx}-M\frac{F'^2}{f_{stoich}}\frac{\partial u}{\partial F}\frac{dF_{out}}{dx}\right\}1\Big/\frac{\partial u}{\partial T}$$

An expression for $dR/d\theta$ in Equation (A2.1) is now required. Krieger and Borman (1966) present an approximation for the gas constant R:

$$R=287+(20F) \text{ (J/kgK of original air)} \quad \textbf{(A2.20)}$$

However, this is in terms of the original mass of air in the mixture and must be converted to express R in terms of the total mass. This is achieved by multiplying by the mass of air and dividing by the total mass as follows:

$$R\times\frac{m_a}{m}=R\times\frac{m_a}{m_a+m_f}=\frac{R\times\frac{m}{F'}}{\frac{m}{F'}+\frac{mFf_{stoich}}{F'}}=\frac{R}{(1+Ff_{stoich})}=\frac{R}{F'} \quad \textbf{(A2.21)}$$

Equation (A2.20) should therefore be written as:

$$R=\frac{287}{F'}+\left(\frac{20\times F}{F'}\right) \quad \textbf{(A2.22)}$$

which, on differentiating gives:

$$\frac{dR}{d\theta}=-\frac{20F'\frac{dF}{d\theta}-(287+20F)\frac{dF'}{d\theta}}{F'^2} \quad \textbf{(A2.23)}$$

but:

$$F' = 1 + Ff_{stoich} \Rightarrow \frac{dF'}{d\theta} = f_{stoich}\frac{dF}{d\theta} \tag{A2.24}$$

$$\therefore \frac{dR}{d\theta} = \frac{1}{F'^2}\left(20F' - 287f_{stoich} - 20Ff_{stoich}\right)\frac{dF}{d\theta} \tag{A2.25}$$

$$\frac{dR}{d\theta} = \frac{\left(20F' - 287f_{stoich} - 20Ff_{stoich}\right)}{m} \times \left\{\left(\frac{F_{in}}{F_{in}'} - \frac{F}{F'}\right)\frac{dm_{in}}{d\theta} - \left(\frac{F_{out}}{F_{out}'} - \frac{F}{F'}\right)\frac{dm_{out}}{d\theta} - \frac{M}{f_{stoich}}\frac{dF_{in}}{dx} + \frac{M}{f_{stoich}}\frac{dF_{out}}{dx}\right\} \tag{A2.26}$$

There are now a complete set of equations for all three terms on the right hand side of Equation (A2.1). Putting these together gives:

$$\frac{dp}{d\theta} = \frac{1}{V}\left\{\frac{R}{\partial u/\partial T}\left\{h_{in} - u - \frac{\partial u}{\partial F}\left(F'^2\frac{F_{in}}{F_{in}'} - FF'\right)\right\}\frac{dm_{in}}{d\theta} - \frac{R}{\partial u/\partial T}\left\{h_{out} - u - \frac{\partial u}{\partial F}\left(F'^2\frac{F_{out}}{F_{out}'} - FF'\right)\right\}\frac{dm_{out}}{d\theta} + \frac{R}{\partial u/\partial T}\left\{\frac{dQ}{d\theta} + M\frac{\partial u}{\partial F}\frac{F'^2}{f_{stoich}}\frac{dF_{in}}{dx} - M\frac{\partial u}{\partial F}\frac{F'^2}{f_{stoich}}\frac{dF_{out}}{dx}\right\} + T\left(20F' - 287f_{stoich} - 20Ff_{stoich}\right)\left\{\left(\frac{F_{in}}{F_{in}'} - \frac{F}{F'}\right)\frac{dm_{in}}{d\theta} - \left(\frac{F_{out}}{F_{out}'} - \frac{F}{F'}\right)\frac{dm_{out}}{d\theta} - \frac{M}{f_{stoich}}\frac{dF_{in}}{dx} + \frac{M}{f_{stoich}}\frac{dF_{out}}{dx}\right\} + \left\{RT\frac{dm_{in}}{d\theta} - RT\frac{dm_{out}}{d\theta}\right\}\right\} \tag{A2.27}$$

This can be rearranged to give:

$$\frac{dp}{d\theta} = \frac{1}{V} \times \left\{\left\{\frac{R}{\partial u/\partial T}\left\{h_{in} - u - \frac{\partial u}{\partial F}\left(F'^2\frac{F_{in}}{F_{in}'} - FF'\right)\right\} + T\left(20F' - 287f_{stoich} - 20Ff_{stoich}\right)\left(\frac{F_{in}}{F_{in}'} - \frac{F}{F'}\right) + RT\right\}\frac{dm_{in}}{d\theta} - \left\{\frac{R}{\partial u/\partial T}\left\{h_{out} - u - \frac{\partial u}{\partial F}\left(F'^2\frac{F_{out}}{F_{out}'} - FF'\right)\right\} + T\left(20F' - 287f_{stoich} - 20Ff_{stoich}\right)\left(\frac{F_{out}}{F_{out}'} - \frac{F}{F'}\right) + RT\right\}\frac{dm_{out}}{d\theta} + \frac{R}{\partial u/\partial T}\frac{dQ}{d\theta} + \left\{\frac{R}{\partial u/\partial T}F'^2\frac{\partial u}{\partial F} + T\left(20F' - 287f_{stoich} - 20Ff_{stoich}\right)\right\}\left\{\frac{M}{f_{stoich}}\frac{dF_{in}}{dx} - \frac{M}{f_{stoich}}\frac{dF_{out}}{dx}\right\}\right\} \tag{A2.28}$$

Equation (A2.28) now gives the rate of change of pressure in terms of the mass flows in and out, their properties and the properties within the control volume. Since any flows in will be from an adjacent control volume, the properties of the incoming flow will be known. Similarly the

properties of any outgoing flows will be those of the gas within the control volume (also known). If Equation (A2.28) is applied to all the control volumes (say n in total), there will be n equations with n+2 unknowns. However, if the flow rates into the port at each end are known, the problem can be solved. This can be achieved by applying compressible flow equations to the restrictions (valves or throttle) at either end. The resulting set of simultaneous equations can then be solved using matrix inversion to give the pressure rise in the port and flow rates between control volumes

A2.2. Calculating gas composition when using the Runge Kutta method

The end values of mass, temperature and F can be found by using the Runge Kutta method for the numerical integration. Assume that there are four estimates for the mass flow rates in and out with their corresponding F values, and similarly for the rate of change of temperature. Thus:

$$\begin{aligned}
\frac{dm_{in}}{d\theta} &= \frac{1}{6}\frac{dm_{in}}{d\theta}_1 + \frac{1}{3}\frac{dm_{in}}{d\theta}_2 + \frac{1}{3}\frac{dm_{in}}{d\theta}_3 + \frac{1}{6}\frac{dm_{in}}{d\theta}_4 \\
\frac{dm_{out}}{d\theta} &= \frac{1}{6}\frac{dm_{out}}{d\theta}_1 + \frac{1}{3}\frac{dm_{out}}{d\theta}_2 + \frac{1}{3}\frac{dm_{out}}{d\theta}_3 + \frac{1}{6}\frac{dm_{out}}{d\theta}_4 \\
\frac{dT}{d\theta} &= \frac{1}{6}\frac{dT}{d\theta_1} + \frac{1}{3}\frac{dT}{d\theta_2} + \frac{1}{3}\frac{dT}{d\theta_3} + \frac{1}{6}\frac{dT}{d\theta_4}
\end{aligned} \qquad \textbf{(A2.29)}$$

The resulting value of F at the end of the step can be estimated from knowledge of the flows into and out of the control volume and their associated F values:

$$F_{end} = \frac{1}{f_{stoich}}\left(\frac{m_f}{m_a}\right)_{end} = \frac{1}{f_{stoich}}\left\{\frac{\frac{mFf_{stoich}}{F'} + \frac{F_{in}f_{stoich}}{F'_{in}}\frac{dm_{in}}{d\theta}\Delta\theta - \frac{F_{out}f_{stoich}}{F'_{out}}\frac{dm_{out}}{d\theta}\Delta\theta}{\frac{m}{F'} + \frac{1}{F'_{in}}\frac{dm_{in}}{d\theta}\Delta\theta - \frac{1}{F'_{out}}\frac{dm_{out}}{d\theta}\Delta\theta}\right\}$$

$$\Rightarrow F_{end} = \left\{\frac{\frac{mF}{F'} + \left(\frac{F_{in}}{F'_{in}}\frac{dm_{in}}{d\theta} - \frac{F_{out}}{F'_{out}}\frac{dm_{out}}{d\theta}\right)\Delta\theta}{\frac{m}{F'} + \left(\frac{1}{F'_{in}}\frac{dm_{in}}{d\theta} - \frac{1}{F'_{out}}\frac{dm_{out}}{d\theta}\right)\Delta\theta}\right\} \qquad \textbf{(A2.30)}$$

But:

$$\frac{F_{in}}{F'_{in}}\frac{dm_{in}}{d\theta} = \left\{\frac{1}{6}\left(\frac{F_{in}}{F'_{in}}\frac{dm_{in}}{d\theta}\right)_1 + \frac{1}{3}\left(\frac{F_{in}}{F'_{in}}\frac{dm_{in}}{d\theta}\right)_2 + \frac{1}{3}\left(\frac{F_{in}}{F'_{in}}\frac{dm_{in}}{d\theta}\right)_3 + \frac{1}{6}\left(\frac{F_{in}}{F'_{in}}\frac{dm_{in}}{d\theta}\right)_4\right\} \qquad \textbf{(A2.31)}$$

and:

$$\frac{F_{out}}{F'_{out}}\frac{dm_{out}}{d\theta} = \left\{\frac{1}{6}\left(\frac{F_{out}}{F'_{out}}\frac{dm_{out}}{d\theta}\right)_1 + \frac{1}{3}\left(\frac{F_{out}}{F'_{out}}\frac{dm_{out}}{d\theta}\right)_2 + \frac{1}{3}\left(\frac{F_{out}}{F'_{out}}\frac{dm_{out}}{d\theta}\right)_3 + \frac{1}{6}\left(\frac{F_{out}}{F'_{out}}\frac{dm_{out}}{d\theta}\right)_4\right\} \quad \textbf{(A2.32)}$$

Also:

$$\frac{1}{F'_{in}}\frac{dm_{in}}{d\theta} = \left\{\frac{1}{6}\left(\frac{1}{F'_{in}}\frac{dm_{in}}{d\theta}\right)_1 + \frac{1}{3}\left(\frac{1}{F'_{in}}\frac{dm_{in}}{d\theta}\right)_2 + \frac{1}{3}\left(\frac{1}{F'_{in}}\frac{dm_{in}}{d\theta}\right)_3 + \frac{1}{6}\left(\frac{1}{F'_{in}}\frac{dm_{in}}{d\theta}\right)_4\right\} \quad \textbf{(A2.33)}$$

and:

$$\frac{1}{F'_{out}}\frac{dm_{out}}{d\theta} = \left\{\frac{1}{6}\left(\frac{1}{F'_{out}}\frac{dm_{out}}{d\theta}\right)_1 + \frac{1}{3}\left(\frac{1}{F'_{out}}\frac{dm_{out}}{d\theta}\right)_2 + \frac{1}{3}\left(\frac{1}{F'_{out}}\frac{dm_{out}}{d\theta}\right)_3 + \frac{1}{6}\left(\frac{1}{F'_{out}}\frac{dm_{out}}{d\theta}\right)_4\right\} \quad \textbf{(A2.34)}$$

Equations (A2.31) to (A2.34) can be substituted into Equation (A2.30) to calculate the value of F at the end of the step. This method ensures that the principle of conservation of mass is not violated and all masses of air and exhaust gas are accounted for.

Appendix 3

ANLAYSIS AND PRESENTATION OF EXPERIMENTAL RSULTS

A3. Analysis and Presentation of Experimental Results

A3.1. Estimating variance

Two methods are available for estimating the experimental error variance σ^2 in a Central Composite Rotatable Design (CCRD) of experiment. The first considers the sum of squares of the residuals which is defined as:

$$SS_E = \sum_{i=1}^{n} (y_i - \hat{y}_i)^2 \qquad \textbf{(A3.1)}$$

Myers and Montgomery (1995) stated that the expected value of SS_E can be related to the variance through the following relationship:

$$E(SS_E) = \sigma^2 (n - p) \qquad \textbf{(A3.2)}$$

where n is the number of observations made in the experiment and p the number of parameters to be evaluated in the regression model. The difference between the two is often referred to as the number of degrees of freedom (ν). An unbiased estimator of σ^2 can therefore be written as:

$$\hat{\sigma}^2 = \frac{SS_E}{(n - p)} \qquad \textbf{(A3.3)}$$

The circumflex is introduced to indicate that the value generated by Equation (A3.3) is an estimate of the variance. Myers and Montgomery (1995) demonstrated how this estimate is dependent on the regression model used. An independent estimate can, however, be generated if repeat tests are conducted at one or more points in the experiment. In the case of a CCRD, a number of repeated tests will have been conducted at the centre points, and these can now be used to generate an independent estimate of the variance. The error sum of squares from the centre points alone is defined as:

$$SS_{Ec} = \sum_{i=1}^{n_c} (y_i - \bar{y}_i)^2 \qquad \textbf{(A3.4)}$$

Only one parameter (the mean value of the centre point readings) is required in Equation (A3.4), so the number of degrees of freedom in this case will be one less the number of centre points. An estimate of the variance can therefore be written as:

$$\hat{\sigma}^2 = \frac{SS_{Ec}}{(n_c - 1)} \qquad \textbf{(A3.5)}$$

A3.2. Standard errors and tests of significance

The estimated value of σ^2 can be used to define a 'standard error' for each parameter b in the regression model β:

$$se(b_j) = \sqrt{\hat{\sigma}^2 C_{jj}} \qquad \textbf{(A3.6)}$$

C_{jj} is the diagonal element of $(\mathbf{X'X})^{-1}$ corresponding to b_j and $\mathbf{X}$ is the matrix of test points used in the linear regression. The standard error can be used in conjunction with the Student's t table to test for significance of each of the parameters b_j. The probability of an individual parameter b_j equalling an arbitrary value β^* can be calculated by using the following 't' value:

$$t_j = \frac{b_j - \beta^*}{se(b_j)} \qquad \textbf{(A3.7)}$$

The null hypothesis can be tested by setting β^* equal to zero to test for t_j having no significance in the regression model.

$$t_j = \frac{b_j}{se(b_j)} \qquad \textbf{(A3.8)}$$

The 't' value for each parameter can be calculated to give a relative significance value for each factor. These can then be compared to the value corresponding to the 95% confidence level.

A3.3. Presentation of results

The results from the regression analysis have been presented in graphical form. Three types of graph have been used. The first is a significance plot showing the factors in the regression model found to be significant with a confidence greater than 95%. The influence of each factor is given in terms of standardised t value calculated from Equation (A3.8). An example of a significance plot is shown in Figure A3.1.

The second type of graph shows results from the modelled response. The regression equation is used to plot a series of contour maps showing the effects of two of the variables while the others are set to their corresponding centre-point value (Figure A3.2)

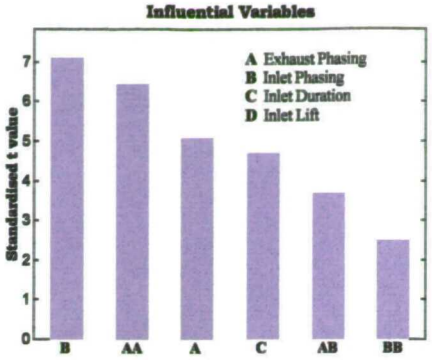

Figure A3.1
Example of a significance plot showing factors significant at greater than 95% confidence

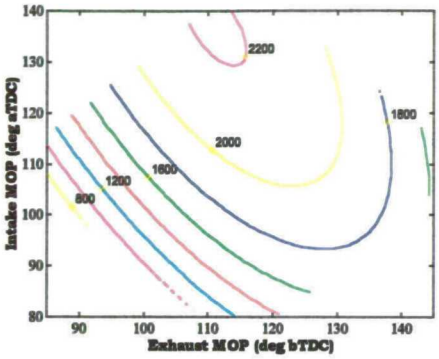

Figure A3.2
Example of a contour plot showing the modelled response as a function of two variables

The last type of graph is one showing the residuals produced from the regression analysis. Addition of error bars at the 95% confidence limits help to indicate any outliers (coloured red). Any trends in the residual plots indicate model inadequacy and the nature of such trends can help in judging the kind of abnormality present.

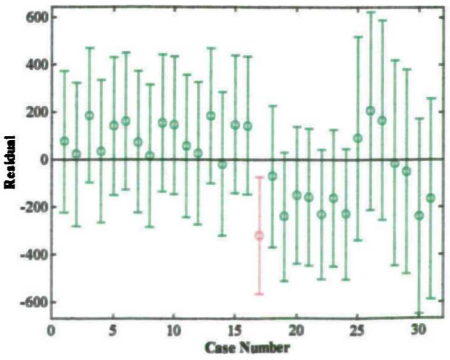

Figure A3.3
Example of a residual plot used for determining outliers and checking model adequacy

Appendix 4

LIST OF INSTRUMENTS

A4. List of Instruments

Instrument & Response Measured	Make	Model	Serial No.
Engine load dynamometer	Heenan & Froude	Dynamatic Mk I	80-242
Cylinder pressure transducer	Kistler	6121	497023
Osilloscope for logging cylinder pressure, and crank angle	Nicolet	4094	85BO1332
Heated chemiluminescence analyser for NOx measurements	Signal Instruments	4000VM	13108
Heated flame ionisation detector for hydrocarbon measurements	Signal Instruments	3000HM	13726
Non-dispersive infra-red analyser for CO and HC measurements	Horiba	Mexa-321E	E40489
Fuel flow meter	AVL	730	987
Plenum pressure transducer	Druck	PDCR910	1979901
Barometric pressure	Prosser	N/A	21064

Appendix 5

RESULTS SUMMARY SHEETS FOR PHASE 1 ENGINE TESTS

List of Result Summary Sheets

NOx Emissions at idle (ignoring lift)
Values in ppm

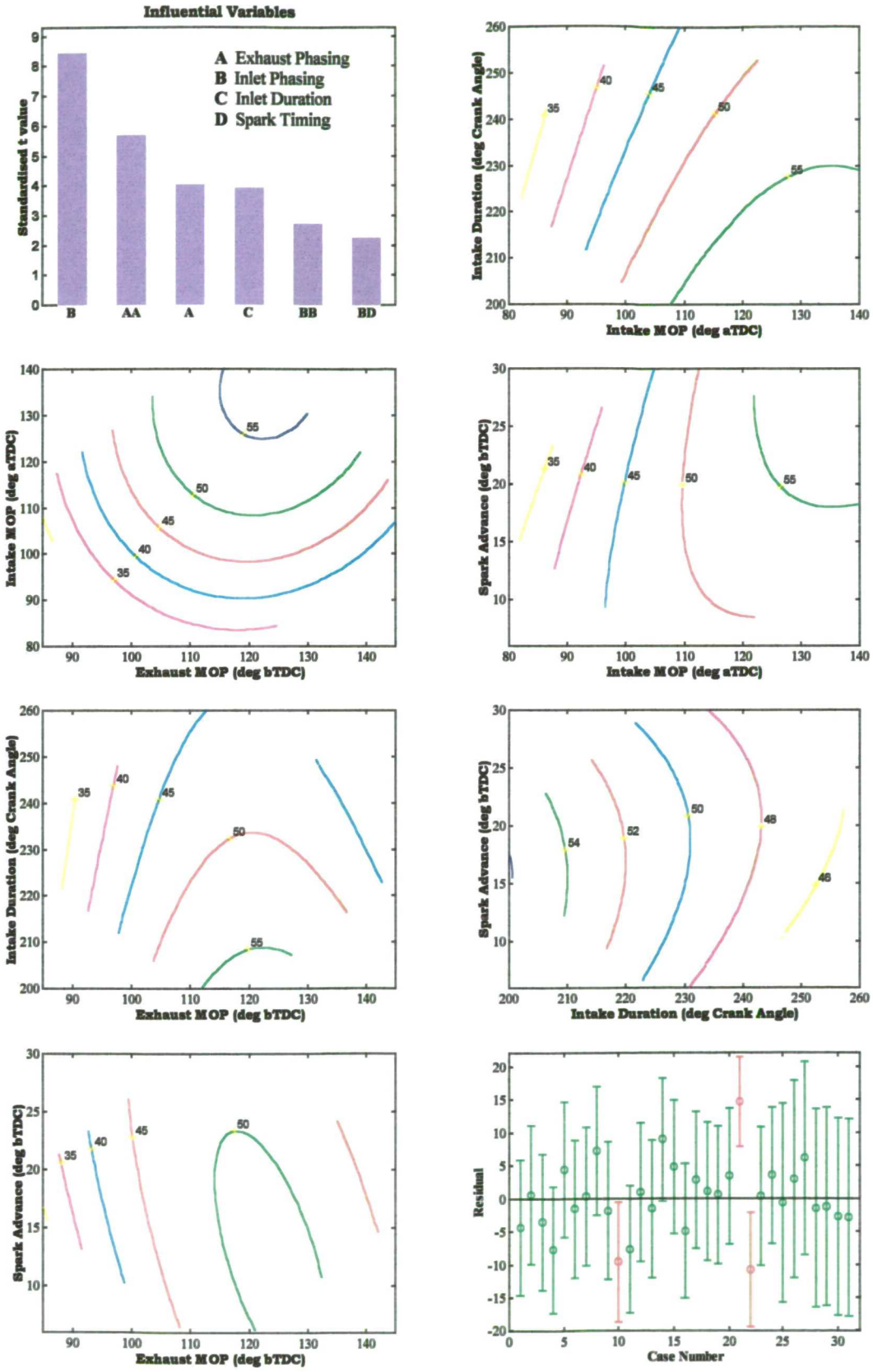

NOx Emissions at 1000 rev/min, 1.0 bar BMEP
Values in ppm

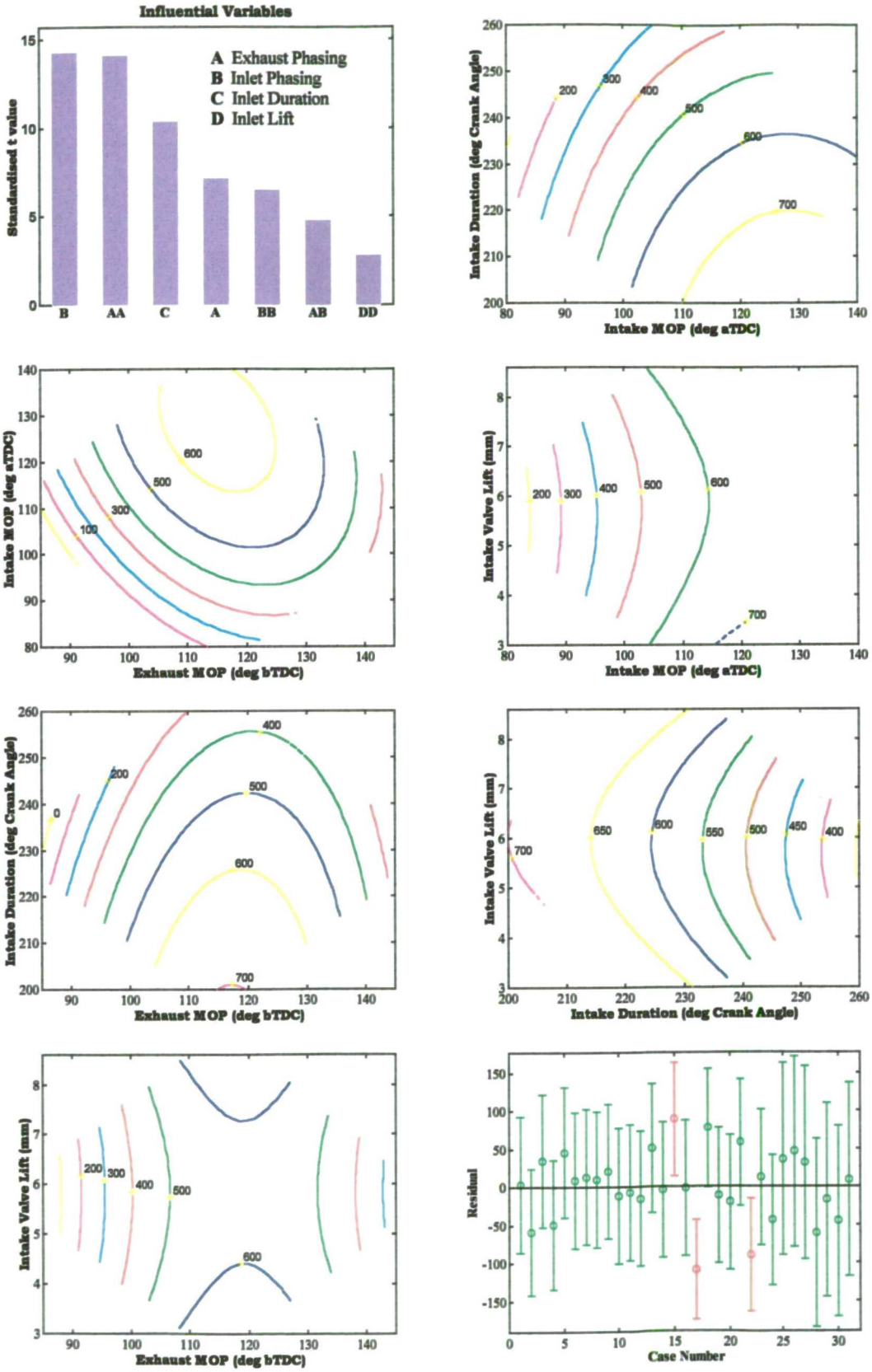

NOx Emissions at 1500 rev/min, 2.62 bar BMEP
Values in ppm

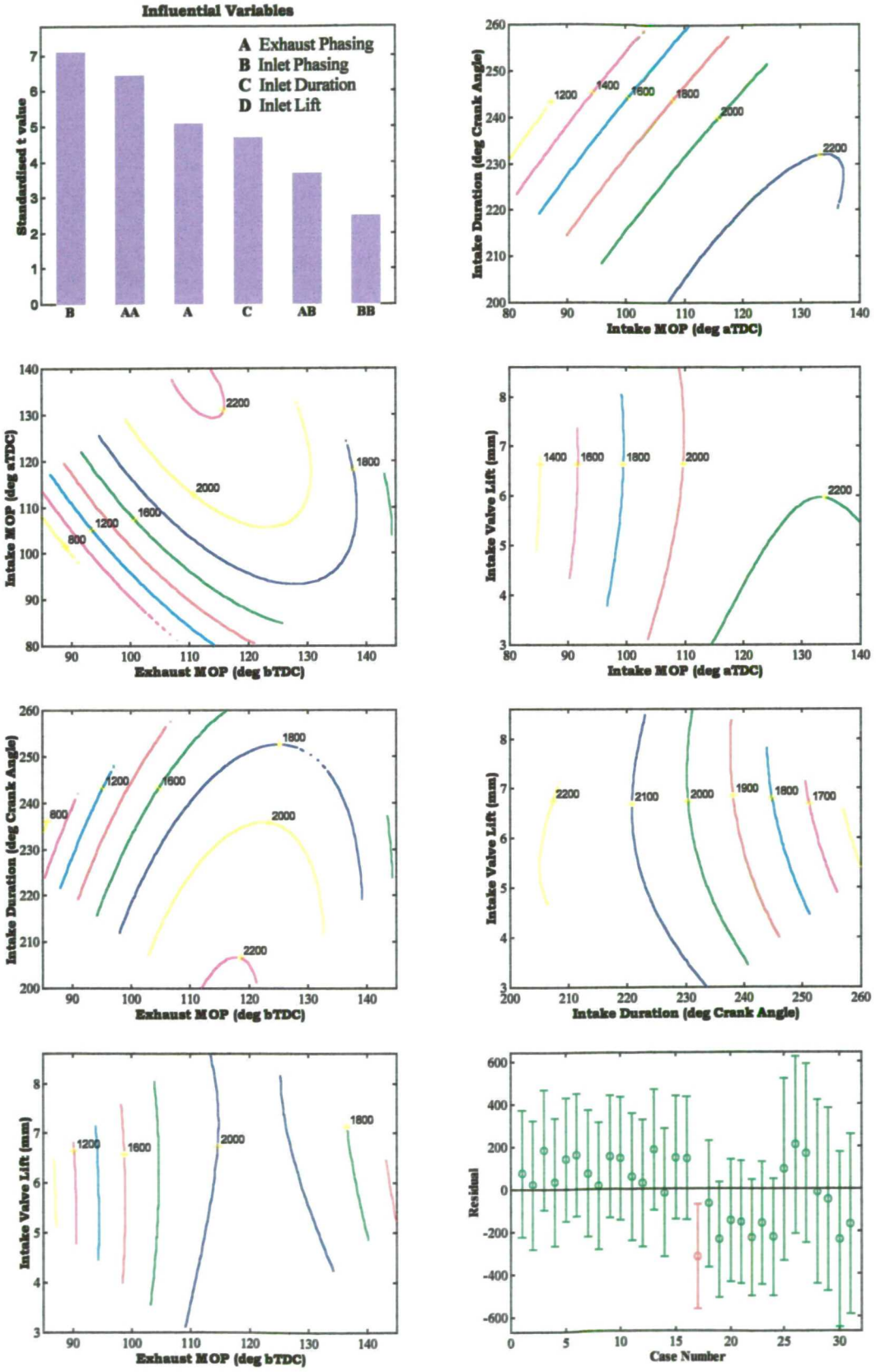

NOx Emissions at 2500 rev/min, 5.5 bar BMEP
Values in ppm

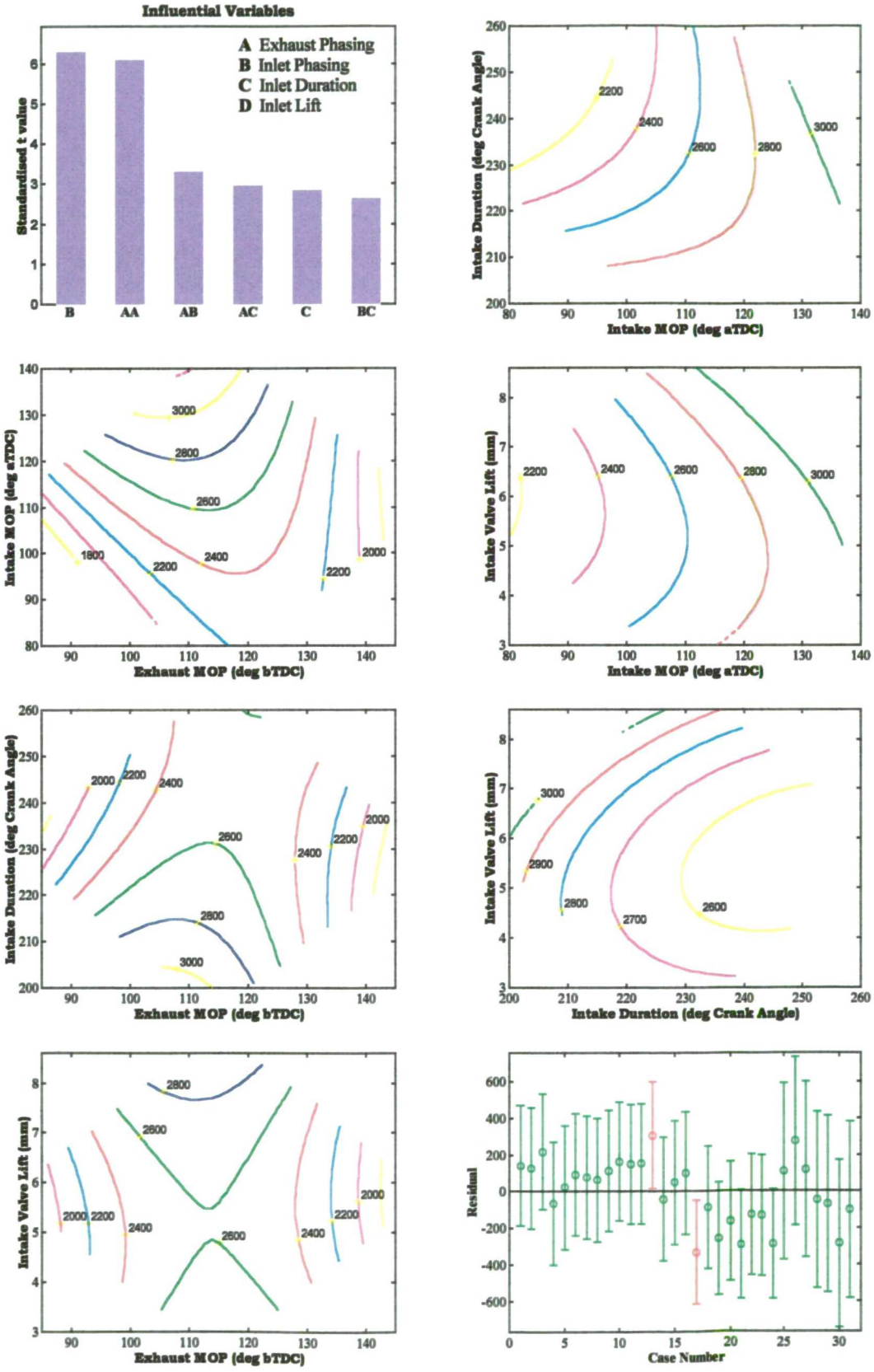

HC Emissions at idle (ignoring lift)
Values in ppm

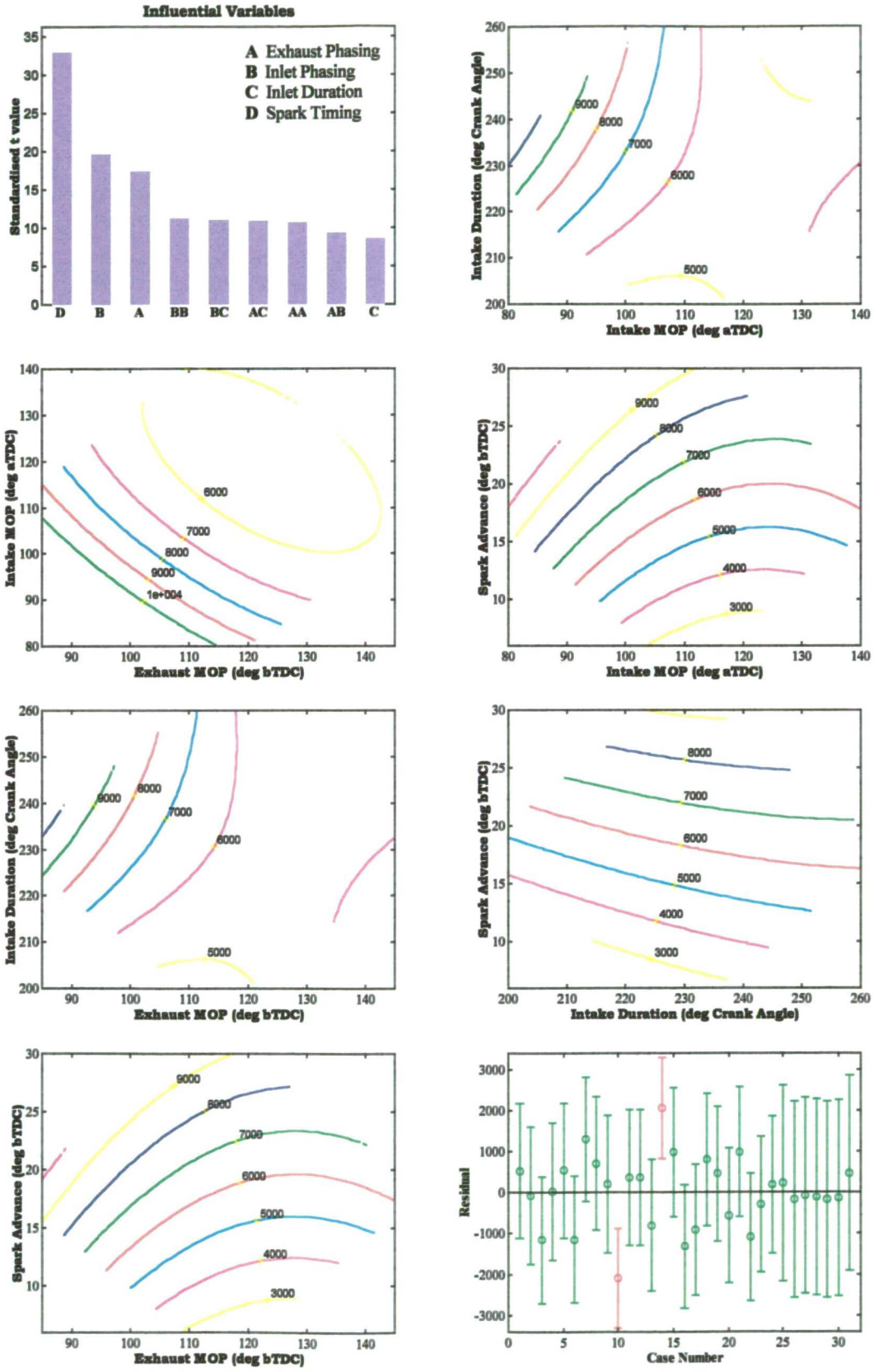

HC Emissions at 1000 rev/min, 1.0 bar BMEP
Values in ppm

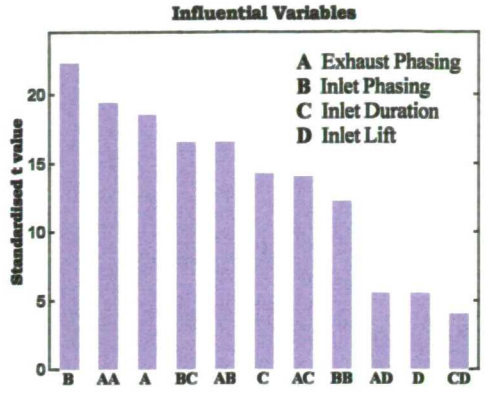

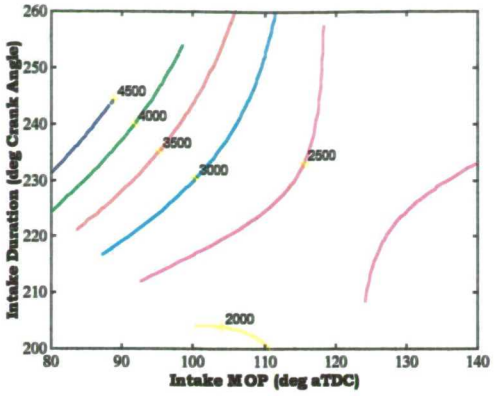

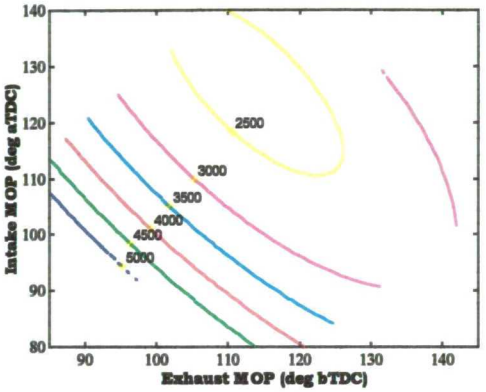

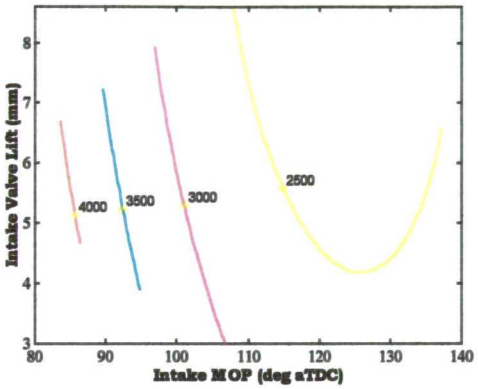

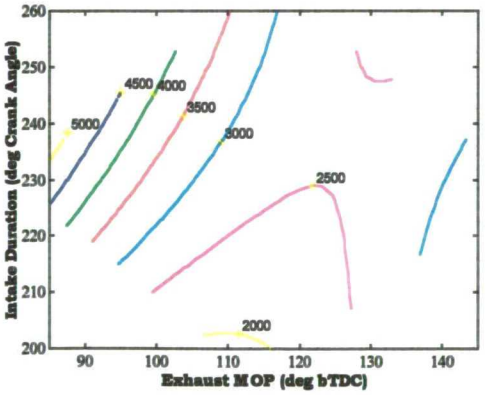

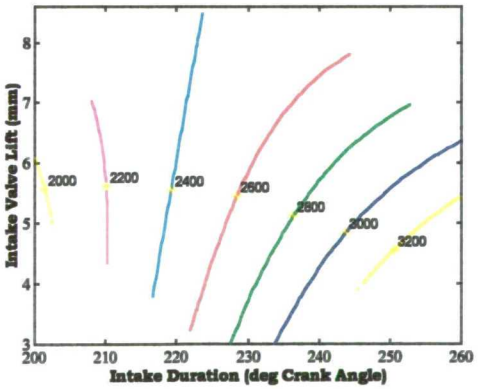

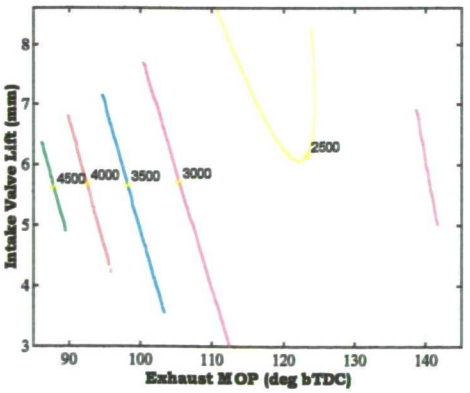

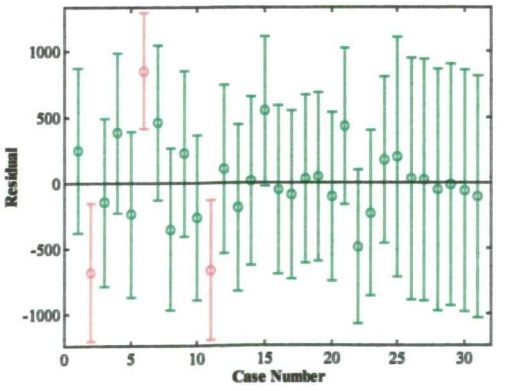

HC Emissions at 1500 rev/min, 2.62 bar BMEP
Values in ppm

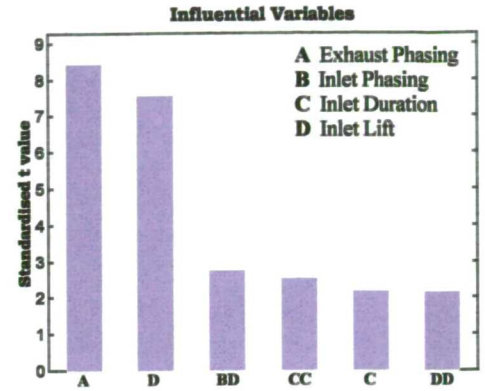

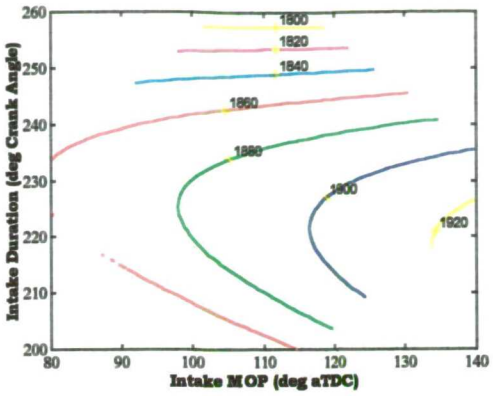

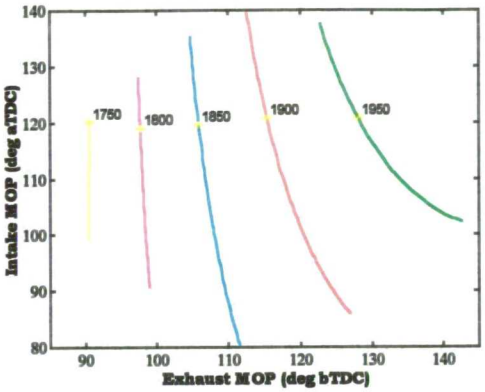

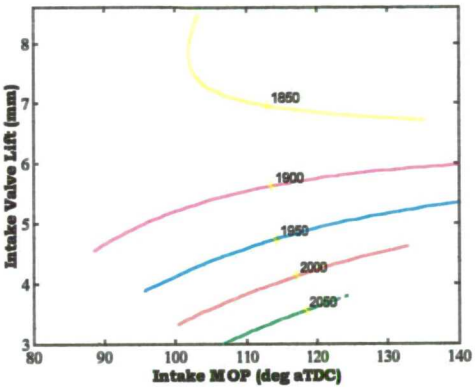

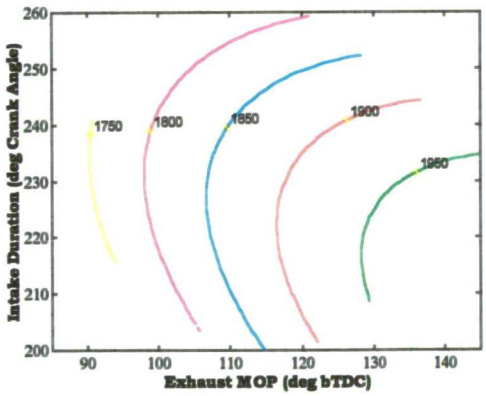

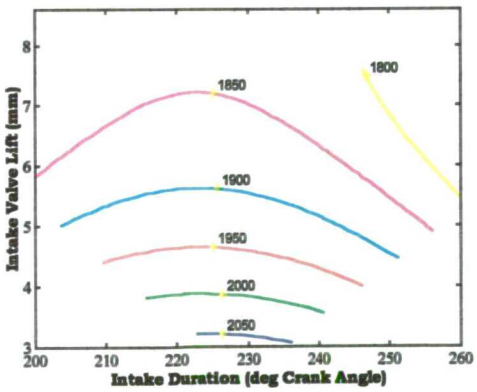

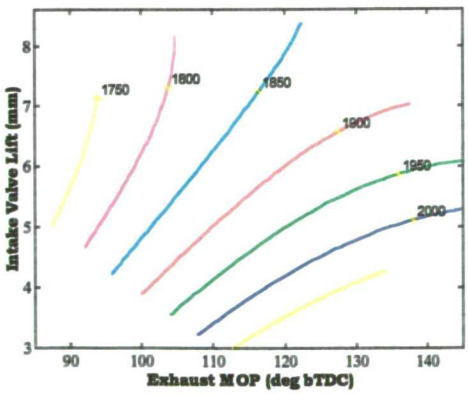

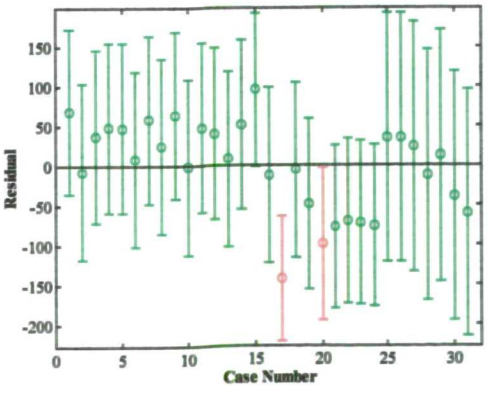

HC Emissions at 2500 rev/min, 5.5 bar BMEP
Values in ppm

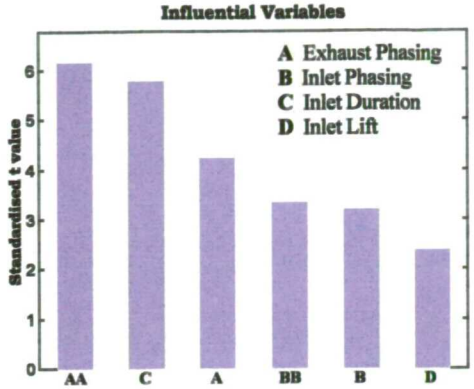

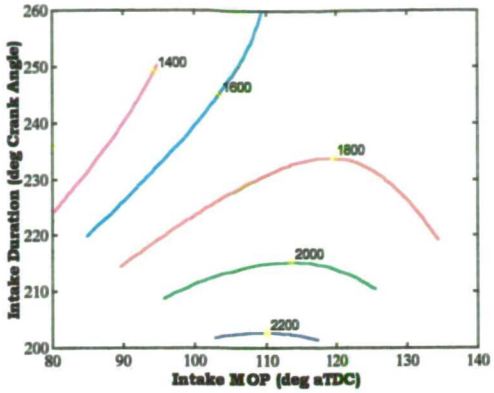

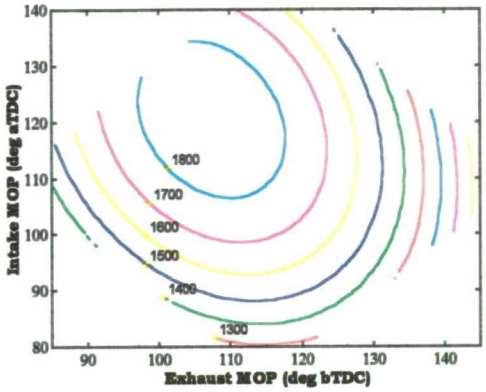

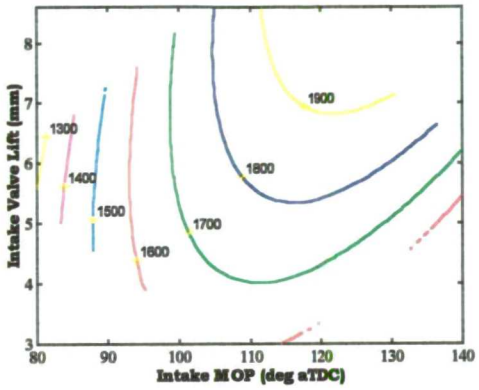

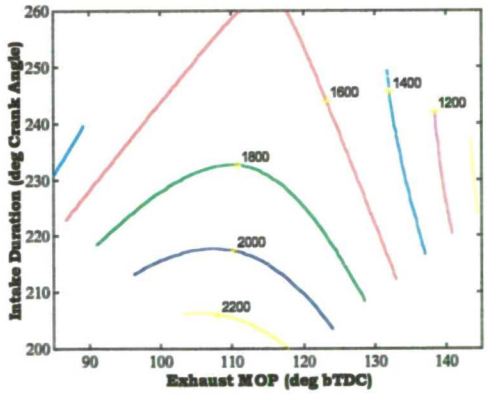

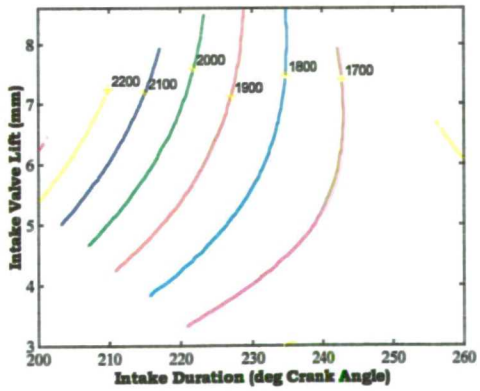

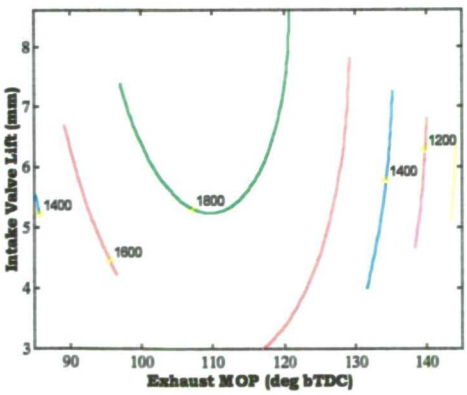

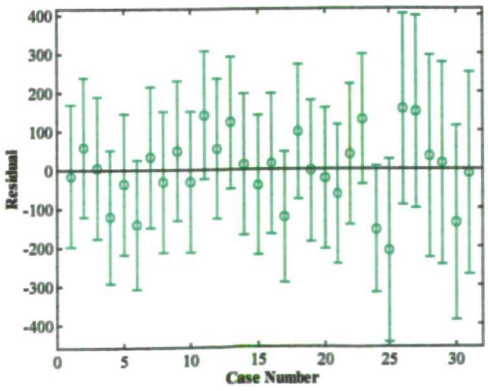

Fuel Consumption at Idle
Values in g/min

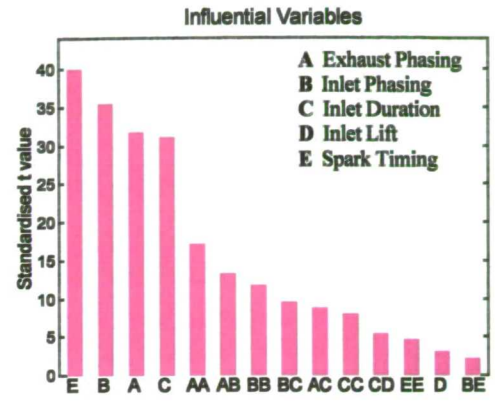

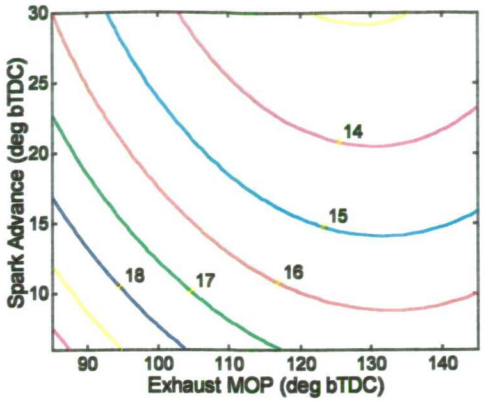

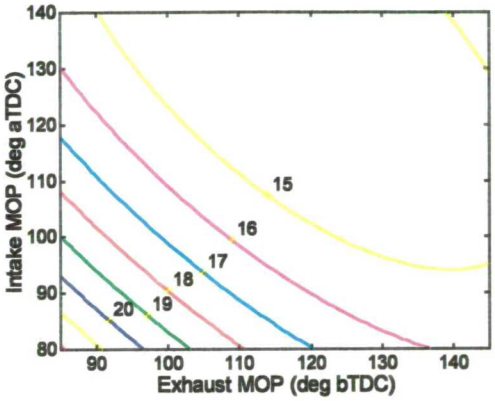

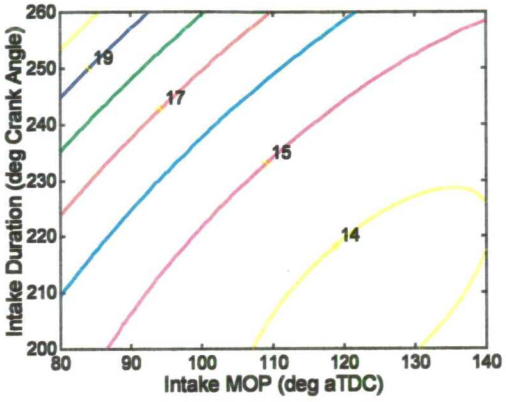

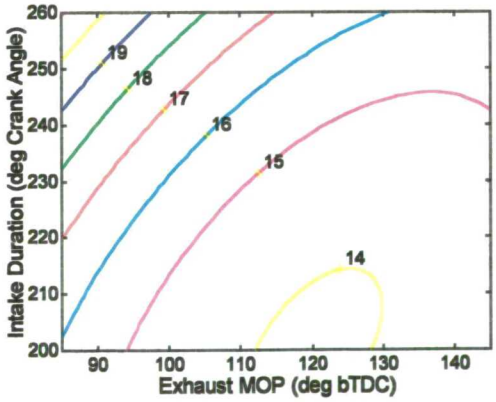

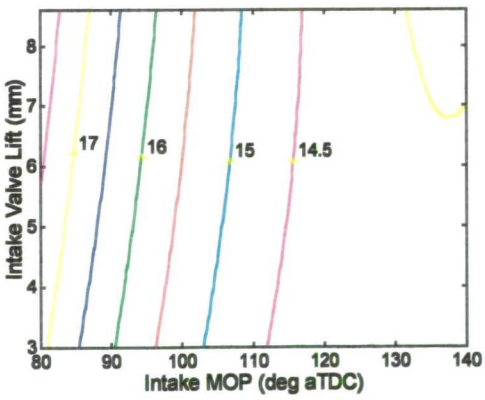

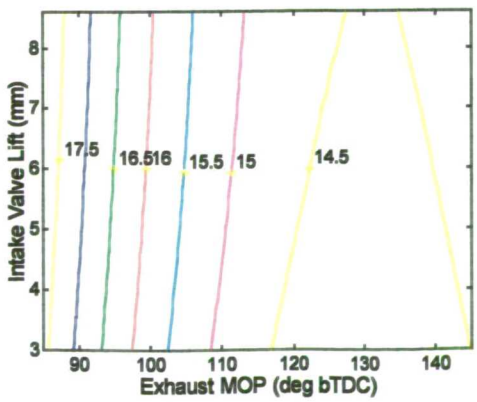

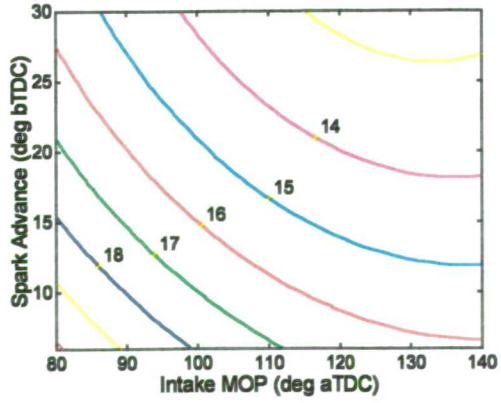

Fuel Consumption at Idle
Values in g/min

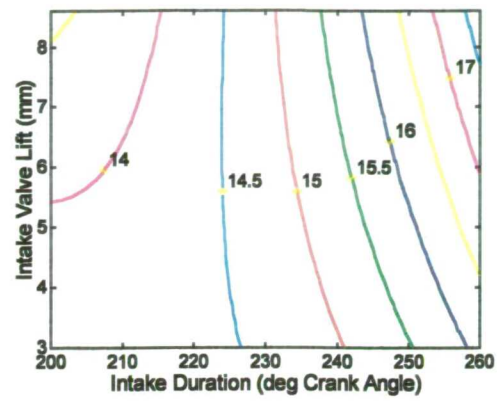

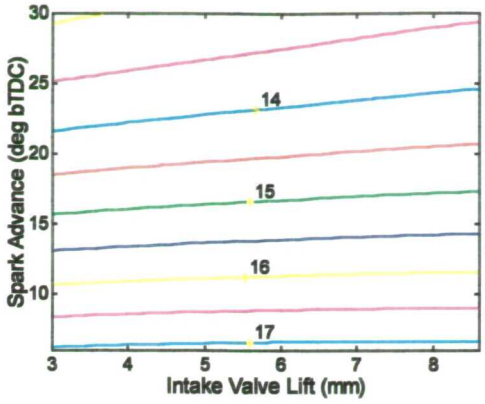

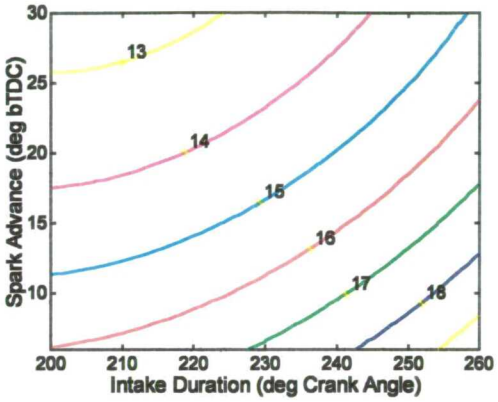

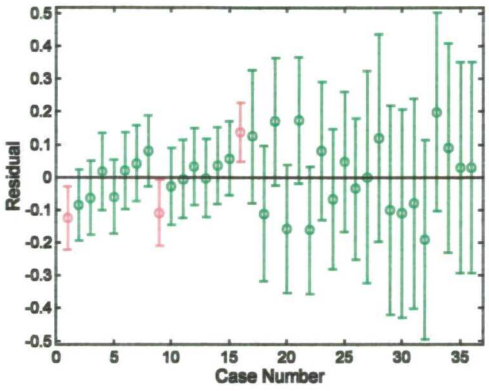

BSFC at 1000 rev/min, 1.0 bar BMEP
Values in g/kWh

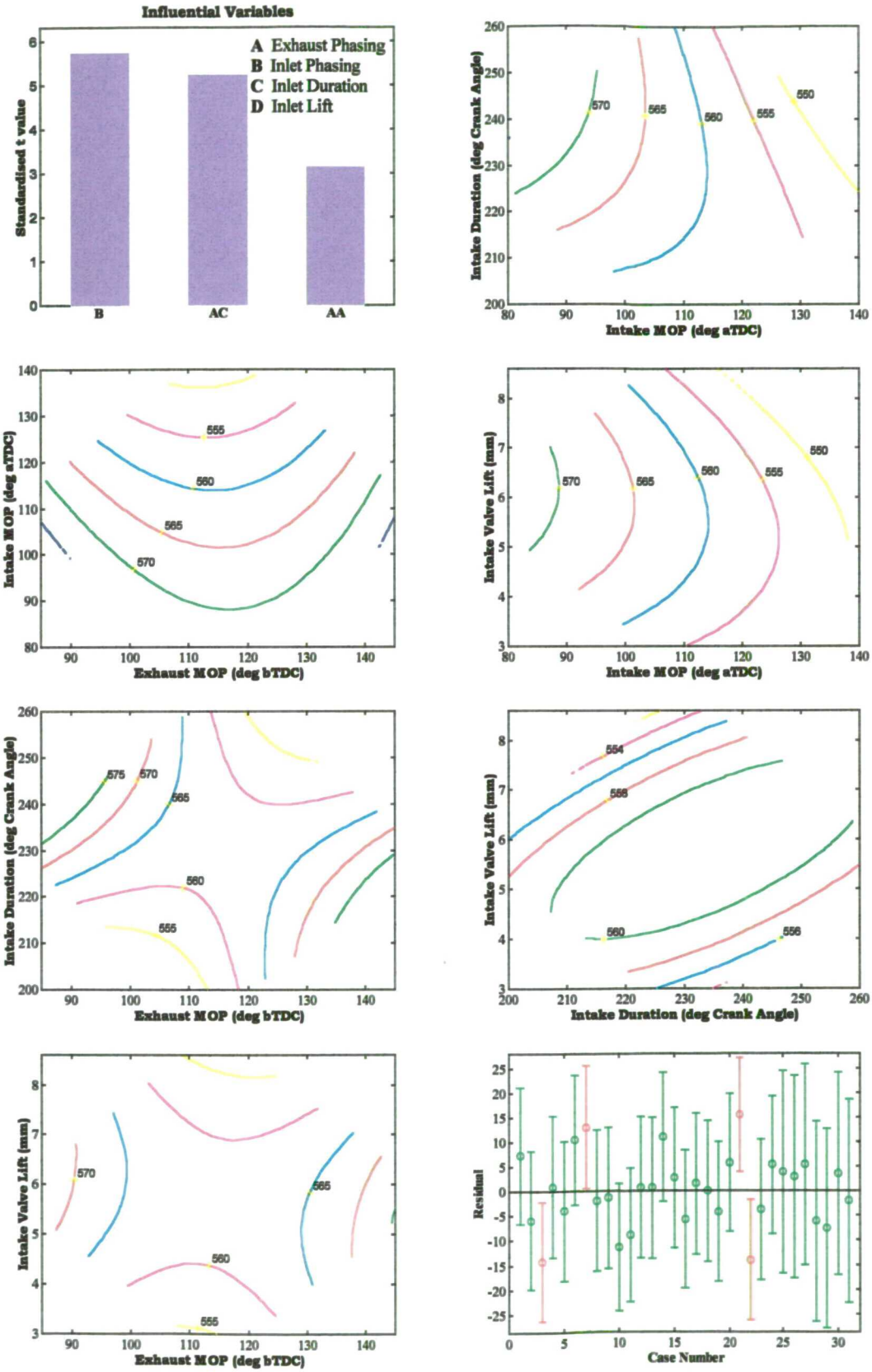

BSFC at 1500 rev/min, 2.62 bar BMEP
Values in g/kWh

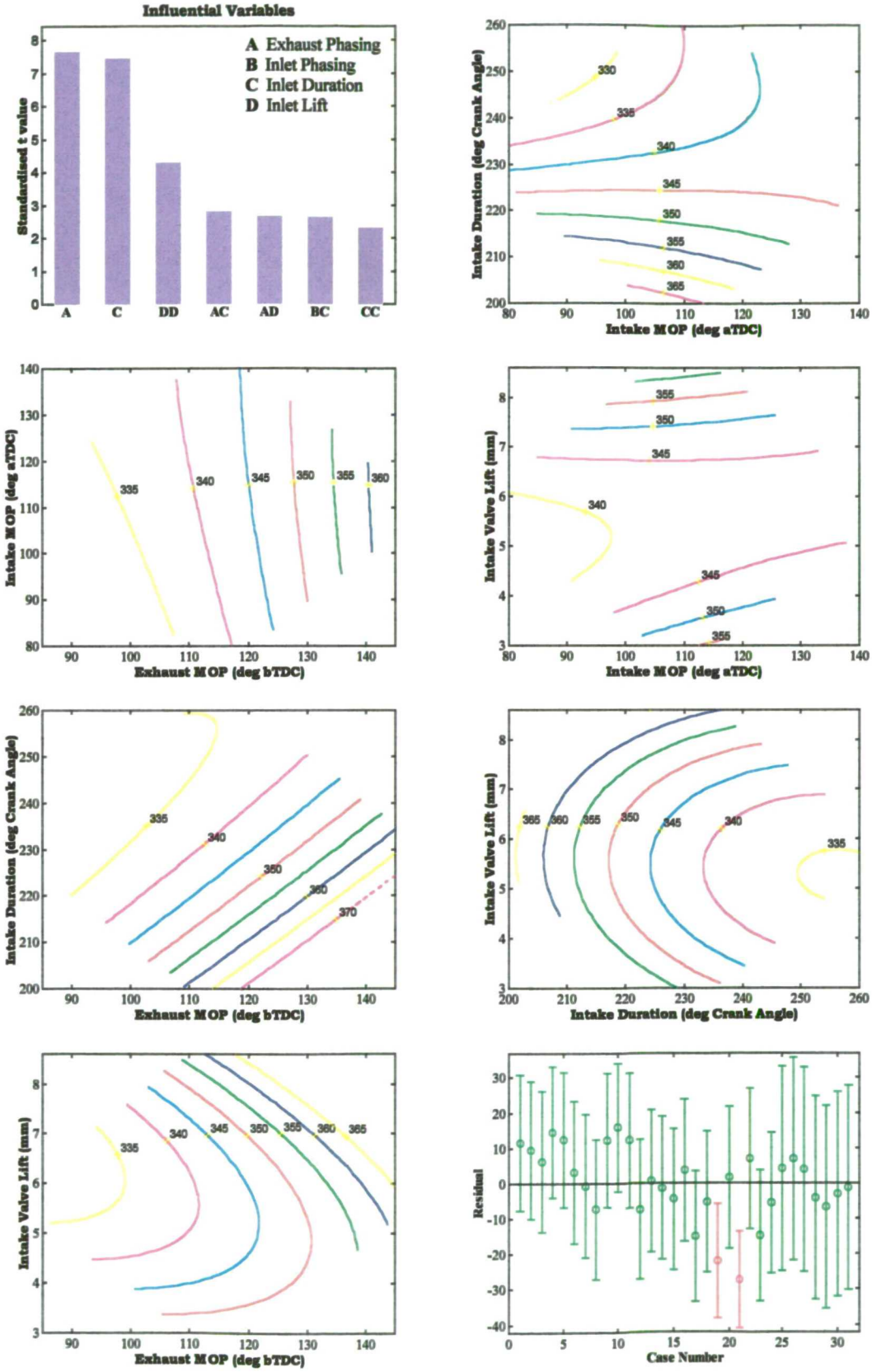

BSFC at 2500 rev/min, 5.5 bar BMEP
Values in g/kWh

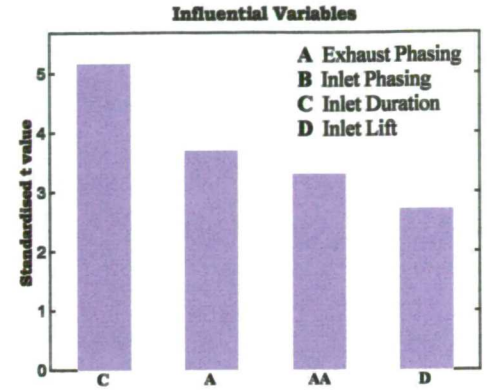

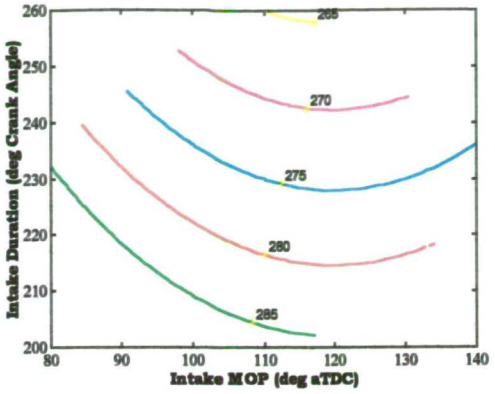

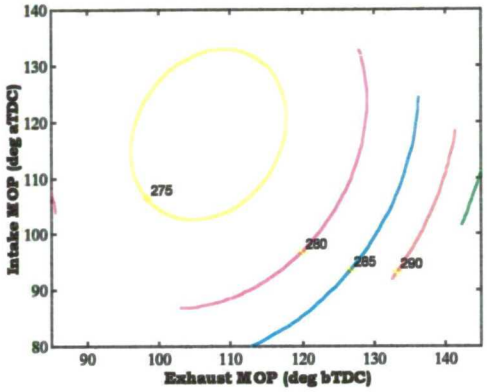

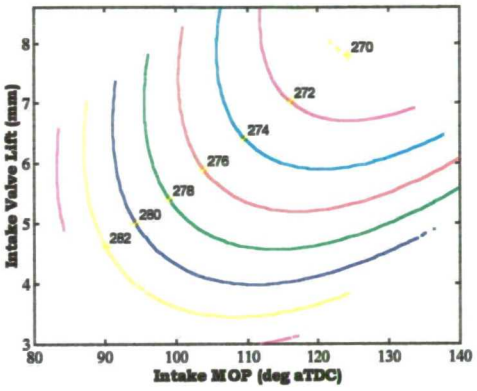

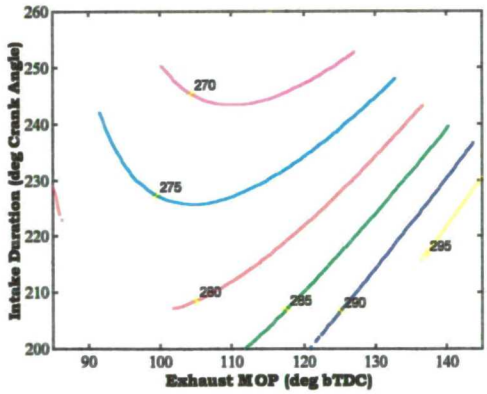

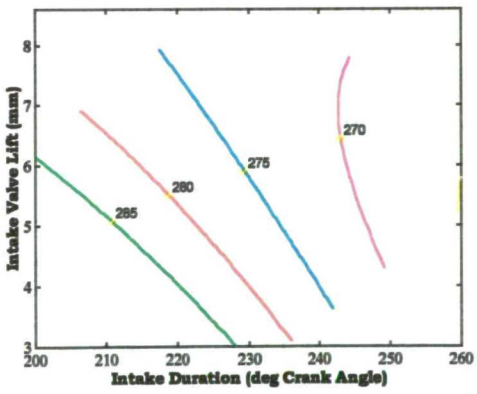

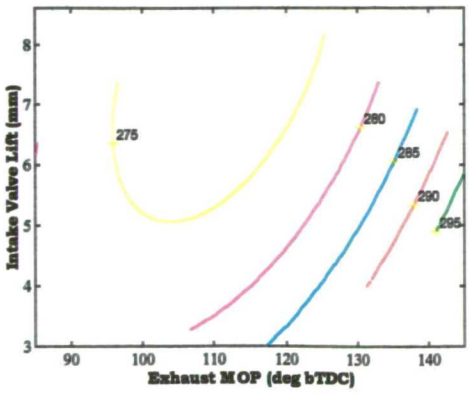

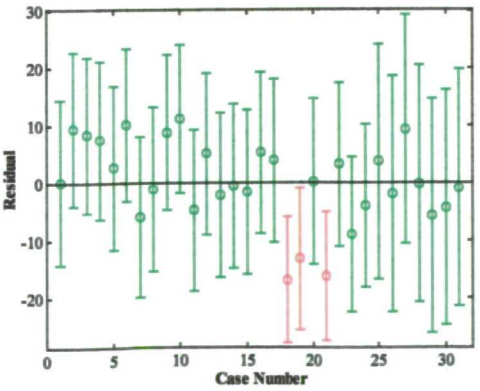

Exhaust Gas Temperature at Idle (Ignoring Lift)
Values in °C

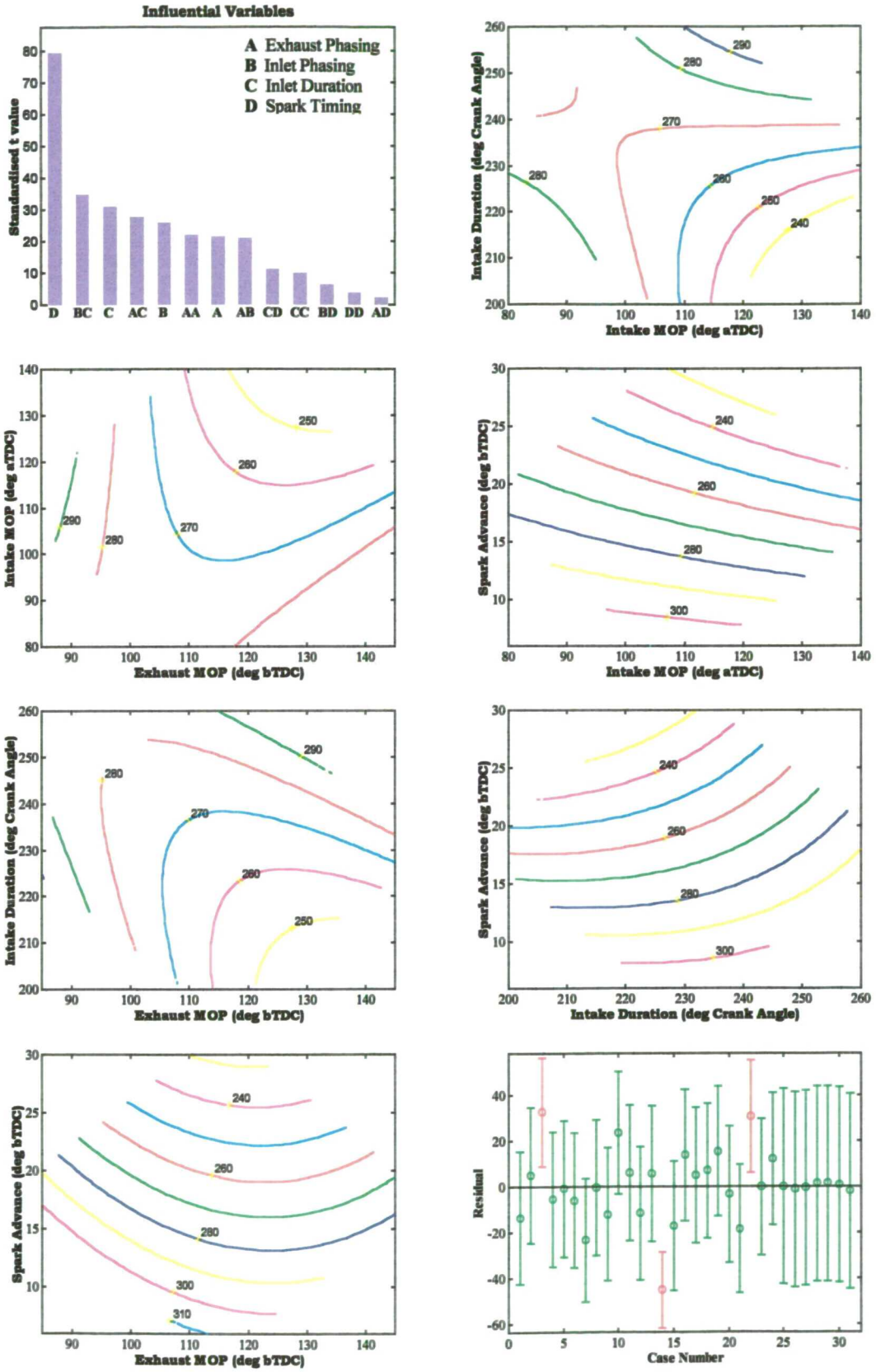

Exhaust Gas Temperature at 1000 rev/min, 1.0 bar BMEP
Values in °C

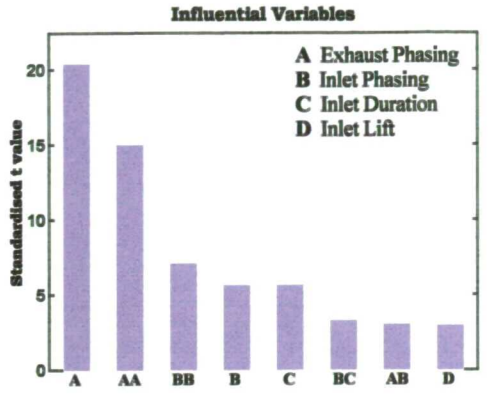

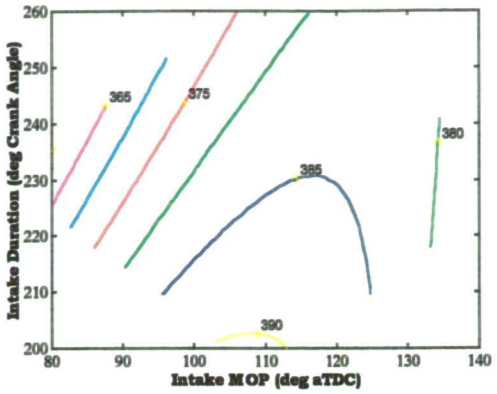

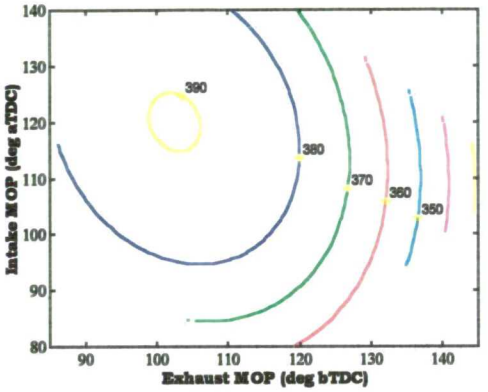

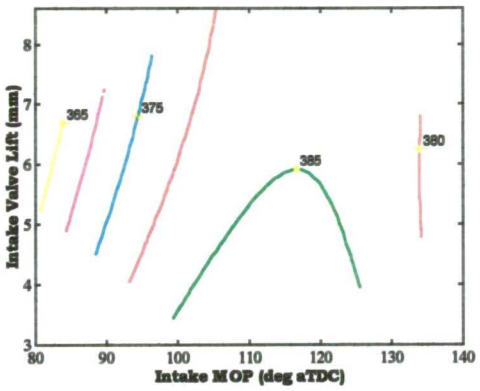

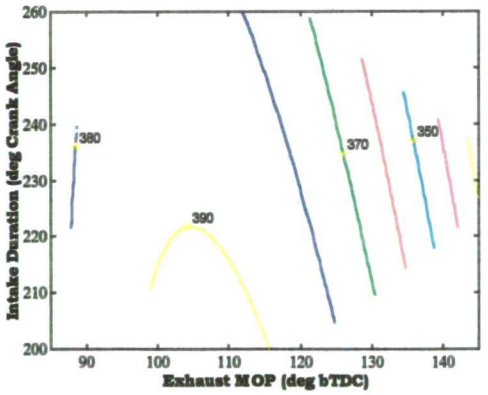

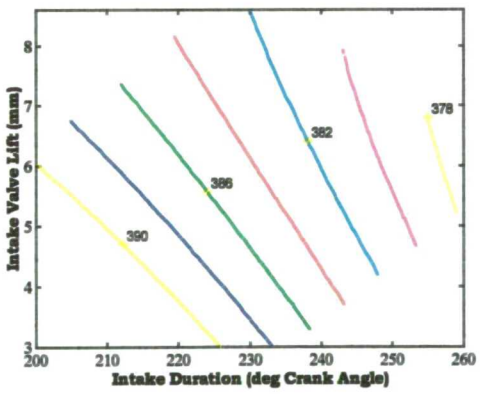

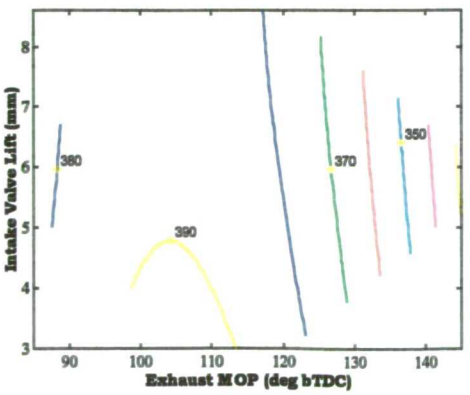

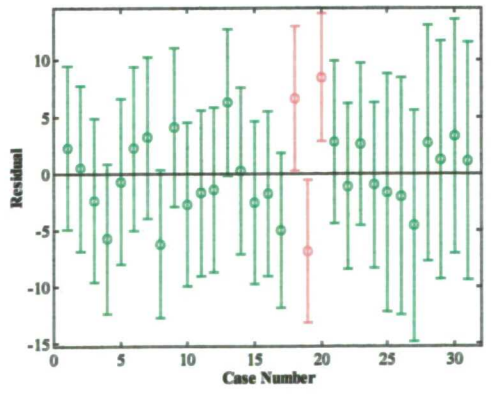

Exhaust Gas Temperature at 1500 rev/min, 2.62 bar BMEP
Values in °C

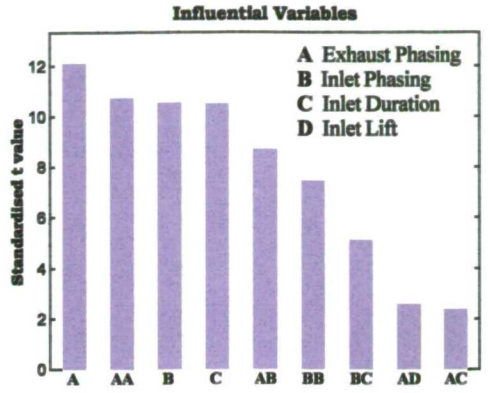

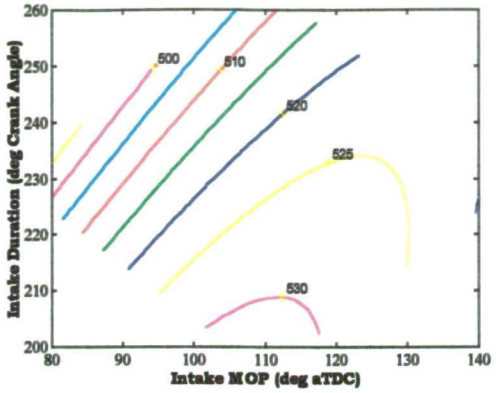

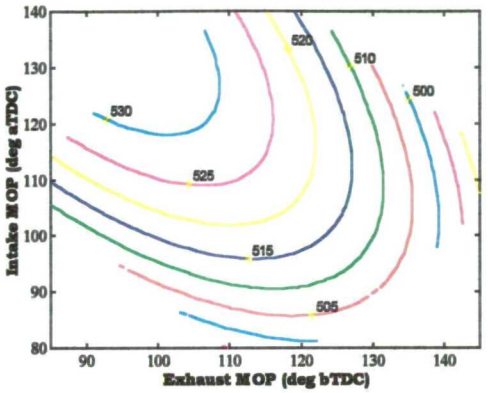

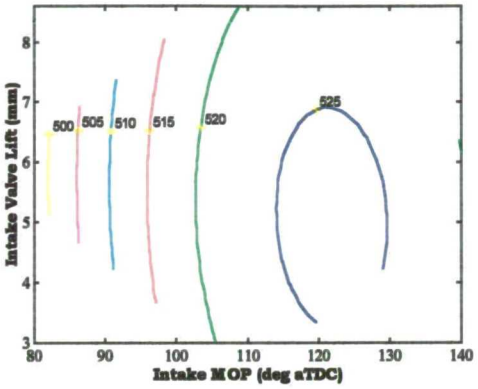

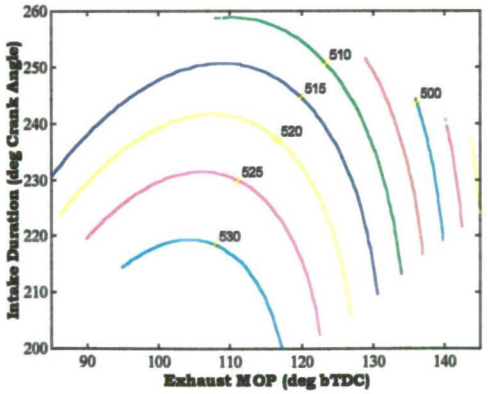

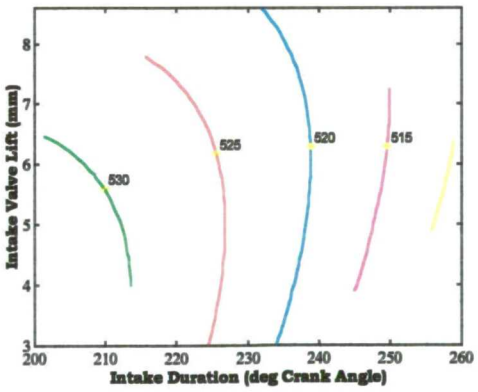

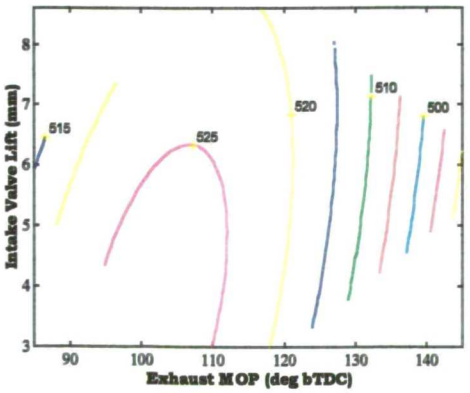

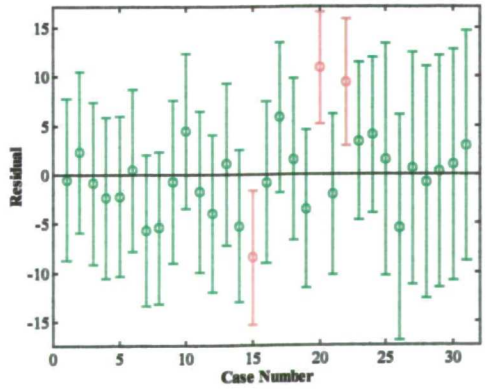

Exhaust Gas Temperature at 2500 rev/min, 5.5 bar BMEP
Values in °C

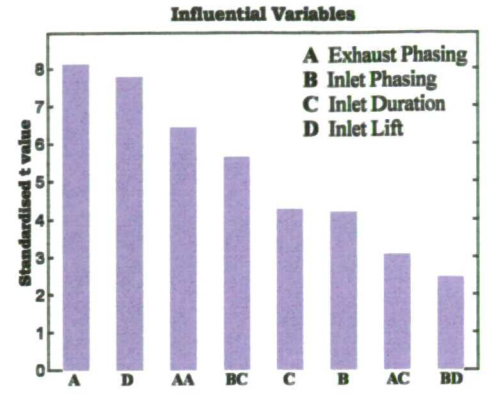

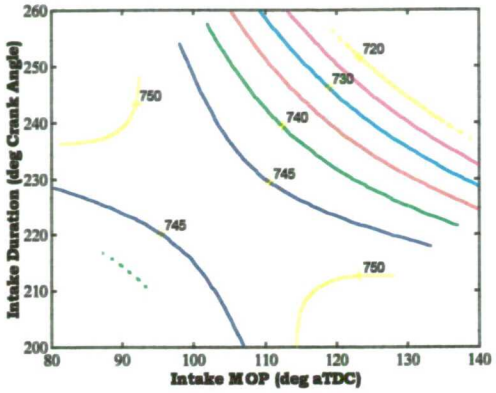

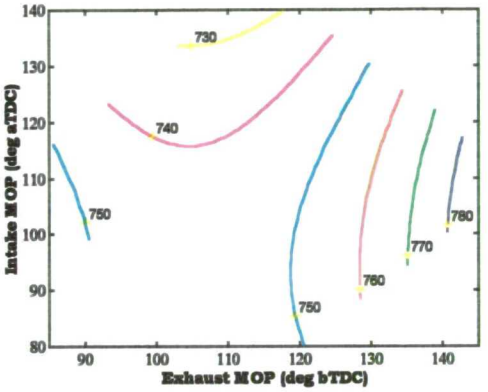

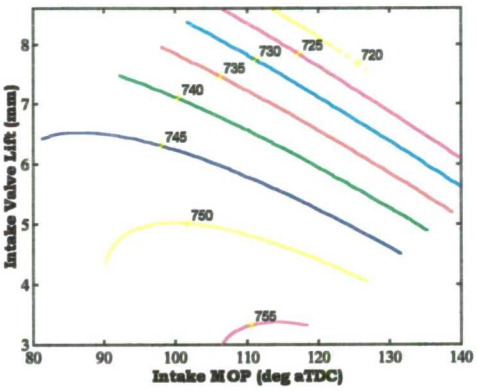

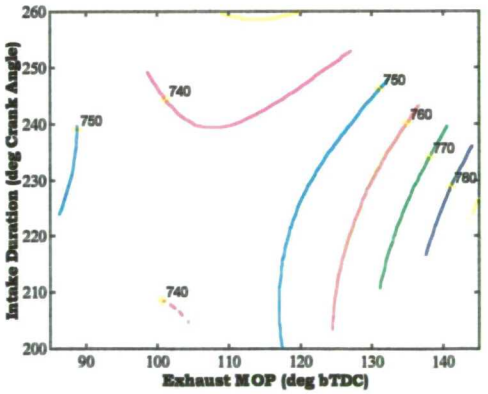

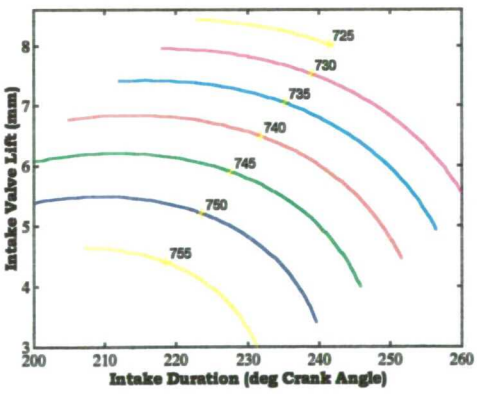

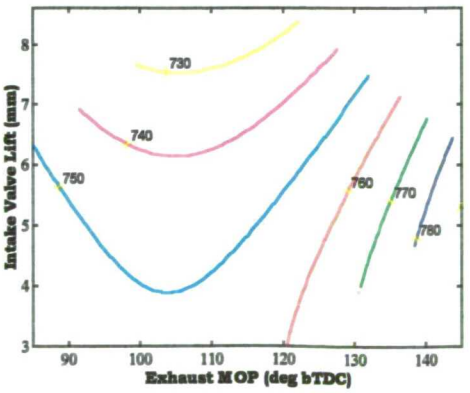

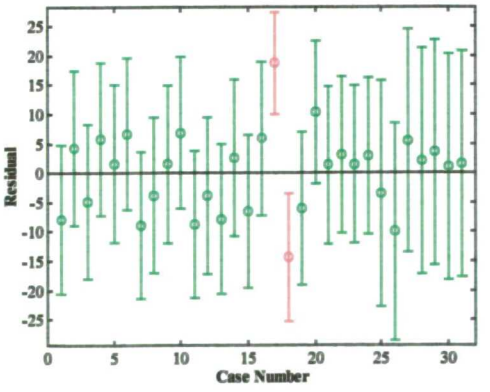

MBT-1% Spark Angle at 1000rpm, 1.0 bar BMEP
Values in °ca bTDC

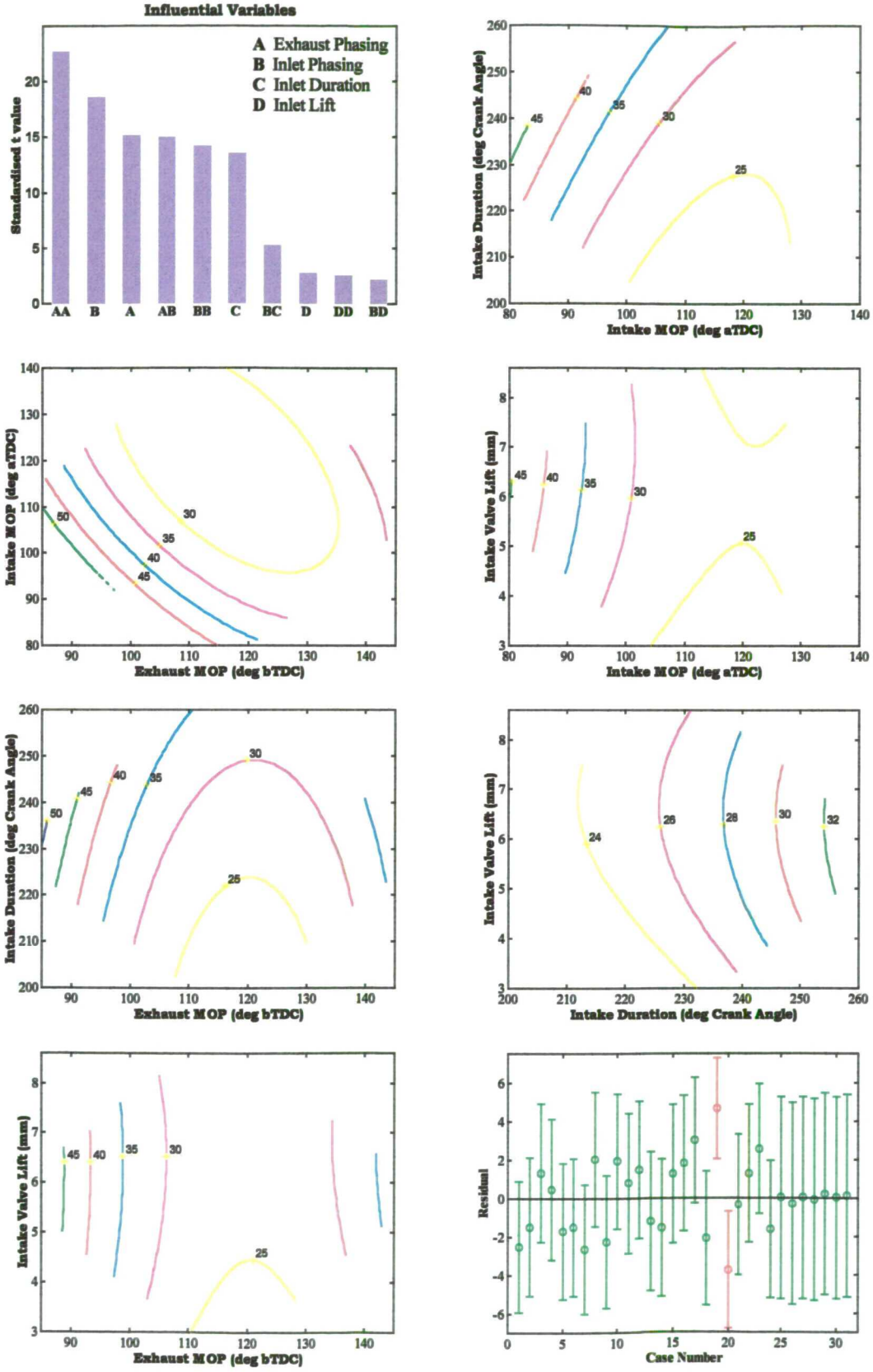

MBT-1% Spark Angle at 1500rpm, 2.62 bar BMEP
Values in °ca bTDC

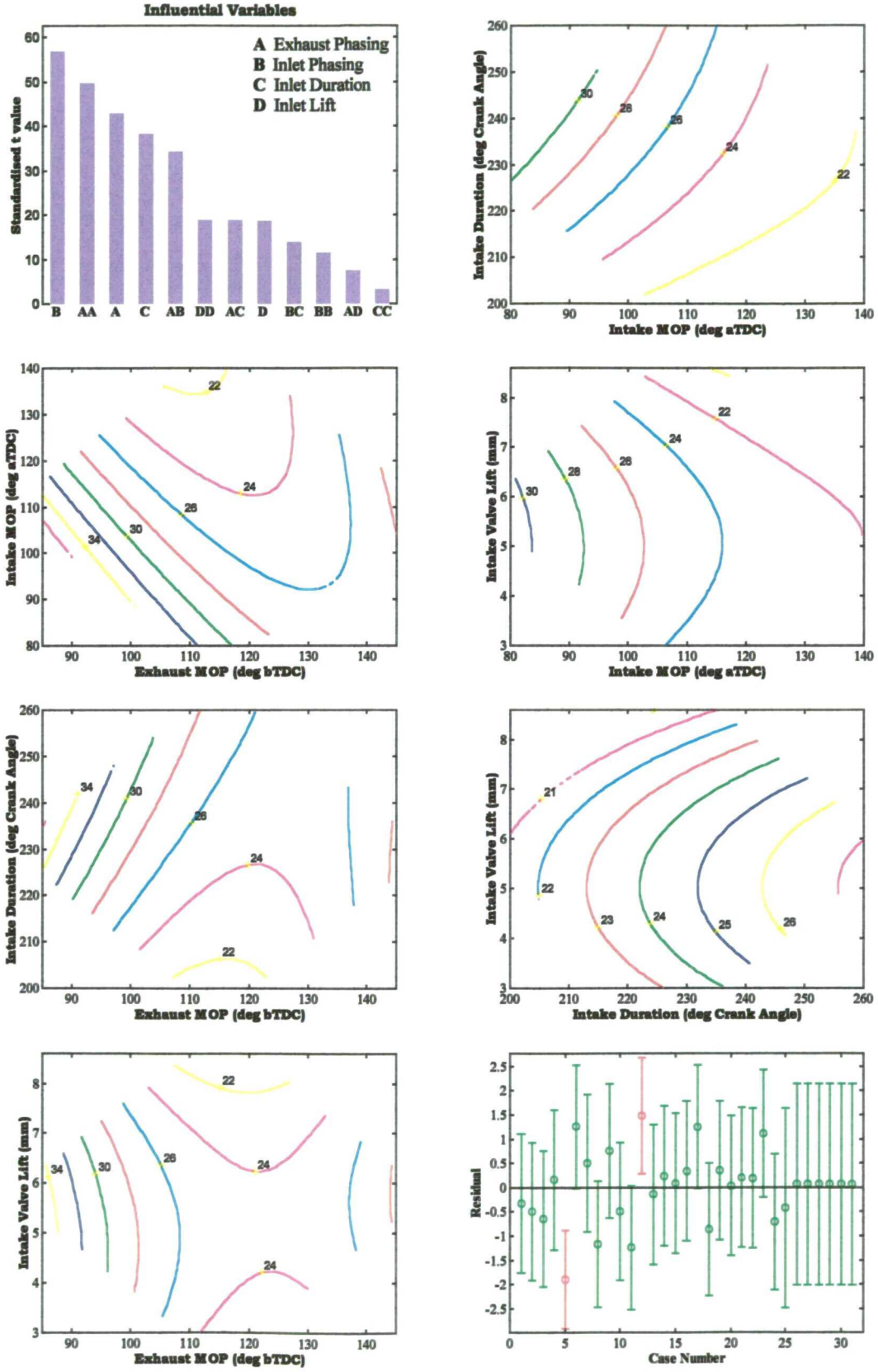

MBT-1% Spark Angle at 2500rpm, 5.5 bar BMEP
Values in °ca bTDC

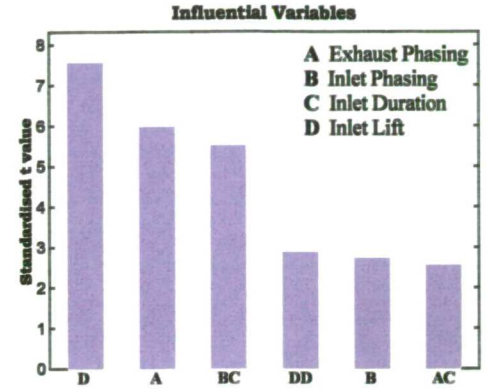

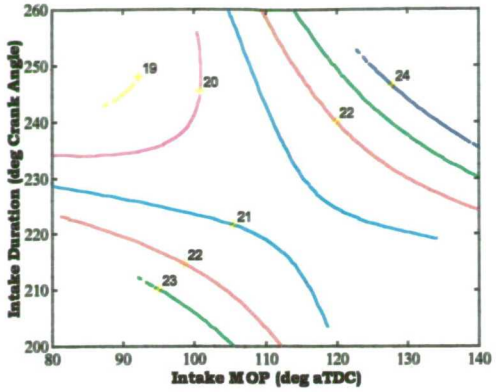

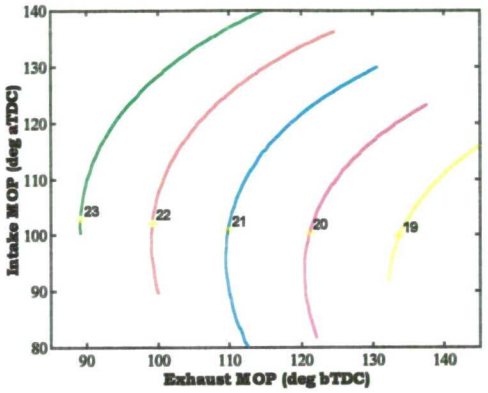

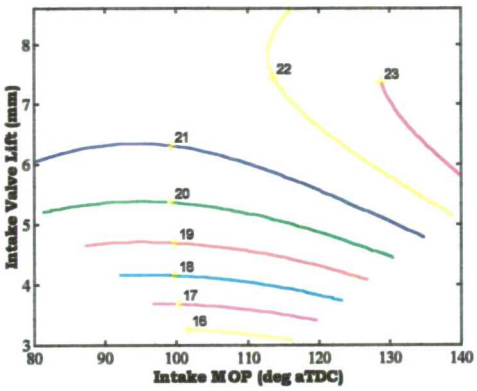

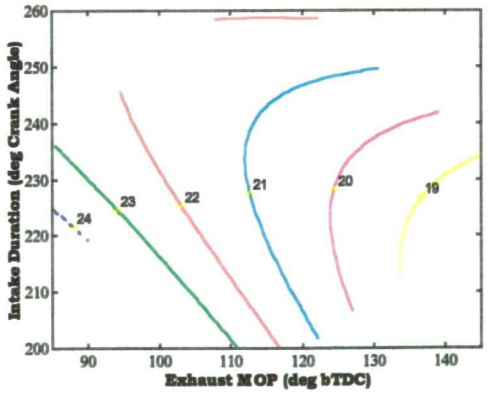

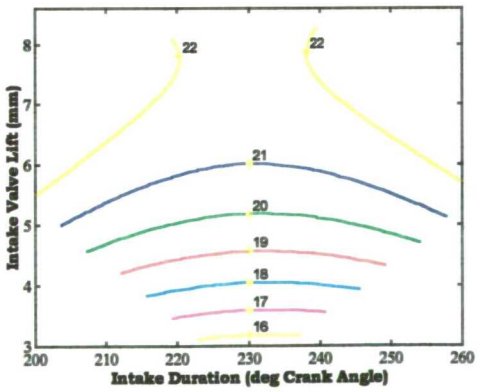

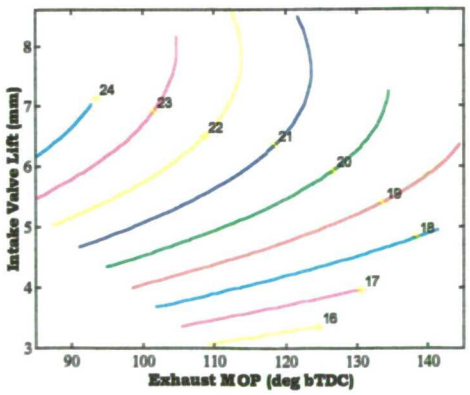

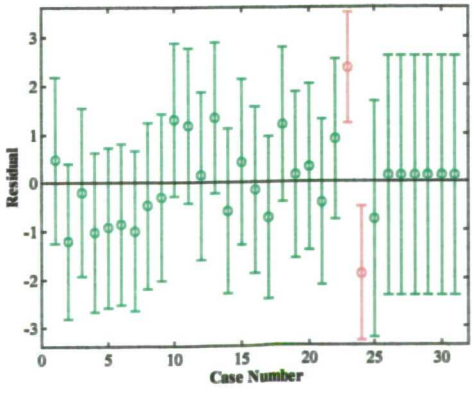

0 - 80% Burn Duration (From Spark Angle) at Idle
Values in °ca

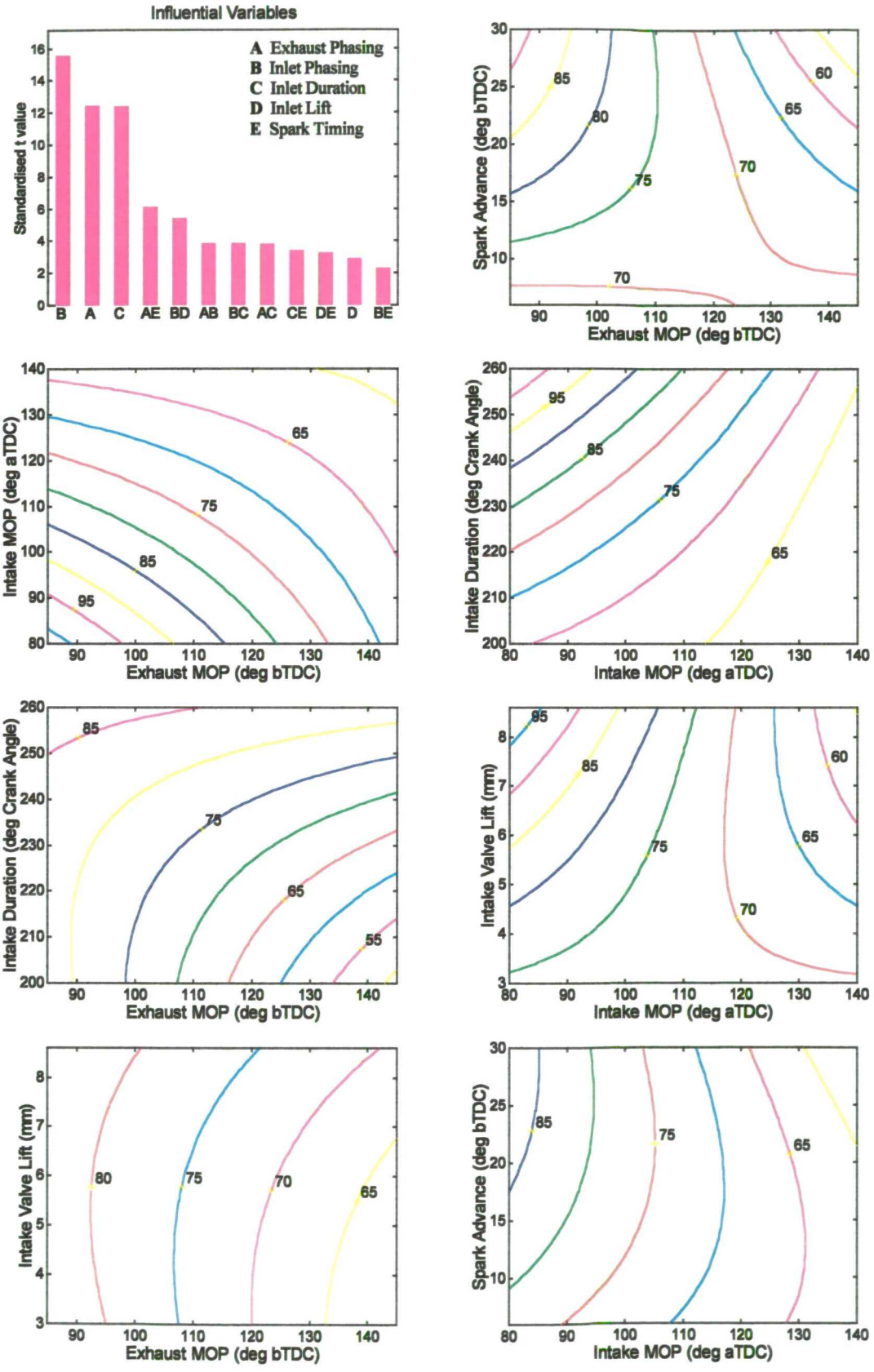

0 - 80% Burn Duration (from Spark Angle) at Idle
Values in °ca

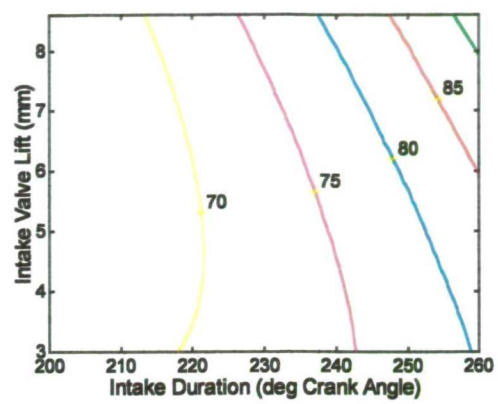

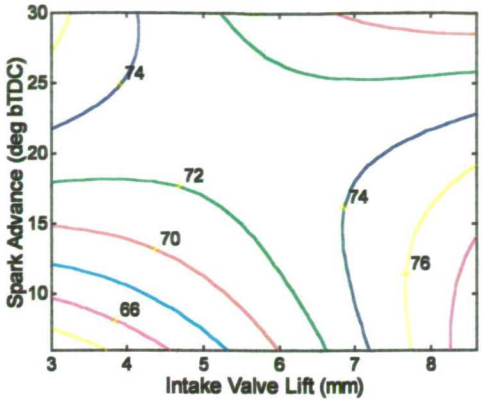

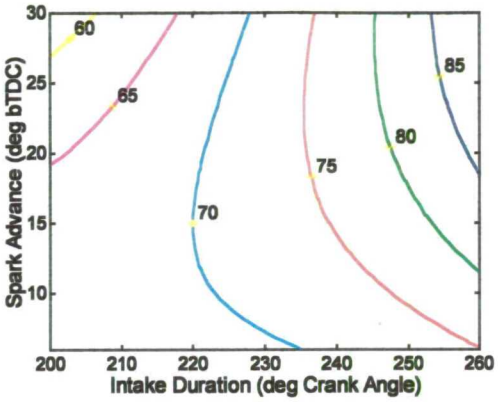

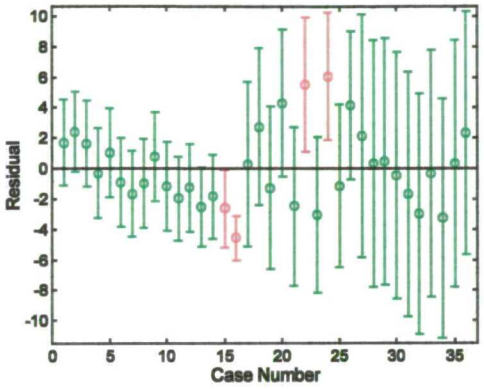

0 - 80% Burn Duration (from Spark Angle) at 1500rpm, 2.62 bar BMEP
Values in °ca

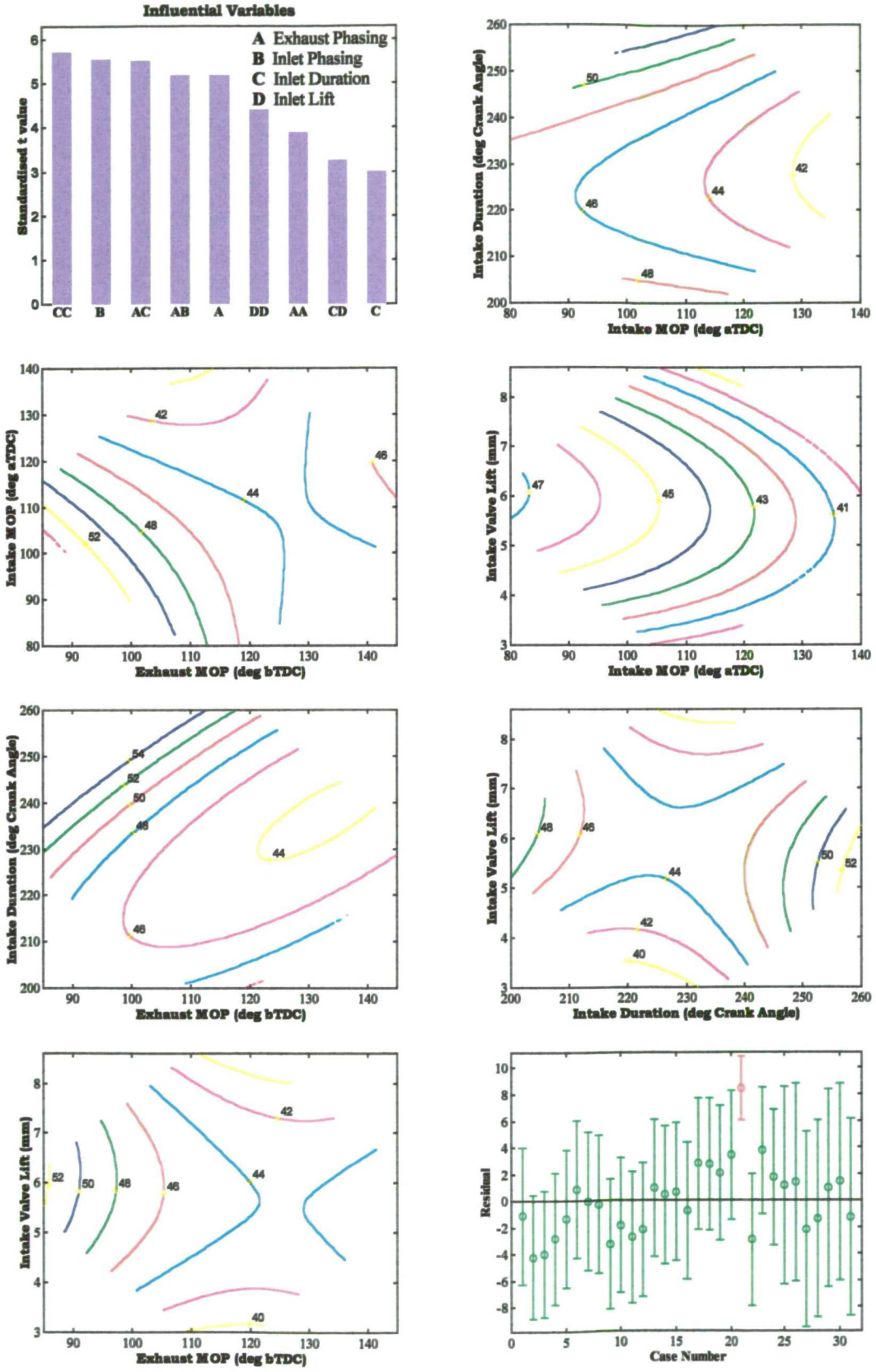

Appendix 6

RESULTS SUMMARY SHEETS FOR PHASE 2 ENGINE TESTS

List of Result Summary Sheets

NOx Emissions at idle
Values in ppm

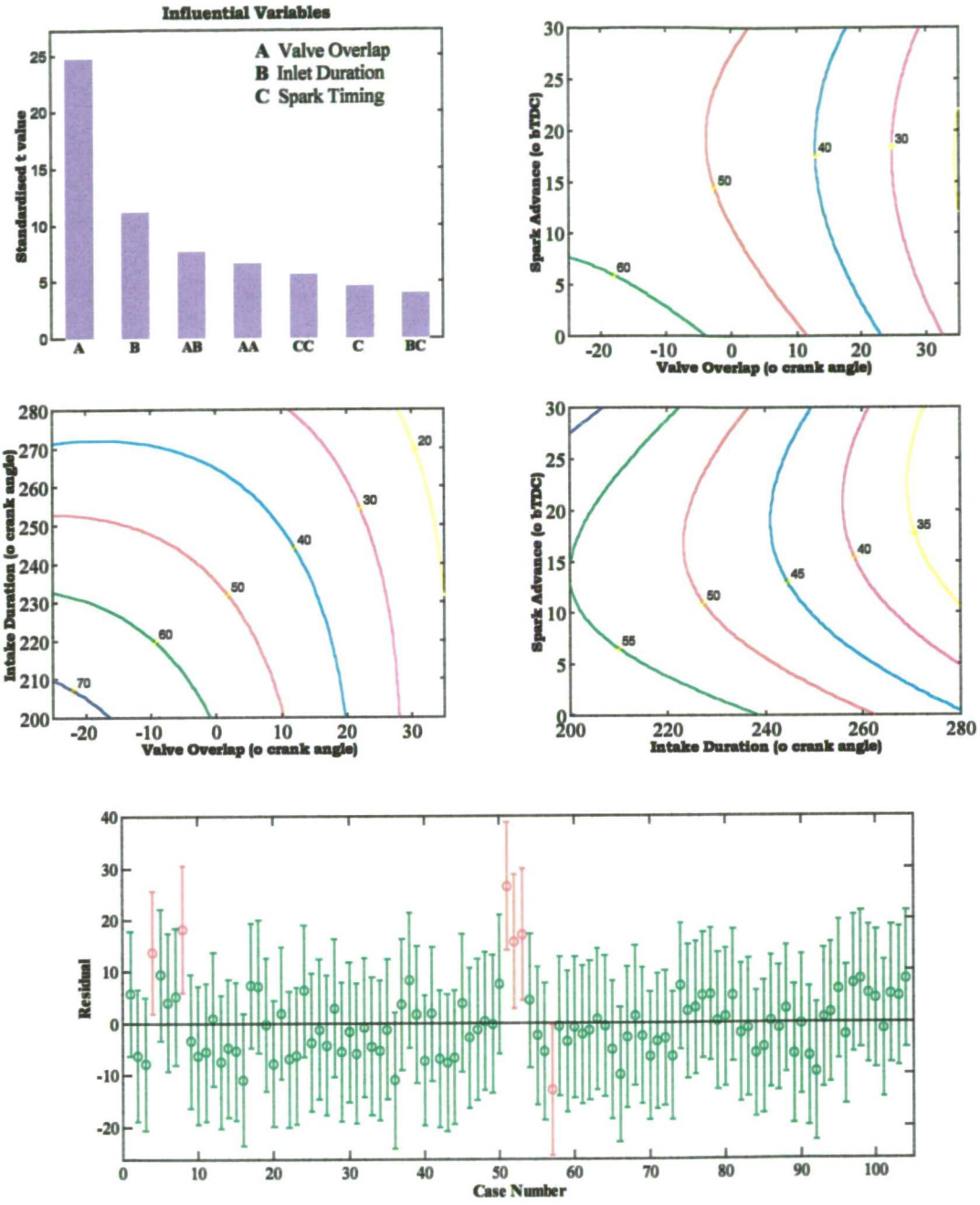

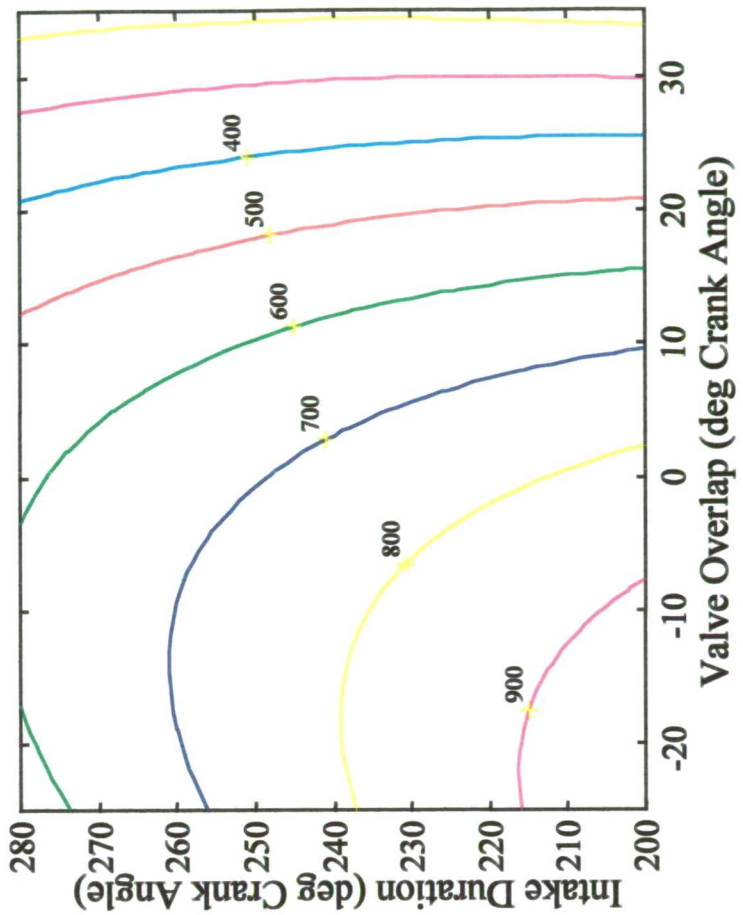

NOx Emissions at 1000 rev/min, 1.0 bar BMEP
Values in ppm

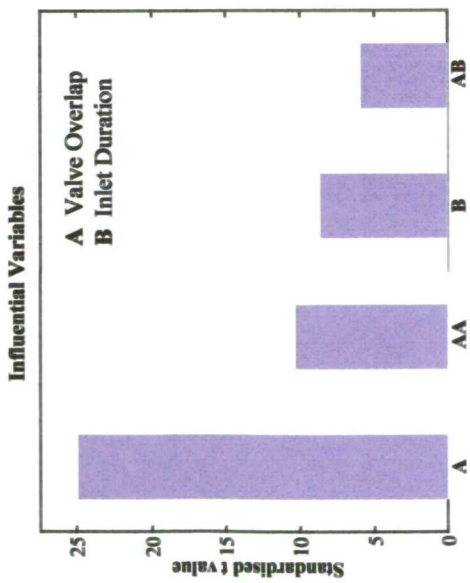

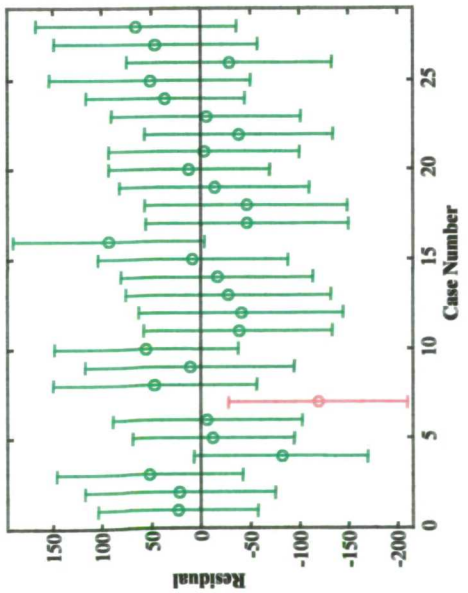

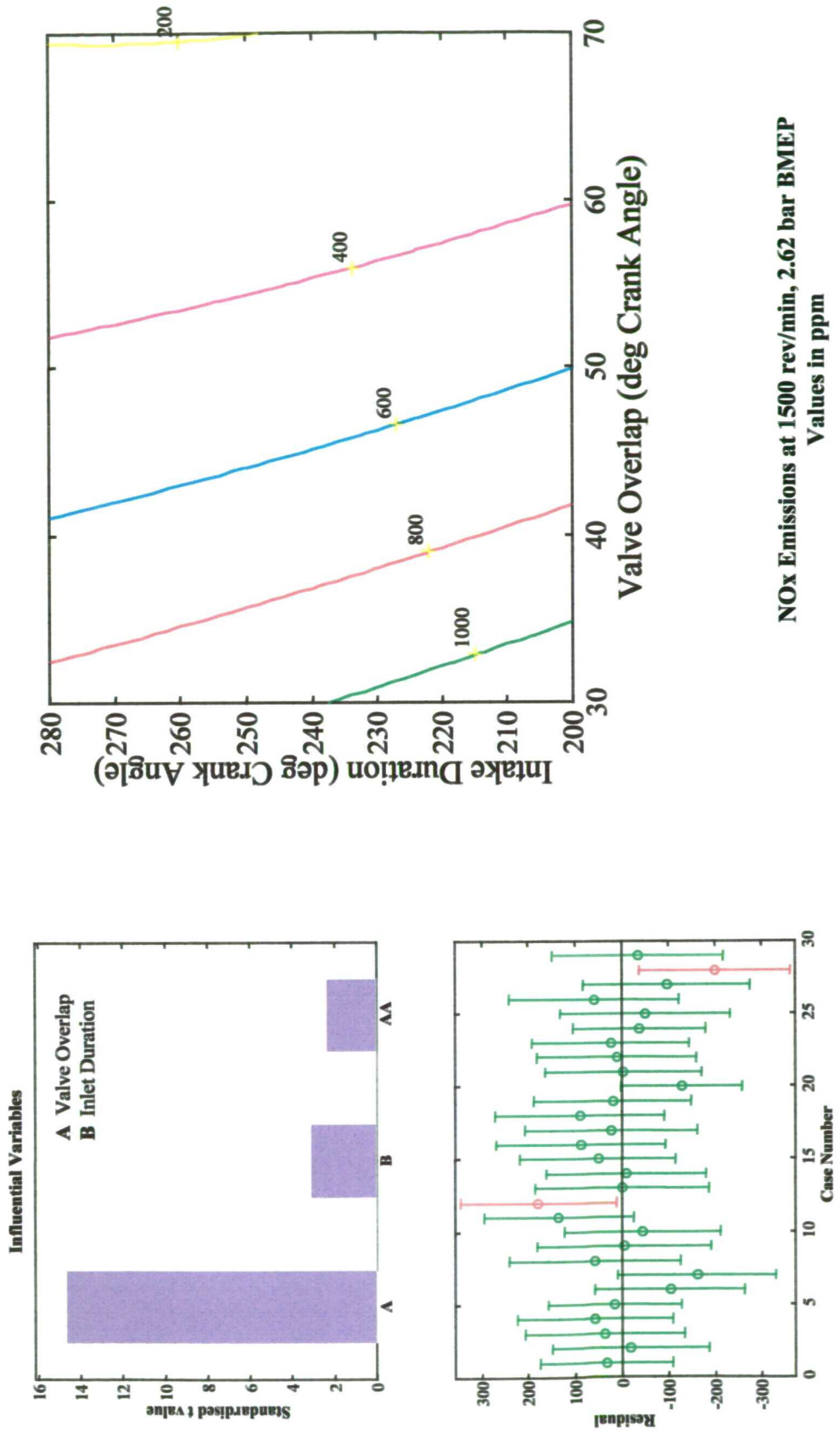
NOx Emissions at 1500 rev/min, 2.62 bar BMEP
Values in ppm
Intake Duration (deg Crank Angle)
Valve Overlap (deg Crank Angle)
200
400
600
800
1000
Influential Variables
A Valve Overlap
B Inlet Duration
Standardised t value
A
B
AA
Residual
Case Number

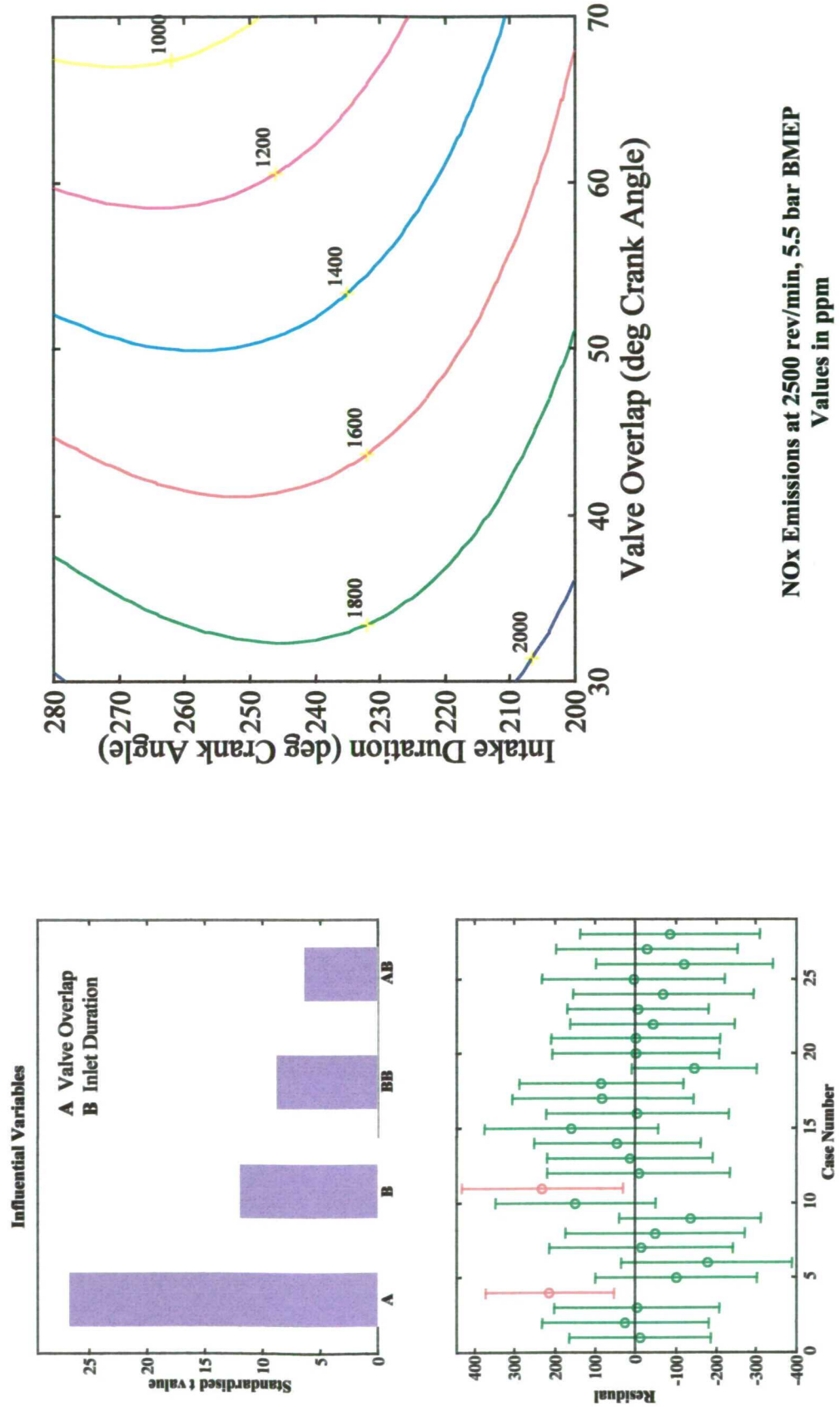
NOx Emissions at 2500 rev/min, 5.5 bar BMEP
Values in ppm
Intake Duration (deg Crank Angle)
Valve Overlap (deg Crank Angle)
1000
1200
1400
1600
1800
2000
Influential Variables
A Valve Overlap
B Inlet Duration
Standardised t value
A
B
BB
AB
Residual
Case Number

HC Emissions at Idle
Values in ppm

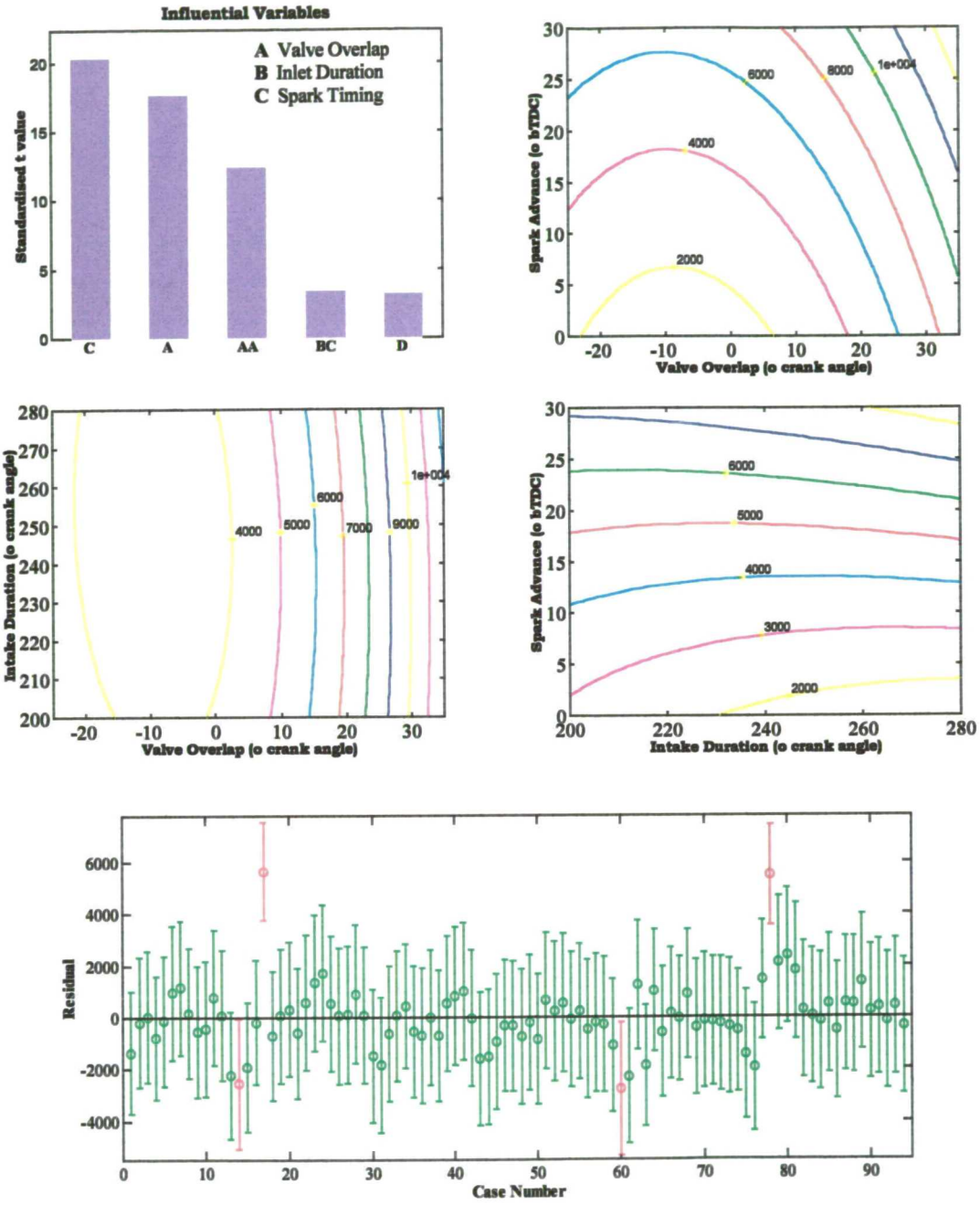

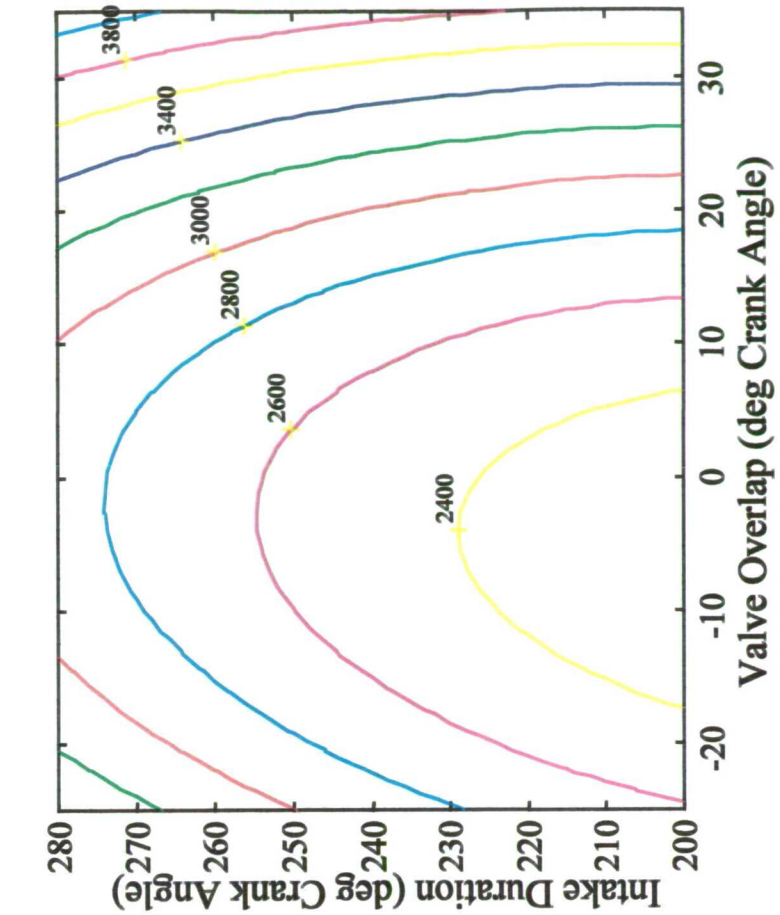
HC Emissions at 1000 rev/min, 1.0 bar BMEP
Values in ppm
Intake Duration (deg Crank Angle)
Valve Overlap (deg Crank Angle)
2400
2600
2800
3000
3400
3800

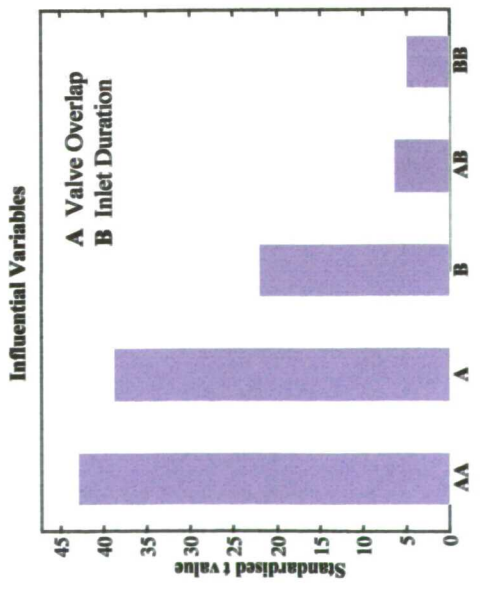
Influential Variables
A Valve Overlap
B Inlet Duration
Standardised t value
AA
A
B
AB
BB

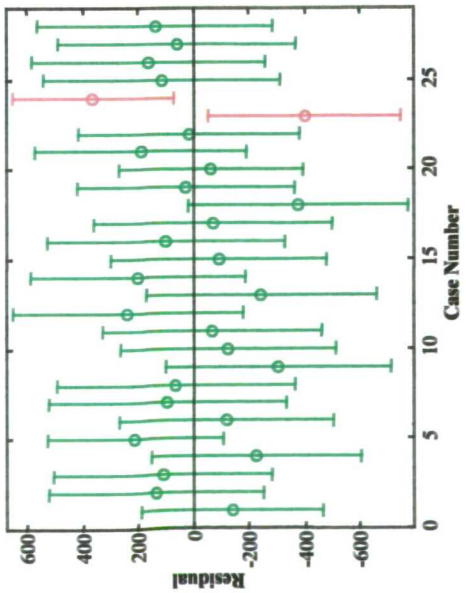
Residual
Case Number

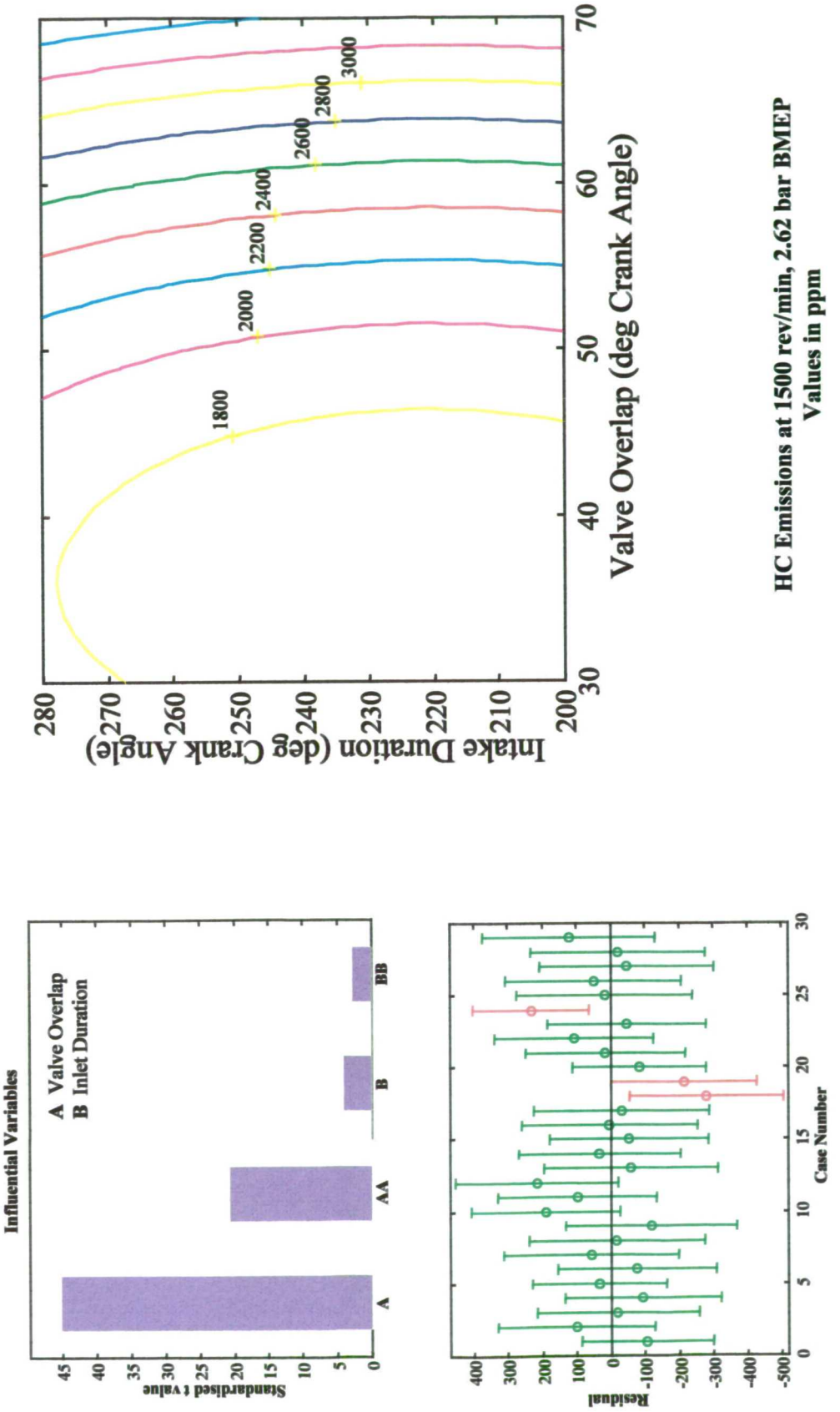
HC Emissions at 1500 rev/min, 2.62 bar BMEP
Values in ppm
Intake Duration (deg Crank Angle)
Valve Overlap (deg Crank Angle)
1800
2000
2200
2400
2600
2800
3000
Influential Variables
A Valve Overlap
B Inlet Duration
Standardised t value
A
AA
B
BB
Residual
Case Number

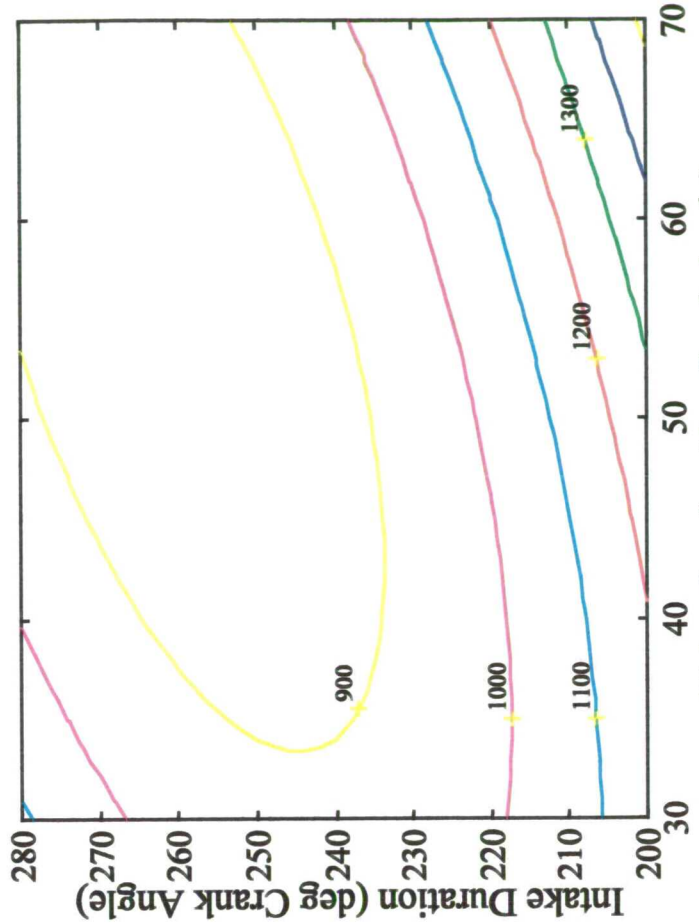

HC Emissions at 2500 rev/min, 5.5 bar BMEP
Values in ppm

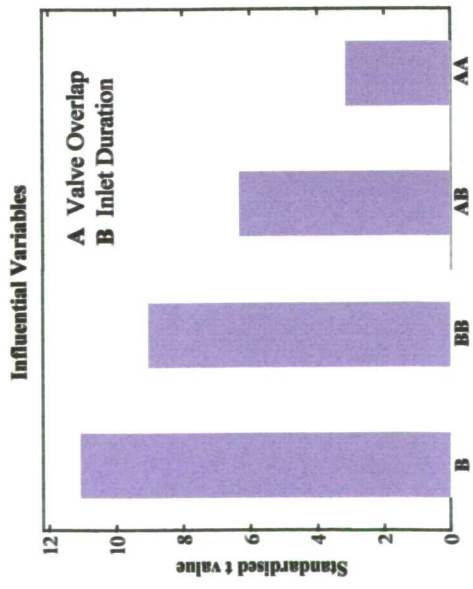

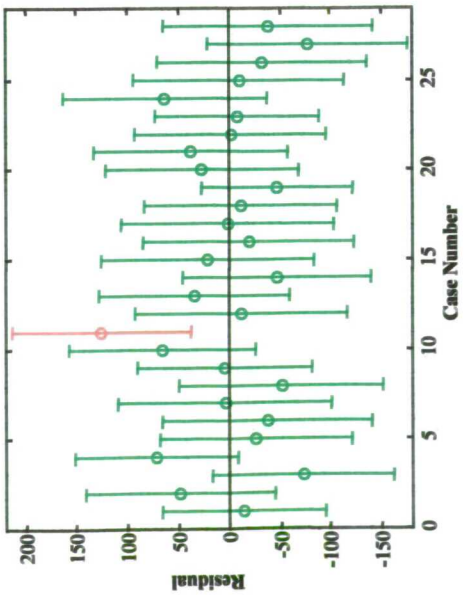

Fuel Consumption at Idle
Values in g/min

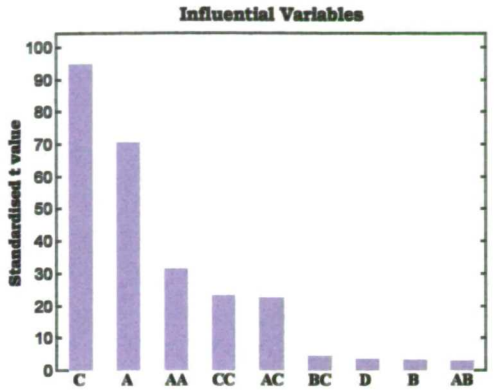

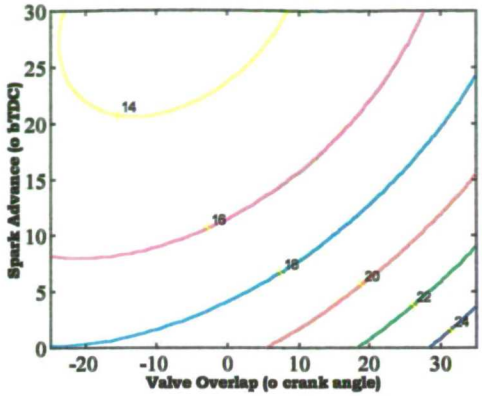

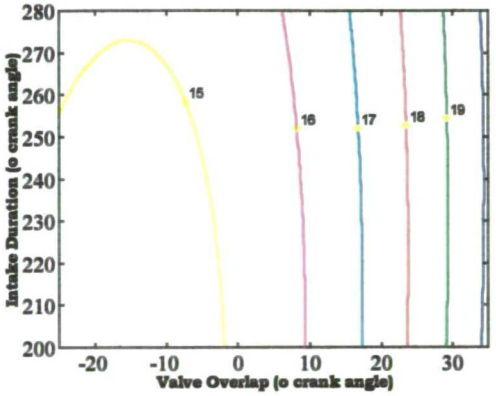

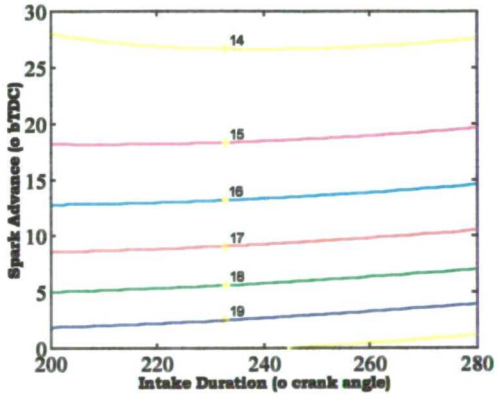

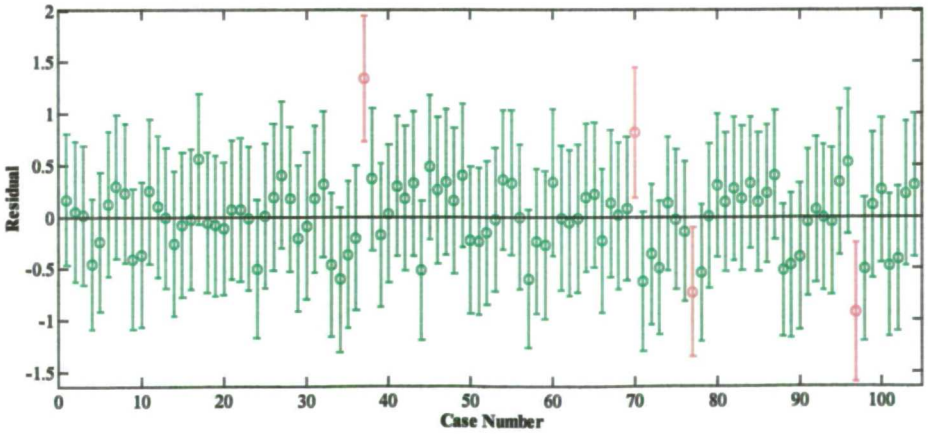

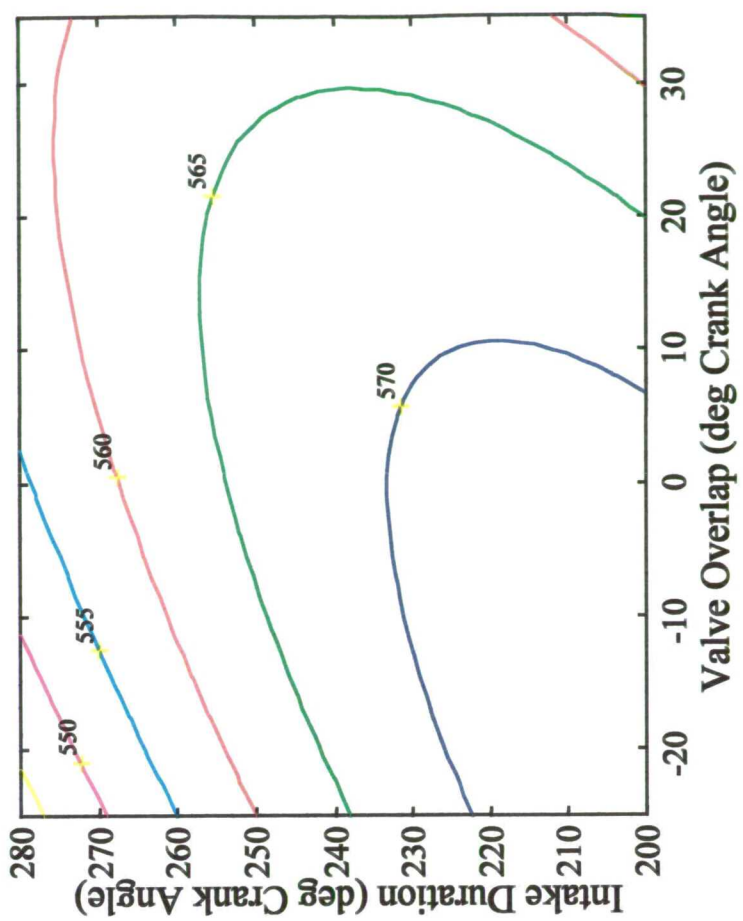

Brake Specific Fuel Consumption at 1000 rev/min, 1.0 bar BMEP
Values in g/kWh

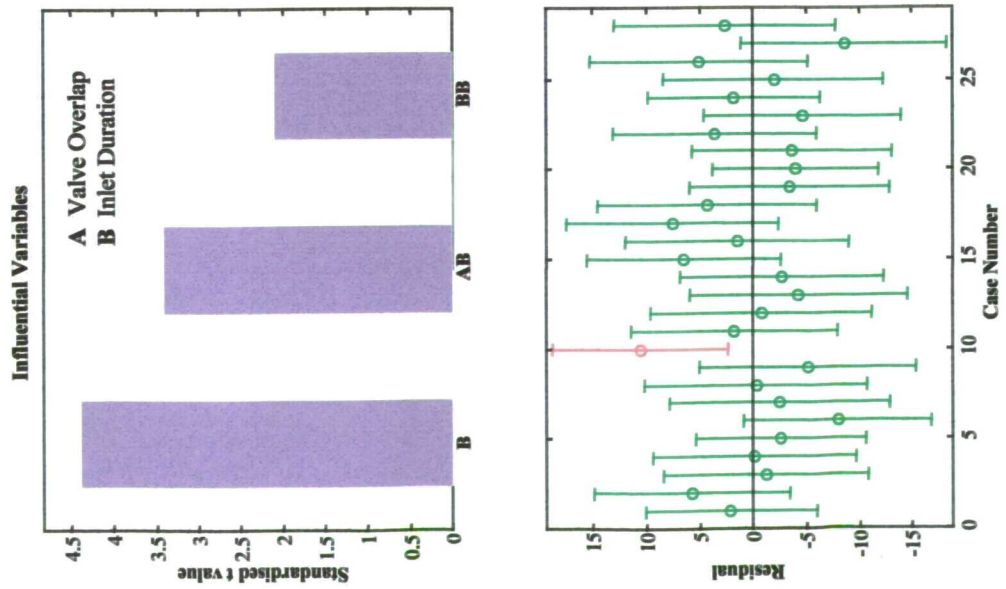

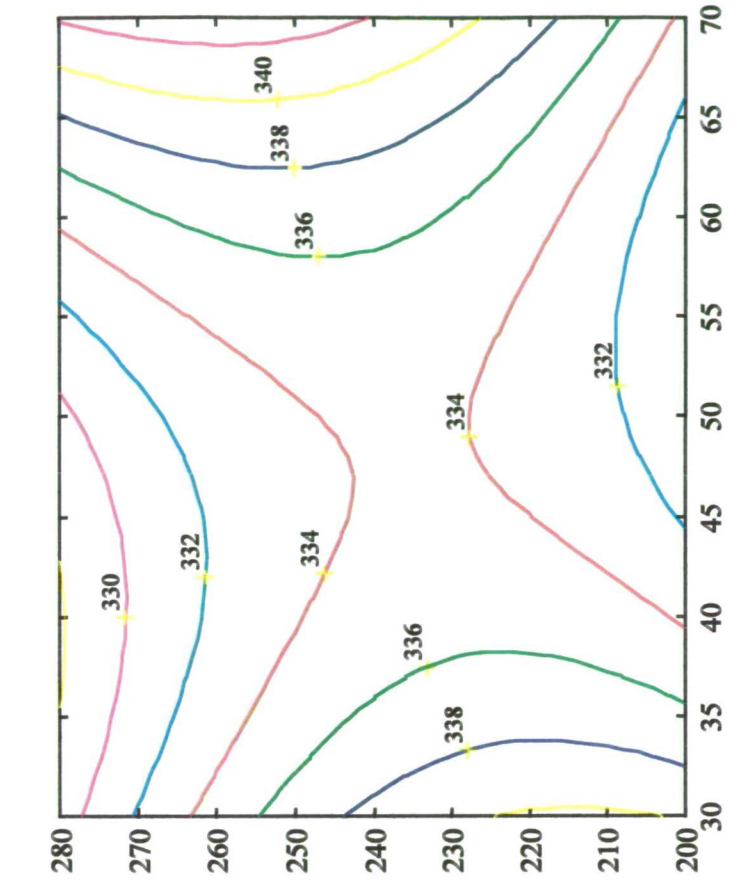

Brake Specific Fuel Consumption at 1500 rev/min, 2.62 bar BMEP
Values in g/kWh

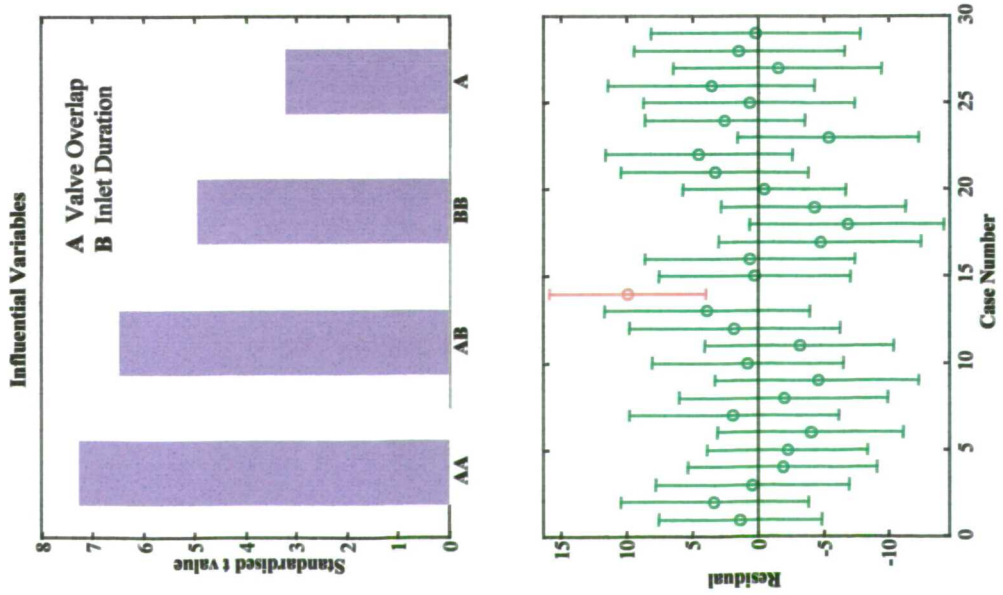

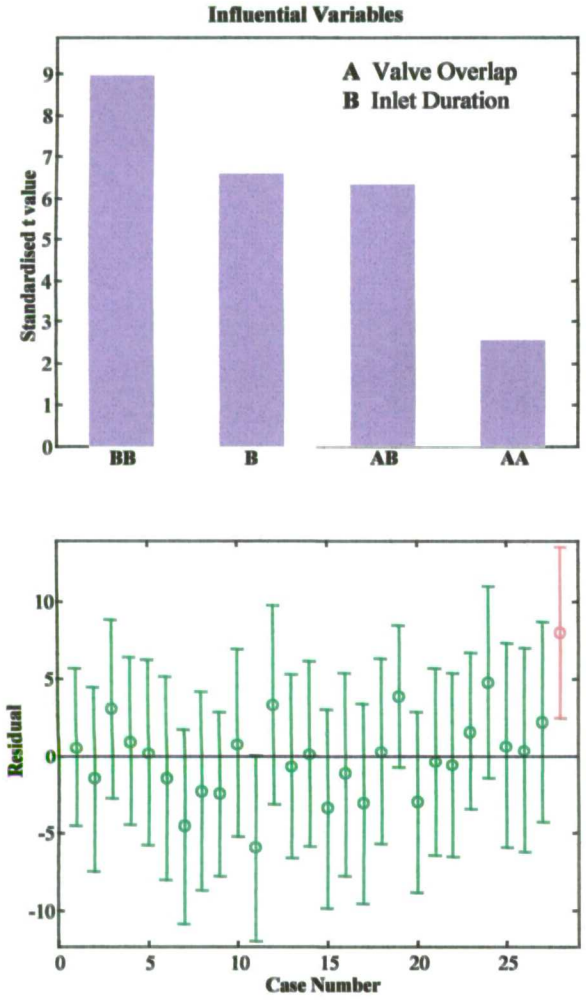

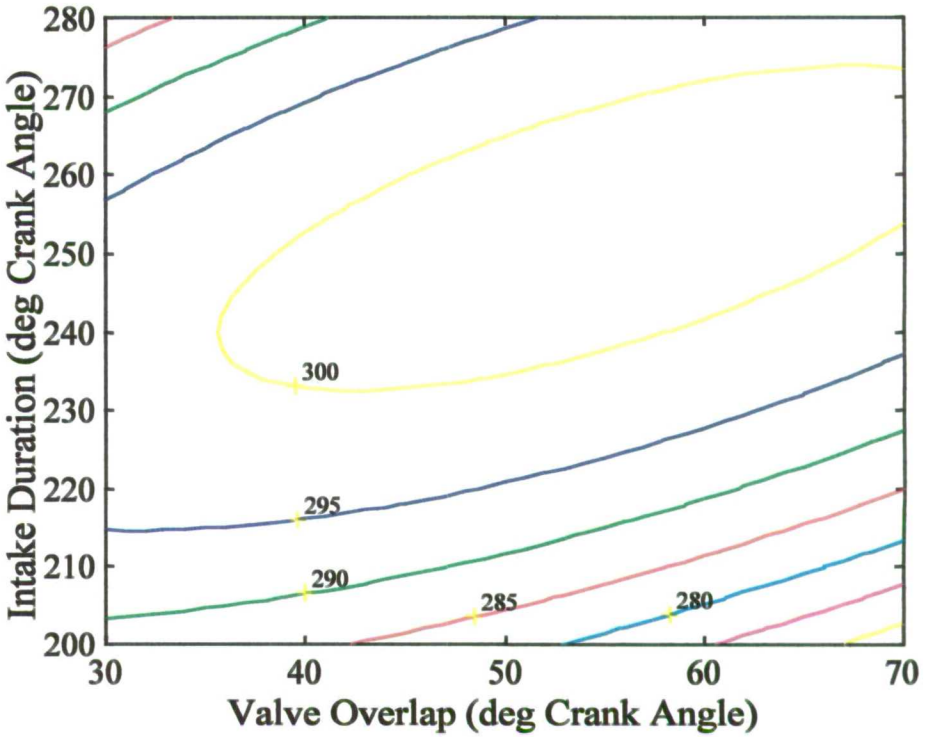

Brake Specific Fuel Consumption at 2500 rev/min, 5.5 bar BMEP
Values in g/kWh

Exhaust Gas Temperature Emissions at Idle
Values in °C

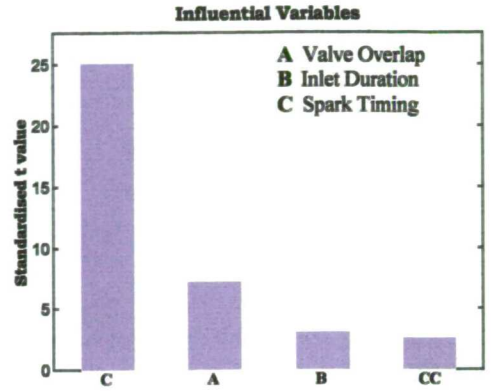

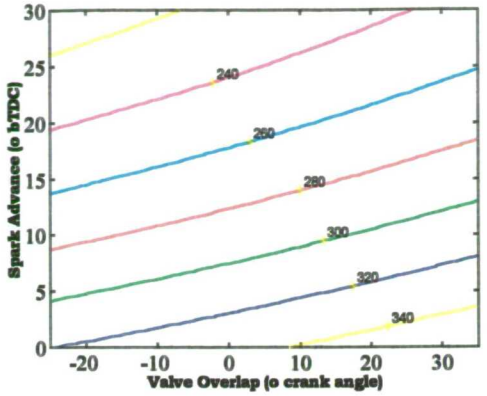

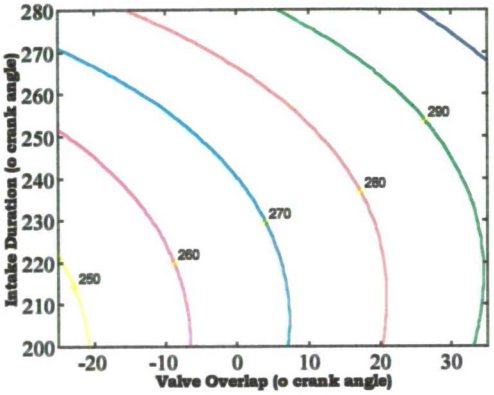

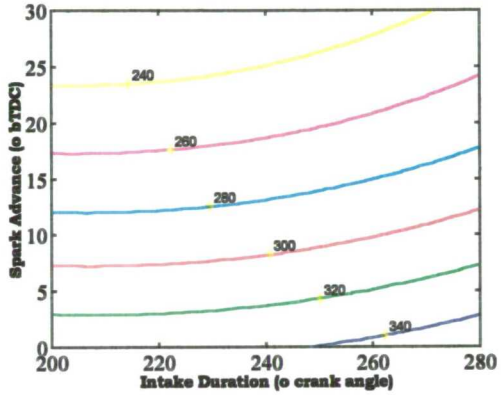

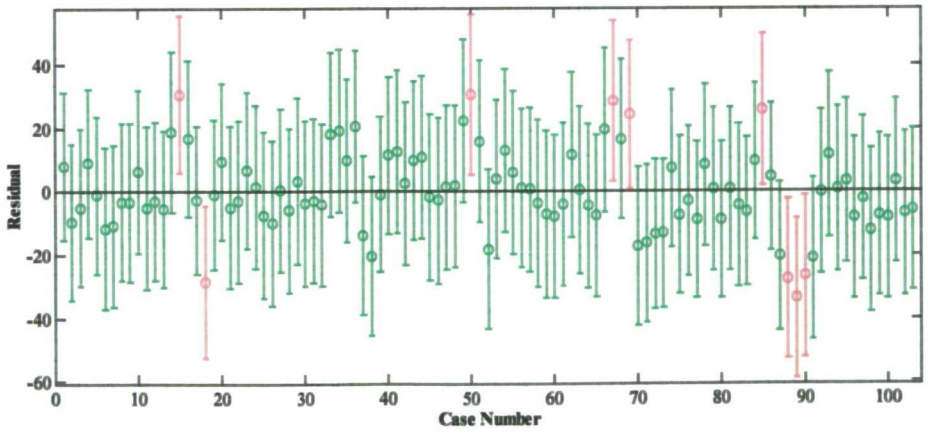

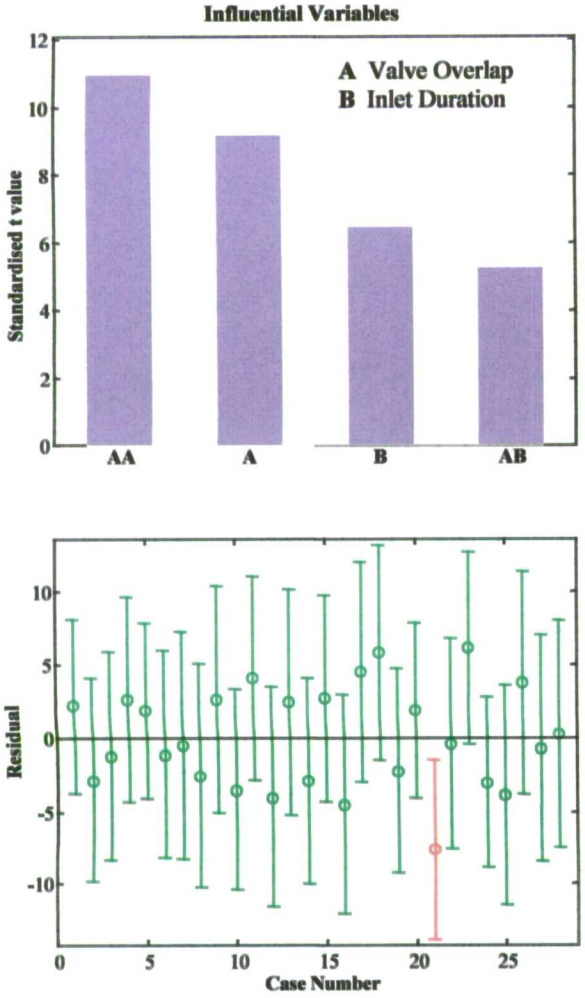

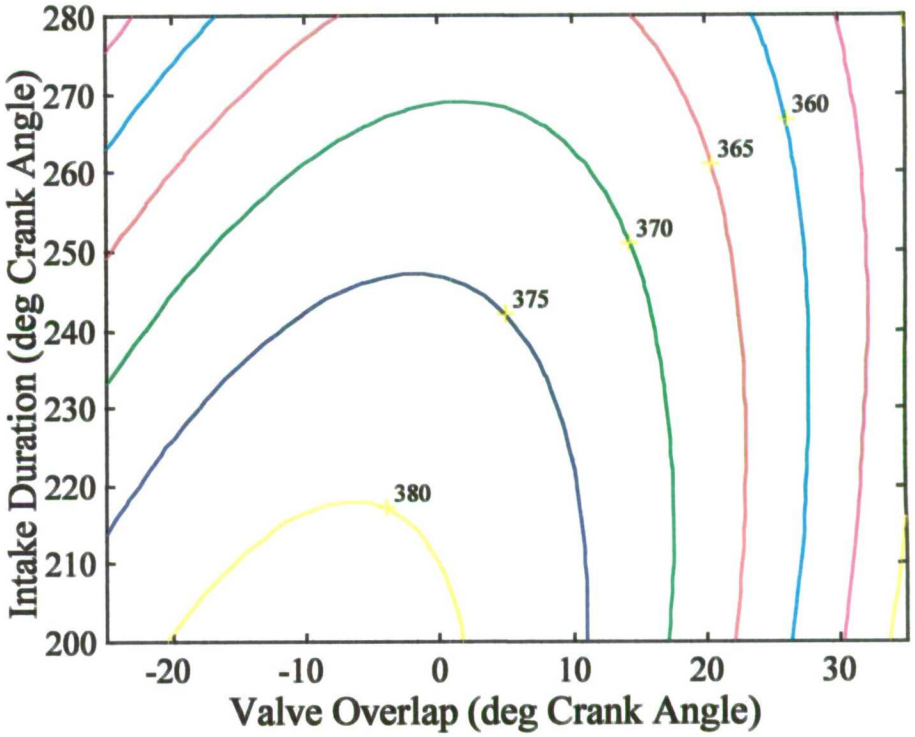

Exhaust Gas Temperature at 1000 rev/min, 1.0 bar BMEP
Values in °C

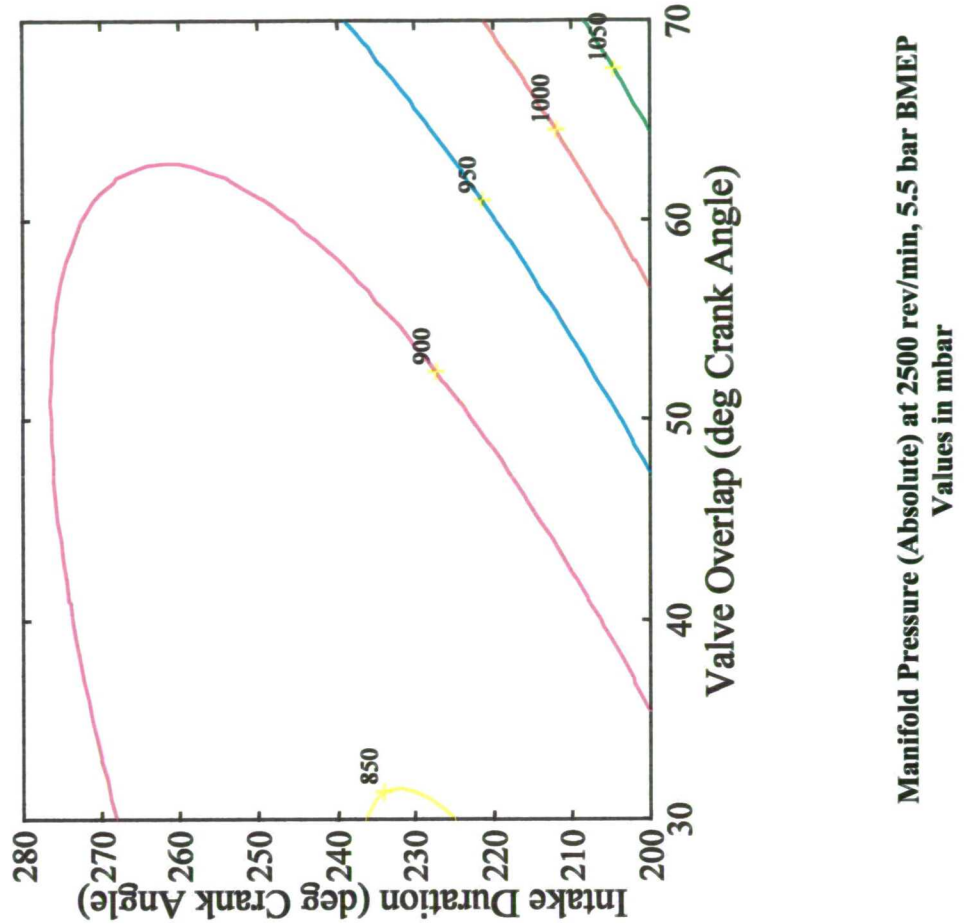
Manifold Pressure (Absolute) at 2500 rev/min, 5.5 bar BMEP
Values in mbar
Intake Duration (deg Crank Angle)
Valve Overlap (deg Crank Angle)
850
900
950
1000
1050

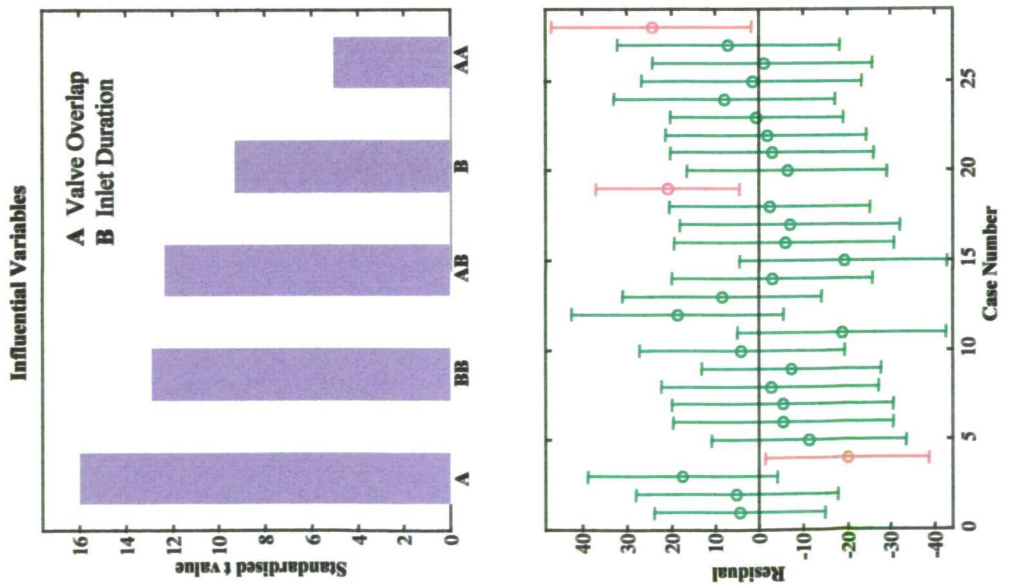
Influential Variables
A Valve Overlap
B Inlet Duration
Standardised t value
A
BB
AB
B
AA
Residual
Case Number

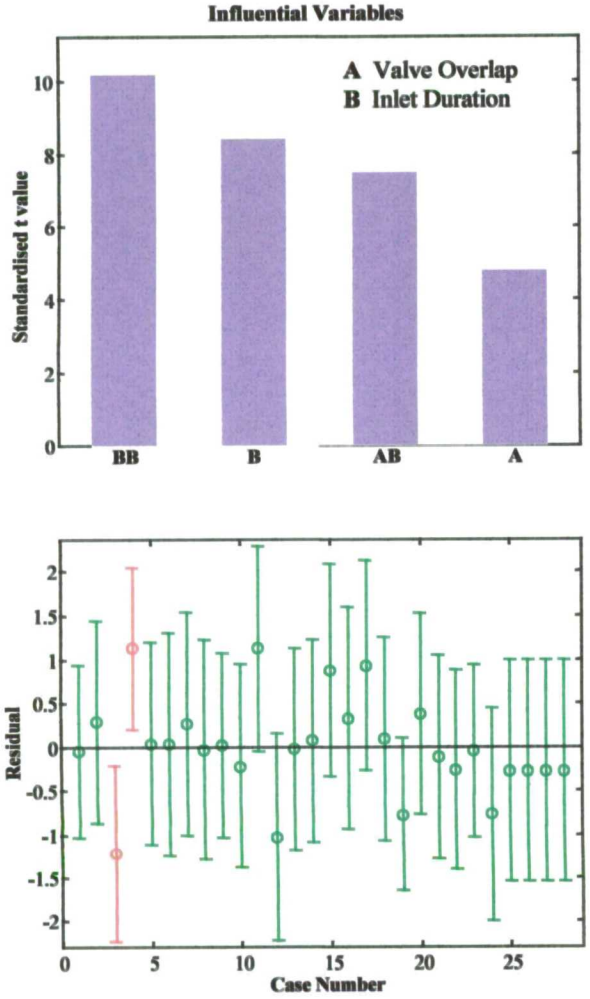

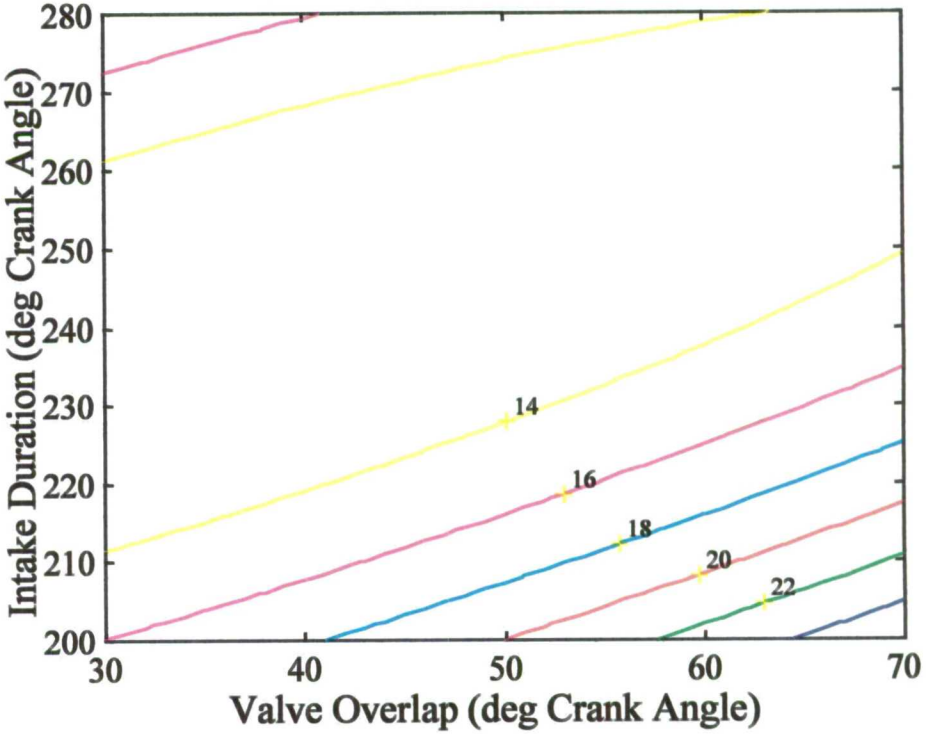

Knock - 2 °ca Spark Angle at 2500 rev/min, 5.5 bar BMEP
Values in °ca bTDC

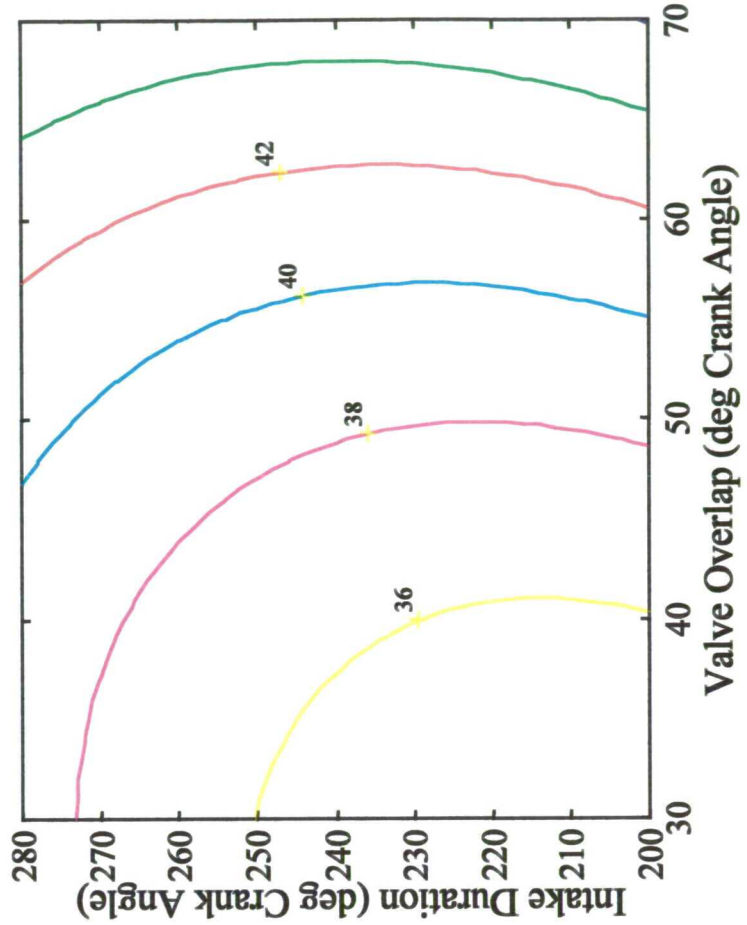

0 - 80% MFB Burn Duration at 1500 rev/min, 2.62 bar BMEP
Values in °ca

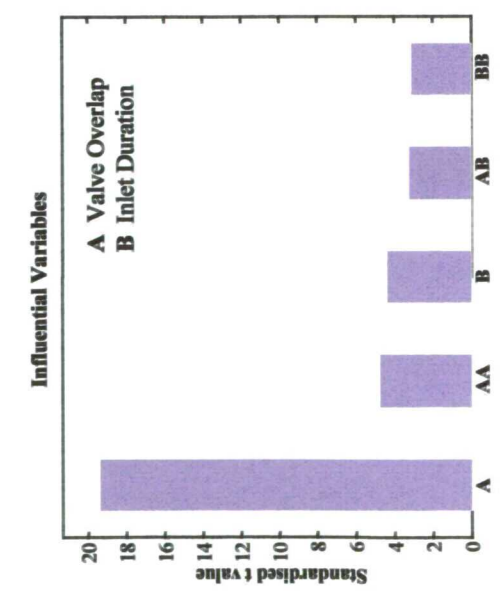

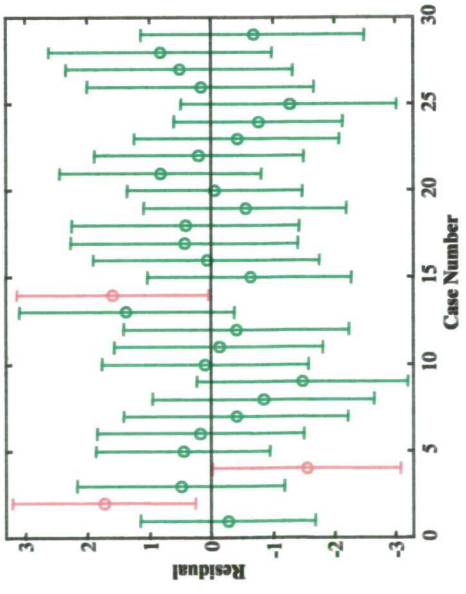

REFERENCES

References

Ahmad, T & Theobald, M A (1989), "A survey of variable valve actuation technology", SAE 891674

Ando, H (1996), "Combustion control technologies for gasoline engines", IMechE Seminar on lean burn combustion engines, Publication No. S433/001/96, IMechE Headquarters, London, UK, 3-4 December, 1996, ISBN 1357-9193

Annand, W J D (1963), "Heat transfer in the cylinders of reciprocating internal combustion engines", Proc. IMechE, Volume 177, No. 36

Annand, W J D & Roe, G E (1974), "Gas flow in the internal combustion engine", G T Foulis & Co. Ltd, UK ISBN 0-85429-160-1

Anon, "AJ-V8 engine and 5HP24 transmission introduction", Jaguar Technical Guide

Anon (1994), "Emissions 2000 - European Exhaust Emissions Regulations 1992 to 2000", Ford Power Products, UK

Baker, T G (1995), "Port throttling applied to a high-performance 4-valve S.I. engine", PhD Thesis, Department of Mechanical Engineering, University College London

Baker, T G, Nightingale, C J E (1996), "Port throttling and port de-activation applied to a 4-valve SI engine", SAE 96 Congress SAE 960587

Barraclough S (1996), Flow bench data for intake valves on Jaguar AJ26 engine. Internal Jaguar document

Boam, D J, Finlay, I C, Biddulph, T W, Ma, T, Lee, R, Richardson, S H, Bloomfield, J, Green, J A, Wallace, S, Woods, W A & Brown, P (1992), "The sources of unburned hydrocarbon emissions from spark ignition engines during cold starts and warm-up", Combustion in Engines - Technology, Applications and the Environment, IMechE Conference Proceedings, C448/064/92

Box, G E P & Draper, N R (1987), "Empirical model-building and response surfaces", John Wiley & Sons, USA

Box, G E P, Hunter, W G & Hunter, J S (1978), "Statistics for experimenters", John Wiley & Sons, USA

Box, G E P & Wilson (1951), "On the experimental attainment of optimal conditions", Journal of the Royal Statistical Society, Series B, Vol. 13, No. 1

Daniels, J (1996), "Emissions - can there be a point of diminishing returns?", Automotive Engineer, August/September 1996

Davies, O L (1954), "The design and analysis of industrial experiments", 1st edition, Oliver and Boyd, Edinburgh

de Boer, C D, Johns, R J R, Grigg, D W, Train, B M, Denbratt, I & Linna, J R (1990), "Refinement with performance and economy for four-valve automotive engines" IMechE C394/053/90

DeLosh, R G, Brewer, K J, Buch, L H, Ferguson, F W & Tobler, W E (1981), "Dynamic computer simulation of a vehicle with electronic engine control", SAE 810447

Demmelbauer-Ebner,W, A Dachs & H P Lenz, (1991), "Variable valve actuation for the optimisation of engine torque", SAE 910447

Diamond, W J (1989), "Practical experiment designs for engineers and scientists", 2nd edition, Van Nostrand Reinhold

Dopson, C & T Drake (1991), "Emissions optimisation by camshaft profile switching", SAE 910838

Dresner, T & Barkan, P (1989), "A review and classification of variable valve timing mechanisms", SAE 890674

Duckworth, R F & Barker, L (1996), "A comparative study of variable camshaft phasing and port throttling for performance and emissions", SAE 960580

Endres, H, Schulte, H & Krebs, R (1990), "Combustion system development trends for multi-valve gasoline engines", SAE 900652

Endres, H, Neuβer, H J & Wurms, R, (1992), "Influence of swirl and tumble on economy and emissions of multi-valve SI engines", SAE 920516

Finney, D J (1945), "The fractional replication of factorial arrangements", Annals of Eugenics, Vol. 12, London

Fisher, R A (1935), "The design of experiments", Oliver and Boyd, Edinburgh

Fry, M D (1994), "Optimisation of mixture preparation in an SI engine", PhD Thesis, Department of Mechanical Engineering, University College London

Gray, C (1988), "A review of variable engine valve timing", SAE 880386

Grohn, M (1990), "The new camshaft adjustment system by Mercedes-Benz - design and application in 4-valve engines", SAE 901727

Hadded, O, Stokes, J & Grigg, D W (1995), "Low emission vehicle technology for ultra low emission vehicle and European stage 3 emission standards", Proc. IMechE, Vol. 209, Part D: Journal of Automotive Engineering

Harada, K (1992), "Development of Air-Assisted Injector System", SAE 920294

Harrington, D L & Bolt, J A (1970), "Analysis and digital simulation of carburettor metering", SAE 70082, SAE Trans., vol. 79

Heywood, J B (1988), "Internal combustion engine fundamentals", McGraw-Hill International ISBN 0-07-100499-8 1988

Horie, K, Nishizawa, K, Ogawa, T, Ajazaju, S & Miura, J (1992), "The development of a high fuel economy and high performance four-valve lean burn engine", SAE 920455

Inoue, K, Nagahiro, K, Ajiki, Y & Kishi, N (1989), "A high-power, wide torque range, efficient engine with a newly developed variable-valve-lift and timing mechanism", SAE 890675

Inoue, T, S Matsushita, K Nakanishi & H Okano (1993), "Toyota lean combustion system - the third generation system", SAE 930873

Johansson, B & Soderberg, F (1996), "The effect of valve strategy on in-cylinder flow and combustion", SAE 960582

Joyce, M J, Carling, J, Clough, M & Corkill W J, (1996), "A new Jaguar engine for the 21st Century", International IMechE seminar on the application of powertrain and fuel technologies to meet emissions standards, IMechE Headquarters, London, UK, 24 – 26 June, 1996, IMechE, Publication No. C517/003/96

Kiyota, Y, Akishino, K & Ando, H (1992), "Concept of lean combustion by barrel-stratification", SAE 920678

Kreuter, P, Heuser, P & Schebitz, M (1992), "Srategies to improve SI performance by means of variable intake lift, timing and duration", SAE 920449

Kreyszig, E (1993), " Advanced engineering mathematics", 7th edition, John Wiley and Sons, Inc. ISBN 0-471-59989-1

Krieger, R B & Borman, G L (1966), "The computation of apparent heat release for internal combustion engines", ASME paper 66-WA/DGP-4, in Proceedings of diesel gas power, ASME 1966

Kyriakides, S C & Glover, A R (1989) "A study of the correlation between in-cylinder air motion and combustion in gasoline engines", Proc. IMechE, Vol 203, Part D, C55/88/89

Leone, T G, Christenson, E J & Stein, R A (1996), "Comparison of variable camshaft timing strategies at part-load", SAE 960584

Ma, T H (1988), "Effect of variable engine valve timing on fuel economy", SAE 880390

Maekawa, K, Ohsawa, N & Akasaka, A (1989), "Development of a valve timing control system", SAE 890680

Mikulic, L A, Quissek, F & Fraidl, G K (1990), "Development of low emission high performance four valve engines", SAE 900227

Miller, M J & Nightingale, C J E (1990), "Measurement of the changes in mixture preparation that occur during flow past the inlet valve of a spark ignition engine", Proc. IMechE, International Conference on Automotive Power Systems, C394/004

Min, K, Cheng, W K & Heywood, J B (1994), "The effects of crevices on the engine-out hydrocarbon emissions in SI engines", SAE 940306

Mowll, D, Robinson, D R, and Pilley, A D (1996), "Baysian experimental design and its application to engine research and development", SAE 961157

Myers, R H & Montgomery, D C (1995), "Response surface methodology: process and product optimisation using designed experiments", John Wiley & Sons, ISBN 0-471-58100-3

Namazian, M & Heywood, J B (1982), "Flow in the piston-cylinder-ring crevices of a spark-ignition engine: effect on emissions, efficiency and power", SAE 820088

Newman C E, Stein, R A, Warren, C C & Davis, G C (1989), "The effects of load control with port throttling at idle - measurements and analyses", SAE 890679

Nogi, T, Ohyama, Y *et al.* (1988), "Mixture formation of fuel injection systems in gasoline engines", SAE 880558

Norris, R D (1991), "A high speed variable valve timing mechanism for engines", Autotech Congress, Proc. IMechE, C427/1/154

Pilley, A D, Beaumont, A J, Robinson, D & Mowll, D (1994), "Design of experiments for optimisation of engines to meet future emissions targets", International Symposium on Advanced Transportation Applications, Ref. 94EN014

Pischinger, F & Kreuter, P (1984), "Electromagnetically operating actuator", US Patent No. 4,455,543

Poole, C J, Hancock, R J & Cairns, D C (1992), "Cosworth MBA engine", SAE 920849

Press, W H, Teukolsky, S A, Vetterling, W T & Flannery, B P (1995), "Numerical recipes in C", 2nd edition, Cambridge University Press, ISBN 0-521-43108-5

Rogers, G F C & Mayhew, Y R (1992), "Engineering thermodynamics work and heat transfer", 4th edition, Longman Group Ltd, London

Rokita, R, Bandel, W & Herzog, P (1993), "Mixture preparation optimisation for gasoline engines on a dynamic flow test rig", Proc. IMechE, C448/067

Saikalis, G, Byers, R & Nogi, T (1993), "Study on air assist fuel injector atomisation and effects on exhaust emission reduction", SAE 930323

Seabrook, J (1995), "Combustion and emissions optimisation in a high-performance SI engine", PhD Thesis, Department of Mechanical Engineering, University College London

Shibano, K, Kamimaru, S, Yamada, T & Watanabe, K (1992), "A newly developed variable valve timing mechanism with low mechanical friction", SAE 920451

Shin, Y, Min, K & Cheng, W K (1995), "Visualisation of mixture preparation in a port fuel injection engine during warm-up", SAE 952481

Stein, R A, Galietti, K M & Leone, T G (1995), "Dual-equal VCT - a variable camshaft timing strategy for improved fuel economy and emissions", SAE 950975

Stivender, D L (1968), "Intake valve throttling (IVT) - a sonic throttling intake valve engine", SAE 680399

Stokes, J, Lake, T H, Christie, M J & Denbratt, I (1994), "Improving the fuel economy/NO_x emissions trade-off for gasoline engines with the CCVS system", SAE 940482

Stone, C R & Kwan, E (1989), "Variable valve actuation mechanisms and the potential for their application", SAE 890673

Stone, C R (1992), "An introduction to internal combustion engines", 2nd edition, Macmillan, ISBN 0-333-55084, 1992

Stone, C R, Carden, T R & Podmore, I (1993), "Analysis of the effect of inlet valve disablement on swirl, combustion and emissions in a spark ignition engine", Proc. IMechE, Part D, Vol. 207, pp. 295-305

Stone, C R, & Ladommatos, N (1992), "The measurement and analysis of swirl in steady flow", SAE 921642

Taguchi, G (1987), "System of experimental design", Volume 1, UNIPUB/Kraus International Publications, New York USA

Taylor, G (1998), "A study of the pressure variations in the inlet manifold of a 4-cylinder, 16-

valve, SI engine", 3rd Year Project Report, Department of Mechanical Engineering, University College London

Thompson, N D & Wallace, J S (1994), "Effect of engine operating variables and piston and ring parameters on crevice hydrocarbon emissions", SAE 940480

Titolo, A (1991), "The variable valve timing system - application on a V8 engine", SAE 910009

Tsatsami, V (1987), "Inlet manifold processes of SI engines under cold operating conditions", PhD Thesis, Department of Mechanical Engineering, University College London

Tuttle, J H (1980), "Controlling engine load by means of late intake valve closing", SAE 800794

Tuttle, J H (1982), "Controlling engine load by means of early intake valve closing", SAE 820408

Urata, Y, Umiyama, H, Shimisu, K, Fujiyoshi, Y, Sono, H & Fukuo, K (1993), "A study of vehicle equipped with non-throttling SI engine with early intake valve closing mechanism", SAE 930820

Watson, N & Janota, M S (1982), "Turbocharging the internal combustion engine", Macmillan, London, ISBN 0-333-24290-4

Wentworth, J T (1971), "The piston crevice volume effect on exhaust hydrocarbon emissions", Combustion Science Technology, vol. 4, pp 97-100

Wilson, N, Dopson, C & Muddell, G (1992), "Lotus active valve train research system", Lotus engineering publication, ref. 1794/92

Wilson, N, Watkins, A J & Dopson, C (1993), "Asymmetric valve strategies and their effect on combustion", SAE 930821

Winterbottom, A (1996), Facsimile communication detailing five-variable CCRD, Department of Acturial Science, City University, London

Yates, F (1935), "Complex experiments", Supplement to Journal Royal Statistical Society, Volume 2, pp 181-247